INFLUENCE OF SHEAR LAG ON THE COLLAPSE

OF WIDE-FLANGE GIRDERS

A thesis submitted for the degree of

Doctor of Philosophy

in the Faculty of Engineering of the

University of London

by

António Ressano Garcia Lamas

Dipl. Civ. Eng., MSc, DIC

Department of Civil Engineering

Imperial College of Science and Technology

London

June 1979

To Joan, António Miguel, Luís

and my parents

CONTENTS

INFLUENCE OF SHEAR LAG ON THE COLLAPSE OF

WIDE-FLANGE GIRDERS

by

António Ressano Garcia Lamas

ABSTRACT

The study reported in this thesis deals with an analytical investigation into the collapse of wide flanges of box girders in a shear lag environment taking into account the effects of plasticity and large deflections.

An analytical model of a simply supported box girder plate assemblage was developed to reproduce the most severe shear lag effects under point loading at mid-span. The numerical solution uses finite differences and dynamic relaxation and was calibrated against other proven numerical techniques.

An experimental study of isolated flange plates loaded under similar shear lag conditions has been programmed to provide data to validate the theoretical research and to investigate some problems associated with stiffened flanges that have not yet been modelled analytically. A special testing rig constructed for this programme is described in the thesis.

The analytical work involves the identification and study of the characteristics of the principal flange modes of failure and the associated upper bounds to its capacity. A parametric study on unstiffened flanges explains in terms of the aspect ratio and the slenderness parameters the interaction between these two modes: the failure in shear of the web-flange connections, directly associated with the shear lag effects, and the failure by inelastic buckling in compression. The results can be used to estimate the degree of redistribution that can be assumed at collapse. The application of these conclusions to stiffened flanges when edge panel buckling can be avoided is also investigated. The thesis demonstrates that additional problems are involved when the edge panels fail in combined shear and compression. Methods to extend the present solution to account for these effects are outlined.

The conclusions regarding redistribution are compared with other proposals. A method for approximating the degree of redistribution that can be assumed at collapse is proposed and used to interpret available experimental results from tests on large scale box girders.

ACKNOWLEDGEMENTS

CHAPTER   1

INTRODUCTION

1.1   IDENTIFICATION OF PROBLEM AND REVIEW OF PREVIOUS WORK

The flanges of a beam subjected to bending are normally strained in shear across their width.   In wide flanges these shear strains may produce a highly non-uniform distribution of longitudinal direct stresses with the maximum values occurring at the web-flange junction.   This *shear lag* effect makes it impossible to apply directly the elementary theory of bending in the calculation of stresses and deflections.   For design purposes, in the linear-elastic range, it is normal to use the concept of an effective width over which the longitudinal stresses are assumed to be uniformly distributed.   With this device simple bending theory may be used to predict peak stresses and/or deflections.   For stress calculations the effective width can be expressed as

$$b_e = (\sigma_{av}/\sigma_{max})b \qquad\qquad 1.1$$

where σ_{av} and σ_{max} are the average and the maximum values of the longitudinal stress distribution across a flange of width b, Fig. 1.1. The ratio b_e/b is usually known as the effective width ratio and thus calculated as:

$$b_e/b = \sigma_{av}/\sigma_{max} \qquad\qquad 1.2$$
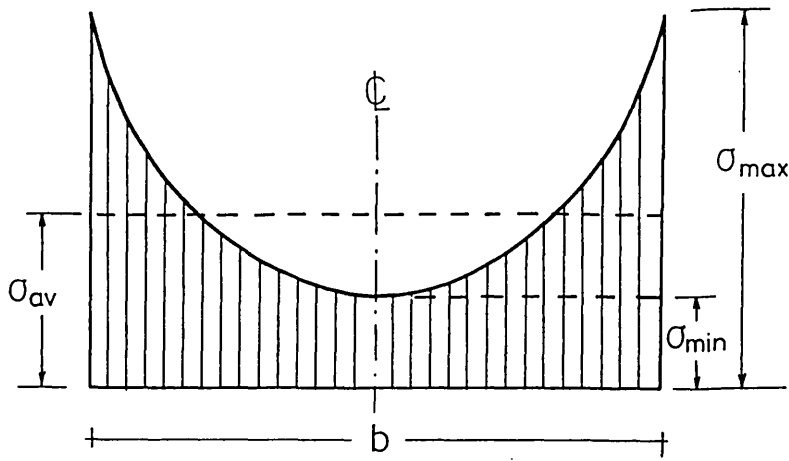
Fig. 1.1   Distribution of longitudinal stresses in flange subject to
shear lag effects

For convenience in design the term effective width has been
associated with other non-uniform stress distributions.   It is used,
for example, in the context of compressive plate buckling to express
the non-uniform stressing due to the development of large deflections.
The confusion between these two concepts*was discussed by Schade[1].

Historically the study of this problem can be traced back to
von Karman[2],   through Chawalla and others[3-5].   The
necessity of considering shear lag effects in design first arose in
aircraft construction[6][7] but soon naval architects[1][8] and
civil engineers were also concerned with the same problem.   The deter-
mination of effective widths for bridge deck flanges has been the subject
of several investigations[10-13].

The extensive study of the shear lag phenomenon in box girder
bridges conducted by Moffatt and Dowling[13][14] constitutes, however,
the major contribution towards the understanding of the effects of the
various parameters involved.   Their design proposals have already

* the shear lag effective width concept is associated with a first order
effect while the"buckling effective width"is associated with a second
order one.
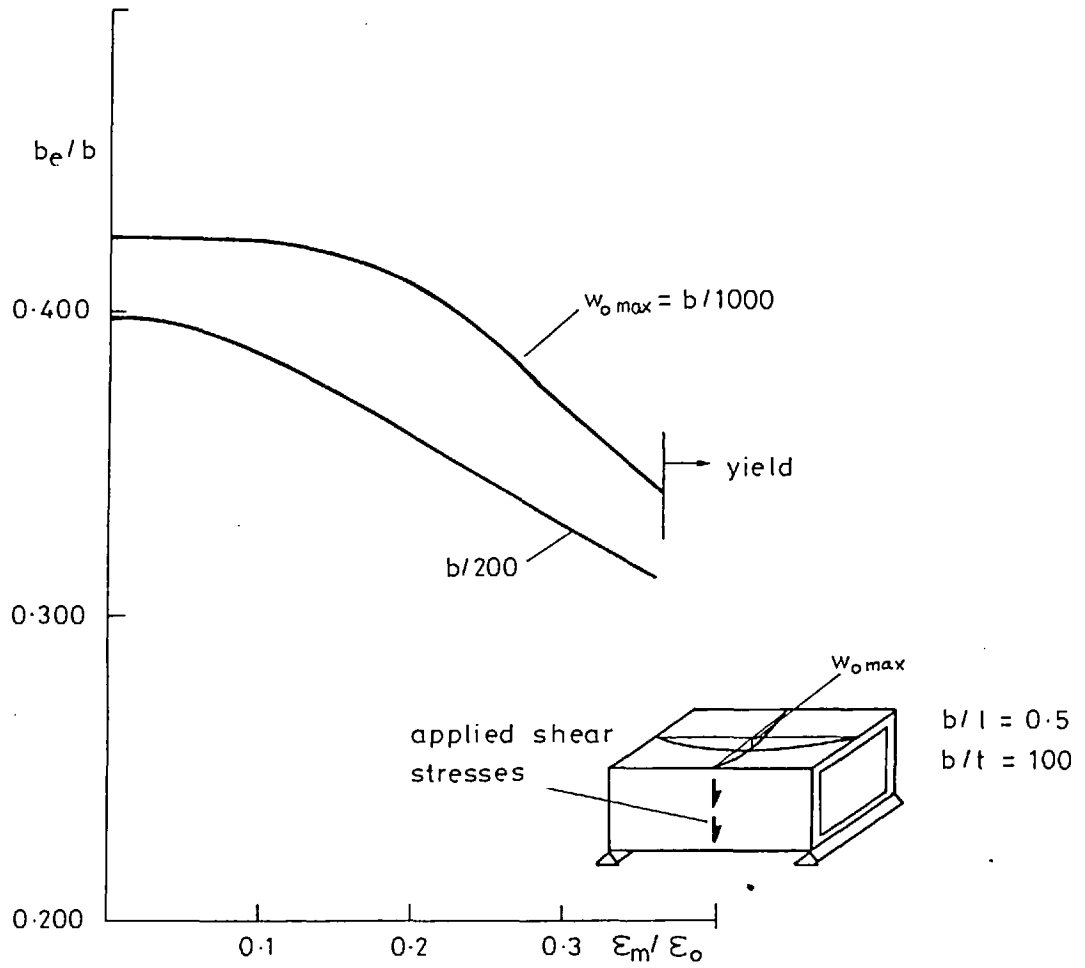
Fig. 1.2   Reduction of elastic effective width ratios due to non-linear
geometric effects

influenced several codes of practice*. These proposals isolate the
flange aspect ratio b/ℓ as the main parameter affecting shear lag,
while adjustments in effective widths were proposed to allow for other
parameters such as loading type, amount of stiffening, cross-sectional
dimensions etc. The application of these results is however limited
to cases where a linear-elastic approach is valid.

In many real structures slender, initially distorted flanges
develop large out-of-plane deflections when compressed thus increasing
the non-uniformity of the in-plane stress distribution. The initial
distortions can reduce the values of effective width ratios from the
early stages of loading. This was shown by the author in reference (18)
and is illustrated in Fig. 1.2 for a compression flange of a simply
supported box girder under a point load at mid-span. The variation of
the elastic effective width ratio with loading† is greatly influenced by
the amplitude of the initial imperfect shape indicating that non-linear
shear lag effects cannot be neglected in slender flanges.

First in-plane yielding is likely to occur at an earlier stage
than predicted by neglecting out-of-plane movement. Further loading
eventually produces a redistribution of stresses through plastic action.
In the context of ultimate load calculations it is necessary to establish
the extent to which redistribution can take place.

---

* - *Merrison Committee, steel box girder bridges design rules, reference(15).*
- *Department of the Environment, Interim rules for design and construction
  of plate girders and rolled section beams in bridges, Tech. Memo, BE 3/76,
  Jan. 1976.*
- *ASCE, Recommendations on box girder bridge design.*
- *Czechoslovak Standard for Steel Bridges, draft of revised CSN 73205.*
- *DnV Rules, Appendix C, DnV, 1977.*
- *BS 5400, Part 5, and draft of Part 3, references(17 and 16).*

† *see method of presenting results in section 1.3.*

This problem was first considered for steel box girder bridges by the Merrison Committee in their appraisal rules[19]. In the calculation of the collapse limit in stiffened flanges it was permitted to consider full redistribution* when flange failure was governed by the failure of plate panels. Such redistribution was not allowed when failure was associated with torsional buckling of open-section stiffeners. This somewhat intuitive limitation was intended to ensure that advantage of redistribution was not taken in cases of inadequate post-buckling capacity[20].

Some studies have been made of the interaction between in-plane shear lag and out-of-plane buckling action. Bogunovic[21] was probably the first to investigate theoretically the elastic buckling of plates in non-uniform compression due to shear lag effects produced in plating eccentrically stiffened by open stiffeners with loading uniformly distributed along their length. The bending deflection of the stiffeners was not considered thus reducing the problem to a bifurcation analysis of critical loads.

Later, Maquoi and Massonnet[22] presented the results of an analytical study on the elastic large deflection behaviour of an orthotropic plate panel acting as a compression flange of a double web beam subjected to a bending moment distribution produced by point loading. The effect of initial imperfections was considered and, as in reference (21), Fourier series solutions were used. This study was an extension of a previous investigation by the same authors[23] of the ultimate capacity of orthotropic flanges in axial compression. As material non-

---

* *full redistribution in the sense that non-uniform compression associated with shear lag can be neglected at collapse, and the ultimate effective width associated with buckling of a uniformly compressed flange plate may be adopted.*

linearity was not considered the Volmir-Skaloud criterion for the collapse of plates in compression was used. This assumes that the ultimate flange strength is reached when the mean membrane stress along the longitudinal edges (adjacent to the webs) is equal to the uniaxial yield stress. These edges were assumed to be free to pull in.

It was as a conclusion of this study that Maquoi and Massonnet (22)(24) proposed a design method for considering the effects of shear lag in the calculation of the ultimate strength of stiffened flanges.

To explain these proposals it is necessary to introduce the extension of the effective width ratio concept, defined in expression (1.2), into the non-linear range. It will be designated for a flange plate cross section by ψ defined* by taking not the maximum longitudinal stress, but the yield stress, thus:

$$\psi = \sigma_{av}/\sigma_o \qquad\qquad 1.3$$

Maquoi and Massonnet defined the efficiency of a compression flange panel located between two cross stiffeners by the ratio of the average longitudinal stress at the mid-length of the panel and of the yield stress in compression, when their collapse criterion is just satisfied. It would be equivalent to the value of ψ at the mid-length section at collapse. They proposed that this efficiency could be approximated by multiplying the elastic shear lag effective width ratio by the buckling effective width factor for the plate in axial compression†. This method will be discussed in more detail in Chapter 5, and it will be shown that it leads to a too conservative design.

The consideration of plasticity in the plane stress analysis of

* *see also section 1.3.*

† *these authors suggested Faulkner's* [25] *formula for its calculation.*

plate girders was the basis of a numerical study by Albrecht[26] using a finite element solution. Some results of this study concern the determination of the ultimate load capacity of simply supported box girders under mid-span point loading. Analysing these results Albrecht, and later Roik[27], recognised that plastic flow could produce redistribution of longitudinal stresses from the web to the flanges while increasing the shear forces on the web. As will be shown in Chapter 4 the web shear capacity places an upper limit on the flange efficiency (measured by ψ) which, in a plane-stress context, can be expressed in terms of the b/ℓ parameter. These authors, however, did not recognise that theoretically, their results should be related to this upper bound expression. Their conclusions, therefore, were simply statements of the influence of shear stresses on the reduction of effective width ratios for cases with high b/ℓ values. Albrecht's results will be discussed in more detail in section 4.3 since they also provide numerical confirmation of the flange failure modes identified in this thesis.

It is interesting to note that Roik's[27] and Maquoi and Massonnet's[22] papers were presented at the same conference in 1976, both dealing separately with the two non-linear effects (material and geometric non-linearities) that must be considered in the study of the influence of shear lag on flange collapse. These theoretical investigations had been stimulated by experimental work which had started years before at Imperial College.

Results of this programme of tests related to the shear lag problem were presented at the same conference by Dowling, Moolani and Frieze[28]. The tests were conducted on three pairs of large scale box girder models. They will be designated by Models 1 and 2, 3 and 4,

9 and 10, retaining the notation used in the original paper since these tests have been reported elsewhere[29-32]. The two models of each pair had the same cross-sectional dimensions (see Table 6.1) and material properties. The first model of each pair was tested as a simply supported beam under central point load (Fig. 6.1). The second models were tested under two point loading to produce pure moment over the central region so that the flanges in this area could be assumed to be under uniform axial stress. The effects of shear lag in the first models were then studied by comparison of results with the other model in the pair. The elastic behaviour of Models 1, 3 and 9 provided a good confirmation of the shear lag effects predicted by the elastic finite element approach reported in reference (13). Comparison of ultimate moment results led the authors to conclude that in the first two models the presence of shear lag in the flanges had no significant weakening effect on the strength of the girder.

Model 9 was designed with a higher b/ℓ ratio (Table 6.1) to exaggerate the shear lag effects. Redistribution of stresses in the compression flange was also identified. Plate buckles developed first in the edge panels while the central bay deflected inwards. The formation of these buckles progressed across the mid-span cross section towards the longitudinal central line. Unfortunately, partly due to different initially deflected shapes, the compression flanges of Models 9 and 10 failed in different modes; the central bay of Model 9 failed by plate compression, while that of Model 10 failed by stiffener outstand compression. The quantification of the shear lag effects in the collapse of Model 9 was thus more difficult.

Observation of the behaviour of this model showed that the

strain in the plate approximately followed the elastically predicted

shear lag distribution almost up to the ultimate load. The ratio of

strains corresponding to $\sigma_{max}/\sigma_{min}$ (see Fig. 1.1) was maintained at

all cross sections and for this model was approximately 3 at the mid-

span. This was certainly also verified in the tests on Models 1 and 3

where this ratio was approximately 2.

The authors concluded that for full redistribution to be possible,

the stiffener/plate combination near the edges would have to sustain

without significant unloading* a level of compression straining predic-

table by multiplying the strain needed to cause plate panel collapse by

the elastic ratio of $\sigma_{max}/\sigma_{min}$. On Model 9 this redistribution was

accompanied by local plate buckling, thus causing permanent deformations

before ultimate capacity was reached. Serviceability considerations

led Dowling et al.((28) and discussion to reference(14)) to propose for

design an arbitrary limit of 2 on the ratio of $\sigma_{max}/\sigma_{min}$, with correspond-

ing restrictions on the slenderness of the plate and stiffener outstands.

Although no point-loaded model failed by stiffener compression,

an attempt was made to extend to these cases the conditions for full

redistribution. According to the suggested conditions, the stiffener

outstands and the plate panels should be capable of being strained to 2.5

times and 4.0 times the yield strain respectively, without significant

unloading. The authors[28] further concluded that these restrictions

can be satisfied by flats with a d_s/t_s ratio of $0.4\sqrt{E/\sigma_{os}}$ and plate

panels with maximum slenderness of $2.77\sqrt{E/\sigma_{op}}$.

These proposals although based only on a small number of experi-

* for design recommendations "significant unloading" was defined as a
fall-off in load carrying capacity greater than 10 per cent of the
maximum load.

ments were included in the Draft of the British Bridge Code[16] since they correspond to an improved approach in comparison with the earlier Merrison Rules' criteria for redistribution. They are still restricted to placing a limitation on plate geometries for which full redistribution may be assumed. Outside these limits a greater knowledge of the mechanism of redistribution would be needed to specify the reduction of collapse effective widths due to shear lag effects.

To validate the possibility of extending the proposals to cases of failure by stiffener compression another box girder (Model 12) was purposely designed to induce this mechanism of failure in a point-loading test. To achieve this, slender stiffeners were used and an outwards initial distortion (away from the stiffener outstands) was imposed on the central panel (Fig. 6.7). The same shear lag characteristics of Model 9 were retained, namely the b/ℓ flange aspect ratio and stiffening factor α (see Table 6.2). The tests on this model were carried out before the Steel Plated Structures Conference, 1976, but were not reported in reference (28).

In 1976, the author joined the Imperial College team working on this project and played a major role in the calibration, instrumentation and testing of Model 12. The behaviour of this model will therefore be described in more detail in Chapter 6. The observed collapse mode was initiated by torsional buckling of the central panel stiffeners situated at a quarter width of each side of the longitudinal central line. Local tripping failure of these stiffeners at mid-span was noticed prior to the maximum load being attained.

This very interesting phenomenon was somewhat unexpected. In Model 10*, although the stiffeners were more stocky, the general mode of

* loaded to produce pure bending over the central span such that the flange could be assumed to be under uniform axial compression.

failure also corresponded to stiffener compression and lateral deflections were observed at the mid-span in all the stiffeners. The higher straining of the quarter width stiffener outstands in Model 12 thus had to be attributed to some interaction of shear lag effects with this mode of failure. An analytical explanation of this phenomonon is presented in this thesis. After testing Model 12, the experimental evidence relating to the interaction of flange mechanisms at failure in a shear lag environment indicated that a fundamental investigation of the problem was needed. This was the theme suggested for the research project reported in this thesis.

To the author's knowledge only two works on the subject have, however, been presented since then. Carlsen, Søreide and Nordsve[33] using a finite element program for large deflection elastic-plastic analysis of plates, examined the problem of the ultimate load of a stiffened compression flange. However, plate panel buckling was only approximately considered. To simulate the shear lag type of loading an axial end shortening was applied to isolated simply supported flange panels in accordance with the elastic shear lag strain distribution. This was based on the experimental observations by Dowling et al.[28], that is, the strain distributions follow the elastic pattern almost up to collapse. The type of loading and the approximations considered were too speculative for their conclusions regarding redistribution to influence the understanding of the failure mechanisms. Crisfield[34], also using a finite element approach, analysed the inelastic behaviour of a single box girder under point load at mid-span. The compression flange was divided into three equal panels by two longitudinal stiffeners. This study was presented in a discussion to reference (33) and the plate characteristics

were chosen to induce local panel buckling. However, the overall

dimensions, namely the b/ℓ flange ratio of 1 to 3, were not chosen to

enhance shear lag effects. Considerable redistribution was achieved

as should be the case for girders with such dimensions according to the

results presented in this thesis.

1.2 SCOPE OF THE THESIS

The results of the research reported in this thesis are organized

in three main chapters. Firstly, the basic modes of failure of a com-

pression flange under a shear lag type of loading are discussed.

Secondly, the interaction between the mode of failure directly

associated with shear lag effects and the failure by inelastic buckling

in compression is investigated. This initially involved a parameteric

study of unstiffened flanges concentrated on the effects of the main

parameter influencing shear lag, the flange aspect ratio b/ℓ, and the

main parameter influencing buckling, the plate slenderness b/t. The

effects of initial imperfections and material properties were also studied.

The conslusions drawn from this parametric study were tested on stiffened

flange cases where overall collapse in plate compression was the governing

buckling mode. The results presented were chosen to illustrate the main

differences associated with orthotropy of form in the context of shear

lag/buckling interaction. Only compression flanges divided into three

panels by two longitudinal stiffeners were used in this study. The problems

associated with panel buckling in stiffened flanges were examined in the

same context but were not treated in detail.

Finally, an attempt to correlate the general conclusions of the

parametric study with the experimental information available from the box

girder models tested at Imperial College is presented.

A computer program purposely developed to analyse a complete model of a simply supported box girder plate assemblage was used in all these studies. Limitations in the formulation of the stiffener-plate interaction restricted the analysis of stiffened compression flanges to only a few cases where panel buckling occurs. The program was also used in an attempt to numerically explain the failure of Model 12 (introduced in Section 1.1) by stiffener torsional buckling.

1.2.1   Analytical Model

The computer program used throughout this thesis is based on an analytical modelling of a box girder plate assemblage where the most severe shear lag effects can be reproduced (i.e. by point loading). This required a careful modelling of the web-flange connections. The compression flange was assumed to be free from rotational restraint from the webs in order to simulate an independence from web buckling. Consequently out-of-plane bending effects on the webs and·tension flange behaviour were eliminated. This allows a considerable numerical economy. Plasticity effects were considered in all the plates and thè modelling of large deflections on the compression flange behaviour followed recent numerical analysis of isolated plates[35][36].

Unstiffened and eccentrically stiffened compression flanges were considered. The discrete character of the stiffener action in vertical bending was taken into account (torsion and lateral bending were neglected).

The box girder model, Fig. 1.3,was considered simply supported and loaded under point load, generally at the mid-span, by applying over the web depth either uniformly distributed displacements or shear stresses. As an alternative a uniformly distributed load over the webs
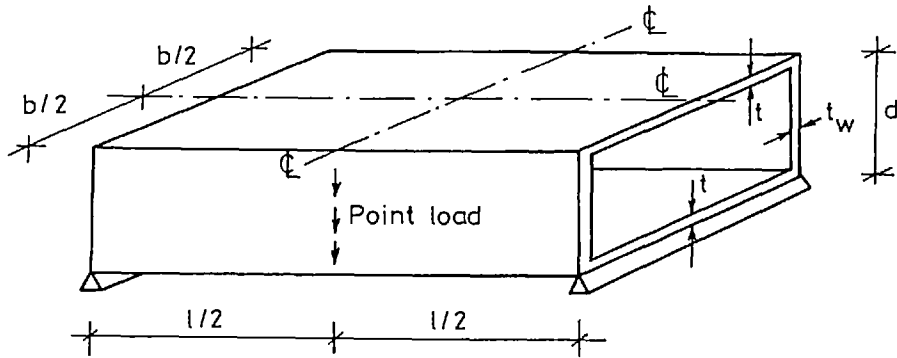
Fig. 1.3   Box girder model
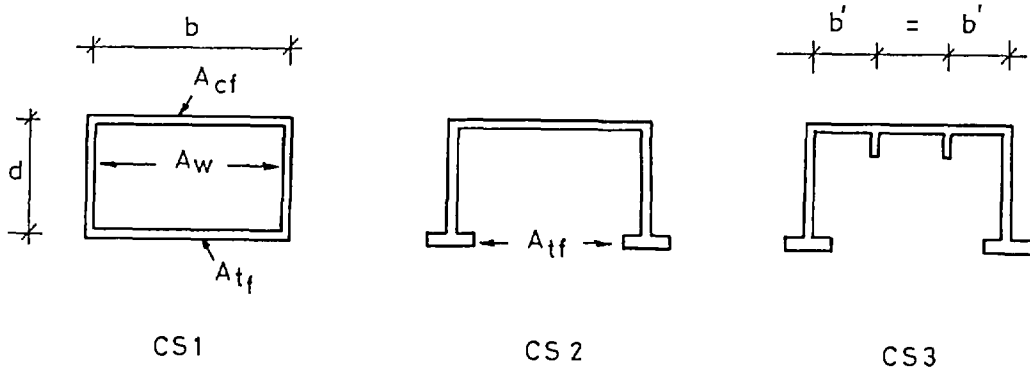
Fig. 1.4   Closed and open types of cross sections

was also allowed for in the program, but this type of load was not considered in the thesis. Closed and open types of cross sections were studied (Fig. 1.4).

A computer program based on this model was written in Fortran IV. Its results were calibrated against other numerical techniques since no accurate experimental data was available for this purpose.

1.2.2   Design of a Flange Testing Rig

It was for the reason mentioned above that a programme of experimental tests was proposed for funding to the Department of Transport. The aim of this proposal was to provide experimental verification for the analytical approach which was being developed.

A rig was designed by the author in which it will be possible to test a series of small scale unstiffened and stiffened flange panels. The principal features of the rig are that:

1.   it can be re-used for several ultimate flange tests as the webs are constructed from very high yield steel;

2.   it will apply shear loading to the edge of the flange panels in a manner representative of that occurring in actual flanges;

3.   it will allow the flanges to pull in freely and rotate freely at their junctions with the webs;

4.   it will allow plates of various aspect ratios and slendernesses to be tested under the most severe shear lag loading condition, i.e. point loading.

Details of the rig are shown in Appendix II. Its manufacture required highly skilled workmanship under close supervision. For this reason the work was carried out in the Imperial College Civil Engineering workshops and supervised by the author. It is now near completion.

1.3   SOME DEFINITIONS AND NOTES ON PRESENTATION

The net compression or tension force at a flange cross section can be measured at any stage of loading by the inelastic effective width ratio ψ defined for unstiffened flanges in expression (1.3). The ultimate capacity of a flange of a simply supported girder under point load at mid-span will then be given by the maximum value of ψ at that cross section (ψ_{max}).

The definition (1.3) of ψ is also valid for stiffened flanges if σ_{av} is taken as the average longitudinal stress over the plate and the stiffener cross sections and by defining a flange *equivalent yield stress* to allow for different materials in the plate and the stiffeners. For the compression flange these quantities are defined as follows

$$\sigma_{av} = \left(\int \sigma_y \, dA\right)/A_{cf} \qquad\qquad 1.4$$

$$\sigma_{ocf} = (\sigma_{op}A_p + \sigma_{os}A_s)/A_{cf} \qquad\qquad 1.5$$

where σ_{op} and σ_{os} are the yield stresses of the plate and the stiffener materials respectively (for the other symbols see the Notation).

The geometric stiffening factor α defined as

$$\alpha = A_s/A_p \qquad\qquad 1.6$$

expresses the distribution of the total cross-sectional area of the flange (A_{cf}) between the plate and the stiffeners

$$A_p = \frac{1}{1+\alpha} A_{cf} \qquad\qquad 1.7$$

$$A_s = \frac{\alpha}{1+\alpha} A_{cf} \qquad\qquad 1.8$$

The definition of α can also be extended to account for different material

properties by introducing an *equivalent stiffening factor* defined as

$$\alpha' = \alpha \, \sigma_{os}/\sigma_{op} \qquad\qquad 1.9$$

This enables the distribution of the flange squash load between the plate and the stiffeners to be expressed as

$$\sigma_{op}A_p = \frac{1}{1+\alpha'} \, (\sigma_{ocf}A_{cf}) \qquad\qquad 1.10$$

$$\sigma_{os}A_s = \frac{\alpha'}{1+\alpha'} \, (\sigma_{ocf}A_{cf}) \qquad\qquad 1.11$$

These expressions will be used in Chapter 4.

The behaviour of the flanges under loading will be described in all the figures by the variation of ψ in relation to the mean longitudinal strain ε_m along the web-flange connection (non dimensionalised by dividing it by the yield strain value). This provides a convenient coordinate system for comparisons with results of isolated plate behaviour in displacement controlled axial compression (or tension).

The criteria for choosing dimensions and material properties described in section 5.2 were followed, unless specified otherwise, in all examples.

CHAPTER   2

THEORETICAL MODEL

2.1   CHOICE OF THEORETICAL MODEL

To accurately reproduce the edge stresses associated with shear lag effects on a compression flange it was necessary to model a complete unit of a box girder. Considerable attention was needed to ensure that the web-flange interaction was reproduced correctly. Special care was taken to represent a point load so that the severe shear lag effects that occur under localised loading could be obtained.

Extensive information was available from a series of tests on large scale box girders[32] and from numerical parametric studies of elastic shear lag effects[13] conducted at Imperial College. This enabled appropriate support and loading conditions to be chosen and simplifications in the analytical model to be made. . Most of these relate to boundary conditions. For example, the idea of separating flange behaviour from possible complication by web buckling by assuming no rotational compatibility at the common edge arose from a study of earlier work.

This boundary condition was only included, however, after considering the possibility of mechanically reproducing it in a test rig. Such a rig* has been designed by the author, and is being constructed to provide controlled experimental data to further validate the theoretical research contained within this thesis.

To   interpret   the shear lag effects on the flanges it was

* see Appendix II

necessary to compare them with results for similar plates loaded in axial compression. Isolated plates could have been analysed using available programs[32][36] but, instead, it was found convenient to organize the present program to consider the compression flange separately. The appropriate boundary conditions are described in section 2.5.5.

To model the behaviour of the compression flange the von Karman large deflection equations, as modified by Marguerre[37], to incorporate the effects of initial distortions, were used. The decision to isolate the compression flange from the effects of web buckling led to the assumption that the web and tension flange could be described by plane stress equations thus considerably simplifying the numerical solution.

For the parametric study a further simplification was introduced by considering the compression flange as part of an open box, as represented in Fig. 1.4 by cross-sections CS2 and CS3. This simplification was justified by experimenting numerically with both models as described later.

The investigation of shear lag/buckling interaction was first conducted on unstiffened flanges, but the action of stiffeners was later considered mainly to study the differences associated with orthotropy of form. The derivation of the plate-stiffener interaction presented in this chapter can be considered as a simplified and refined reformulation of the ideas contained in a paper by Basu, Djahani and Dowling[38] for studying discretely stiffened plates. The stiffener actions on the plate are derived as line loads in terms of plate deformations and adapted to be used with finite differences and dynamic relaxation in the

method of solution.   This problem illustrates how this numerical tech-
nique can be conveniently extended to consider structural discontinuities.

The material behaviour was assumed to be elastic-perfectly plastic
yielding according to the von Mises yield criterion.

Two different options were available to deal with plasticity in
the compression flange: the multi-layer method and the single-layer approach.
Both methods were applied successfully to similar plate analysis (using
finite differences and dynamic relaxation) by Harding[35] and Frieze[36],
respectively.

The multi-layer approach, extensively used in finite-element
analysis[39][40], consists of dividing the plate thickness into layers,
the yield of each being determined by the von Mises yield criterion.
After a load increment, stress-strain relationships can be determined at
each layer using a Prandtl-Reuss flow rule.   These are integrated through
the thickness to obtain plate rigidities for use in terms of stress and
strain resultants for the next increment of loading.

The single-layer, or 'area' approach, uses a function of the six
stress resultants and an associated flow rule to assess yield over the
whole thickness and to directly calculate tangential rigidities.
Ilyushin's general yield surface derived for shells from the von Mises
criterion has been the basis of approximate yield functions used with this
method.   The method assumes that the plate at a point is either elastic
or at yield over the whole thickness.   The intermediate elastic-plastic
states and the continuous loss of stiffness from the onset of surface
yielding, in a combination of in-plane and bending strains,are thus neglec-
ted.   The unloading from a previous plastic state is also assumed to be

a sudden full-thickness elastic process.

These are considerable disadvantages in comparison with the multi-layer method which, if used with a sufficient number of layers, is capable of modelling the real behaviour as closely as the theoretical yield assumptions allow. The multi-layer method, however, requires considerably more computer storage. This was the main reason for utilising the single-layer approach in the present research.

Theoretically this method should overestimate the ultimate capacity of plates but results obtained for plates in axial compression using the two methods compare satisfactorily (see Fig. 3.18, section 3.5.5). This is perhaps due to the fact that although the single-layer approach delays the detection of plasticity, in predominantly in-plane loading cases the differences should not be very significant. It is also possible that during the loading history a delayed yielding of some points can be compensated by simultaneous elastic (therefore more sudden than in reality) unloading of other points previously at yield.

Crisfield[41] and Frieze[42] have documented the use of the single layer approach in plate analysis but both authors employ the same approximation to Ilyushin's yield surface. In the present research another more rigorous expression is also used and both are compared for some cases. A detailed description of the method is presented in section 2.4 to allow comments to be made on its limitations.

Despite the inability to reproduce the transition between fully elastic and plastic states, the concept of using a yield surface expressed in stress resultants is of such appeal in its simplicity, when compared with the multi-layer method, that it suggests that more research should
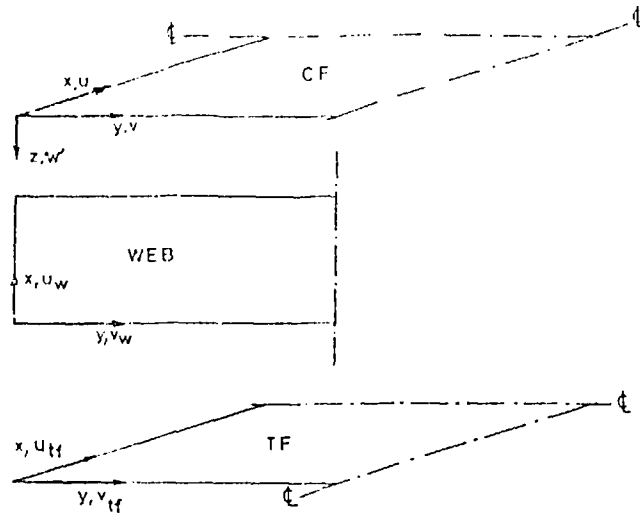
Fig 2·1   Coordinate systems of axes
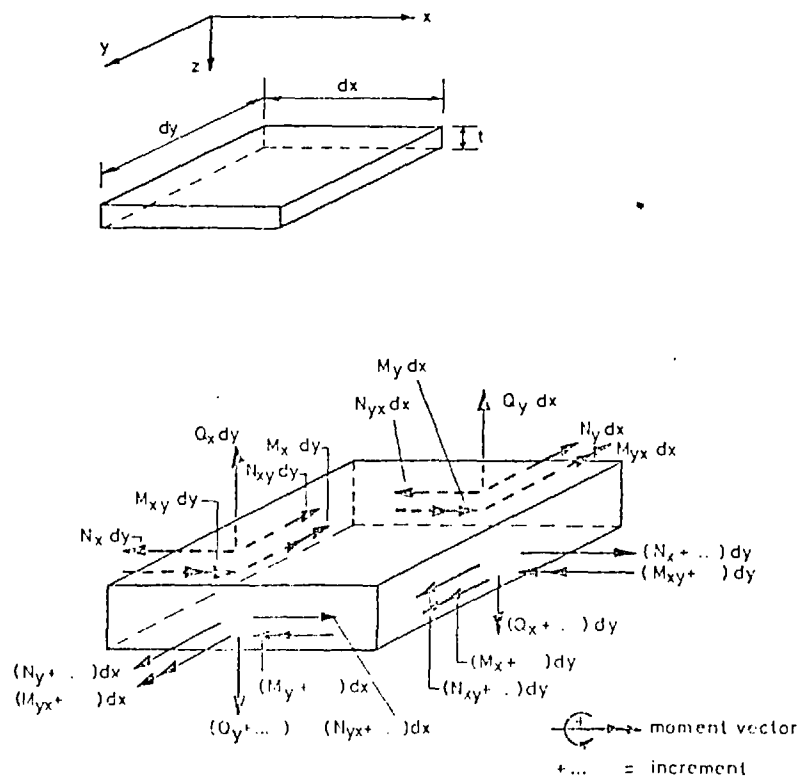
Fig 2·2   Plate element showing positive
directions of stress resultants

be directed to combining the advantages of the two methods. Crisfield[43] has already attempted this by using a pseudo hardening parameter to describe that transition, chosen as an acumulated equivalent plastic curvature. In this way he is able to bring the ultimate capacity of plates in axial compression closer to the multi-layer values. In so far as post-collapse unloading is concerned, however, the stress-strain relations inexplicably diverge. This discrepancy may be either due to the inaccuracy of the approximate yield surface used or to the choice of the transitional parameter but the idea is certainly promising. In the present research the use of a more accurate yield function did not present any problems and it is therefore intended to experiment with it in a similar form in future work.

2.2   PLATE EQUATIONS

The coordinate systems of axes used for each plate are indicated in Fig. 2.1 .

Only the governing equations for the compression flange are presented. The plane stress equations can easily be obtained by omitting the terms involving bending or out-of-plane quantities in the relevant equations. The expressions for the strain resultants in terms of midplane displacements and the equilibrium equations of an element of plate (Fig. 2.2) are independent of material properties and can be summarised as follows:

in-plane strains

$$\varepsilon_x = \partial u/\partial x + \tfrac{1}{2}(\partial w/\partial x)^2 + (\partial w/\partial x)(\partial w_o/\partial x)$$

$$\varepsilon_y = \partial v/\partial y + \tfrac{1}{2}(\partial w/\partial y)^2 + (\partial w/\partial y)(\partial w_o/\partial y)$$

$$\varepsilon_{xy} = \partial u/\partial y + \partial v/\partial x + (\partial w/\partial x)(\partial w/\partial y) +$$
$$+ (\partial w/\partial x)(\partial w_o/\partial y) + (\partial w/\partial y)(\partial w_o/\partial x) \qquad 2.1$$

curvatures $\qquad \chi_x = -\partial^2 w/\partial x^2$

$$\chi_y = -\partial^2 w/\partial y^2$$

$$\chi_{xy} = -\partial^2 w/\partial x \partial y \qquad\qquad 2.2$$

equilibrium in

x direction: $\partial N_x/\partial x + \partial N_{xy}/\partial y = 0$

" y " : $\partial N_y/\partial y + \partial N_{xy}/\partial x = 0$

" z " : $\partial^2 M_x/\partial x^2 + 2(\partial^2 M_{xy}/\partial x \partial y) + \partial^2 M_y/\partial y^2 +$

$$+ N_x(\partial^2(w + w_o)/\partial x^2) + 2N_{xy}(\partial^2(w + w_o)/\partial x \partial y) +$$

$$+ N_y(\partial^2(w + w_o)/\partial y^2) = 0 \qquad\qquad 2.3$$

The sign convention for the stress resultants is indicated in Fig. 2.2 where positive stresses are represented acting on the plate element. In the present study no external lateral loading acting on the plate was considered.

For elastic-plastic treatment of the step-by-step loading, finite incremental strain-displacement relationships can be obtained from expressions (2.2) by simply subtracting from the current values those calculated in the previous load increment. For example, the expression for the increment of the first strain component is:

$$\Delta\varepsilon_x = \partial u/\partial x - \partial u_p/\partial x + \tfrac{1}{2}(\partial w/\partial x - \partial w_p/\partial x)((\partial w/\partial x + \partial w_p/\partial x) +$$

$$+ 2(\partial w_o/\partial x)) \qquad\qquad 2.4$$

where subscript p designates previous values.

The strain increments are designated for convenience of presentation, as components of a strain increment (6×1) column vector $\Delta\varepsilon$. Corresponding increments of stress resultants (ΔN) can be added to the previous stresses to obtain the current total stresses involved in the

equilibrium equations (2.3). Using matrix form, the column vector of current total stress, N, is therefore calculated as follows

$$N = \Delta N + N_p \qquad\qquad 2.5$$

The stress-strain relations can be expressed in linear incremental form, for generality, as follows:

$$\Delta N = C \, \Delta\epsilon \qquad\qquad 2.6$$

C being a (6×6) symmetric matrix of coefficients representing instantaneous or tangential rigidities. For elastic loading and unloading this matrix reduces to the usual set of plate elastic rigidites:

$$
C^e = \begin{bmatrix}
C_x & C_1 & 0 & & & \\
C_1 & C_y & 0 & & 0 & \\
0 & 0 & C_{xy} & & & \\
\hline
& & & D_x & D_1 & 0 \\
& 0 & & D_1 & D_y & 0 \\
& & & 0 & 0 & D_{xy}
\end{bmatrix} \qquad\qquad 2.7
$$

For an isotropic plate:

$$C_x = C_y = C_1/\nu = C = Et/(1 - \nu^2)$$

$$C_{xy} = C(1 - \nu)/2 = Et/2(1 + \nu)$$

and

$$D_x = D_y = D_1/\nu = D = Et^3/12(1 - \nu^2)$$

$$D_{xy} = D(1 - \nu) = Et^3/12(1 + \nu)$$

$$\qquad\qquad 2.8$$

The calculation of C depends on the yield assumptions and the description of the elastic-plastic behaviour. The method followed in this study is discussed in section 2.4.3.

2.3   STIFFENED FLANGES

Only stiffeners with thin rectangular cross sections were considered. As referred to before the main purpose of analysing stiffened plates was to investigate the effects of orthotropy of form in the context of shear lag/buckling interaction. Consequently, all the flanges studied had only a few stiffeners and most were simply divided into three panels by two longitudinal stiffeners. For these cases neglecting the torsional rigidity of the stiffener was compatible with the assumption, used throughout this study, of flange edges being free from bending restraints from the webs. The effects of the small torsional rigidity of these thin stiffeners would in any case be difficult to consider in an elastic-plastic treatment and would unnecessarily complicate the program.

These effects were disregarded by assuming that the stiffeners behave as beams connected to the bottom face of the flange by a fictitious "door hinge" imposing compatible axial straining and vertical rotations. Similarly, the resistance to lateral bending of the stiffeners in the x-direction, following the u displacements of the plate, was neglected. The cross sections of these beams can then be assumed to remain plane for vertical bending and axial straining.

Using the above assumptions, the longitudinal strain in the stiffener at a distance z from the mid-plane of the plate can be obtained from the Marguerre equation for the corresponding strain in a plate layer at that depth as:

$$\varepsilon_z = \partial v/\partial y + \tfrac{1}{2}(\partial w/\partial y)^2 + (\partial w/\partial y)(\partial w_o/\partial y) - z\partial^2 w/\partial y^2 \qquad 2.9$$

The corresponding stresses can be calculated using a simple elastic perfectly plastic stress-strain relation in the following way:
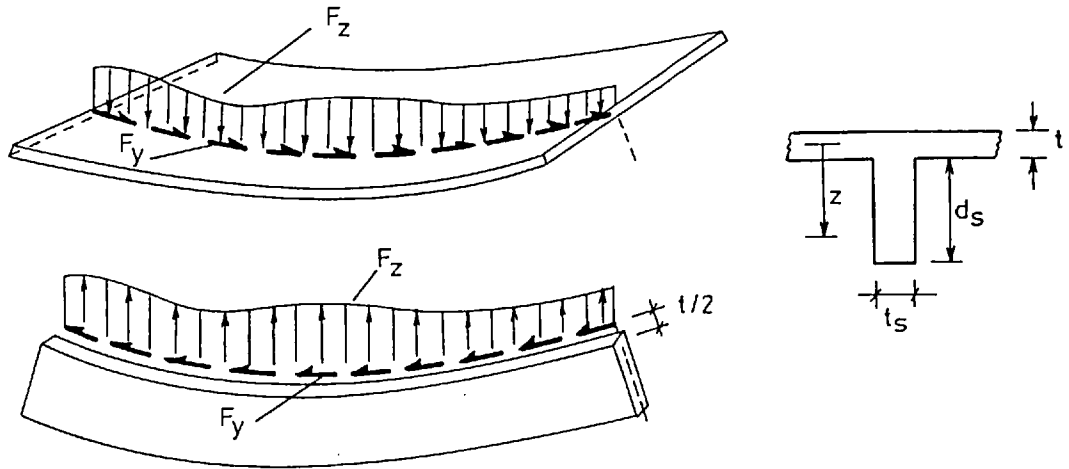
(a) interaction line forces
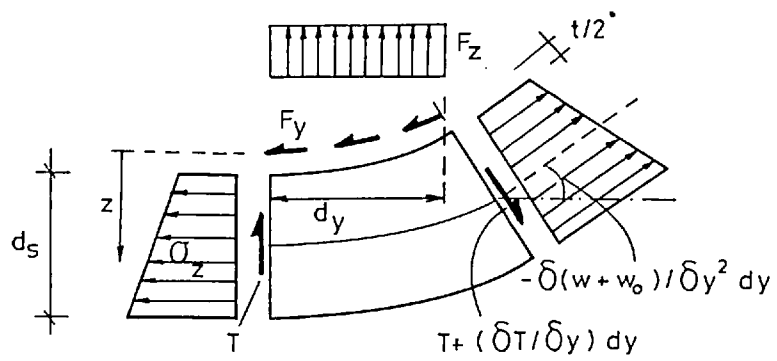
(b) actions on deformed element of stiffener

Fig. 2.3   Stiffener-plate interaction forces

$$\sigma_z = E\epsilon_z \quad \text{if} \quad |\epsilon_z| < \epsilon_o$$

or

$$\sigma_z = \pm\sigma_o \quad \text{if} \quad |\epsilon_z| \geq \epsilon_o$$

2.10

The interaction of stiffener and plate can be treated by considering longitudinal and vertical line loads acting along the connection at the plate *mid-plane level* as indicated in Fig. 2.3a where the forces per unit length are denoted by F_y and F_z.

The equilibrium equations for an element of stiffener, as represented in Fig. 2.3b, if referred to the system of axes centred at the mid-plane level, provide expressions for these forces. For that purpose the axial force N_s at the stiffener cross section and the moment M_s of the stresses σ_z in relation to an axis parallel to the x direction and centred at mid-plane level :

$$N_s = t_s \int_{t/2}^{t/2 + d_s} \sigma_z dz \qquad 2.11$$

$$M_s = t_s \int_{t/2}^{t/2 + d_s} \sigma_z z dz \qquad 2.12$$

Equilibrium of forces along y gives:

$$F_y = \partial N_s / \partial y \qquad 2.13$$

and along z gives

$$N_s (\partial^2 (w + w_o) / \partial y^2) dy + (\partial T / \partial y) dy - F_z dy = 0 \qquad 2.14$$

Moments about the axis/provide a beam equilibrium equation between T parallel to the x direction and M_s:

$$T = \partial M_s / \partial y \qquad 2.15$$

By substitution the following expression is obtained:

$$F_z = \partial^2 M_s / \partial y^2 + N_s (\partial^2 (w + w_o) / \partial y^2)$$
          2.16

This derivation of the plate-stiffener interaction forces can be considered as a simplified version of the elastic approach[38] which considers the torsion and lateral bending of the stiffener and consequently involves the derivation of two extra corresponding line loads.   In this approach it was assumed that the stiffener cross sections do not distort and remain plane and normal to the plate mid-surface along the line of intersection.   Shear strains in the stiffener were also neglected. This elastic formulation was extended by Djahani[44] for the elastic-plastic analysis of stiffened plates, assuming that the stiffener elastic torsional rigidity (warping rigidity was not included) applies throughout the loading history.   This should overestimate somewhat the torsional stiffness in the plastic range.   To consider the complexity of a full solution of the coupled compression-bending-twisting problem would seem, however, unjustified in the presence of other simplifications that have to be introduced, namely, stiffener local buckling effects.   This was also the view of other authors who dealt with similar stiffeners in plate analysis[45].

In comparison, the present simplified model should, therefore, lead to a lower bound to Djahani's results for the plate ultimate capacity. On the other hand, it must be emphasised again that, in all the flanges to which the present analytical model was applied, the torsion of the stiffeners was not expected to have a significant effect.   Some assessment of the importance of the neglected effects will be made during the discussion to the calibration of the numerical program.

The presence of the line interaction forces F_y and F_z, implies
a discontinuous distribution of the in-plane and transverse shear forces
on the plate across the stiffener line. Theoretically, this would
require the flange to be subdivided into panel strips between stiffeners,
with longitudinal common edges on which these line actions would be
included as boundary conditions. However, in the solution described
later, a discretization based on finite difference technique allows the
derivation of special equilibrium equations for nodes on the stiffener
lines, to approximate this discontinuity problem.

When more interaction components are considered other discon-
tinuities in the corresponding stress resultants should be taken into
account. Basu, Djahani and Dowling[38] in their approach, however,
derived equilibrium equations for plate elements over stiffener lines by
considering these line forces distributed over a finite plate width.
The method of solution of references(38) and (44) subsequently uses an
intermediate differential formulation of those equations in terms of dis-
placements which are, in the author's opinion, somewhat misleading regard-
ing the problem of boundary conditions. It could be argued that as
finite difference forms are in any case used for calculating the deriva-
tives there is an implicit 'smearing' of the line forces and consequently
of the discontinuities. However, ignoring these discontinuities, the
equilibrium equations involve an order of derivatives for which there are
then, apparently, insufficient boundary conditions. The problem of the
boundary conditions at the end cross section of the stiffened flange is
discussed in section 2.5.2.

2.4   PLASTICITY

This section deals with the method adopted to describe the elastic-plastic range of the compression flange behaviour.

The elastic-plastic behaviour of the webs and tension flange can again be considered a particular case of the general formulation by reducing the general yield function to the terms involving only in-plane stress resultants.   All the other expressions in section 2.4.3 remain valid.

2.4.1   Ilyushin's Yield Criterion

In the context of a deformation theory, Ilyushin[46] studied, with the usual thin shell assumptions, the problem of elastic-plastic material behaviour in shells of arbitrary geometry.   Neglecting the influence of transverse shear stresses in the yield condition he demonstrated, apparently for the first time, that a finite relationship between the six stress resultants* exists when all layers over the shell thickness are sufficiently strained to have yielded according to von Mises criterion.   This can be considered as a full-depth yield condition. As pointed out by Crisfield[43] this would presuppose that in cases where membrane action is not predominant, unrealistic large curvatures would be required before yield could be established by such a criterion, though similar limitations are common to most yield criteria used in limit analysis.

The relationship was formulated in parametric form choosing, for convenience of the various integrations involved in the calculation of

* components of the vector $\underset{\sim}{N}$ in expression (2.5).

the stress resultants, two parameters, λ and μ. These are defined as ratios of equivalent strains* at three different depths over the normal to the mid-surface:

$$\lambda = e_2/e_1 \qquad \mu = e_o/e_1 \qquad\qquad 2.17$$

Subscripts 1 and 2 respectively indicate the negative and positive faces of the shell and e_o is the minimum value of the equivalent strain distribution. In some cases this minimum corresponds to a layer within the shell thickness (referred to by Ilyushin as bending-dominant cases) and for others to a fictitious depth outside the shell (in-plane dominant). The physical interpretation of these parameters is, however, not important to the study of the yield condition and it is only sufficient to point out that by definition they verify the inequalities:

$$0 \leqslant \mu \leqslant \lambda \qquad\qquad 2.18$$
$$\mu \leqslant 1$$

The original Ilyushin yield condition was derived by expressing in terms of λ and μ the following three non-dimensional quadratic forms of the stress resultants:

$$Q_t = (N_x^2 - N_x N_y + N_y^2 + 3N_{xy}^2)/N_o^2$$

$$Q_m = (M_x^2 - M_x M_y + M_y^2 + 3M_{xy}^2)/M_o^2 \qquad 2.19$$

$$Q_{tm} = (N_x M_x - \tfrac{1}{2} N_x M_y - \tfrac{1}{2} N_y M_x + N_y M_y + 3N_{xy} M_{xy})/N_o M_o$$

where $N_o = \sigma_o t$ and $M_o = \sigma_o t^2/4$.

*equivalent strain: $e = \dfrac{2}{\sqrt{3}} \sqrt{\varepsilon_x^2 + \varepsilon_x \varepsilon_y + \varepsilon_y^2 + \tfrac{1}{4}\varepsilon_{xy}^2}$
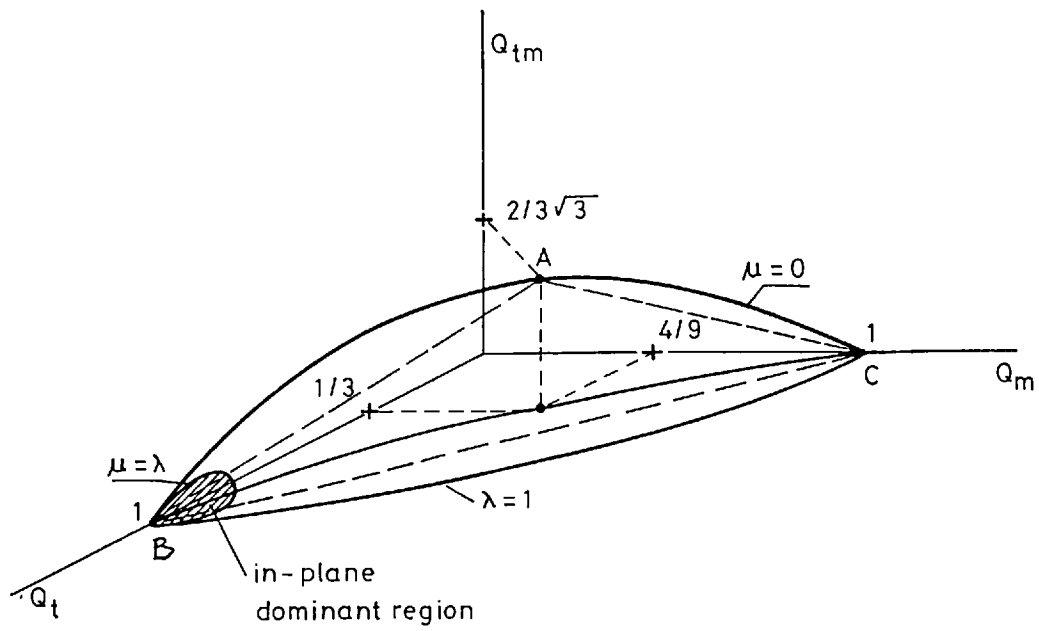
a) Sketch of the positive half of the surface
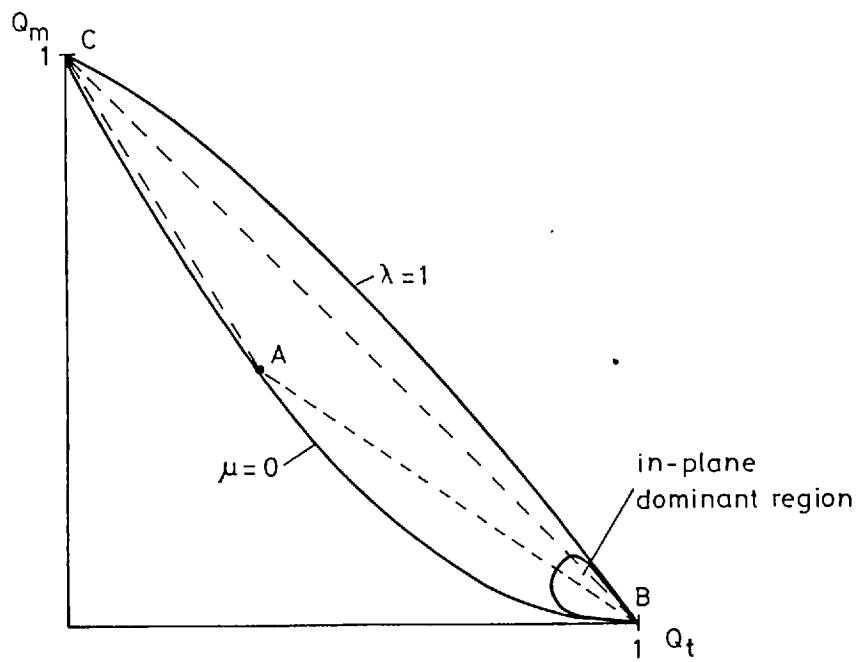
b) Projection of the surface on the $Q_{tm} = 0$ plane

Fig 2·4   Ilyushin's yield surface

Using Ilyushin's notation the parametric expressions are:

$$Q_t = \frac{1}{\Delta_1^2} (\mu^2\Psi^2 + \Phi^2)$$

$$Q_m = \frac{4}{\Delta_1^4} (\mu^2(\mu^2 + \Delta^2)\Psi^2 + (4\mu^2 + \Delta^2)\Phi^2 +$$
$$+ 2\mu^2\Delta\Phi\Psi - 2\mu^2\Psi\chi + 2\Delta\Phi\chi + \chi^2)$$

$$Q_{tm} = \frac{2}{\Delta_1^3} (\mu^2\Delta\Psi^2 + \Delta\Phi^2 + \mu^2\Phi\Psi + \Phi\chi)$$

2.20

where

$$\Delta_1 = \left| \sqrt{1 - \mu^2} \pm \sqrt{\lambda^2 - \mu^2} \right|$$

$$\Delta = (1 - \lambda^2)/\Delta_1$$

$$\Phi = \lambda - 1$$

$$\Psi = \left| \ln \frac{1 + \sqrt{1-\mu^2}}{\mu} \pm \ln \frac{\lambda + \sqrt{\lambda^2-\mu^2}}{\mu} \right|$$

$$\chi = \left| \sqrt{1 - \mu^2} \pm \lambda\sqrt{\lambda^2 - \mu^2} \right|$$

These auxiliary variables are calculated using the positive sign for bending dominant situations and the negative sign for in-plane dominant cases.

Expressions (2.20) represent in the space of the variables Q_t, Q_m and Q_{tm} a surface which is, consequently, a three-dimensional image of a yield surface in the space of the six stress resultants.

Ilyushin studied some properties of this continuous and convex surface in the Q_t, Q_m and Q_{tm} space. As Q_t and Q_m are non-negative forms, all the surface is situated in the first quadrant of the coordinate system (Q_t, Q_m, Q_{tm}) and is symmetric* about $Q_{tm} = 0$, the positive

* values corresponding to $\lambda' = 1/\lambda$ and $\mu' = \mu/\lambda$ mirror those for λ and μ.

values corresponding to $\mu \geq 1$. Only half the surface needs to be examined and a sketch of its shape is given in Fig. 2.4a. Most of the surface corresponds to bending dominant situations and only a small portion, not touching the coordinate planes, to in-plane dominant ones. The two zones are separated by lines where $\mu = \lambda$.

Ilyushin also showed that the surface is limited by lines corresponding to $\mu = 0$ where

$$Q_m = (1 - Q_t)^2 \qquad\qquad 2.21a$$

and $\qquad |Q_{tm}| = (1 - Q_t)\sqrt{Q_t} \qquad\qquad 2.21b$

The maximum values of Q_{tm} are attained over these lines and the absolute maximum corresponds to a point A (Fig. 2.4) of coordinates ($Q_t = 1/3$; $Q_m = 4/9$; $Q_m = 2/3\sqrt{3}$). The projection in the plane $Q_{tm} = 0$ of $\mu = 0$ is represented in Fig. 2.4b, together with the intersection of the surface with this plane corresponding to $\lambda = 1$ and drawn using values given by Ilyushin.

2.4.2 Approximate Expressions for Ilyushin's Yield Surface

The parametric form (2.20) of the yield surface is not directly usable in practical problems where an explicit expression of the stress resultants is required. Several approximate expressions for the 'exact' surface have been proposed in Q_t, Q_m and Q_{tm} space. They have been reviewed by Robinson[47] in a comparative study of their relative accuracy.

Ilyushin[46] has pointed out that the straight line joining the points B and C, Fig. 2.4b, closely approximates the line $\lambda = 1$. He therefore suggested that a good linear approximation to the surface could be obtained by considering two planes passing by that straight line and

the points where Q_{tm} has relative maxima (point A in Fig. 2.4). Such planes are defined by

$$Q_t + Q_m + \frac{1}{\sqrt{3}} |Q_{tm}| = 1 \qquad\qquad 2.22$$

Robinson[47] has concluded that this approximation is the best of all the other linear proposals. It has been used with success in several research analyses of plates[41,42,44] and incorporated in the present computer program as an optional yield condition.

As the true surface is convex a considerable part of the linear approximation is contained within it. This therefore leads to a conservative or 'safe' estimation of yield. 'Unsafe' regions can however be found outside the lines AB and AC and the larger differences between the surface and the planes, measured along Q_{tm}, occur over the limiting line $\mu = 0$ as should also be expected from convexity. Using expressions (2.21) it is possible to calculate the coordinates $Q_t = 0.683$ and $Q_m = 0.100$, corresponding to the considerable maximum difference of 0.113.

Most of the 'unsafe' area lies near or on the in-plane dominant region, as can be seen from Fig. 2.4b. This contradicts the possibility of extending to all in-plane loading analyses of plates the general impression[48] that this approximation is conservative.

Results for plates in compression using this linear surface compare well with those obtained from a more rigorous approximation. This agreement could be explained perhaps by assuming that over the whole plate safer assessments of yield can be compensated by unsafe ones.

The approximate yield surface of expression (2.22) does not vary smoothly across the straight line $Q_t + Q_m = 1$ on the plane $Q_{tm} = 0$ and

this constitutes a major disadvantage for its use with an associated flow rule. To obviate this problem Crisfield[40] suggested that the normal to the surface over this line and at all points for which $|Q_{tm}| < 10^{-4}$ should be considered horizontal and directed perpendicularly to $Q_t + Q_m = 1$. This suggestion was followed in the present numerical analysis.

From the non-linear approximations available Robinson[47] quotes two proposed by Ivanov[49]:

$$Q_t + \tfrac{1}{2}Q_m + \sqrt{\tfrac{1}{4}Q_m^2 + Q_{tm}^2} = 1 \qquad\qquad 2.23$$

$$Q_t + \tfrac{1}{2}Q_m + \frac{\tfrac{1}{4}(Q_t Q_m - Q_{tm}^2)}{Q_t + 0.48Q_m} + \sqrt{\tfrac{1}{4}Q_m^2 + Q_{tm}^2} = 1 \qquad\qquad 2.24$$

and concludes that they represent a substantial improvement over the linear expression(2.22). Both coincide with Ilyushin's surface over the limit corresponding to $\mu = 0$ or $Q_m = (1 - Q_t)^2$, and the second is almost 'exact'. Robinson compared the accuracy of the various expressions based on calculated values of Q_t, Q_m and Q_{tm} using expressions(2.20)over a fine mesh of λ and μ values. Substitution in the first members of the various approximations produces results that are either greater than unity (the approximation being 'safe') or smaller ('unsafe'). From Robinson's results it is possible to conclude that:

$$0.935 \leqslant \exp.(2.22) \leqslant 1.133$$

$$1.000 \leqslant \exp.(2.23) \leqslant 1.096 \qquad\qquad 2.25$$

$$0.990 \leqslant \exp.(2.24) \leqslant 1.002$$

The improved accuracy of the second Ivanov approximation is obvious and it was therefore introduced as an option, mainly for checking the use of

expression (2.22),in the numerical program. Its analytical complexity did not present any problem in the numerical treatment but it was certainly the reason why Haydl and Sherbourne[50] preferred to use the first Ivanov approximation in the limit analysis of circular plates under lateral loading. The Ivanov surfaces have also the advantage of being smooth and differentiable throughout.

As the numerical solution considers both expressions (2.22) and (2.24) they will be designated for convenience as Iluyshin I and Ilyushin II respectively.

2.4.3   Expressions for Plate Tangential Rigidities

Using the assumptions of incremental plastic theory, Olszak and Sawczuk[51] showed that a yield surface for shells of "von Mises material" could also be derived in six-dimensional stress resultant space. The form of the surface would be similar to the one given earlier by Ilyushin based on deformation theory, thus clearing doubts about the possibility of using it in an incremental plastic analysis. From Drucker's postulation[52] as the Prandtl-Reuss flow law is valid for the material, a flow rule associated with that yield criterion can be accepted in generalised stress-strain rate space[53]. This conclusion had already been arrived at by Onat[54] for Ilyushin's surface.

For convenience the yield surface expressed in (2.20) will be represented by

$$f(N_i) \; = \; 0 \qquad\qquad i=1, \; \dots, 6 \qquad\qquad 2.26$$

where N_i are the stress components of vector $\underset{\sim}{N}$ defined in equation (2.5). The plastic potential flow rule is taken in the form

$$\Delta \varepsilon^P = \gamma f, \qquad\qquad \gamma \geqslant 0 \qquad\qquad 2.27$$

where $\Delta \varepsilon^P$ is the plastic component of the vector $\Delta \varepsilon$ of strain resultants; γ is the unknown flow parameter representing the magnitude of the strain rate $\Delta \varepsilon^P$; and $f,$ is a column vector of components $f,_i = \partial f / \partial N_i$ $(i = 1, \ldots, 6)$.

For perfectly plastic flow the stress increment vector ΔN must remain tangential to the yield surface or

$$f,^T \Delta N = 0 \qquad\qquad 2.28$$

Elastic incremental stress-strain relations can be written using (2.6) as

$$\Delta N = C^e (\Delta \varepsilon - \Delta \varepsilon^P) \qquad\qquad 2.29$$

Substitution of (2.27) and (2.29) in (2.28) gives

$$\gamma = \frac{f,^T C^e \Delta \varepsilon}{f,^T C^e f,} \qquad\qquad 2.30$$

Substituting this expression back into (2.29) and using appropriate associativity of matrix multiplication a relation between ΔN and $\Delta \varepsilon$ follows:

$$\Delta N = C^e \Delta \varepsilon - \frac{C^e f, f,^T C^e}{f,^T C^e f,} \Delta \varepsilon \qquad\qquad 2.31$$

Hence, the matrix C of tangential rigidities defined in (2.6) can be expressed as:

$$C = C^e - \frac{C^e f, f,^T C^e}{f,^T C^e f,} \qquad\qquad 2.32$$

The calculation of these rigidites by the direct use of a yield function of stress resultants is the fundamental difference between the single layer and the multi-layer approaches.

The use of an approximate expression in place of Ilyushin's correct yield function in the above expressions involves a degree of error difficult to estimate. The flow rule applied to the two-planes approximation (Ilyushin I, eq.(2.22)) corresponds to a constant direction for the normals on each half of the surface and clearly Ivanov's expression (Ilyushin II, eq.(2.24)) has an even greater advantage in this respect.

2.5   BOUNDARY CONDITIONS AND LOADING

The boundaries of the plates forming the box girder model can be divided for convenience of presentation into four categories:

- fictitious boundaries associated with symmetry simplifications;

- edges situated at the ends of the box and where the support conditions are defined;

- longitudinal edges between web and flange plates; and finally

- the web cross sections (in general at mid-span) over which vertical point loading is applied.

In this section the analytical conditions considered at the various boundaries are presented with reference to any special numerical treatments which are needed. These are discussed in detail in Chapter 3. A particular approach was also needed to deal with most of the conditions in the plastic range.

The various boundary conditions are summarized in Fig. 2.5 for a quarter of a closed box for the case of double symmetry.

2.5.1   Conditions Along Lines of Symmetry

Due to longitudinal symmetry of geometry and loading, symmetry of behaviour can be assumed for all cases, thus reducing the problem to
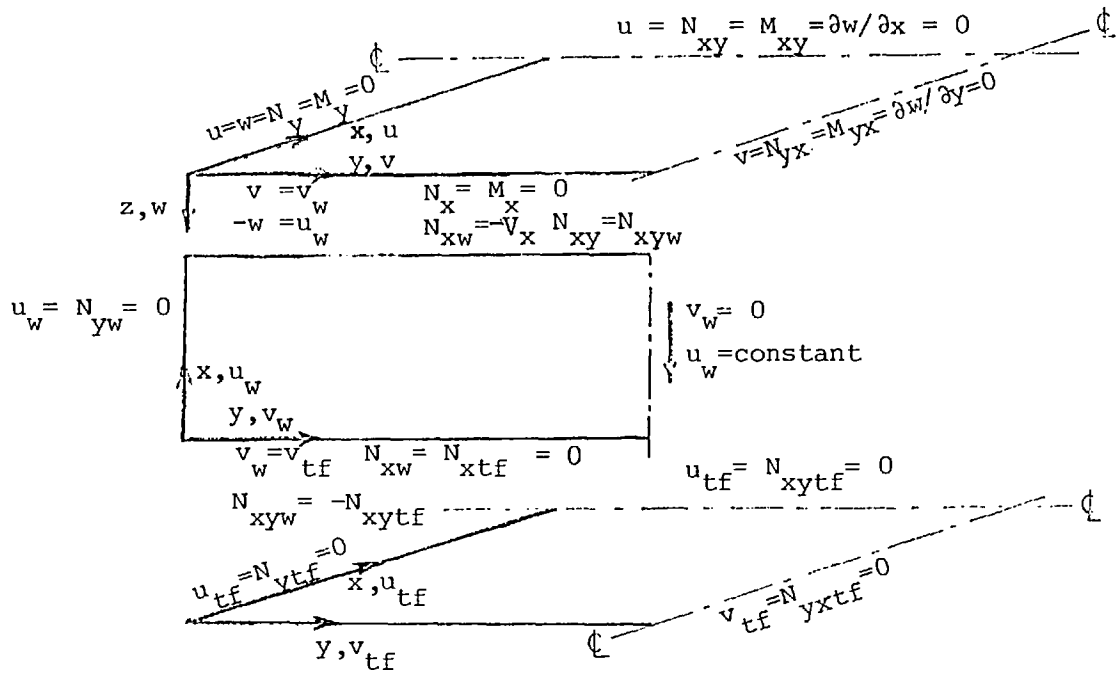
Fig. 2.5   Summary of boundary conditions for double symmetry

the analysis of half a box girder. In most cases symmetry about the mid-span cross section can also be considered and only a quarter of the box has to be modelled (Fig. 2.5).

Symmetry can be introduced by assuming in-plane displacements and slopes of out-of-plane displacements to be zero across the corresponding sections (represented in Fig. 2.5 by the central lines) and shear stress and twisting moment resultants to vanish along them.

Where mid-span symmetry cannot be assumed, the possible longitudinal rigid-body movement of the beam was prevented by fixing a point in the web-compression flange junction in that direction. This was usually at the point loading section.

2.5.2 Conditions at the Supports

The beam ends were assumed to be closed by diaphragms which are infinitely rigid in-plane but with no out-of-plane rigidity. This assumption provides an overall support condition equivalent to zero vertical displacement of the points on the web edges at those sections, together with a local simple support for the compression flange plate. This corresponds to zero tangential displacements ($u = 0$) and zero direct in-plane stresses ($N_y = 0$) at the edges of all the plates connected by the diaphragm. There are two additional conditions for the compression flange, viz. $w = 0$ and $M_y = 0$.

Along the compression flange edge the kinematic conditions correspond to $\varepsilon_x = \chi_x = 0$ and in elastic solutions $N_y = 0$ is therefore associated with $\varepsilon_y = 0$ and similarly $M_y = 0$ with $\chi_y = 0$.

In the plastic range, however, stress increments are dependent on all strain resultants as indicated by expression (2.6). Thus increments

of ε_y and χ_y would have to be calculated from the zero stress conditions ($N_y = M_y = 0$) as follows:

$$\Delta\varepsilon_y = -\frac{1}{C_{22}} (C_{23}\Delta\varepsilon_{xy} + C_{25}\Delta\chi_y + C_{26}\Delta\chi_{xy})$$

$$2.33$$

$$\Delta\chi_y = -\frac{1}{C_{55}} (C_{52}\Delta\varepsilon_y + C_{53}\Delta\varepsilon_{xy} + C_{56}\Delta\chi_{xy})$$

where C_{ij} are the components of matrix $\underset{\sim}{C}$ with $C_{22}, C_{55} \neq 0$. The relations could be further simplified and expressed only in terms of $\Delta\varepsilon_{xy}$ and $\Delta\chi_{xy}$ but they are sufficient to illustrate the complexity of the boundary conditions in the plastic range.

In stiffened compression flanges the boundary conditions at the end cross sections raise in general problems even in the elastic range. To achieve the same boundary conditions used for the unstiffened plate there must be no longitudinal stresses applied over the whole cross section, for the free to pull in condition, and no net moment* for the free to rotate condition. At the end cross sections the same supporting diaphragms used for the unstiffened flanges are assumed. It is then also possible to substitute on the plate edge the condition of zero longitudinal stress by $\varepsilon_y = 0$, and the zero bending moment condition by $\partial^2 w/\partial^2 y = 0$. These two conditions extended to stiffener locations ensure zero longitudinal strains (given by expression (2.9)) and consequently zero stresses (2.10) at the stiffener end cross sections. Hence, the diaphragm assumption makes possible the translation of the two stress edge conditions (free to pull-in and free to rotate) into displacement conditions ($\varepsilon_y = \partial^2 w/\partial y^2 = 0$) which are valid for the whole stiffened edge.

---

* about a line of rotation

To impose a fully fixed condition for the stiffened plate end cross section would also present no special difficulty. However, a combination of applied longitudinal stresses with a free rotation condition seems difficult to model with the present eccentric stiffener formulation. Supposing, for example, that it was intended to apply an axial compressive load with no eccentricity in relation to the plate mid-plane level. At the plate edge this corresponds again to zero applied bending moment ($M_y = 0$) which would still be equivalent to $\partial^2 w / \partial y^2 = 0$. Where the stiffeners are located this edge condition would not be sufficient. It should also be required that at the stiffener and cross section the moment of the applied stresses should be zero in relation to the plate mid-plane level, that is $M_s = 0$ (expression (2.12)). However, the basic assumption that the stiffener cross sections remain plane implies that the longitudinal membrane strain now existent at the plate over the stiffener position is transmitted to the whole stiffener cross section. At this section, the zero curvature only ensures that the longitudinal strains and the corresponding stresses* vary uniformly over the stiffener depth, but they would not have a zero M_s moment. This condition seems therefore impossible to enforce without violating compatibility. These boundary condition problems were not discussed in references (38) and (44). They are of a similar nature to those encountered in finite element analysis where over boundaries equilibrium and compatibility cannot always be assured simultaneously.

Numerically, when a discretising technique is used, it is possible to simulate the condition of zero net moment in relation to

---

* *Due to Poisson effects and different Young's modulus the stresses on the stiffener end cross section would be different from the longitudinal stresses on the plate.*

the plate mid-plane level by assuming zero values of N_s and M_s, at the stiffener end cross section, independently of the compatibility assumptions. This solution was, in fact, investigated and adopted for studying isolated stiffened flanges in axial compression (section 3.5.4). For these cases the loading was applied by longitudinally displacing the plate end cross sections which were assumed to remain straight.

Experimentally, in tests of isolated stiffened panels, the end cross sections are usually welded to relatively stocky stiffeners[55]. In axial loading a simple support condition is in general achieved by applying the load to these end stiffeners at an assumed neutral axis level and allowing rotation about the loading line. Basically this corresponds to assuming at the stiffened panel end cross sections a distribution of longitudinal stresses such that its overall moment about that line is zero. There is a difference between this free rotation condition and the one that was discussed above for the present numerical study. In fact, the torsional and lateral bending rigidities of the end stiffeners of such test panels can provide, during the loading history, some local clamping to the plate edge and some redistribution of longitudinal stresses. This can be achieved while respecting the overall zero moment condition. In the case of the load level coinciding with the plate mid-plane it would thus be possible to imagine that at the stiffener end cross sections some longitudinal stresses can exist.

On tests of stiffened cylinders under axial compression[56] a different approach has been attempted to model the condition of free rotation at the end edges. It consists in tapering the stiffeners near the ends and supporting the plate edge in a circular groove on the loading blocks, thus allowing it to rotate freely. This is perhaps a

closer physical interpretation of what was assumed in the present ana-
lytical solution.

It can be argued that the difference between the two ways of
achieving the free rotation, which have been discussed, reduces to some
end effects with little influence on the overall panel behaviour.
However, when local panel buckling occurs near the loaded ends inducing
overall collapse, there is scope for justifying some more refinement of
boundary conditions. For comparison with test results, it would there-
fore be interesting to be able to model numerically the stiffened plate
support condition where realistic end stiffening exists. This is not
possible with the present numerical solution and the influence of assum-
ing at the stiffener end cross sections that $M_s = 0$ is discussed in
Section 3.5.4.

The stiffened plate boundary conditions should also be analysed
from the point of view of the plate-stiffener interaction which was
formulated in terms of the line forces F_y and F_z (expressions (2.13) and
(2.16)). Here again, the assumption of end diaphragms is useful. In
terms of stiffener equilibrium considered as a beam the vertical reactions
to the distributed load F_z can be assumed to be provided by the diaphragm
at the ends, although these reactions are not calculated in the solution
process. These line loads correspond, as discussed before, to di-
continuities in the plate in-plane and transverse shear forces. For
plate equilibrium at an end which is free to pull in, the value of F_y
should vanish. Similarly, when this section is supposed to be simply
supported the continuous zero value for the plate curvatures along the
end edge indicates that the transverse shear force $Q_x{}^*$ must also

* $Q_x = -D(\partial^3 w/\partial x^3 + \partial^3 w/\partial x \partial y^2)$

vanish along y = 0 (Fig. 2.1). Therefore F_z should also be zero at this end section. These two conditions cannot be guaranteed in the present formulation and the stiffener ends correspond most probably to plate singularity points. To prove this suggestion would involve an investigation beyond the aims of this thesis. It should however be recalled that in plane-stress problems of load diffusion from a stiffener to a plate medium the ends of the stiffener correspond in general to plate singularities[57][58].

As will be shown in the next chapter, the numerical solution method which was used does not require the calculation or assumption of end values for these two line loads. The effects of the singularities, if any, do not seem to influence the results and no high stress concentration was detected numerically in the plate around the ends of the stiffeners.

2.5.3   Conditions at Plate Junctions

Interaction of plate edges was treated in the following manner:

1.   At all longitudinal web edges compatibility of longitudinal displacements and continuity of the shear stress flow was assumed.

2.   The edges of the compression flange were made to deflect to follow the vertical displacements of the web.

3.   The edges of the flanges were assumed free to pull in and the compression flange edges free to rotate.

The numerical handling of the web-flange interactions presented some difficulty, particularly for those aspects concerned with longitudinal compatibility and equilibrium. The accurate modelling of these

conditions is obviously essential to the study of the shear lag problem. This led to the derivation of a special equation of equilibrium for an 'edge' element (Fig. 3.6), with finite dimensions, to calculate the longitudinal displacements on the edge without having to make assumptions regarding the variation of shear flow across it. This variation can be very rapid at some points due to shear lag and web deep-beam effects. This technique is similar to the one used for the nodes over the stiffener lines, mentioned before, and is also capable of dealing with any distribution of longitudinal stresses across the edge including discontinuities. Pronounced differences between values of N_y on the web and on the flange can occur on the common edge. This occurs not only in the elastic range, due to different thicknesses and boundary conditions, but mainly due to plastic flow of stresses if the plates are made of different materials. This will be also discussed in detail later.

The same approach could be used to ensure compatibility of vertical displacements on the web-compression flange connection, by considering the vertical equilibrium of 'edge elements'. Instead, as in reference (59), this condition was indirectly introduced by calculating these displacements on the web taking into account any external load distributed over its edge and the flange reaction ($V_x = \partial M_x / \partial x + 2 \partial Mxy / \partial y$). The corresponding deflection is then imposed on the compression flange boundary. This process, compared with the former, proved to have a more stabilising effect on the flange behaviour for the application of the dynamic relaxation technique. The disadvantage is that it relies heavily on the use of fictitious node values to express in finite difference form the flange reaction and its effects on the web. These approxi-

mations are perfectly acceptable since the shear lag effects are not too dependent on the accuracy of modelling the flange boundary deflections.

Once it was established that the compression flange ultimate capacity was not influenced by the type of cross section (see Chapter 5), girders with an open section (CS2 and CS3 in Fig. 1.4) were used in some cases, for economy of numerical computation.

In the open stocky tension flanges shear lag can be neglected and the longitudinal stresses can be assumed to be uniformly distributed over the width. Compatibility of axial straining (ε_y) of the web-flange junction is then sufficient to calculate the total axial force on the flange as:

$$N_{tf} = \tfrac{1}{2} A_{tf} E_{tf} \varepsilon_y \qquad\qquad 2.34$$

where $\tfrac{1}{2}A_{tf}$ is the cross-sectional area of one flange plate. Plasticity was introduced by limiting the absolute value of this force to a maximum corresponding to uniaxial yield stress.

From equilibrium considerations used in normal beam theory the shear stress on the web edge can be expressed as:

$$N_{xy} = -\partial N_{tf}/\partial y \qquad\qquad 2.35$$

With the other boundary condition at this edge being the same as before ($N_x = 0$), the web analysis involves only web variables. This considerably reduces the computing time.

2.5.4   Point Loading Idealisation

As mentioned in the introduction, to follow the post-buckling behaviour, an incremental displacement controlled loading was used.

The point loading (for most cases at mid-span) was modelled by applying uniform vertical displacements over the depth of each web. In physical terms this corresponds to assuming that an interior infinitely rigid diaphragm exists at that section. As observed by Dowling[29] experimentally and later proved theoretically by Wittrick[60], this gives rise to a singularity at the point of the web-flange junction.

In box girder bridges the point load generally corresponds to support cross sections where load bearing diaphragms are located. The present approach is therefore a more realistic representation of actual loading than, for example, the application of a displacement at a single point down the web as in reference (26). Both ideas were tested numerically with the present computer program and it was found that a localised displacement induces an even more severe singularity and, through dissipation of the concentrated stress, tends to smooth the overall bending moment distribution around that section. This clouds the effects of the point loading on shear lag.

To comment on the singularity problem it is useful to refer to Williams'[61] results for the analysis of a plate corner. Williams has shown that at a right angle corner unbounded stresses may occur if one edge is restrained (normal and tangential displacements being fixed) and the other free. If vertical displacements are imposed in a symmetric beam the web-flange junctions at the mid-span cross section represent plate corners in similar conditions. Assuming the plates to have no flexural rigidity Wittrick[60] subsequently concluded that the singularity problem was inherent to interior diaphragms since around them the stress distributions have in general a symmetric component. The situation is different at an end diaphragm where theoretically there should be no singularity.

In the present analysis, the bending of the compression flange produces vertical reactions on the web and, therefore, the theoretical assumptions which eliminate the singularity at the end cross section are not totally fulfilled. However, it is always possible to imagine that at the support the concentrated plate reaction is absorbed in the rigid end diaphragm and to assume numerically a zero vertical stress on the web to avoid any stress concentration.

Wittrick concluded that the possibility of a singularity at a stress concentration point is sufficient to cause divergence in any finite element solution, while attempting to study the concentration by mesh refinements. The same conclusion applies to the use of the finite difference method in the present numerical program as will be discussed later (section 3.5.3).

The effect of the singularities on the web is indirectly transmitted to the flanges even if they are not connected to the fictitious diaphragm as the adopted boundary conditions indicate. However, this 'separation' must help to moderate the propagation of the local high straining, and it was found numerically that this has only a very localised effect on the stress distribution. In practice, these effects are diffused by yielding of the material and should not have any overall significance since they happen in the context of displacement controlled loading. They were therefore accepted in ultimate load calculation even in cases where the webs are theoretically assumed to remain elastic.

On the other hand, for some elastic calculations, for example of shear lag effective width ratios, the singularity would completely confuse the results for the loaded cross section. Following reference (13) the point loading was therefore modelled, for these cases, by

applying uniformly distributed shear stresses over the depth of the web.
For numerical reasons, however, this loading was only introduced in
cases of symmetry about the loaded cross section.

The presence of the singularities was recognised by Dowling[29]
during the series of box girder tests conducted at Imperial College.
The first models (Models 1 and 3) under point loading included a load
bearing diaphragm at the centre.   In Model 3, for example, the stress
concentration at the web-diaphragm-tension flange junction was noticeable
in the early stages of loading and later became very pronounced to the
extent of producing necking and cracking of the flange.   In later simi-
lar tests[30] (Models 9 and 12) to avoid this problem the full-width
diaphragms were replaced by tapered stiffeners on the webs through
which the load was applied (Figs. 6.2   and   6.3).

2.5.5   Boundary Conditions for an Isolated Flange in Compression

The computer program developed for the analysis of box girders
was adapted to study the compression flange in isolation.   As previously
mentioned, the purpose of this option was to provide results for a plate
under axial end compression to compare with those obtained for a shear
lag type of loading.   Therefore, only the boundary conditions associated
with the loading and the overall deflection of the longitudinal edges,
whose effect was neglected, were changed.   The flange was assumed to
be simply supported at its four edges and loaded by applied uniform
axial displacement (v = constant) of the end cross-sections.   The longi-
tudinal edges were assumed to be free from shear stresses.   The end
cross-sections remained straight but all the other boundary conditions
were unchanged namely, the restrained tangential displacement (u = 0).
For the reasons already discussed, to restrain in-plane displacements at

this end edge and to free the adjacent one introduces a singularity at the corner. In all numerical results thiscornerconsequently yields at a very early stage but such stress concentration does not affect the overall behaviour in strain controlled loading.

For stiffened flanges, problems with the boundary conditions at the end cross sections arise. These were discussed in detail in Section 2.5.2.

CHAPTER   3

NUMERICAL SOLUTION

3.1   INTRODUCTION

Finite differences (FD) and dynamic relaxation (DR) have been successfully applied to large deflection elastic-plastic analyses of isolated plate panels (references (35) and (36)) and thin walled box-column plate assemblages[59]. The combination of these two techniques has proved to date to be faster and less demanding in computer storage than finite element solutions. With FD and DR it is also possible to follow special variations of displacements or stresses, either by using non-uniform meshes of by simply choosing appropriate interpolating functions. Thus the solution technique can be improved by examining the initial results. This is advantageous when the objective is to develop an economic computer program for a parametric study. The approximations involved can also be directly assessed and the accuracy can be increased by a simple physical understanding of the problem.

The usual FD and DR technique for isolated plate analysis had to be extended to consider in the context of box girder plate assemblages three specific problems:

  - the plate connections

  - the stiffener action

  - the point loading stress distributions at the cross section
    to which it is applied.

These problems involve rapid variations and discontinuities of stress distributions which cannot be easily considered by usual finite difference techniques. They are discussed in section 3.3 and the proposed method for their solution is detailed in Appendix I. The method was developed to avoid reducing excessively the mesh sizes near these zones, or

making inaccurate approximations of the difficult stress distributions.
For the shear lag study the problem of modelling the web-flange connections
is obviously very important. The proposed method of solution was checked
against available finite element elastic solutions.

The other plate boundary conditions did not present any problems
in the elastic range and fictitious nodes were used when necessary. In the
plastic range the boundary conditions had to be treated in the manner of
reference (36) as mentioned in the previous chapter. The numerical treat-
ment of the plasticity condition and the stress-strain relations in the
inelastic range presented some problems associated with the finite diffe-
rence mesh arrangement and the incremental loading. The solutions to
these problems are presented in section 3.4.

A computer program was specially designed for the parametric study.
Certain results of this program were compared with other numerical solutions
some of which have been experimentally verified. The calibration of the
program was organised to separately study the different aspects of modelling
the box girder since no comparable analysis of full elastic-plastic/buckling
behaviour was available.

3.2   DISCRETIZATION TECHNIQUES

3.2.1   General Formulation

To establish the displaced configuration of each plate under load-
ing, the variation of each displacement component (u, v and w) was assumed to
be described by a set of values taken over a nodal mesh. The meshes for each
component need not coincide and can be chosen in the most convenient way for
the purpose of defining the respective field. This is the principle of inter-
lacing meshes used to improve the accuracy of the finite difference solution.

The distributions of stress resultants can be similarly treated
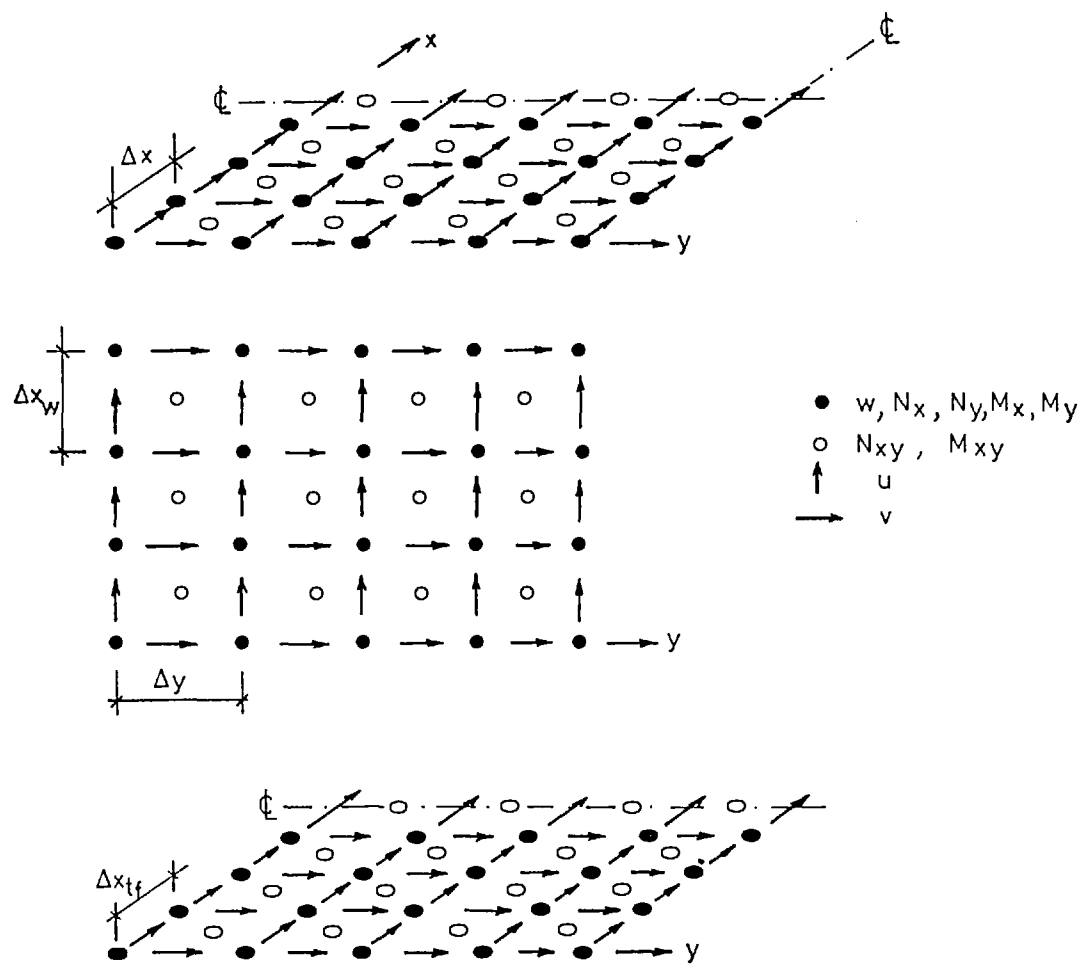and in general defined over another six nodal meshes. These distributions

Fig. 3.1   Mesh arrangement for finite differences

need not be smooth and may have sharp variations requiring a careful choice of node positions.

For the constitutive relations, generalised strains have to be calculated at all stress nodes either directly or by interpolation of the strain distributions over neighbouring nodes. In principle, strain distributions can be defined over other sets of nodes but it is convenient to make stress and strain meshes coincide.

For the present solution interlacing rectangular uniform meshes were chosen based on other plate analyses[35][36]. The relative position of the various meshes is presented in Fig. 3.1. The spacing in the y-direction was assumed to be the same for all plates.

A uniform mesh restricts the choice of boundary nodes and requires some experimentation to find the best location of nodes over the boundaries. Some boundary conditions were easy to consider in this respect. For example, considerations of longitudinal symmetry suggested that N_{xy}, M_{xy} and u nodes should be placed over the flange longitudinal central line. However, to accurately calculate the net longitudinal force at the point loading cross section, N_y nodes were positioned over this section, even in the case of models with double symmetry. This choice also has the advantage of placing on the web a line of vertical displacement nodes over the point loading cross section for the application of displacement controlled loading. On the other hand, such a mesh arrangement does not allow a direct modelling of the point loading by applied uniform shear stresses over the web depth (see section 3.5.1). For convenience in the treatment of the stress variations across the web-flange junctions and stiffener positions these lines were also made to coincide with the N_y nodal lines.

Values of the plate-stiffener interaction line forces F_y and F_z were calculated over v and w nodes respectively. For these calculations equations (2.13) and (2.16) were written in finite difference form using
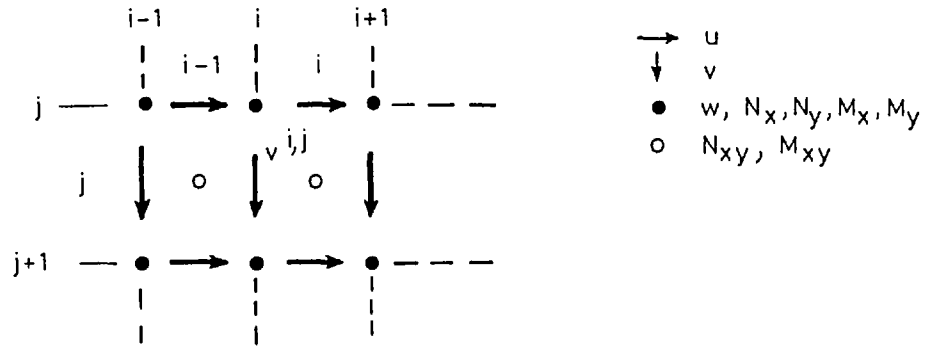
Fig. 3.2   Position of node $v^{i,j}$ on the interlacing mesh
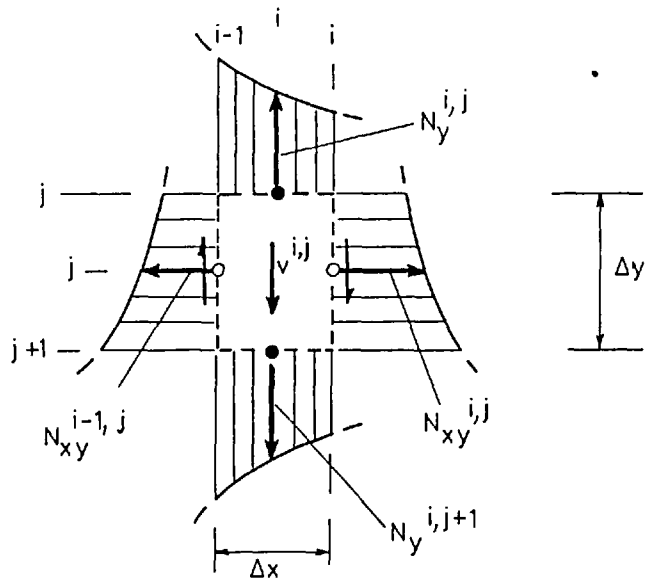
Fig. 3.3   Stresses with longitudinal component acting on 'finite element' of plate centred at node $v^{i,j}$

values of the stiffener internal forces N_s and M_s defined at cross sections over N_y plate nodes.

The calculation of N_s and M_s required a further discretization consisting of dividing the stiffener depth into horizontal layers. At each layer the longitudinal strain and stress are given by expressions (2.9) and (2.10). The integrations involved in the definition of N_s and M_s are substituted by appropriate summations of corresponding quantities for each layer. This is necessary to trace the spread of plasticity in the stiffener.

To study the compression flange in isolation the mesh arrangement described in Fig. 3.1 was retained. Axial compression was applied by resorting to fictitious v nodal displacements at the end cross sections.

Once the mesh arrangement is established, local equilibrium in each direction can be defined over corresponding displacement nodes by expressing equations (2.3) in finite difference terms using adjacent stress nodal values. For example, on the $v^{i,j}$ node of Fig. 3.2 the equation for equilibrium in the y direction takes the form:

$$(N_y^{i,j+1} - N_y^{i,j})/\Delta y + (N_{xy}^{i,j} - N_{xy}^{i-1,j})/\Delta x = 0 \qquad 3.1$$

where central finite differences are used due to the convenient disposition of the various nodes in the interlacing mesh.

This equation can also be interpreted as representing, under certain conditions, the equilibrium of the forces applied to a rectangular plate 'finite element' centred at the displacement node $v^{i,j}$ and with boundaries over adjacent lines of N_y and N_{xy} nodes. Such an element is represented in Fig. 3.3. The distributed loads acting on the boundaries which contribute to the equilibrium in the y-direction are the plate stress resultants N_y and N_{xy}. This equilibrium can be expressed as follows:

$$\int_{\text{side } j+1} N_y - \int_{\text{side } j} N_y + \int_{\text{side } i} N_{xy} - \int_{\text{side } i-1} N_{xy} = 0 \qquad 3.2$$

If the stress distributions are such that their average value over each side can be represented by the nodal values then equation (3.2), after dividing by the element area, is equivalent to (3.1). This analogy suggested a way of dealing with equilibrium conditions along web-flange junctions, stiffener lines and the point loading cross section. This is described in the next sections.

Dynamic relaxation was used to assist in the solution of the non-linear set of equilibrium equations described above as these can be considered as relations between nodal displacements.

3.2.2   Equilibrium along Plate Junctions

The flow of shear stresses across the web-flange common edges can vary and includes a point of contraflecture. Thus, making an accurate interpolation of its distribution over the chosen mesh arrangement is difficult. In general, the longitudinal stresses N_y also differ between the web and flanges. This is worsened where different materials are used for the webs and the flanges. For example, in the case where the web is assumed to have a much higher yield stress than the flange, the web may then still be elastic whilst yielding of the flange edge is accompanied by a flow of stresses under constant equivalent stress. This tends to increase the shear at the expense of the longitudinal stress component. In a strain controlled loading this can be reduced to very small values. To illustrate this problem typical stress distributions over a box cross section are represented in Figs 3.4 and 3.5.
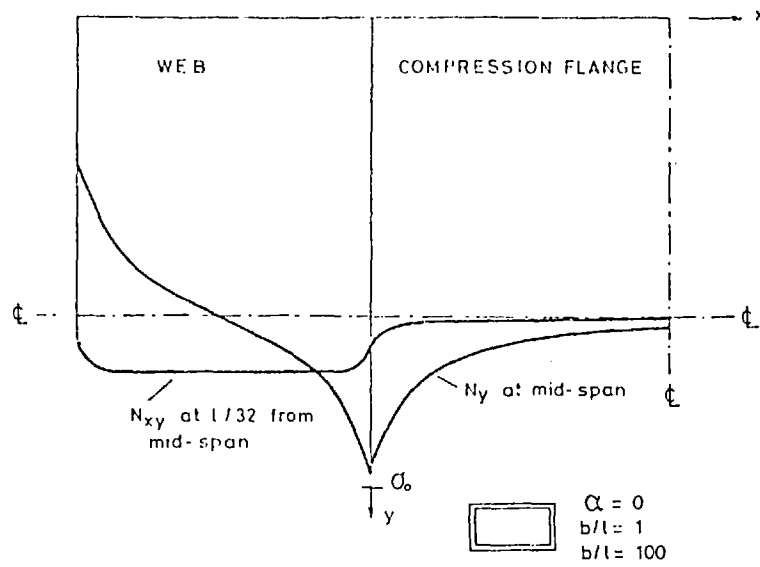
Fig 3·4 Example of elastic stress distributions
across web-flange connection
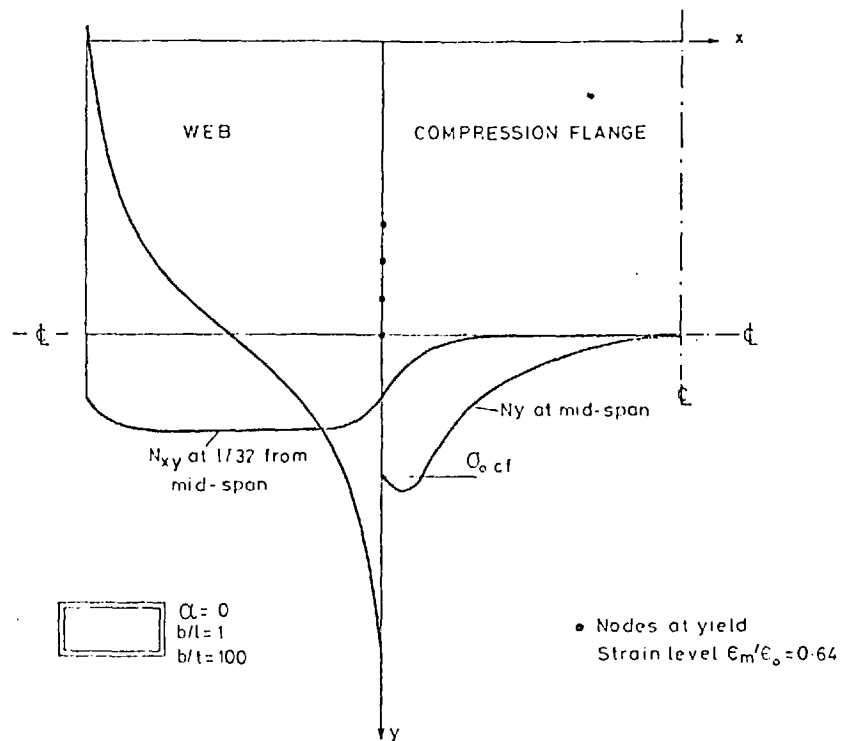
Fig 3·5 Example of stress distributions across
web-flange connection when the flange
edge has partially yielded (elastic webs)

For these reasons, it was found convenient to consider 'finite elements' of the plate connection as shown in Fig. 3.6 for the web-compression flange junction. The elements are centred over a v node and have an unfolded width chosen, for convenience, to be equal to the web mesh spacing in the x direction. It is thus possible to use a wider transverse mesh on the web than on the flanges as outlined in Appendix I.
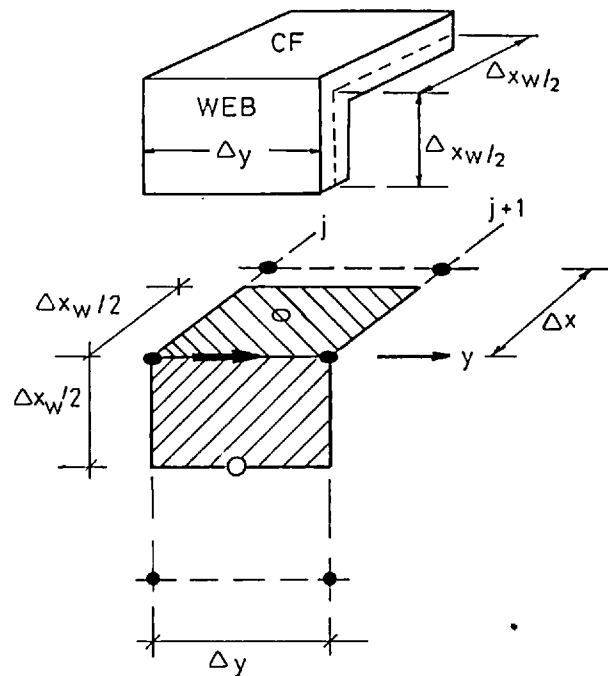
Fig. 3.6 'Finite element' of web-flange connection

Following the analogy mentioned in section 3.2.1 the same approach as used for deriving equation (3.2) can be followed for studying the equilibrium of one of these elements in the y-direction. For this purpose all the stresses acting on the element with a longitudinal component must be considered and integrated. The method of deriving the corresponding equilibrium equation is described in Appendix I.

It is assumed that the resulting equation (I.2) can represent

both the compatibility of longitudinal displacements and the continuity

of the shear stress flow across the web-flange junction. Any other way

of introducing these conditions in the solution process would have to rely

on an approximation for the variation of the shear flow. This would be

difficult and would involve greater inaccuracies than the proposed method

in which interpolations are considered only over well definable stress

distributions.

Apart from invoking the analogy described earlier, no attempt

is made to justify this method. Comparisons are however made later with

other rigorous numerical techniques to show that it produces good results.

Vertical equilibrium equations for similar angle elements were

also derived to implement the compatibility of vertical displacements at

the web-flange junction but, as discussed in section 2.5.3, another

approach was found to be more convenient.

The method just described could also be applied to deal with the

compatibility of rotation in welded web-flange connections. This prob-

lem presents special difficulties[59] when fictitious nodes are used.

An equation of rotational equilibrium of an element of the plate connec-

tion could then similarly incorporate both conditions of equilibrium of

moments and compatibility of rotation.

3.2.3   Equilibrium along Stiffener Lines

Figure 3.7 shows possible distributions of longitudinal and

shear stresses on a stiffened plate in axial compression. The plate-

stiffener interaction line force F_y (defined in (2.13)) produces the

shear discontinuity and the simultaneous cusping of longitudinal stresses

with a local shear lag effect.

To calculate the longitudinal displacements v along the stiffener line, the equilibrium in the y direction of a finite element of plate centred over a v node (Fig. 3.8), can be considered in the same manner as described before.

The stresses acting over the element which contribute to the equilibrium are the shear stresses defined at nodal values over the longitudinal edges and the cusping longitudinal stresses on the transverse sides. These are obtained by interpolating the longitudinal stress distributions over appropriate N_y nodes. The action of the stiffener on the plate element can be replaced by the line force F_y. The derivation of the equilibrium expression is given in Appendix I.

The vertical equilibrium at stiffener positions could also be studied considering finite elements of the plate centred over w nodes. This would enable the discontinuity in Q_x across the stiffener line to be taken into account (with the corresponding cusping of the M_x moment distribution as discussed in section 2.3). However, since the present stiffener formulation already neglects the discontinuity in the M_x distribution that exists due to the stiffener torsion, this refinement was not introduced. The vertical equilibrium over the stiffener position was thus treated following reference (38). In this approach the F_z interaction line force is assumed to be uniformly distributed over a width of plate equal to Δx. It is then included as a lateral load in the normal equilibrium equations written for the w nodes over the stiffener.

$\alpha = 0.25$

$b/l = 1.0$

$b'/t = 60$

$l/r = 40$

$\varepsilon_m/\varepsilon_o = 0.900$

(see also fig 4.12)

scale N/mm
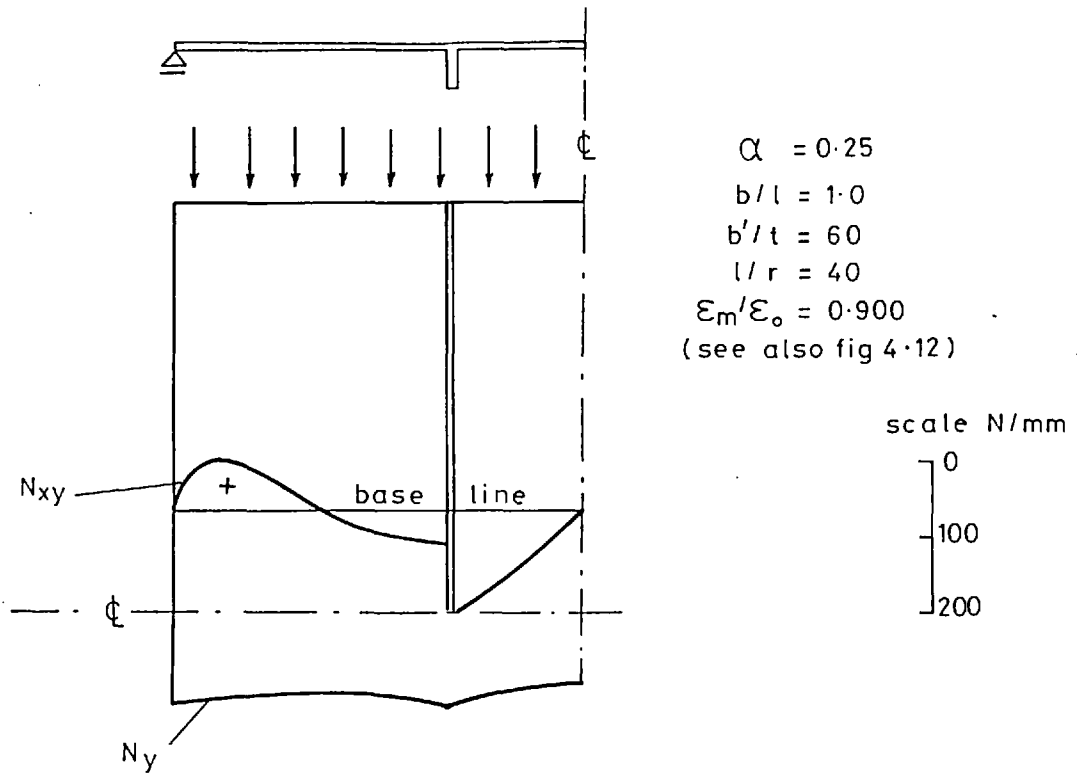
Fig. 3.7   Stiffened flange in axial compression. Example of stress
distributions over cross section at distance $l/8$ from mid-length
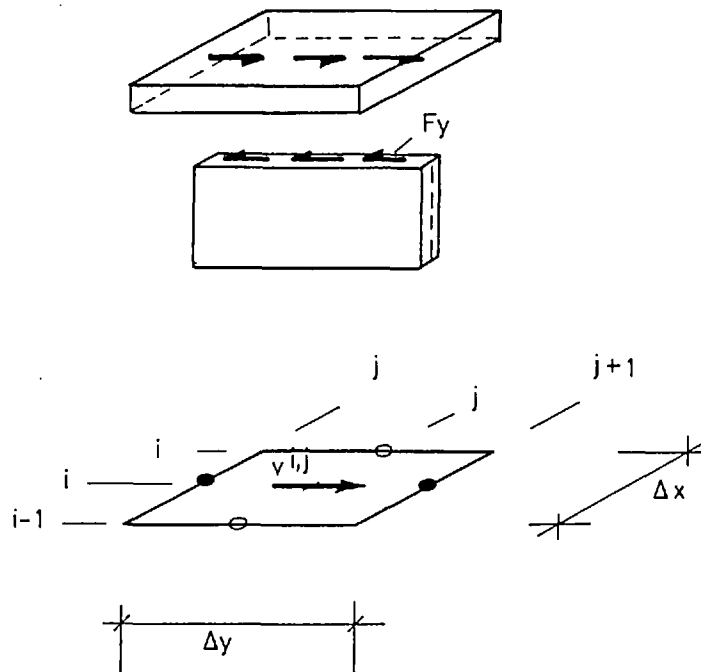
Fig. 3.8   'Finite element' of plate over stiffener line

3.2.4   Equilibrium over the Point Loading Cross Section

On the compression flange the chosen mesh arrangement (Fig. 3.1) has u and w nodes over the point loading cross section.   For most cases this section coincides with the mid-span and symmetry can be assumed. Thus, by using appropriate boundary conditions only one quarter of the box need be analysed (see Fig. 2.5).   Since the symmetry conditions are not directly associated with displacements or stresses defined at nodes u and w, fictitious symmetric or anti-symmetric nodal values have to be introduced.   These are required to calculate over the section the u and w displacements and all the stress components except those assumed to vanish due to their anti-symmetric distribution (N_{xy} and M_{xy}).

The shear lag effect, associated with the point loading condition, produces not only a very high longitudinal stress peak but also sharp variations of N_x due to the symmetry and Poisson effect.   The assumption of N_x being zero on the flange along the web-flange connection further complicates the distribution of these stresses near the web. Figure 3.9 illustrates the typical shape of these distributions in the elastic regime.

The peaks and cusping of in-plane stresses are particularly pronounced in the elastic range for cases of loading by uniform vertical displacements over the depth of the web.   This is due to the singularity discussed in section 2.5.4.   Yielding of the material smoothes the peak of the longitudinal stresses.   However,over a mid-span cross section, the zero/symmetry condition allows a combination of N_x and N_y stresses
                     shear
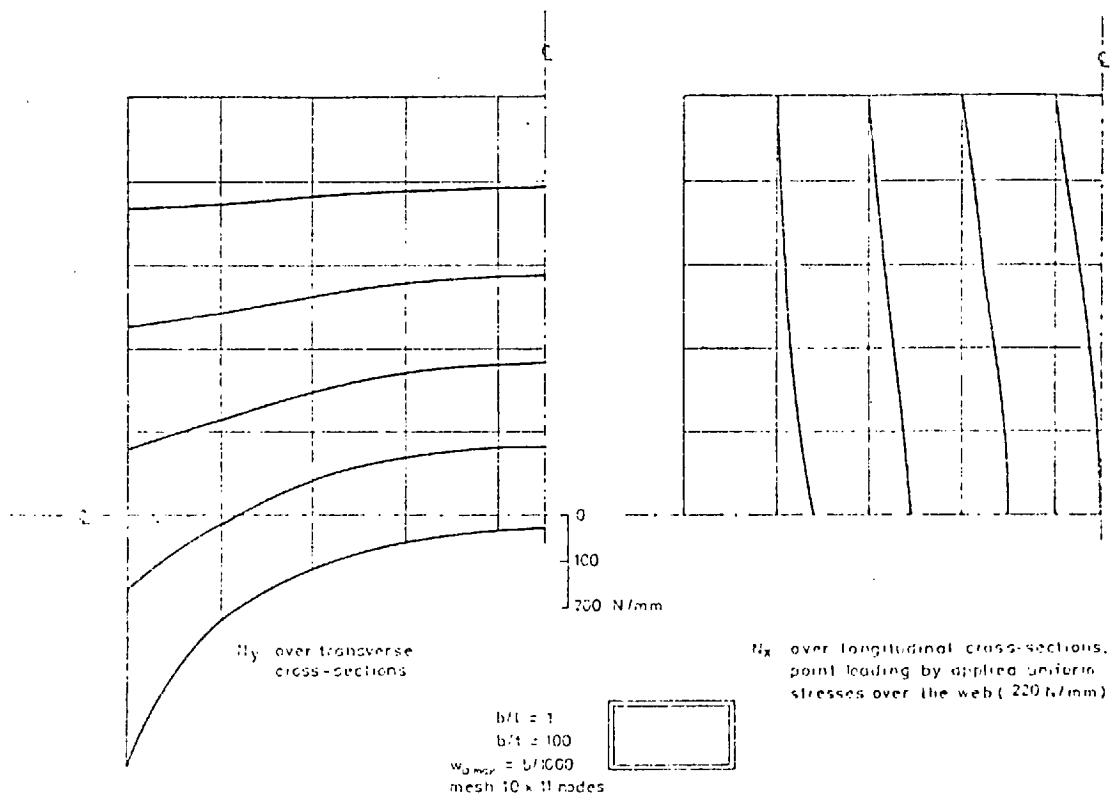
Fig. 3.9   In-plane stresses on compression flange due to point loading

such that N_y can exceed uniaxial yield stress (see Fig. 3.5).

As the capacity of the flanges is measured by the longitudinal

net compression or tension force over the point loading cross section,

an accurate calculation of stresses over this section is required. This

was attempted by reverting to the 'finite element' technique to express

the equilibrium on both flanges around this section.   Since irregularities

in the stress distributions are quite localised, it was found sufficient

to apply this refinement only to the derivation of equilibrium equations

in the x-direction for u nodes over the section (see Appendix I).

Over the web the applied vertical displacement loading corresponds

to a line where displacements are completely defined. Hence, no special treatment of equilibrium conditions was required.

3.3   DYNAMIC RELAXATION

Dynamic relaxation is particularly suitable for the solution of non-linear structural problems and is usually associated with a finite difference formulation of the governing equations. A detailed description of the DR technique will not be given here since it is adequately documented elsewhere (36)(62-66). Essentially, however, the method consists of transforming the 'static' equilibrium equations into equations of 'motion' by adding terms involving viscous damping (proportional to velocity) and inertia (acceleration). The application of a load increment is assumed to alter equilibrium and activate the motion of the structure. The solution proceeds as a step-by-step integration in time of the equations of 'motion', expanded in finite difference form in time. The 'static' governing equilibrium equations are, in finite difference form, highly non-linear expressions of the nodal displacements but are linear in time in terms of displacements.

The process is basically a substitution technique: previous out-of-balance forces (expressed by the 'static' expressions) are used to calculate velocities and displacements. From these new out-of-balance forces can be calculated for the next time increment. The technique is easily programmable since the full solution matrix is never formed and the various sets of equations are kept separate and invoked at different time instants:

1.   invoke displacement boundary conditions in which loading increment conditions can be incorporated;

2.   calculate strains from strain-displacements expressions;

3.   calculate stresses from constitutive relations;

4.   invoke stress boundary conditions;

5.   calculate out-of-balance forces;

6.   calculate velocities and new displacements;

7.   repeat sequence until convergence is reached.

For stress applied loading the sequence would start at step 4.

It is the use of the governing equations in separated forms that makes it easy and advantageous to express equilibrium along particular lines or boundaries in the way described in section 3.2.

The solution technique is similar to following the 'physical' oscillations of the various nodal points after the sudden application of a load increment to a structure which is originally in a state of equilibrium.

The method involves the choice of three sets of parameters: the damping factors, the time increments and the material densities.   If damping factors are chosen to be near critical values, the oscillations converge to the steady state solution.

Using the fictitious densities and unit time increment techniques proposed by Cassell[65] and discussed for plate analysis in reference (36) the convergence depends only on the estimation of appropriate damping factors.   In the present problem the optimization of these factors was particularly laborious.   It involved the adjustment for each box girder case of two factors for the web, two for the tension flange, three for the compression flange and, in the presence of stiffeners, two additional ones for the plate nodes on the stiffener lines.

During the parametric studies it was frequently possible, for changes in dimensions, to adjust the damping factors from one case to another by extrapolation. However, for no obvious reason, some cases presented difficulties of convergence requiring an independent adjustment of factors. A possible explanation may be related to the fact, pointed out by Chaplin[68], that damping in analogous physical oscillations could only be critically chosen in each plate for one mode of vibration, usually the fundamental one. Therefore, in a plate assemblage some interaction of modes not critically damped could produce general instability.

For each loading increment it was found that very rapid and large initial vertical oscillations of the web had a destabilising effect on the compression flange. To assist convergence an artifice suggested by Frieze and Dowling[59] was used. This consists in not implementing for the first DR cycles the compatibility of the vertical displacements at the web-flange connection. A similar approach was used to improve convergence in the case of stiffened flanges by considering the interaction forces F_y and F_z as being gradually applied to the flange plate. Convergence was controlled by checking the nodal velocities.

For each load increment, within the DR sequence only increments of stress and strain are calculated. However, the equilibrium equations were kept in terms of total stress resultants. This introduces an automatic correction of any out-of-balance forces remaining from the previous load increment.

After each loading increment, tangential rigidities are recalculated and total stresses and displacements stored. For the next increment a linear extrapolation of the previous displaced configuration was taken as a starting approximation to the final solution to reduce the number of iterative cycles.

3.4   NUMERICAL TREATMENT OF PLASTIC BEHAVIOUR

To determine when a node reaches yield, the value of the yield function (Ilyushin I (2.22) or Ilyushin II(2.24)) has to be examined after each loading increment.   If yielding is detected the rigidities are modified according to expression (2.32) for the next increment. The sign of the flow parameter γ (defined in (2.27)) is checked thereafter to monitor any unloading in which case the elastic rigidities (2.7) are restored.   The numerical handling of these aspects involves consideration of the discretization technique and the loading incrementation.

3.4.1   Problems Associated with the Finite Difference Mesh

The interlacing mesh arrangement (Fig. 3.1), although very useful for the finite difference formulation, introduces a considerable complication in the application of the single-layer method described in Chapter 2.   This is due to the fact that at each node of the mesh only certain stress components are calculated but, to assess yield, the full state of stress has to be known.   For the web this problem was solved by averaging the missing stress value using surrounding node values.   For the flanges, in particular for the compression flange, special interpolating subroutines were designed.

Here again, the variation of the stress distributions associated with the web-flange connections, the stiffener lines and the point loading cross section were taken into account.

The present numerical solution is not however yet capable of accurately dealing with the plate yielding at the stiffener position. As mentioned before, the discontinuity of shear stresses on the plate across the stiffener lines should theoretically be treated by separately considering the two plate panels meeting over the stiffener.   This treat-

ment would allow, in the plastic range, the two plate panels to have

different rigidities at their common edge since there they have different

states of stress. However, the present numerical model only considers

one line of plate nodes over the stiffener and only one state of stress

can be defined at these nodes for the yield condition. This was achieved

by averaging the shear discontinuity.

The 'finite element' method described before for dealing with

the equilibrium condition at the web-flange connection was derived mainly

to avoid making assumptions regarding the shape of the shear stress

distribution across this line. It was found to be successful for solving

this problem during the DR sequence. However, after convergence is

achieved for a load increment, it is still necessary to accurately define

the value of the shear stress at the flange edge.

Assuming good convergence is achieved after each load increment

this stress was calculated from the condition of equilibrium of a strip

of flange between two consecutive transversal lines of N_y nodes (lines j

and j+1 in Fig.3.10). The net compression forces over these two lines

can be calculated by numerically integrating the longitudinal stress

distributions.

A good approximation for the value of the shear stress resultant

on the edge over the j line of shear nodes is:

$$N_{xy}^* = \int_o^{b/2} (N_y^{j+1} - N_y^j)dx/\Delta y \qquad\qquad 3.3$$

The interpolating refinements mentioned before could be afforded

in terms of computer time since they are only used once for each loading

increment. However, for strains, a similar problem arises within each

cycle of the DR sequence. As for the stresses these are also calculated
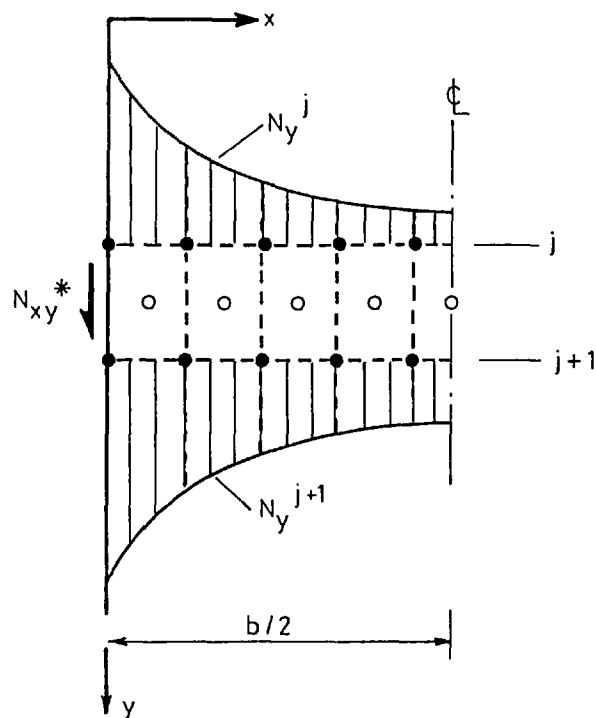
Fig. 3.10   Equilibrium of a strip of flange between consecutive
transverse   nodal lines

over two different nodal meshes.   After the onset of yield, the full

state of straining is required at each stress node but only simple

averaging techniques were used to calculate the missing strains.   This

is not only justifiable in terms of computer time but also because the

strain distributions are much more regular than the stress distributions.

3.4.2   Problems Associated with Load Incrementation

The problem of assuming convenient dimensions for the finite

loading steps required particular attention.   The detection of plasti-

city at each node had to be determined accurately to avoid 'perforation'

of the yield surface, since there is already a delayed accessment of first

yield using the single-layer method.   That is, the 'perforation'

of the yield surface must be well controlled.

Once a node becomes plastic, the size of the next increment still

has to be small, even if the rigidities are calculated correctly, to obtain a flow of stresses tangential to the yield surface. This is necessary to ensure that after a finite loading increment the state of stress remains close to the yield surface.

For each box girder case, a preliminary study enabled a general idea of the loads related to first yielding and to the spreading of plasticity to be obtained. The loading was then organized to have only a very small number of nodes yielding at each increment.

A technique has been proposed by Zienkiewicz[69] for considering points where the yield surface is 'perforated' in a change from an elastic to a plastic state. It consists of automatically subdividing the loading increment effects and has been used mainly in finite element analysis to consider larger load steps[40]. It was, however, decided to dispense with this refinement by keeping the size of the increments small and correcting the stresses after each increment to bring the state of stress back to the yield surface. This also consequently avoids accumulation of errors.

Supposing that after an increment the value of the yield function represented by f* is greater than unity, the correction mentioned above can then be approached in two ways:

1. A simple method consists of multiplying each stress resultant by the inverse square root of f* (to take into account the quadratic form of the function). This method is equivalent to correcting the state of stress along the line of its position vector (Fig. 3.11)

Position in stress space

0 - before load increment

0' - after load increment

$0'_1$ - corrected by first method

$0'_2$ - corrected by second method
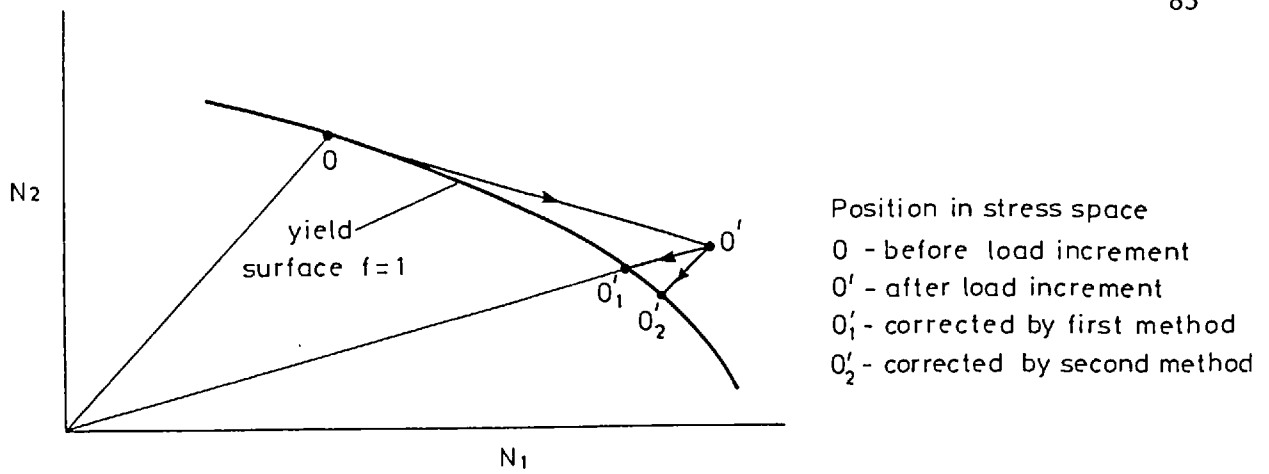
Fig. 3.11   Methods for correcting 'perforation' of the yield surface

2.   The state of stress can, instead, be corrected along the normal

to the yield surface (see reference (69)).   Representing the

difference of f* to unity by Δf, each stress component N_i

should be corrected by the following quantity

$$\Delta N_i = -\Delta f \frac{\partial f / \partial N_i}{\sum_{i=1}^{6} (\partial f / \partial N_i)^2} \qquad\qquad 3.4$$

This is equivalent to reducing each stress proportionally to its

contribution to the value of f.   That is, higher stress com-

ponents would be more severely modified which seems a more sensible

approach.   However, to apply this second method of correction

involves considerably more computer storage since the corrective

quantities (3.4) have to be previously calculated and stored

due to the stress averaging required for the interlacing mesh.

Although the two methods of correction could give different

results, in particular when using the Ilyushin I yield surface (two-plane

approximation), it was found that differences in overall results were not

significant provided that the loading incrementation was well controlled.

The first method was therefore preferred and used in the parametric study.

The numerical treatment of these corrections to the 'perforation' of the yield surface presents a problem associated with the use of the interlacing mesh. At each node of this mesh only stress components that are calculated directly can be corrected. Therefore, at some nodes, the value of the yield function calculated after applying the corrections can be smaller than unity. In the flanges, this frequently occurs at the nodes connected to the webs. This is due to the fact that the state of stress at these nodes depends greatly on the shear transmitted by the web, and corrections on flange nodes have no effect over these stresses. The yielded state of each node after a step load had therefore to be recorded before making the correction.

It must finally be mentioned that, although these corrections partially destroy equilibrium, this is reestablished in the DR loop of the next increment as the equilibrium equations consider total stresses.

3.5 PROGRAM CALIBRATION AND MESH SIZE STUDY

A computer program was written in Fortran IV based on the numerical solution described before. The extensive study of the verification and calibration of the program is reported in this section. In the absence of suitable experimental data comparisons with results from other numerical techniques served as the main basis for these studies.

Most of the examples selected to illustrate the various aspects refer to unstiffened flanges but the same general conclusions from the calibration study can be drawn for stiffened cases.

For choosing appropriate mesh sizes for these cases, consideration must be given to the number of mesh nodes used across the flange width between stiffener positions to model plate panel buckling.

3.5.1   Comparison with Finite Element Elastic Solutions

The numerical method of solution (FD and DR) has been well cali-
brated in the analysis of isolated unstiffened plates in shear[35] and
compression[36], but it remained to be shown that it could also be used
in the solution of box girder plate assemblages.   The efficiency of
the discretization technique described previously for modelling the point
loading shear lag effects was investigated by comparing with the results
presented by Moffatt and Dowling[13] for elastic shear lag effective
width ratios based on a finite element program.

As stated previously, the modelling of the point load by apply-
ing uniform vertical displacements over the web depth involves singu-
larities at the web-flange junction.   The definition of an elastic
effective width ratio at the loaded cross-sections (expression (1.2))
would be meaningless in the presence of these singularities.   This led
Moffatt and Dowling to consider the point load by applying uniform shear
stresses over the web.   To use their results for a comparison, the
same loading was introduced in the present computer program as an alterna-
tive for cases with symmetry about the mid-span loaded section.   This
was achieved by considering a line of fictitious shear nodes on the web
in the mesh arrangement shown in Fig. 3.1.

The loading was applied by ensuring that the average of the
shear stresses at the internal and the fictitious nodes was equal to the
applied stress.

The finite element program developed by Moffatt for the shear
lag study was based on an element with good shear characteristics and
the need for a longitudinally refined mesh near the point loading cross

section was reported[13]. In the parametric study conducted in reference
(13) it was possible to use only one element over the web depth whereas
in the present finite difference formulation several mesh nodes had to
be considered. This is a consequence of using the proposed method for
solving the web-flange connection described before. It requires the
web vertical mesh size to be greater but close to the one used trans-
versely on the flanges. This enhances the deep beam effects in compari-
son with the finite element approach thus increasing the shear lag
gradients. Another difference between the two approaches refers to the
compatibility of rotation at the web-flange connection assumed in the
finite element model. However, this should not greatly affect the com-
parison for very small deflections. Good agreement was generally found
to exist between both results.

This is illustrated by a mesh size study of a $b/\ell = 1$ box girder under
uniform shear stresses applied over the web at mid-span. The elastic
effective width ratios obtained at the loaded cross section by increasing
the number of longitudinal mesh nodes are plotted in Fig. 3.12. They
can be seen to converge to the corresponding value given in reference (13).

According to the authors, the ratios were calculated by taking
as a reference stress the longitudinal stress at the web (σ_{max} in
expression (1.2)).

These results show that the present numerical method is conver-
gent and also indicate that the modelling of the web-flange connection
closely resembles solutions that have been calibrated against experimental
results.

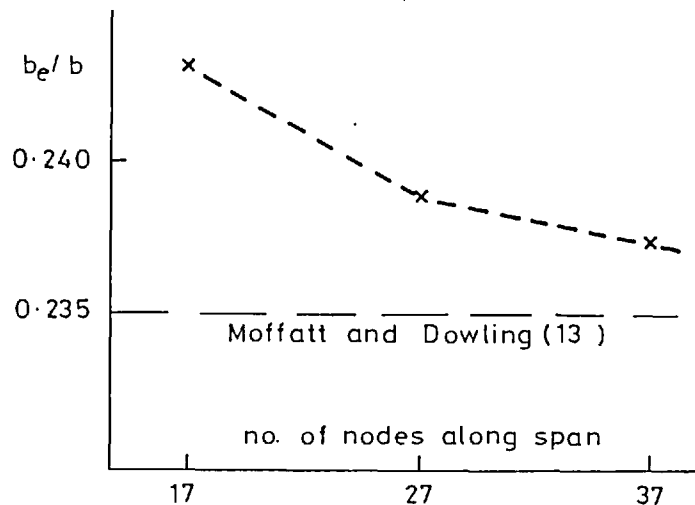That same program[13] was also used to apply uniform displacements

Fig. 3.12   Elastic effective width ratio at mid-span $(b/\ell = 1$; point load).
Mesh size study

over the web at mid-section on a finite element mesh as recommended in

reference (13).   This was compared with the present finite difference

solution calculated over a typical mesh.   The stress distributions

obtained in this case in the presence of the singularities compare

quite well as shown in Fig. 3.13.   The two mesh arrangements are repre-

sented in the same figure.   The good agreement further indicates that

an acceptable degree of accuracy can be achieved by the present solution

with reasonable mesh sizes, like those used in the parametric study, with

the advantage of a considerable economy in computer time.   This is

important since the refined non-uniform meshes recommended by Moffatt

and Dowling for the study of elastic shear lag effects cannot be repre-

sented in the present solution.

3.5.2   Spreading of Plasticity in the Presence of Shear Straining

In a girder under applied uniform displacements if the webs are

assumed to remain elastic, the longitudinal edges of the flanges are

WEB

COMPRESSION FLANGE

N_{xy} at $\frac{1}{4}$ span

N_y at $\frac{1}{4}$ span

N_{xy} at $l/32$ from mid-span

N_y at mid-span

b = l = 1800mm
d = 900mm
t = t_w = 18 mm
E = 205800 N/mm²
σ_o = 235 N/mm²

———— Present
o Moffatt's FE program

stress scale

0   100 200 300
N/mm

8 @ 10   642

8 equal divisions

b/2

applied displacements
u_w = −0.15 mm

d

l/2 = 900mm
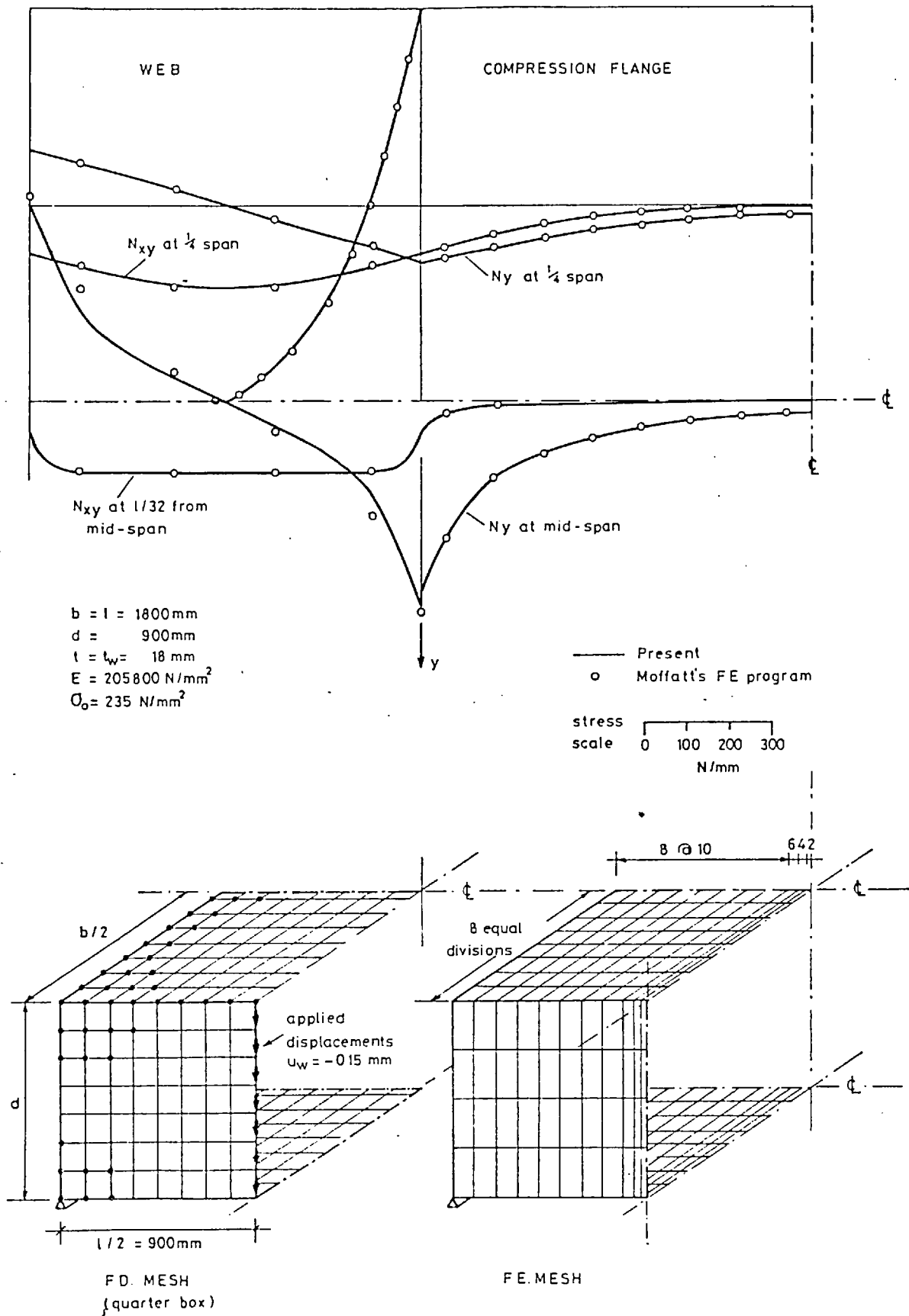
F.D. MESH
(quarter box)

F.E. MESH

Fig 3·13 Elastic stress distributions (b/l = 1)
comparison with finite element solution

effectively loaded under a controlled shear strain.   Consequently, the shear stresses along a flange edge can increase after yield has spread over the whole edge.   This is achieved by plastic flow of stresses under constant equivalent stress with a simultaneous reduction of the other stress components.   These shear stresses should nowhere exceed the value corresponding to von Mises yield stress in pure shear $(\sigma_o/\sqrt{3})$ but errors must be expected due to the discrete nature of the numerical approach.

However, acceptable results can still be obtained with practical mesh sizes.   This is illustrated in Fig. 3.14 where the distributions of shear and longitudinal stresses on the edge of the tension flange of a $b/\ell = 1$ box are represented up to an average edge strain of 1.5 times yield strain.
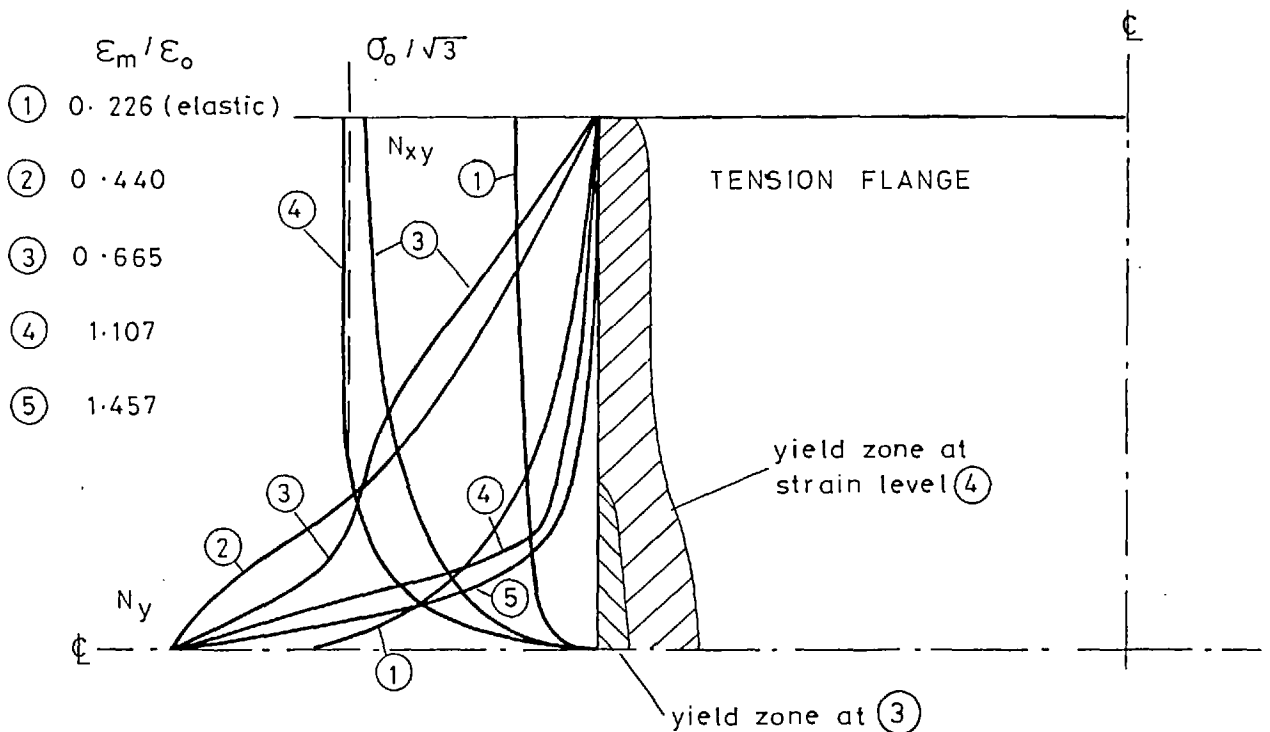
Fig. 3.14   Stress distributions on edge of tension flange; $b/\ell = 1$, $b/t = 60$ (elastic webs - see also Fig. 4.4)

WEB

COMPRESSION FLANGE

N_y along
web-flange
connection

$\propto = 0$
$b/l = 1$
$b/t = 100$

N_y at mid span

——— 16 × 17 nodes on flanges
8 × 17 nodes on webs
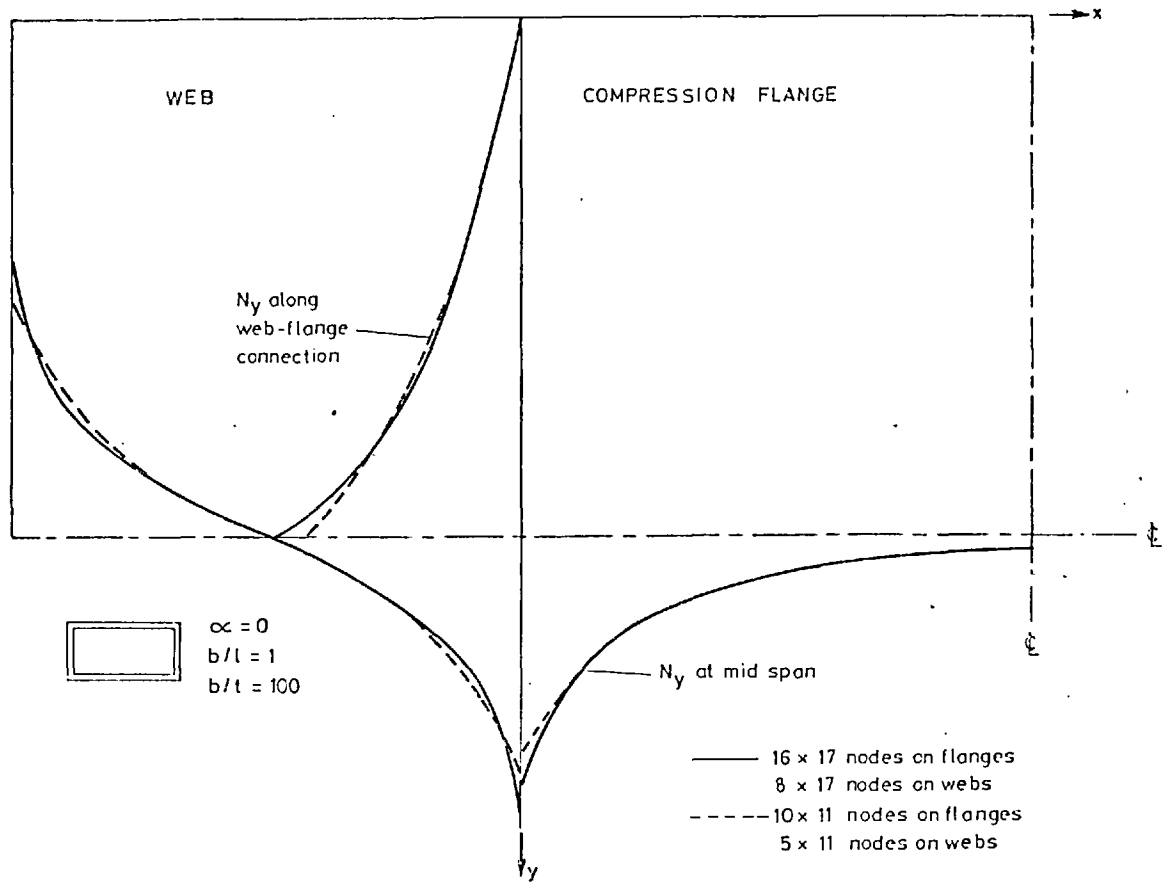- - - - 10 × 11 nodes on flanges
5 × 11 nodes on webs

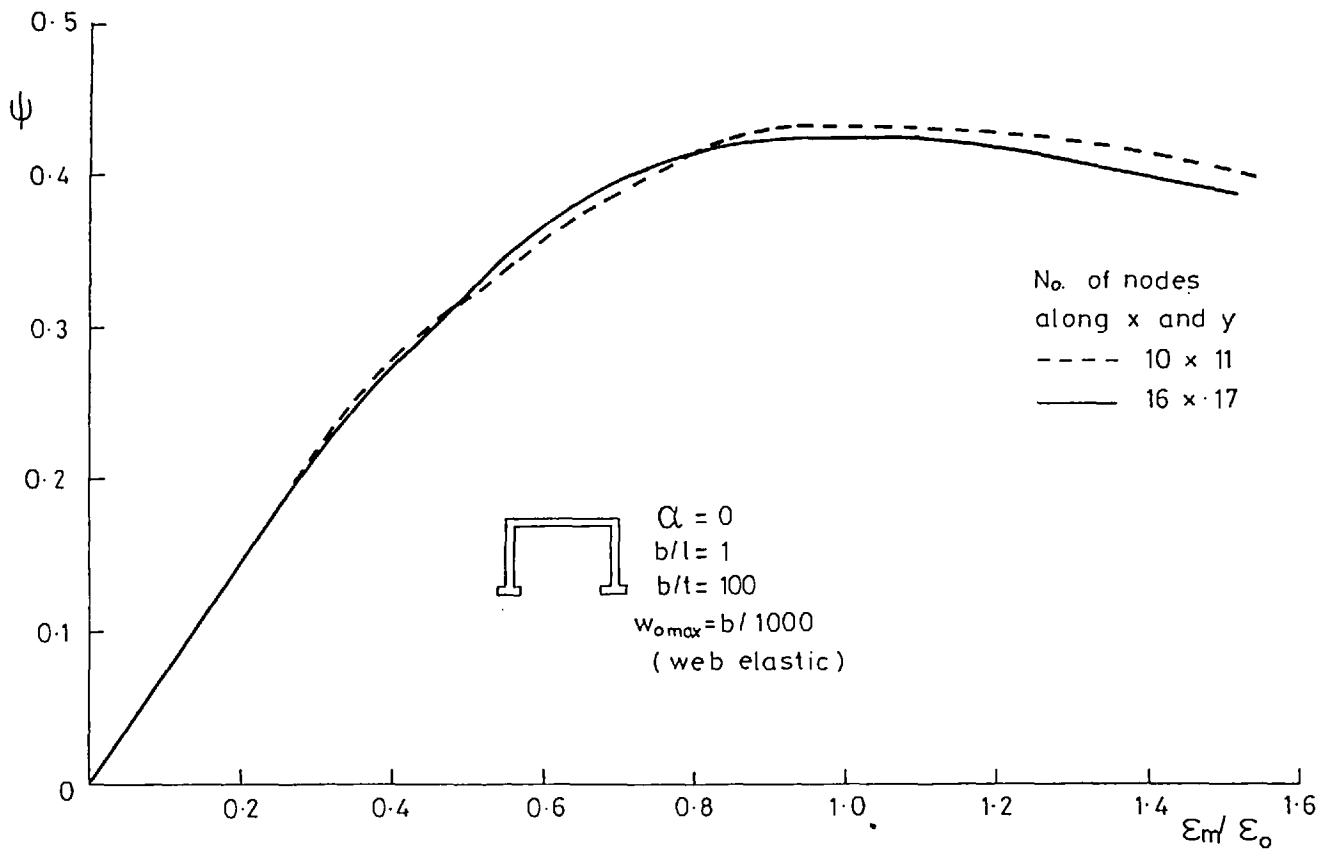Fig. 3.15 Effect of singularities on the stress distributions

Fig 3·16 Mesh size study

3.5.3 Effects of the Singularities and Mesh Size Study

The presence of the singularities at mid-span at the web-flange junction, discussed in section 2.5.4, is detected numerically by the continuously increasing peak stress values when the mesh sizes are refined. However, the effects of these stress concentrations on the overall stress distributions are very localised. Figure 3.15 shows the variation of elastic longitudinal stresses across the flange mid-section and quarter-length section for two different mesh sizes. Although at the mid-span the peak stress value is relatively higher in the smaller mesh, away from this point the differences are negligible as might be expected.

Confidence in the use of this type of loading was confirmed when it was established that once yielding occurs near the stress concentration point the effects of the singularity are further diffused. This is illustrated by the small effect that a mesh refinement beyond a certain size, has on the ultimate strength of the flanges - see Fig. 3.16.

3.5.4 Influence of Simplified Assumptions for Stiffener Formulation

The principal simplifications introduced in the formulation of the plate-stiffener interaction are expressed in the "door hinge" type of connection between the two elements which was assumed while neglecting the effects of the torsion and the lateral bending of the stiffeners. Another important aspect in the treatment of the stiffeners refers to the end boundary conditions that were adopted in the present theoretical model. They were justified in detail in section 2.5.2 and correspond to assuming numerically that the stresses at the stiffener end cross sections are zero (i.e. $N_s = M_s = 0$) to simulate a stiffened plate edge simply supported and loaded (in axial compression cases) at the plate mid-plane level.

To assess the effects of these assumptions two different plates were analysed in compression using the present program and another developed by Webb [70] for an extensive study of stiffened plates. This is based on a stiffener formulation which follows more closely Djahani's [44] approach i.e. considering the effects of the elastic torsional rigidity and the lateral bending of the stiffeners. It uses the same FD and DR method of solution allowing a close comparison since the same mesh sizes can be chosen.

The dimensions of the first plate (Fig. 3.17) were selected to correspond to a case in which there is predominance of overall buckling in the collapse mode. The load is applied by displacing axially the plate end cross sections while keeping them straight and tangentially restrained ($u = 0$). At these sections, to compare with Webb's results, the longitudinal strain calculated at plate level over the stiffeners was firstly assumed to be transmitted to the whole stiffener cross section and the axial stresses were calculated accordingly. This corresponds (see section 2.5.2) to assuming that, although the curvature $\partial^2 w/\partial y^2$ is zero, there are external forces N_s and bending moments M_s (expressions (2.11) and (2.12)) at the stiffener end cross sections. The results obtained by introducing this approach in the present program show, as expected, a lower ultimate load compared with the solution [70] in which the stiffener torsional rigidity and lateral bending are considered. The small differences between the two solutions (represented by the two upper curves in Fig. 3.17) indicate that it is valid to neglect these effects in the case of stiffeners of rectangular cross section.

If these solutions are compared with the results obtained

Fig. 3.17   Stiffened plate in axial compression.   Effect of neglecting
torsion and lateral bending of stiffeners and influence of
end boundary conditions
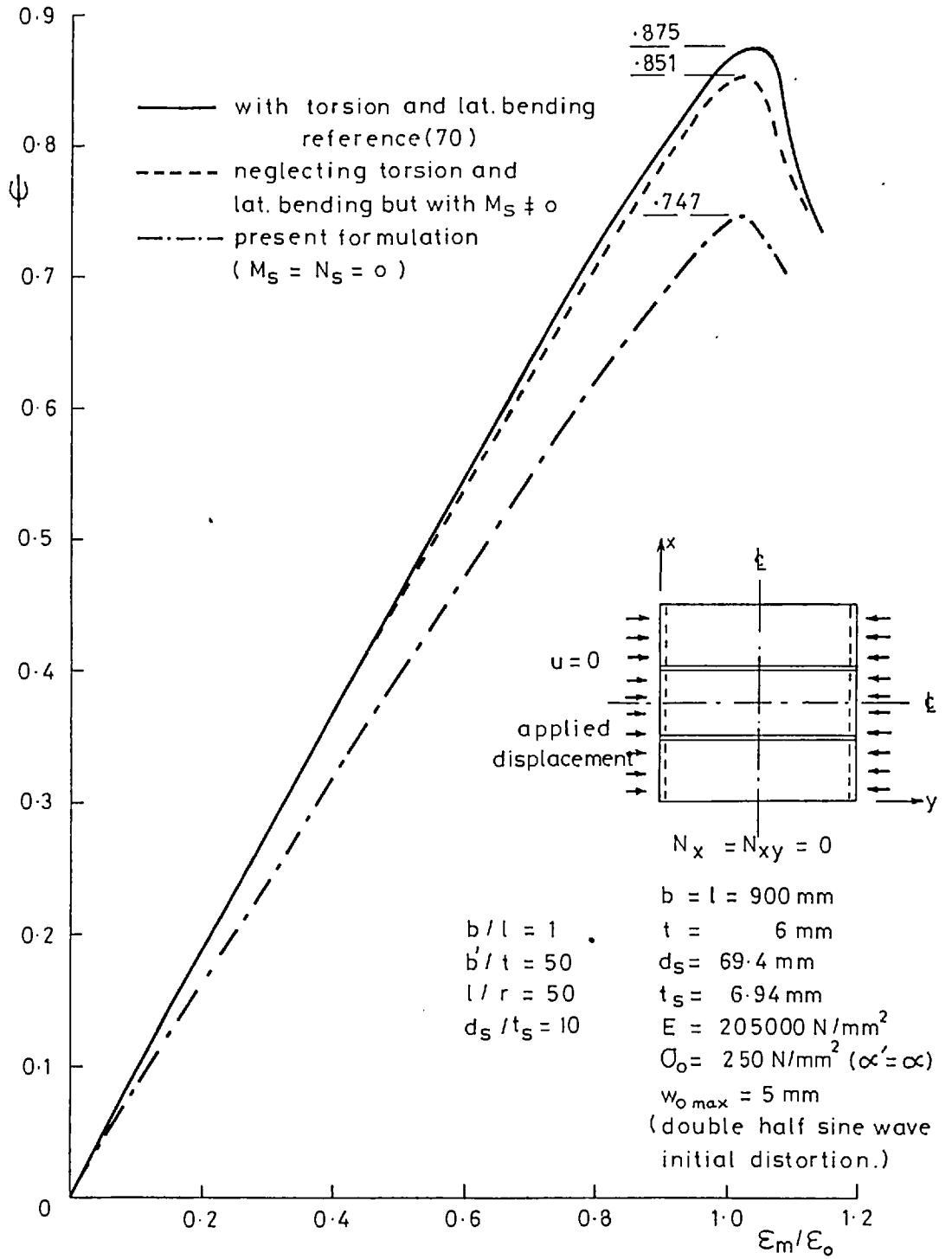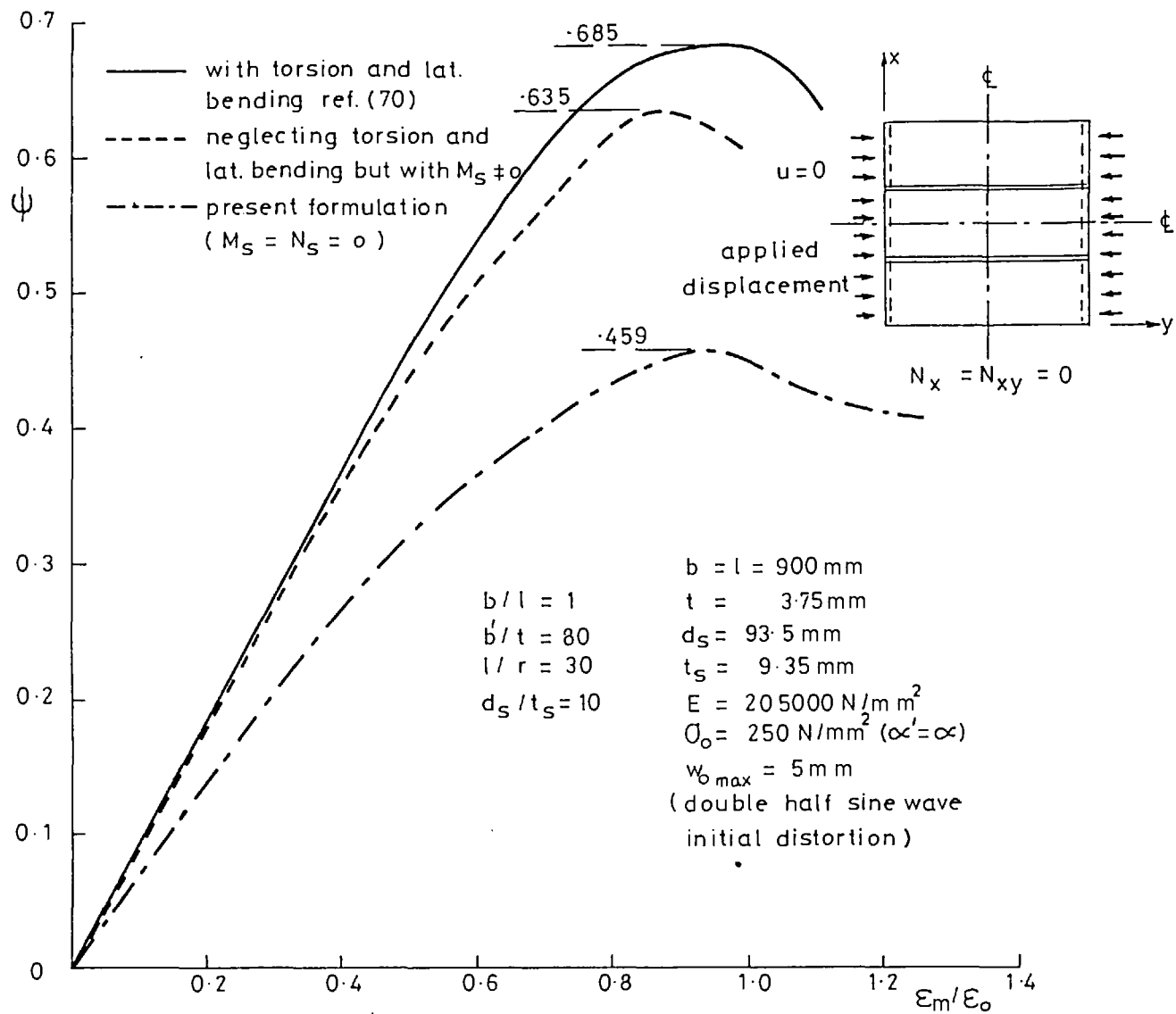
Fig. 3.18   Stiffened plate in axial compression.   Effect of neglecting
torsion and lateral bending of stiffeners and influence of
end boundary conditions

assuming $N_S = M_S = 0$ at the stiffener end cross sections, the differences in behaviour are substantial. This approach corresponds to always maintaining the applied axial load at the plate level whereas, in the first cases, this level is not controlled and varies with loading history. However, as overall buckling is in this case predominant, the mode of failure is not changed by the presence of the bending moments M_S.

In the other stiffened plate used for a similar comparison the cross sectional dimensions (Fig. 3.18) were chosen to increase the stiffener bending rigidity and the plate slenderness. When N_S and M_S are not assumed to vanish at the stiffener ends the collapse mode is associated with small deflections of the stiffeners and the plate panels buckle into nine alternate upwards and downwards bows. The effects of the stiffener torsional rigidity should be more important in this case and this is reflected in a bigger difference between ultimate strengths obtained using Webb's[70] and the present formulation i.e. 0.685 and 0.635, respectively. In this case however, to assume $N_S = M_S = 0$ at the stiffener end cross sections changes the mode of collapse. This assumption increases the influence of the overall buckling mode component and the collapse is associated with the formation of plastic hinges on the stiffeners at the mid-length cross sections. The ultimate strength is drastically reduced to 0.459 which corresponds to a difference of 33% between the two extreme solutions. As discussed in section 2.5.2 the results obtained maintaining N_S and M_S always zero at the ends of the stiffeners should be considered as lower bounds to the flange strength. They seem however to be more reliable for comparing with the behaviour of flanges under the shear lag effects which are effectively loaded along the longitudinal edges at plate level on the assemblage of flange and webs.

3.5.5   Comparison Between Different Assumptions in the Plasticity

        Formulation

The differences between the single-layer and the multi-layer approaches for considering plasticity effects are illustrated in Fig. 3.19 for a plate in axial compression. This case has already served for comparison between different numerical solutions, finite elements and FD, obtained respectively by Crisfield[40] and Harding[35]. The single-layer solutions produce, as discussed in section 2.1 higher ultimate strengths and more pronounced peaks due to a delayed deterioration of stiffness since detection of surface yielding is not possible. For the same reason, the unloading path obtained from this approach is also more abrupt but an acceptably good agreement can be obtained.

The two approximations to Ilyushin's yield surface designated in section 2.4.2 by Ilyushin I (expression (2.22)) and II (2.24) were tested on the same unstiffened plate in axial compression and on compression flanges of point loaded box girders. The results of these tests are illustrated in Figs. 3.20 and 3.21. ·Some small differences on the average stress-strain curves were noticed but for all the cases tested the values of ultimate strengths were not significantly changed.

In the case of the plate in axial compression (Fig. 3.20) the post-ultimate strength unloading is less pronounced using Ilyushin II. This seems to indicate, as suggested in section 2.4.3, that the main differences in the use of the two approximations should be found in the calculation of tangential rigidities rather than in the assessment of first yield. The better agreement of the Ilyushin II unloading path with multi-layer solutions (see Fig. 3.19) confirms the more reliable characteristics of this yield function. However, the differences in
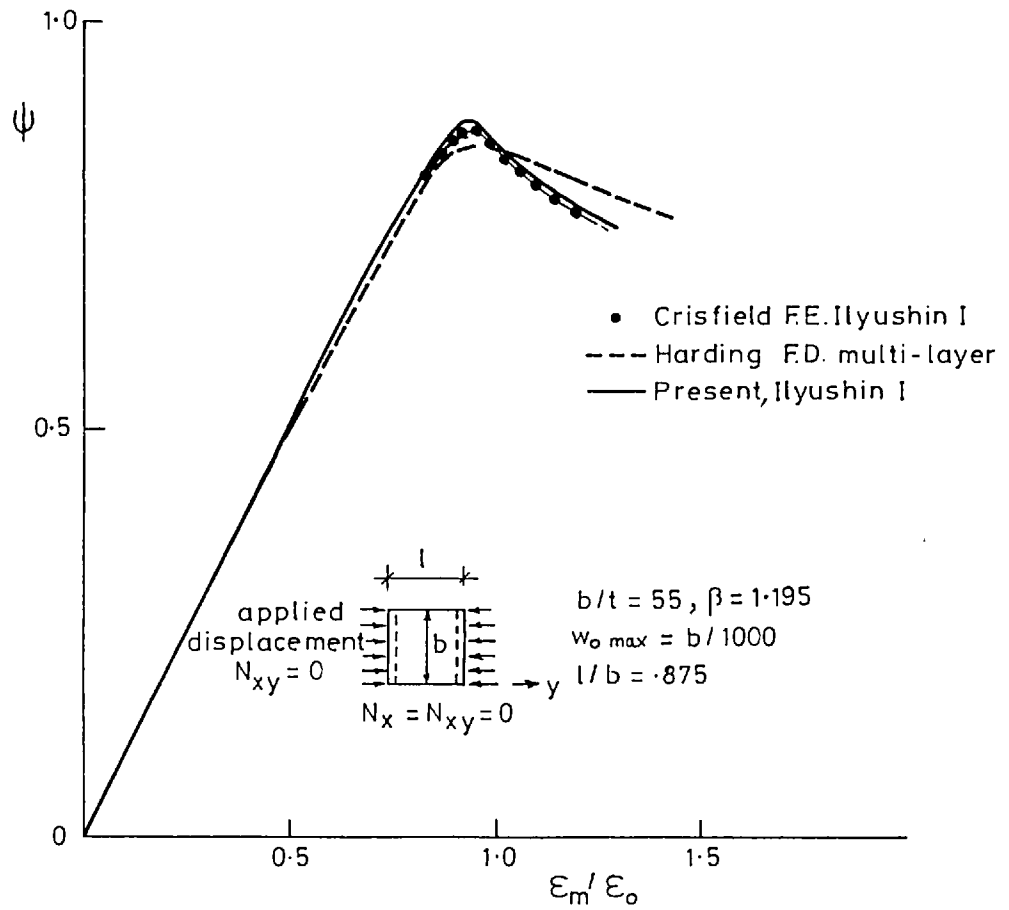
Fig 3·19 Unstiffened simply supported plate under
uniform compressive displacement.
Comparison with other solutions
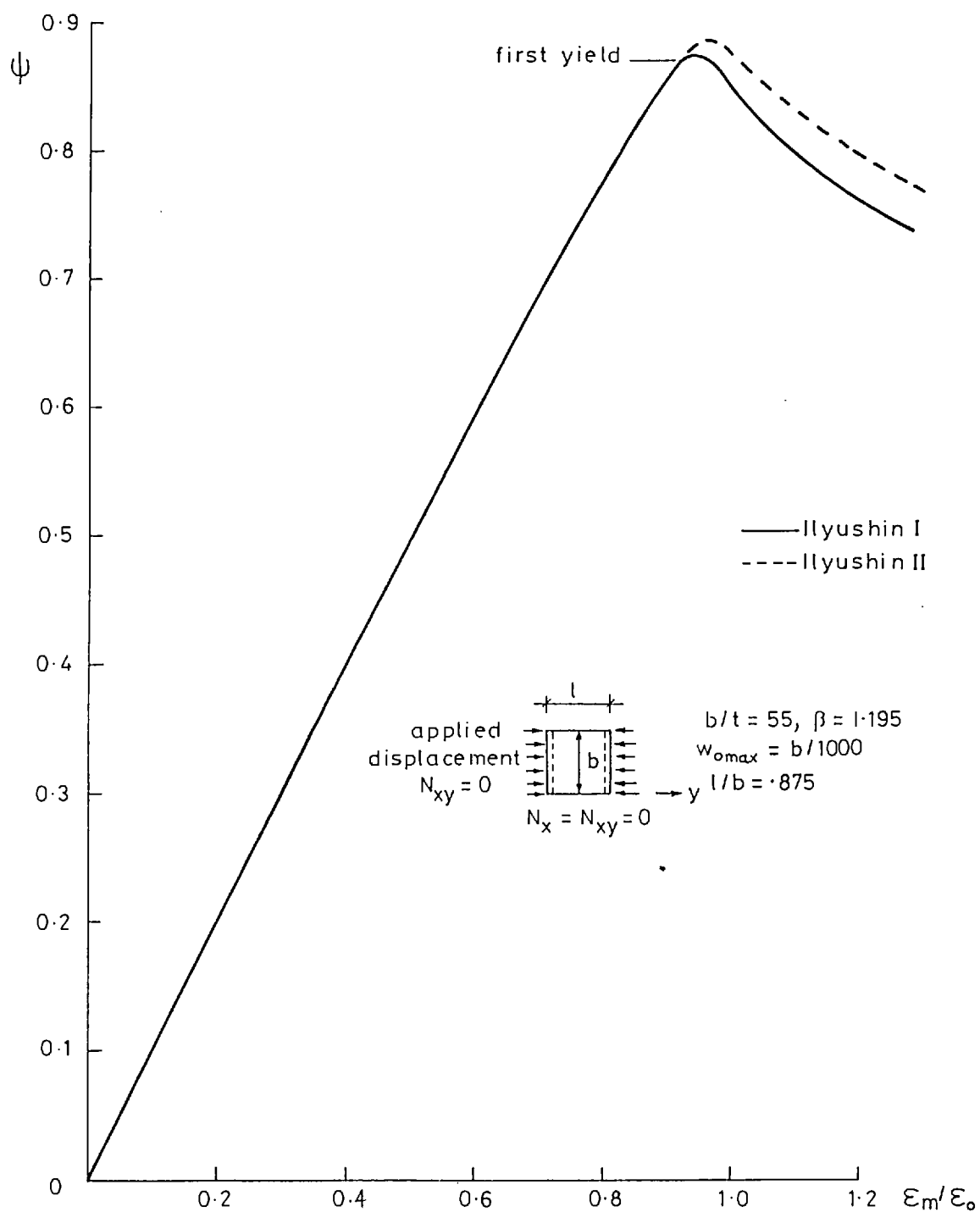
Fig 3·20 Use of different yield functions in the study
of isolated plate in axial compression
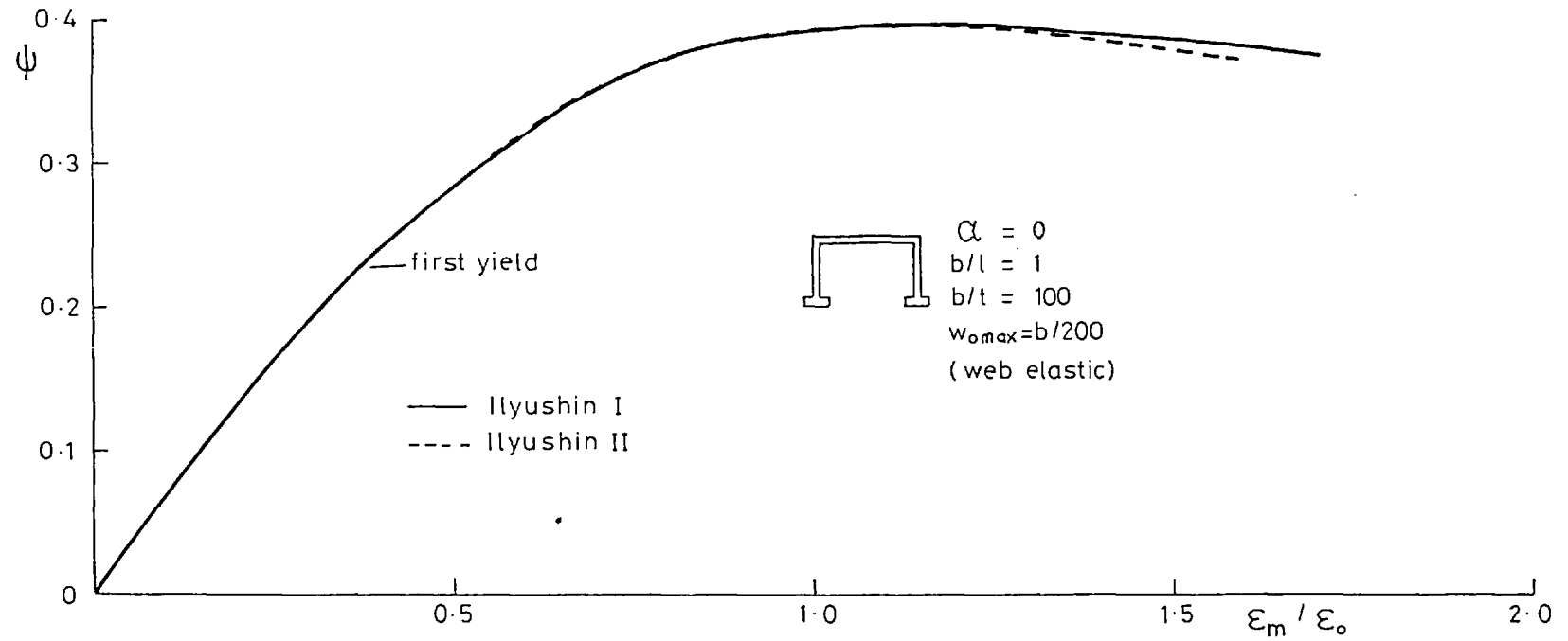
Fig 3·21 Comparison between different yield functions

the unloading paths in Fig. 3.21 might suggest the reverse conclusion but, as they are so small they should not be considered for this appraisal.

Although Ilyushin II should be more reliable, it was mainly utilised as a checking on the use of the Iluyshin I function which was the first to be considered in the program. This one was also the yield criterion more experimented with in previous plate analysis[40][42].

CHAPTER 4

FLANGE MODES OF FAILURE

4.1   RELEVANCE TO LIMIT STATE DESIGN

It was pointed out in the Introduction that the elastic performance of a flange in a shear lag context is generally confined to a reduced level of loading. The high stress concentrations near the web-flange connection at a point loading cross section induce early yielding around these regions. To define a serviceability limit state as the attainment of first yield would be in general a too severe requirement. Dowling et al.[28] identified a criterion for dispensing with the yield condition at service loads in stiffened flanges under shear lag effects. This referred to the development of permanent deformations in the components near the web-flange junctions. The serviceability aspects of the flange behaviour under load are not covered in this thesis which is mainly concerned with the conditions related to the collapse limit state. However, the information provided later may be used by code drafters to help with the formulation of suitable procedures to deal with that limit state.

In the simply supported model under mid-span point loading, the overall collapse mode is associated with the ultimate moment of resistance of the loaded cross section. Whatever assumptions are made regarding the behaviour of the individual plate components, it is normal to expect that some redistribution of longitudinal stresses within the cross section will take place. This process normally involves the mobilisation of the capacity of the flanges to resist bending while the

webs are mobilised to carry shear. Theoretically, such redistribution can continue until either the compression flange or the webs ultimate strengths are reached. These capacities can be obtained separately but must be combined for equilibrium in assessing the girder ultimate load. Compatibility of deformation of the plate components at collapse has to be verified. Interaction between the web and the flange modes of failure must also be taken into account. This interaction can be expected to alter the carrying capacity of the individual plates if these latter strengths are estimated on the basis of commonly used boundary conditions.

A common approach used to calculate the collapse limit state of box girders[15] consists of assuming that the bending moments are ultimately resisted by the flanges and the webs are designed to carry shear alone. To use the ultimate capacities of the flanges and webs in such an approach is appropriate when they approximately correspond to the same collapse load. However, it is mainly in these cases that safeguards against web-flange buckling interaction have to be considered.

As discussed in Chapter 2, the theoretical model was simplified to separate the flange behaviour from web buckling. This is reflected in the modelling of the web-flange connection and in the description of the web behaviour. The analytical model does not allow consideration of the out-of-plane deflections of the web and the ultimate capacity of these components is thus only associated with in-plane yielding. The interaction between web and flange modes of failure was therefore investigated within these limitations.

The present research was, however, focussed on the behaviour of the flanges rather than that of the girder as a whole. By assuming that the web material has a high yield stress, or indeed is very much thicker than the flange, it is possible to model situations where the web shear

capacity does not place any restriction on the maximum longitudinal force the flanges can resist. The flange ultimate capacity obtained in this way can be directly used in the calculation of the maximum moment of resistance. The use of the design approach described in the third paragraph, in any case, neglects the web contribution to bending strength. Depending on the relative strengths of the two components this can be a very conservative approach and thus requires careful consideration in cases where the web's contribution to bending strength may be large.

The ultimate capacity of the flanges will be measured by the maximum value of the inelastic effective width ratio ψ at mid-span (expression (1.3)). When studying a flange (under no limitations imposed by the web strength), redistribution of the longitudinal stresses takes place, beyond the elastic limit, within the cross sections of the flanges. This corresponds to a reduction in the non-uniformity of the elastic shear lag stress distributions through material yielding. The degree of redistribution achieved in this mechanism at collapse can be estimated by comparing the maximum value attained by ψ with the inelastic buckling effective width of the flange plate in axial compression. For this, the buckling load was computed using the same numerical program to consider the compression flange in isolation, simply supported at the four edges and loaded by axially displacing the end edges while keeping them straight. Strain control along the longitudinal edges is lost in this analysis of plates in isolation, in contrast with the situation relating to the same edges in a box girder assemblage. This should result in a more pronounced post-ultimate unloading of isolated slender plates in comparison with the behaviour of similar flanges of box girders. This has been experimentally verified by Dowling et al.[28]

when testing box girders in a pure bending moment situation. However, the purpose of the numerical analysis of isolated flanges is only to compare ultimate capacities and in these values the influence of the unloaded edge conditions is small.

So far, the two types of stress redistribution discussed refer to the ultimate bending resistance of the critical cross section and occur within it. These are the only possible mechanisms of redistribution which are studied with the present simplified model. Redistribution processes associated with web buckling are not included but should be studied in any subsequent extension of this research.

In the case of girders with continuity over more than two supports, redistribution of overall bending moments is posible due to plastic hinge deformations at critical cross-sections. This must also affect the simple mechanisms of stress redistribution investigated in this thesis and possibly invalidate the extrapolation of the results obtained for simply supported girders to cases where continuity exists.

In the elastic regime it is often accepted that each portion of a girder between adjacent sections of zero moment can be treated as an equivalent simply supported beam. The possibility of using this approach to evaluate the elastic shear lag effects over continuous girders was investigated by Moffatt and Dowling[13]. These authors suggested that, in cases of statically indeterminate girders, the distribution of overall bending moments can be done on the basis of a fully effective width. Based on results for simple bending moment distributions they proposed formulae for calculating effective width ratios over the various parts of the continuous girder.

In the context of ultimate limit state it will be shown, for

the simply supported girder case, that the flange ultimate strength depends on the geometric parameter b/ℓ. Assuming that the cross-sectional ultimate moment of resistance can be calculated on the basis of the flange strength alone, this dependence indicates that, when full redistribution is not possible, the moment of resistance is not solely dependent on cross-sectional properties. Therefore, the application of the general theory of plastic hinge mechanisms to the failure of continuous box girders is a complex problem.

4.2 UPPER BOUNDS TO FLANGE ULTIMATE STRENGTH

In the following sections some possible modes of failure of symmetric compression flanges of girders under point load are identified. Corresponding upper bounds to their capacity are also estimated.

4.2.1 Flange Capacity Limited by Web Shear Strength

The main external forces acting on the flanges considered in isolation, Fig. 4.1a, are the shear stresses transmitted by the webs. To consider only these stresses corresponds to heglecting in the analytical model the vertical supporting reactions at the four compression flange edges and, in a real structure, the rotational and in-plane restraints in the connections to the webs and end diaphragms.

The total longitudinal in-plane force on the flanges at any cross section must be in equilibrium with these stresses. For half a box beam the resultant of the shear stresses at each edge (the shear flow) can be represented by T_f, Fig. 4.1b. Using expressions (1.3-5) longitudinal equilibrium of the compression flange gives

$$\psi = 2T_f/\sigma_{ocf}A_{cf} \qquad\qquad 4.1$$

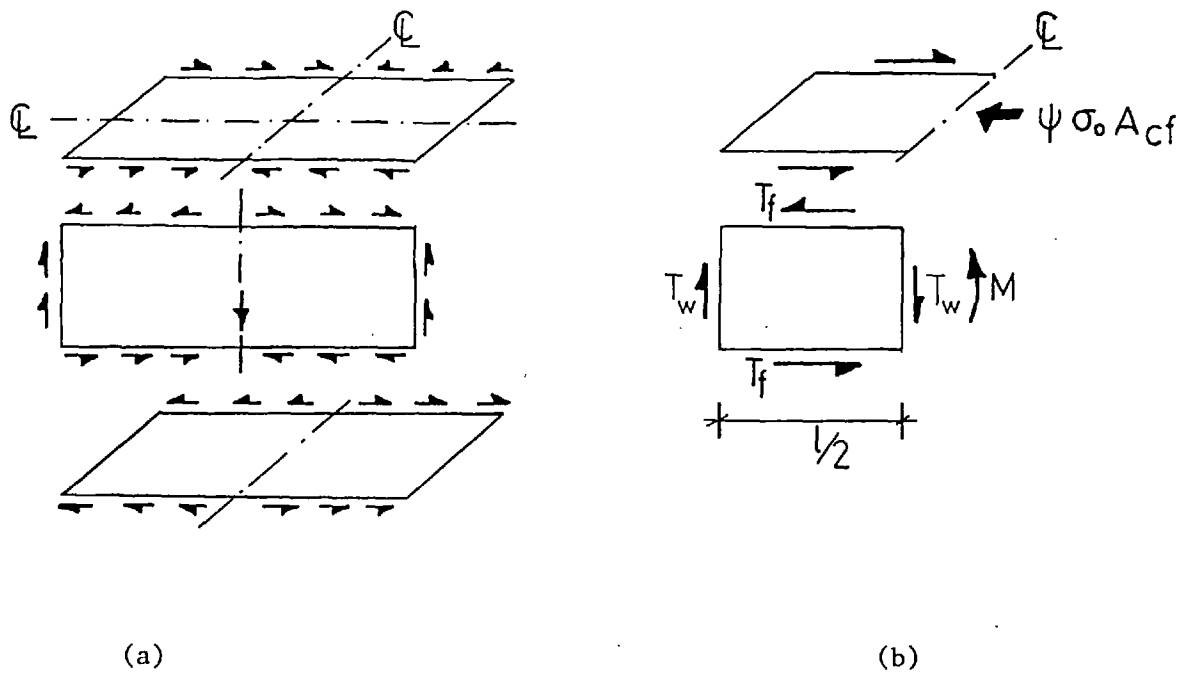(a)   (b)

Fig. 4.1   Flange equilibrium

This indicates that the flange strength is limited by the maximum shear flow that can be transmitted through the longitudinal edges. The shear flow in turn is limited either by the web shear strength or the shear capacity of the flange edge.

In the present model the ultimate strengths of the web and of the tension flange are governed by plane elastic-plastic considerations. Generally, the initial state of stress along the longitudinal edges of both the web and the flanges includes all stress components. After the onset of plasticity in displacement controlled loading cases plastic flow of these stresses under constant equivalent stress will increase the shear at the expense of the other components. Considering the web edge an upper bound to the value of T_f can be identified corresponding to von Mises yield stresses in pure shear along the entire edge i.e.

$$T_f < \frac{\sigma_{ow}}{\sqrt{3}} \frac{t_w \ell}{2} \qquad\qquad 4.2$$

Hence, for the compression flange

$$\psi < \frac{\sigma_{ow}}{\sqrt{3}} \frac{t_w \ell}{\sigma_{ocf} A_{cf}} \qquad\qquad 4.3$$

The squash load of the whole flange $(\sigma_{ocf} A_{cf})$ can be expressed in terms of the plate contribution using equation (1.10). Substituting this expression, inequality (4.3) can be conveniently presented in terms of the shear lag parameter b/ℓ and the equivalent stiffening factor α', (1.9) as follows

$$\psi < \frac{1}{\sqrt{3}} \frac{\sigma_{ow}}{\sigma_{op}} \frac{1}{1+\alpha'} \frac{t_w}{t} \frac{1}{b/\ell} \qquad\qquad 4.4$$

For plate, stiffeners and web of the same material $(\sigma_{ow} = \sigma_{op}$ and $\alpha' = \alpha)$ expression (4.4) takes the simplified form:

$$\psi < \frac{1}{\sqrt{3}} \frac{1}{1+\alpha} \frac{t_w}{t} \frac{1}{b/\ell} \qquad\qquad 4.5$$

For equilibrium of half a web panel considered in isolation, Fig. 4.1b, the shear flow T_f must be in equilibrium with the shear force T_w and the bending moment M at the mid-span cross section. The upper bound on T_f given by expression (4.2), also corresponds to a maximum yield shear value for T_w if M is assumed to vanish under plastic redistribution of stresses. In the cases where the flange capacity is limited by the web strength, it is appropriate to calculate the ultimate moment of resistance on the flange contribution alone using the following expression

$$M_{ult} = \psi_{max} \sigma_{ocf} A_{cf} d \qquad\qquad 4.6$$

$$\psi = \frac{1}{\sqrt{3}} \frac{t_w}{t} \frac{1}{b/l}$$
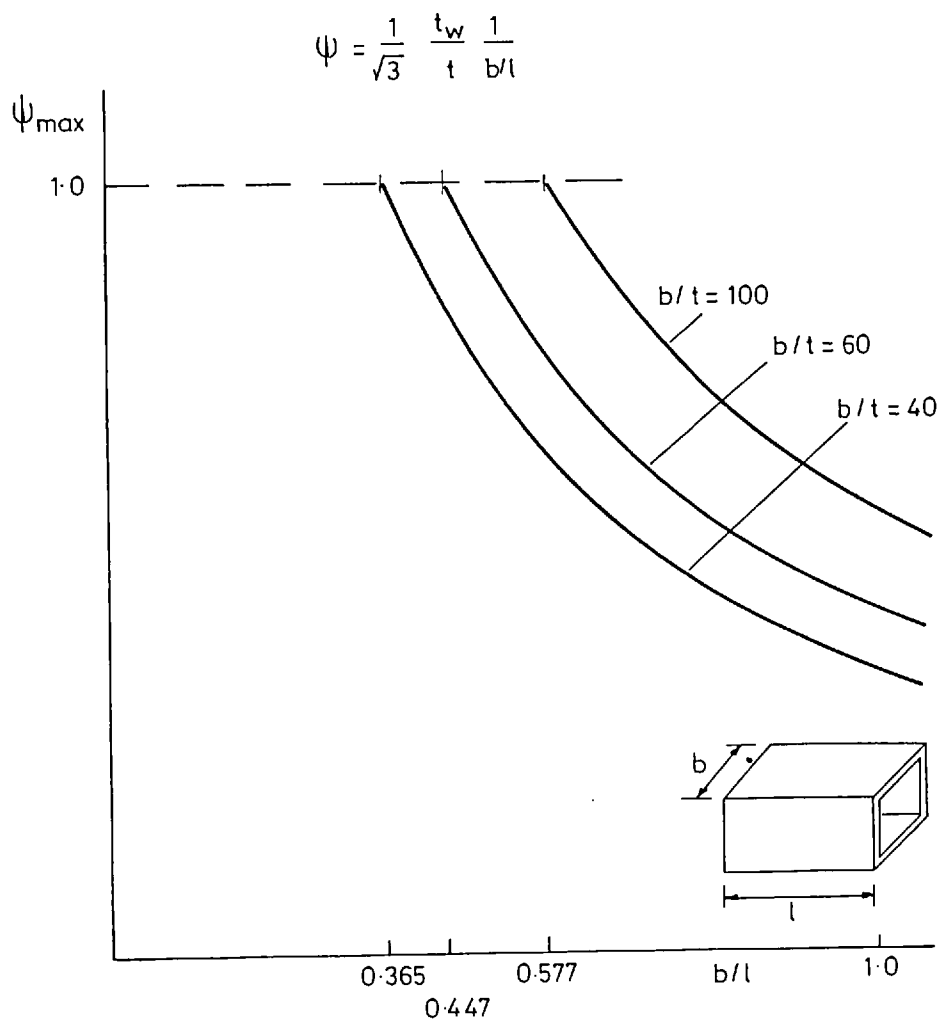

Fig 4·2 Flange capacity limited by web shear strength ($\alpha = 0$)

. For a fixed ratio of thicknesses and a value of α, the upper bounds to the flange capacity, given by the right hand side of inequality (4.5), are hyperbolic functions of b/ℓ. These are illustrated in Fig. 4.2 for unstiffened flanges (α = 0) and for the t_w/t ratios corresponding to the various flange plate slendernesses (b/t) considered in the parametric study. It should be noted for later reference that b/t = 100 corresponds to t_w/t = 1, for the dimensions selected for the numerical examples (see section 5.2). Similar curves could be traced, for example, by fixing t_w/t and considering different values of α.

The significane of these upper bounds will be discussed in section 4.3 together with numerical examples to help interpret their practical applications.

It is reasonable to expect that similar expressions may be derived for an upper bound to the flange capacity when allowance is made for web buckling. From tension field theory the web ultimate shear capacity is dependent on the flange properties but an upper bound estimate should always be possible.

4.2.2   Flange Capacity Limited by Flange Shear Strength

Another upper limit on T_f is given by a similar plastic maximum shear capacity of the flange edge. If this is to govern, and the influence of bending effects is neglected, this capacity can be assumed to correspond to von Mises yield stress in pure shear along the edge of the flange. Then,

$$T_f < \frac{\sigma_{op}}{\sqrt{3}} \frac{t\ell}{2}$$ (4.7)

Substituting in (4.1) gives

$$\psi \quad < \quad \frac{\sigma_{op}}{\sqrt{3}} \ \frac{t\ell}{\sigma_{ocf}A_{cf}} \qquad\qquad 4.8$$

Again, expression (1.10) can be used to relate the flange squash load to the plate squash load to obtain after simplification:

$$\psi \quad < \quad \frac{1}{\sqrt{3}} \ \frac{1}{1+\alpha'} \ \frac{1}{b/\ell} \qquad\qquad 4.9$$

The value of the plate thickness does not appear in this inequality which is also independent of material properties if the plate and stiffeners are made of the same material, that is, $\alpha' = \alpha$. In this case,

$$\psi \quad < \quad \frac{1}{\sqrt{3}} \ \frac{1}{1+\alpha} \ \frac{1}{b/\ell} \qquad\qquad 4.10$$

This expression of the new upper bound to the values of ψ is again represented by a hyperbolic function of b/ℓ. This coincides with the function derived from expression (4.5) when the web and the flange plate have the same thickness. For such cases the curves of Fig. 4.3 represent both upper bounds (those given by (4.5) and (4.10)). Among the unstiffened flanges used as examples this happens for the case of $b/t = 100$ as referred to before. For the other slendernesses studied $t_w/t < 1$ and consequently they correspond to cases where the flange capacity is limited by the web shear strength.

No reference was made in the derivation of these upper bounds to the effects of residual stresses. If the residual stresses can be assumed not to involve shear stressing of the flange edges, their presence near these edges (where they are normally tensile) should not affect the possibility of ultimately reaching yield stress in pure shear along
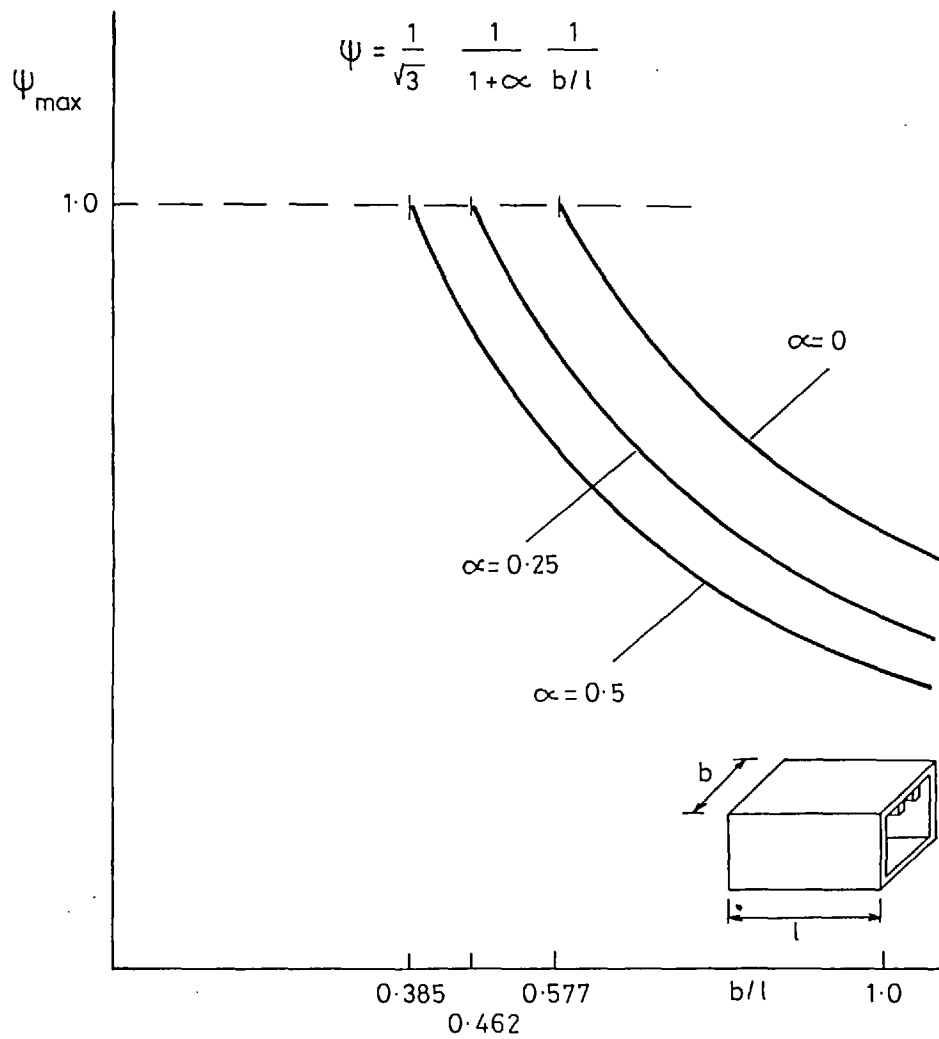
Fig 4·3   Flange capacity limited by flange shear strength

them. Thus, the theoretical maximum values of ψ derived above should still apply. No investigation of the validity of this suggestion was however attempted and the effects of residual stresses were not considered.

It was mentioned for the web in the previous section that out-of-plane deflections can be expected to reduce its maximum shear capacity in comparison with the assumed yield value. Similarly, in a real stiffened flange, the capacity of the plate panels adjacent to the edge to transmit shear must be reduced by buckling interaction. This should depend on the panel slenderness, the rotational restraint from the web and the torsional rigidity of the nearest stiffeners. The present numerical model does not consider these rotational effects and is thus not specially suited for investigating the shear capacity of slender edge panels. However, a few examples will be presented which show a considerable reduction in flange strength compared with the values predicted by the present upper bounds. This must be caused by the reduced capacity of the flange edge panels to transmit shear due to buckling. This ultimate capacity is reached by a combination of shear and varying compression along the length of the panels.

4.2.3   Flange Capacity Limited by Flange Compression Strength

Another obvious upper bound is the full squash load of the flange, i.e.

$$\psi \ \leqslant \ 1 \qquad\qquad\qquad 4.11$$

It intersects the hyperbolas of expression (4.10) at $b/\ell = 0.577$ (or $1/\sqrt{3}$) if $\alpha = 0$; $b/\ell = 0.462$ if $\alpha = 0.25$ and $b/\ell = 0.385$ for $\alpha = 0.5$ (see Fig. 4.3). This shows that the maximum efficiency of even a very stocky flange can never be attained for aspect ratios b/ℓ greater than the values quoted. Many real stiffened flanges have values of α (or α') greater than 0.5 which means that the limitation imposed by the edge shear strength may occur for realistic flange sizes.

The development of out-of-plane deflections in a real flange influences its maximum compressive strength. Thus it is necessary to consider, a more severe upper limit associated with collapse in inelastic buckling rather than the squash load. The presence of residual stresses must certainly now influence the value of this limit but, as stated before, these were not considered in the present research.

4.3   INFLUENCE OF THE UPPER BOUNDS ON FLANGE BEHAVIOUR

4.3.1   Numerical Examples

The upper bounds to the flange capacity were derived from plane-stress considerations regarding the shear strength of the web-flange connection and theoretical conditions of plastic stress flow. Under displacement controlled point loading, these conditions can be numerically reproduced. The influence of these upper limits can be illustrated with a few examples.

The first examples chosen refer to a closed box girder with $b/\ell = 1$ and unstiffened flange plates ($\alpha = 0$) with $b/t = 60$. The choice of dimensions followed the general criteria described in Section 5.2.

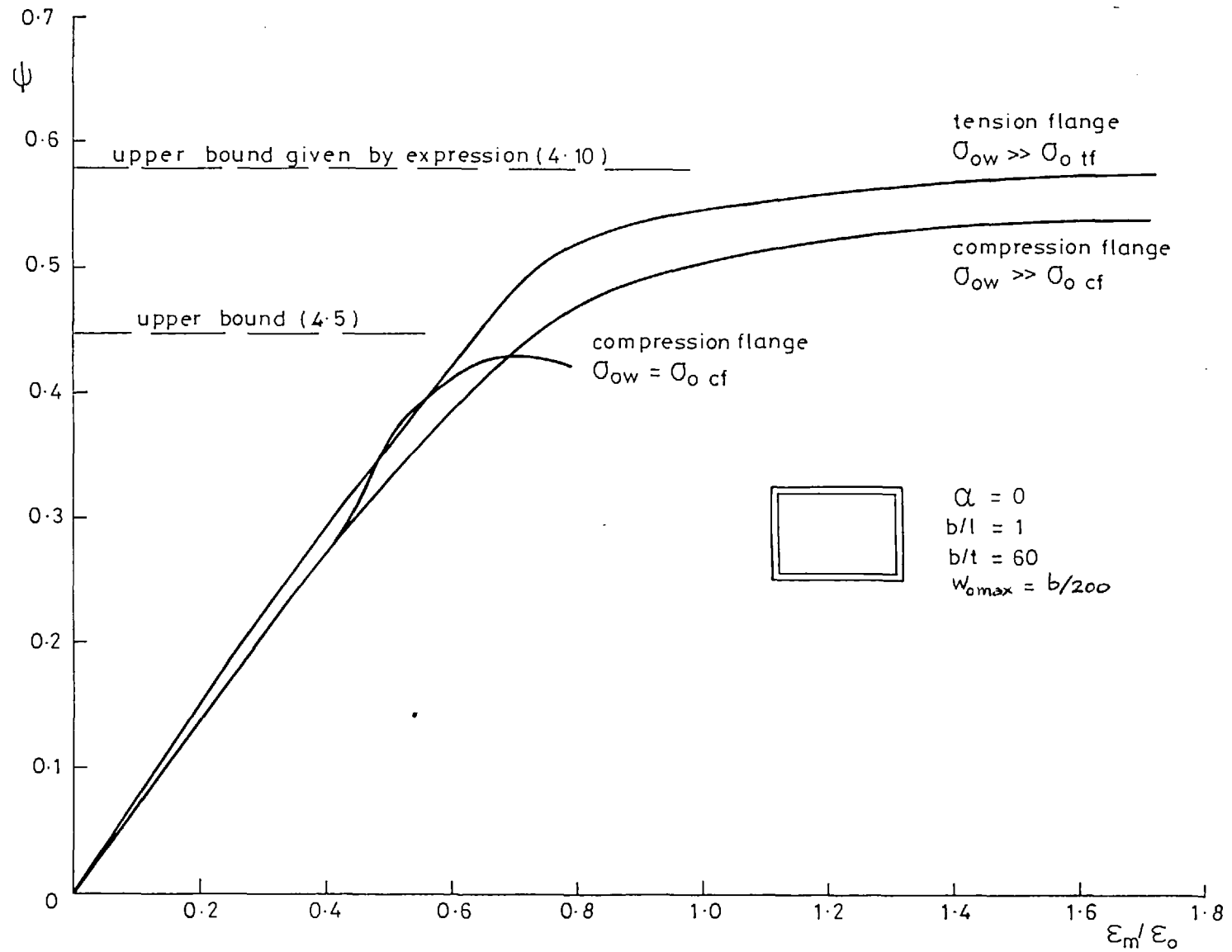For this slenderness $t_w/t = 0.774$ and, for web and flanges of

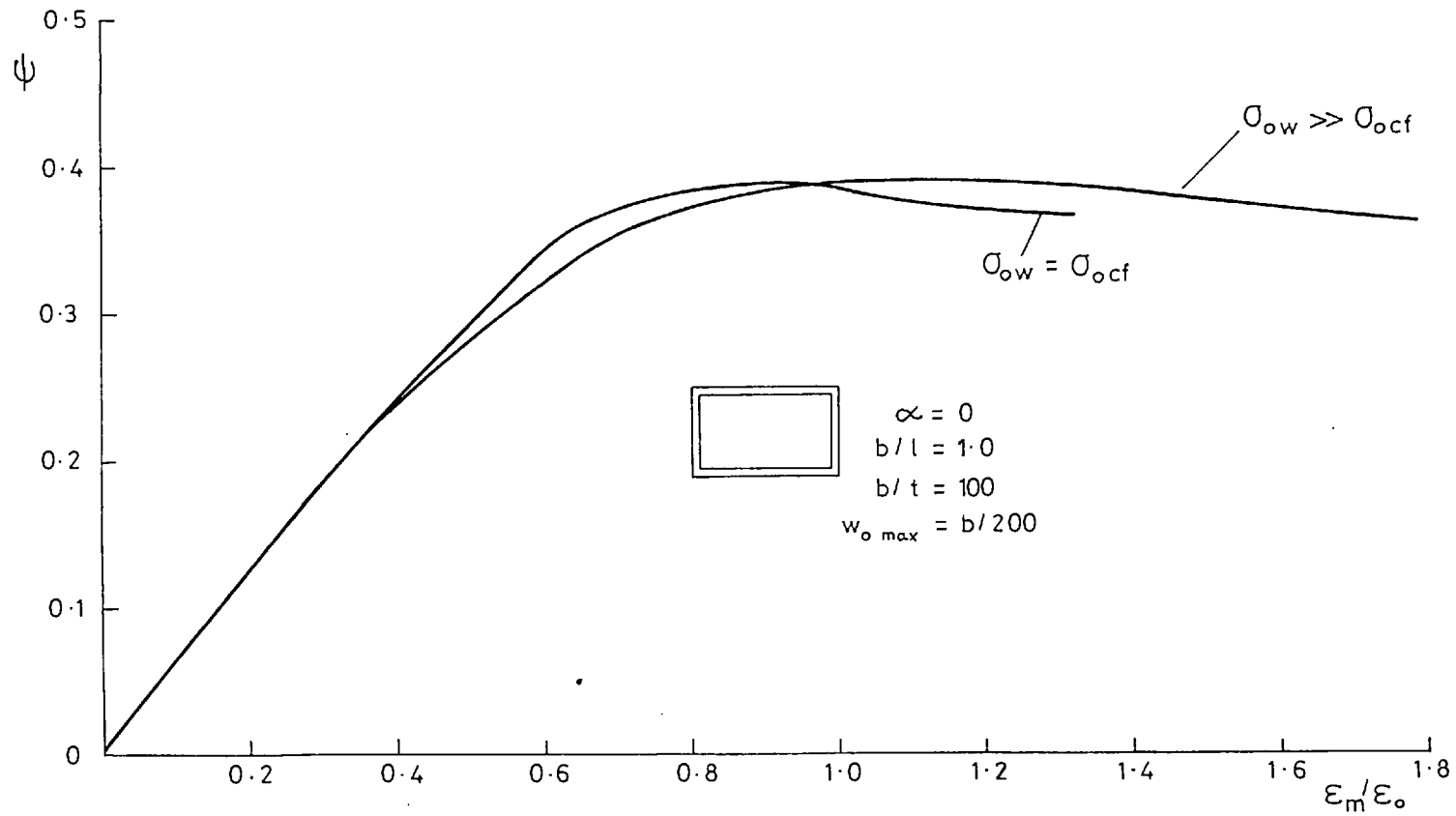Fig 4·4   Influence of upper bounds on flange behaviour

Fig 4·5   Influence of upper bounds on flange behaviour

the same material, the web shear strength should govern. According to expression (4.5) $\psi < 0.447$ (see Fig. 4.2).

By assuming the web material to have a very high yield stress ($\sigma_{ow} \gg \sigma_{ocf}$ or σ_{otf}) the influence of the two upper bounds can be reversed and the flange edge strength made to govern as in expression (4.10). In this case $\psi < 0.577$.

When $\sigma_{ow} \gg \sigma_{otf}$ the tension flange (plane-stress analysis) shows (Fig. 4.4) that a maximum tension force closely approximating the theoretical upper bound value is reached. The mesh size and the other approximations inherent in the discretization technique described in Chapter 3 are responsible for ψ values exceeding somewhat the value of 0.577. This was discussed before since this example has already been used to illustrate in section 3.5 the modelling of the flow of stresses along the web-flange edges in high shear straining.

The compression flange behaviour is represented in the same figure with two different assumptions for the web material: $\sigma_{ow} \gg \sigma_{ocf}$ and $\sigma_{ow} = \sigma_{ocf}$. In the first case the upper limit of 0.577 is not attained due to some buckling interaction. In the second case, the web shear strength restricts the flange capacity from reaching the maximum compression that the flange's own characteristics would allow and this is traduced in a completely different flange behaviour. The values of ψ do not now exceed the 0.447 theoretical maximum. Beyond the maximum strength the values of ψ reduce considerably. This is due to the straining of the longitudinal edge being accompanied by a very rapid increase of vertical displacements of the web-flange connection following plastic deformation of the web.

These deflections induce flange buckling at a much lower mean edge strain

than in the previous case thus causing the fall-off of ψ values.

The same effect is illustrated in Fig. 4.5 for a $b/t = 100$ flange. For this slenderness the expression for the upper bounds (4.5) coincides with (4.10) if $\sigma_{ow} = \sigma_{ocf}$ since $t_w = t$. This means that the ultimate capacity should theoretically be the same in this case as when $\sigma_{ow} \gg \sigma_{ocf}$. Figure 4.5 indicates that this prediction is followed. The different post-peak behaviour is explained by the above interpretation of the plastic deflections when the web yields.

4.3.2 Discussion of Albrecht's Results

The numerical examples quoted indicate that the theoretical upper bounds derived in section 4.2 correspond to maximum flange capacities which should be reproducible in numerical plane stress analyses. The displacement controlled loading used in the present model plays an important role in ensuring that the plastic flow of stresses, required for mobilising that capacity, takes place.

It is therefore interesting to compare these conclusions with the results of the finite element plane stress study of closed box girders conducted by Albrecht[26] and mentioned in the Introduction.

$d = 1000\,\text{mm}$
$t = t_w = 10\,\text{mm}$
$l = 10000\,\text{mm}$
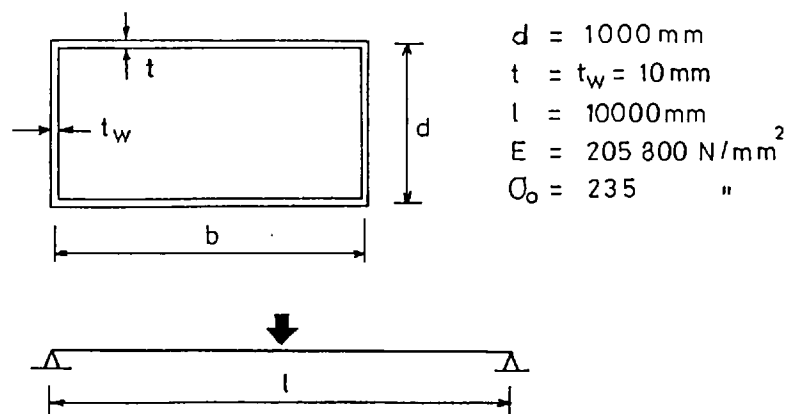$E = 205\,800\,\text{N/mm}^2$
$\sigma_o = 235\quad$ "

Fig. 4.6 General characteristics of simply supported box girders
in reference (26)

This was part of a numerical research into the problem of effective widths of wide flange girders taking account of plasticity effects, and seems to be the only other numerical investigation whose results can be used for comparison.

Albrecht's model was also simply supported and had the general impractical dimensions indicated in Fig. 4.6*. It was loaded by applying vertical displacements to a node at half the web depth at mid-span. As discussed in section 2.5.4 this loading clouds the shear lag point loading effects on the flange but plastic flow of stresses, increasing the shear capacity of the web beyond a fully yielded depth at mid-span, was also reported. This was referred to by Roik[27] in a discussion of these results.

Depending on the dimensions, the collapse of preliminary examples corresponded to either full shear/being reached over the whole web depth or to fully yielded flange cross-sections. The ratio b/ℓ was identified as the parameter controlling the mode of collapse. For higher values of b/ℓ the shearing of the web governed the failure. In these cases parts of the mid-span flange cross section remained elastic. However, the type of loading and the characteristics of the finite elements used produced in-plane N_x stresses at the plate edges of the web-flange connection which were out of equilibrium. These spurious stresses contributed to the reduction of the shear capacity of these edges thus masking the possibility of expressing the flange capacity in terms of a maximum yield shear flow along them. The corresponding upper bounds to this capacity derived in expressions (4.5) and (4.10) were thus not explicitly recognised.

* from page 95 of reference (26)

Albrecht defined effective width (designated by b_m) as the part of the flange width which, if used in the normal expression of the cross-sectional plastic moment, would give the calculated ultimate moment of resistance. That is,

$$M'_{ult} = \sigma_o(b_m t + dt_w/2)d \qquad\qquad 4.12$$

From the numerical results, obtained by keeping ℓ constant ($\ell = 10000$ mm) and changing b, a variation of b_m with b/ℓ was proposed in the form of Fig. 4.7. Although the definition of b_m expresses the reduction of
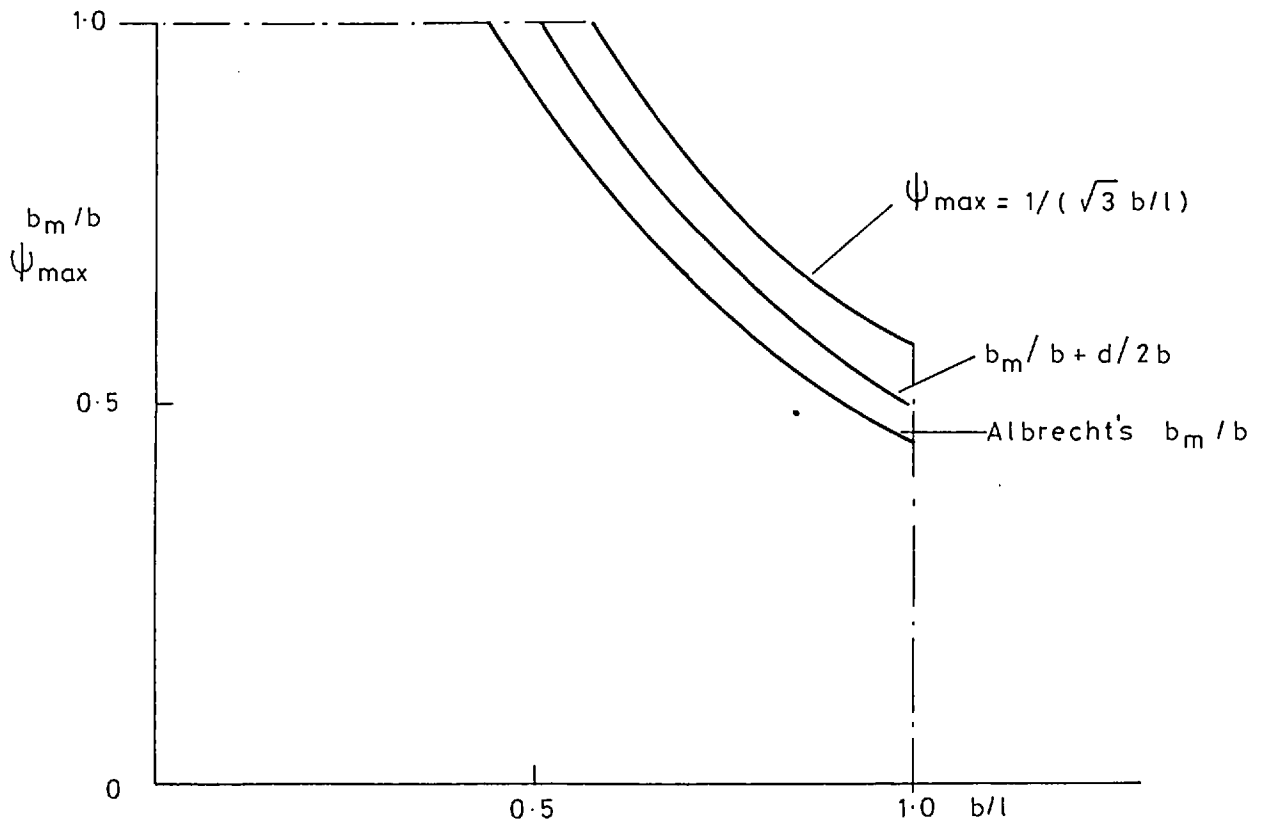

Fig. 4.7   Comparison of present approach with results from reference (26)

plastic moment due to the shear lag type of loading, it exaggerates its

effects on the flange since the web contribution is assumed to be

unaltered. The effective width is thus made to depend on the depth of

the web. This seems inconsistent with the numerical evidence for large

values of b/ℓ indicating that almost full redistribution of longitudinal

stresses from the web to the flanges was possible.

In the context of the upper bounds to the flange capacity dis-

cussed in this chapter these are cases where the web contribution can

be neglected and the ultimate moment of resistance calculated in terms

of ψ_{max} according to expression (4.6). In the present case the value

of ψ_{max} should be given by the right hand side of expression (4.10).

Albrecht's results can be correlated with this approach by

comparing the values obtained by using both expressions of M_{ult} divided,

for convenience, by $\sigma_o btd$. That is, comparing

$$M'_{ult}/\sigma_o bdt = b_m/b + d/2b \qquad 4.13$$

with

$$M_{ult}/\sigma_o btd = \psi_{max} \qquad 4.14$$

By graphically adding to Albrecht's results for b_m/b (Fig. 4.7) the

values of d/2b, calculated for each b/ℓ (from the given ℓ and d values),

it is possible to see that the values of expression (4.13) are consis-

tently below the corresponding ψ_{max} values and are on the 'safer' side.

The reason for this more conservative estimation should however be

attributed to numerical problems, referred to before, rather than to any

deliberate assumption.

Although the upper bounds to the flange capacity, given by

(4.5) and (4.10), are derived from intuitive equilibrium considerations,

their existence and practical significance were not noticed by these earlier researchers[26][27]. A further confirmation that the shear capacity of the web-flange connection was not identified by these authors as limiting the flange efficiency arises from an attempt by Albrecht to study the influence of the web thickness on the girder strength. For $b/\ell = 0.2$ two different thicknesses ($t_w = 10t$ and $t_w = 0.1t$) were experimented with while keeping the other dimensions (Fig. 4.6) constant.

A statement that in the first case the ultimate load was not altered while in the second it was considerably reduced, was the only observation provided. If the mechanism of failure had been understood fully, the explanation tendered within this section, by the use of expression (4.5), would have been presented.

4.4   FLANGE COLLAPSE MODES

4.4.1   Unstiffened Flanges

The significance of the upper bounds discussed before was easily identified for unstiffened flanges. The shear capacity of the loaded edges was seen to impose, for certain values of b/ℓ, a limitation on the flange effectiveness. The other limitation to be considered corresponds to the compressive capacity in inelastic buckling. A different collapse mode is associated with each one of these upper bounds.

The analysis of two cases showing distinctly different modes of failure will illustrate this statement and provide a means of interpreting later the results of the parametric study. The behaviour of two compression flanges of open cross section girders, with the same slenderness $b/t = 60$ but different b/ℓ ratios (1 and 0.5 respectively)
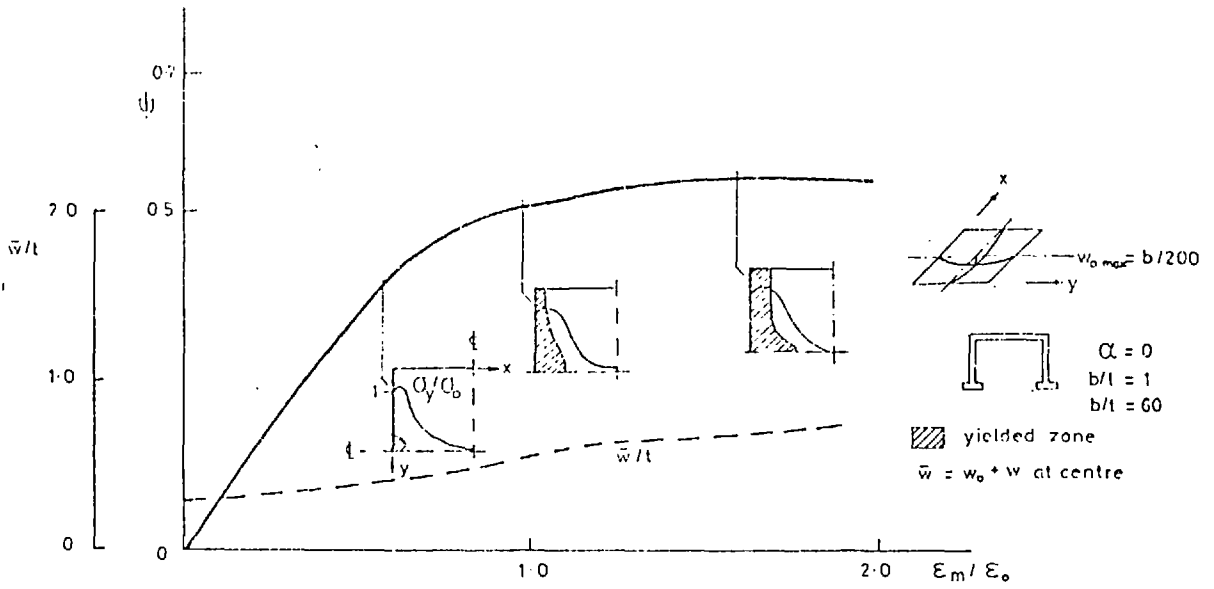
Fig 4·8   Flange collapse mode associated
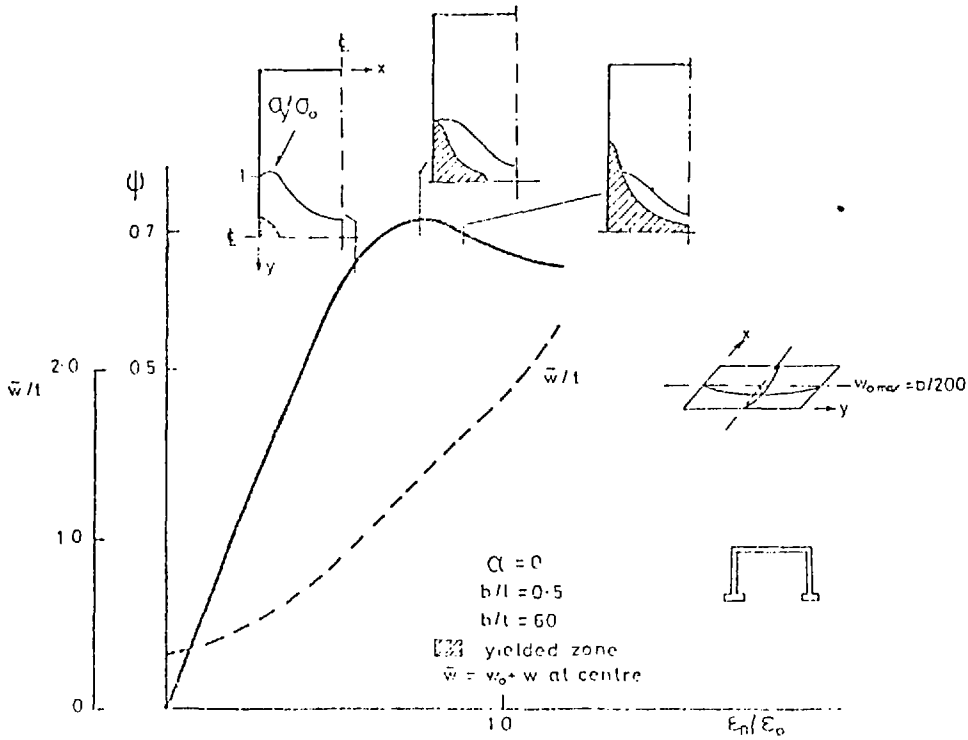with the edge failure in shear

Fig 4·9   Flange collapse mode associated
with inelastic buckling in compression

is represented in Figs. 4.8 and 4.9. The webs were assumed to remain elastic during the loading history thus making the flange failure only dependent on flange characteristics. In both cases the initial imperfections had a half-sine wave shape transversely and longitudinally with the amplitude of b/200.

In both figures 4.8 and 4.9 the spread of plasticity and the distribution of the longitudinal stresses at the mid-span cross section are indicated at various strain levels. The development of the central deflection is also shown.

Due to the more pronounced shear lag effects in the first case, $b/\ell = 1$, the edge yields before any significantly large deflections occur and at an average compression level at mid-span well below the collapse load in axial compression. For this comparison the behaviour of the same plate in compression is also shown in Fig. 4.8. A characteristic of this flange mode of failure is the plateau corresponding to the ultimate load explained by the theoretically infinite ductility assumed for the material. This load (ψ_{max}) is very near the upper limit in plane-stress behaviour of 0.577 (or $1/\sqrt{3}$) predicted by expression (4.10).

In the second case, Fig. 4.9, significant parts of the edge remain elastic providing load paths through which shear stresses can be transmitted from the web to the central zone. This continues until the level of average compression in this area approaches the buckling load under uniform compression, obtained for the previous case, and the full plate width becomes plastic.

The ultimate capacity (ψ_{max}) is smaller than the compressive strength of a square isolated panel due to partial interaction of

shear lag effects. However, the more rapid unloading in comparison with the $b/\ell = 1$ flange, shows the characteristic influence in this mode of failure of inelastic-buckling. The variation with load of the distribution of longitudinal stresses at mid-span demonstrates, in both Figs. 4.8 and 4.9, how the capacity of the compression flange is mobilised to a different extent in each mode of failure. The $b/\ell = 0.5$ example was difficult to compare with the behaviour of a similar isolated plate in compression. In fact, the preferred buckling mode shape of a plate in compression is, for this aspect ratio, longitudinally anti-symmetric about the mid-length cross section. In the flange, the given imperfection shape, although not producing the most severe effects*, induces inelastic buckling in a symmetric mode approximately with the same shape. This is convenient for comparison with the $b/\ell = 1$ flange.

4.4.2   Stiffened Flanges

In cases where panel or stiffener buckling do not occur in the flange failure the same two simple collapse modes illustrated for unstiffened flanges can be identified. They correspond to the predominant edge failure in shear or to the overall buckling in axial compression with the stiffeners deflecting downwards. Again the first mode is associated with the upper bound given by expression (4.10) and the second depends on the column slenderness (ℓ/r) of the stiffener and combined plate width (Fig. 5.1). However, the presence of the stiffeners increases the shear lag effects and the edge failure in shear becomes the predominant collapse mode for smaller values of b/ℓ than in the case of unstiffened flanges.
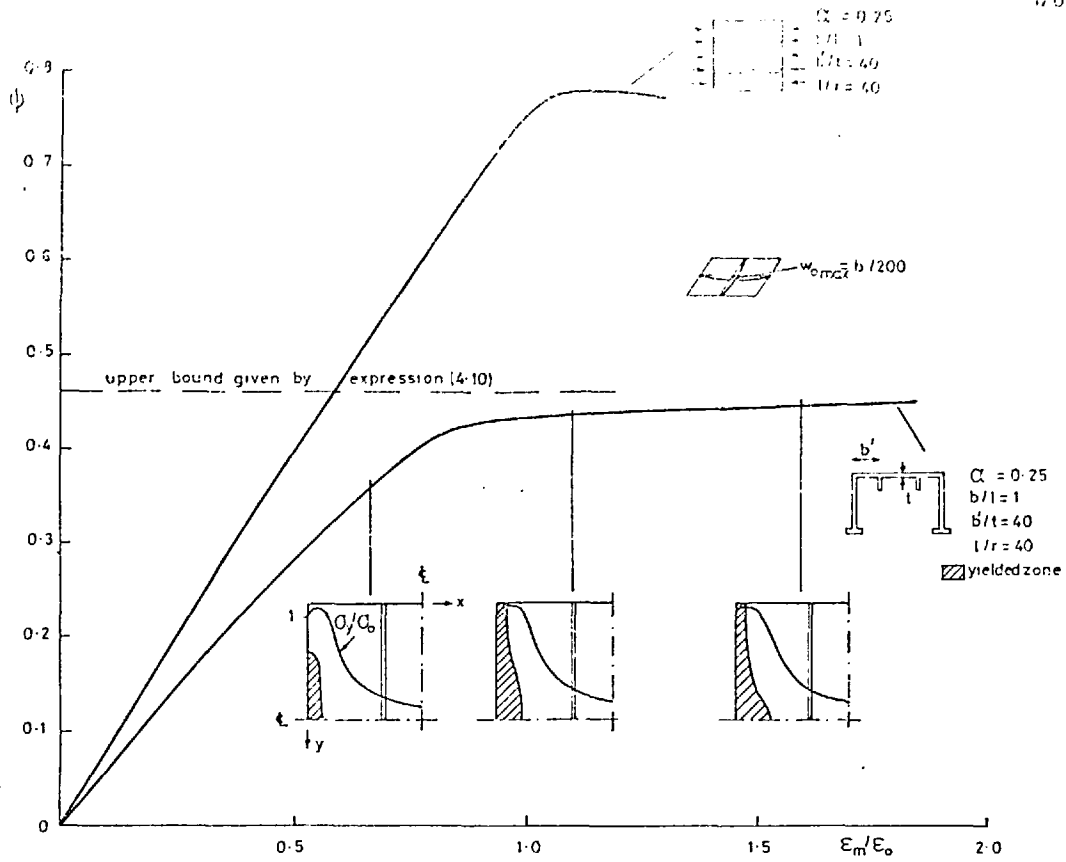
* see section 5.3.

Fig 4·10   Collapse mode of stiffened flange associated
with the edge failure in shear Comparison
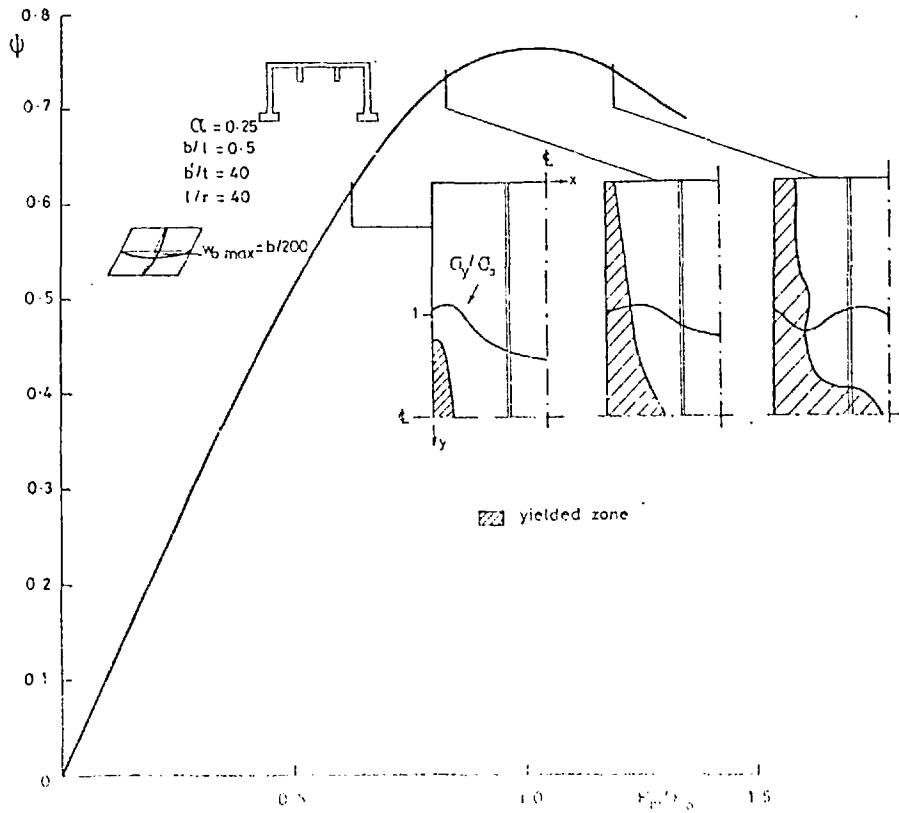with failure in axial compression

Fig 4·11   Collapse of stiffened flange in combined edge
failure in shear and failure in axial compression

The examples chosen to illustrate this aspect refer to flanges simply divided into three equal panels by two longitudinal stiffeners made of the same material as the plate ($\alpha' = \alpha$) and having a stiffening factor $\alpha = 0.25$. Elastic webs of open cross sections were also adopted. Some preliminary numerical experiments showed that it was sufficient to adopt $b'/t = 40$ to ensure that no premature panel buckling took place. The value of $\ell/r = 40$ was chosen to determine the cross-sectional dimensions (see section 5.2). For overall initial distortions half-sine wave shapes were assumed to occur in both directions having a maximum amplitude of $b/200$.

The behaviour of stiffened flanges having the above characteristics and values of b/ℓ of 1 and 0.5 are represented in Figs. 4.10 and 4.11 respectively. The same presentation which was used for unstiffened flanges shows that in the first case the spread of plasticity along the longitudinal edge corresponds to a mode of failure similar to the case of Fig. 4.8. A more pronounced shear lag effect associated with the orthotropy of form ($\alpha > 0$) would indicate, according to expression (4.10), a maximum capacity of 0.462 (see also Fig. 4.3). The values of ψ closely approximate this limit and no fall-off in the carrying capacity is shown. This is similar to the behaviour of the tension flange of Fig. 4.4 indicating that the increase of shear stresses at the edges (under plastic flow) takes place in the absence of large deflections. As in the case of Fig. 4.8 the maximum capacity is much smaller than that of the same stiffened plate in axial compression whose behaviour is also represented in Fig. 4.10.

In the $b/\ell = 0.5$ case (Fig. 4.11) plasticity also spreads along the whole edge before maximum capacity is reached. This capacity is close to the ultimate strength in axial compression ($\psi_b = 0.78$) of the

square panel with the same cross section (Fig. 4.10). Collapse occurs

with the mid-span cross section almost fully yielded. The unloading is

more pronounced than that of the plate in compression. This can be

explained in terms of the upper bounds of Fig. 4.3. For $\alpha = 0.25$ the

intersection of the upper bound corresponding to the edge in shear

(expression 4.5) and the bound corresponding to the compressive strength

occurs for $b/\ell = 0.59$. The value of $b/\ell = 0.5$ is thus very close to

this critical value for which the two modes of failure should theoretically

produce the same ultimate capacity. The interaction between the two

modes is greater in this zone, as was confirmed in the parametric study

(section 5.5.3) thus causing the post-peak fall-off in the flange capacity.

If, instead of avoiding the interaction of panel buckling,

more slender panels are assumed, the buckling of the edge panels should

reduce their capacity to transmit shear, as discussed in section 4.2.2.

This is illustrated by two examples of flanges with the same cross-sectional

dimensions and again different aspect ratios ($b/\ell = 1$ and 0.5). They

were chosen to have only three panels, with $b'/t = 60$, $\ell/r = 40$,

and a stiffening factor of 0.25 for comparison with the $b'/t = 40$ cases

presented before. The initial distortions were assumed to have the same

shape as in the previous cases (half-sine waves in both directions) with

maximum amplitude also given by $b/200$. Elastic webs of open cross

sections were again adopted. The behaviours of these flanges are

represented in Fig. 4.12 together with the behaviour of the $b/\ell = 1$ flange

plate in axial compression.

The capacity of the $b/\ell = 1$ flange is reduced below the upper

bound value of 0.462 which so closely predicted the ultimate strength of

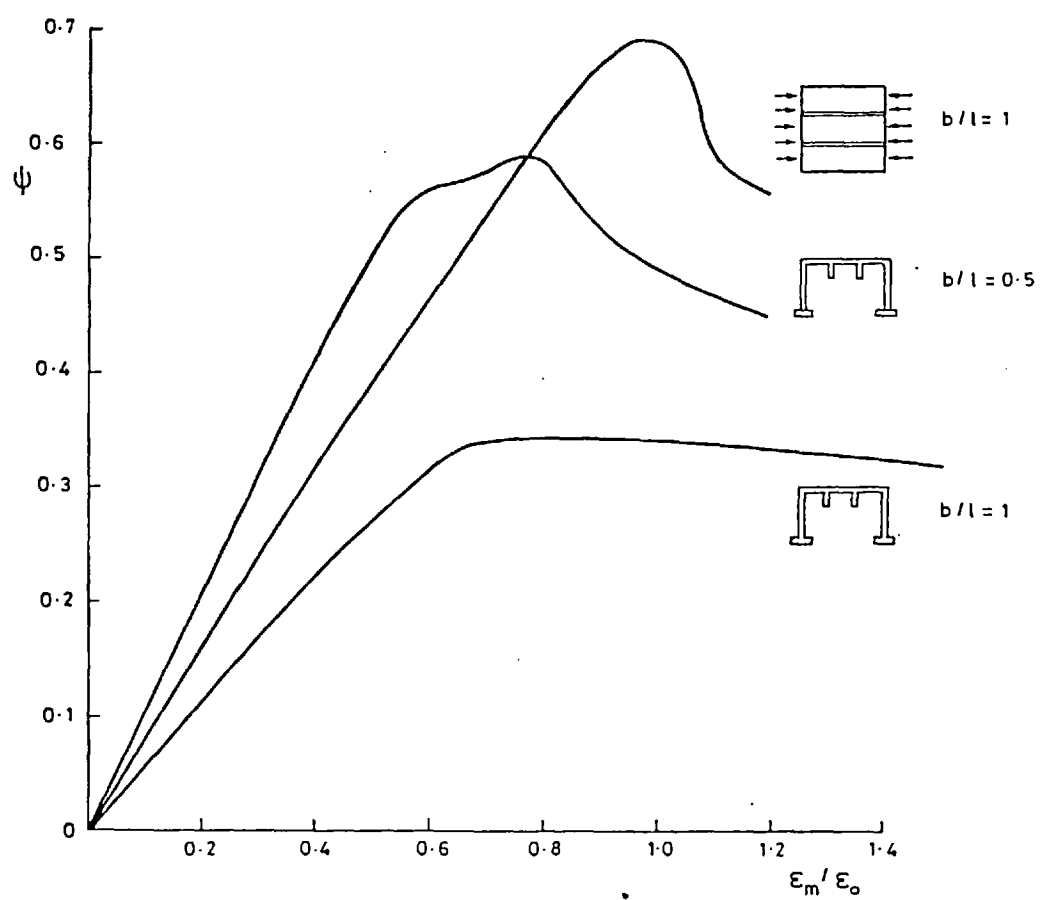the $b'/t = 40$ case with the same aspect ratio. The mode of failure is

Fig 4·12 Influence of shear lag on stiffened
flanges with slender plate panels.
(α = 0·25; B/t = 60; l/r = 40)

now associated with the formation of large panel buckles. In the edge panels the direction of these buckles is slightly inclined in relation to the longitudinal line since they are produced under a combination of shear and compression straining. The buckled shape is shown in Fig. 4.13a together with that of the same plate in compression, Fig. 4.13b. While in the flange the shear loading produces larger and deeper buckles in the edge panels, in the plate in compression the buckles concentrate near the loaded ends.

In the $b/\ell = 1$ flange behaviour, the gentle unloading beyond ultimate load is still characteristic of a predominance of the edge shearing mode of failure in contrast with what would be expected from a more rapid unloading of the slender panels in compression. However, the flange maximum capacity corresponds to a transverse distribution of compressive stresses at mid-span whose average over the edge panels is approximately equal to the buckling stress of a $b/t = 60$ plate in compression.

In the $b/\ell = 0.5$ flange, downwards buckles form first in the edge panels at mid-span followed by the development of alternate buckles (upwards) along the edge and in the central panel. While the buckles propagate the deflections in the first buckle grow considerably. However, ultimate capacity is reached with extensive parts of the edge panels still undistorted. The buckled shape of this flange is also shown in Fig. 4.13c. Perhaps more clear' than in the previous case is the inclined direction of the second buckle in the edge panel due to the shear component.

The value of ψ_{max} is still much smaller than that of the square flange in axial compression. In this case, the average compression in
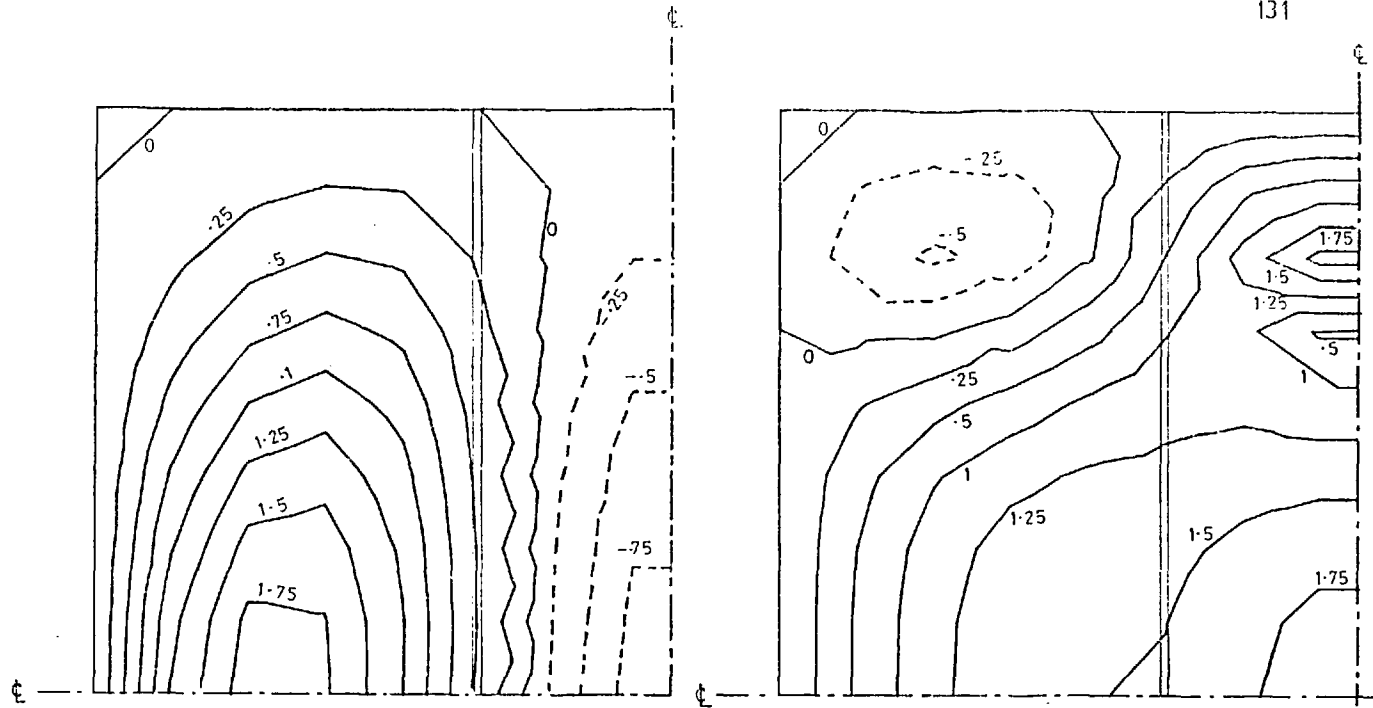
(a)

(b)
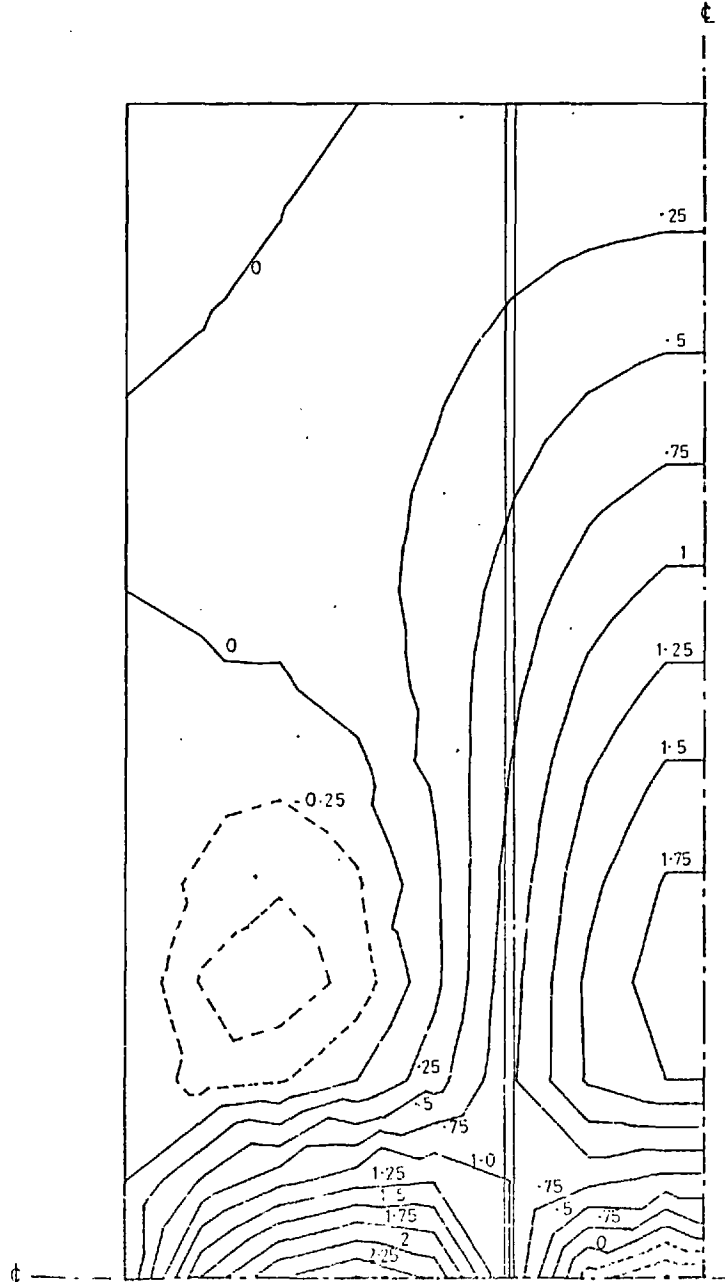
(c)

Out of plane deflections
expressed as multiples
of plate thickness
——— towards stiffener outstand
– – – – away from stiffener outstand
Initial distortions are included,
but deflections due to bending
of the webs were deducted

a) $b/t = 1$
$\varepsilon_m/\varepsilon_o = 1.376$

b) $b/t = 1$
$\varepsilon_m/\varepsilon_o = 1.080$
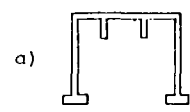
c) $b/t = 0.5$
$\varepsilon_m/\varepsilon_o = 1.129$

$\alpha = 0.25$
$b/t = 60$
$l/r = 40$

Fig 4.13
Buckling mode shapes of
stiffened flanges of fig. 4.12

the edge panels reaches the value of the buckling stress of a b/t = 60

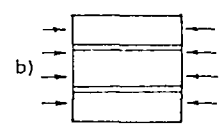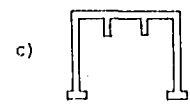plate panel before the central panel is fully mobilised and before the

flange ultimate capacity is attained.   With subsequent straining a   .

process of unloading of the edge panels takes place.

It is possible that the behaviour of the b/ℓ = 1 case could ᵇ

still be understood in terms of the upper bounds used in the previous

cases if the bound derived from the edge plastic shear strength was con-

veniently reduced to correspond to the new inelastic buckling capacity

of the edge panels in shear.   However, the behaviour of the second case

(b/ℓ = 0.5) indicates that the interaction of panel buckling may alter,

in some cases, the simple pattern of interaction identified before between

the modes of failure corresponding to those upper bounds: the edge failure

in shear and the overall buckling mode.   The interaction of these two

modes may be insufficient to interpret the behaviour of such cases and

would thus have to be combined with an assessment of the reduction   of

the flange compressive strength, to take account of post-buckling unloading

of edge components in the shear lag environment.

It was the experimental observation in Model 9 (see section

6.3.2) of a behaviour similar to that of the b/ℓ = 0.5 case, which led

to the identification in reference (28), as discussed in the Introduction,

of the relevance of the post-ultimate strength of the edge plate panels

and stiffeners in the context of full stress redistribution.   This

problem was not investigated within this thesis.

CHAPTER   5

PARAMETRIC STUDY

5.1   INTRODUCTION

The main purpose of this study was to understand the inter-
action between the two principal modes of failure identified in
Section 4.4.   It was based on the analysis of unstiffened flanges and
was thus concentrated on the effects of the main parameter influencing
shear lag, the flange aspect ratio b/ℓ, and the main parameter influenc-
ing buckling, the plate slenderness b/t. To reduce the number of the
other parameters involved a few criteria regarding the fixing of
dimensions were adopted.

The possibility of the webs failing plastically in shear is of
limited interest for the purposes of this study and was removed by
assuming them to be made of a very high yield steel.   Thus a flange
failure depending only on flange characteristics, could be studied and
the only upper bound to be considered is that given by expression (4.9).
However, a further assumption for stiffened flanges was that $\alpha' = \alpha$
thus making expression (4.10) the relevant one.

A further numerical simplification was introduced by consider-
ing only girders with open cross sections of types CS2 and CS3, Fig. 1.4.
The difference in behaviour between open and closed sections was investi-
gated and no difference in the ultimate behaviour of the compression
flanges was found for the several cases considered.   This can be illus-
trated for a $b/\ell = 1$ case by comparing the behaviour of the same com-
pression flange ($\sigma_{ow} \gg \sigma_{ocf}$) in a closed and an open cross section

girder in Figs. 4.4 and 4.8 respectively. This, together with the fact that for b/t = 100 cases (Fig. 4.5) the same ultimate capacity was obtained for different web materials, shows that although the maximum flange strength is controlled by the total shear stress applied along the edges it is not very sensitive to changes in its distribution.

The parametric study of unstiffened flanges was preceded by an investigation of the effects of initial imperfections and their most weakening shape, together with a study of the influence of material properties. These investigations were restricted to a few cases and the observations, although interesting, are insufficient to come to any firm conclusions regarding the shape of initial imperfections having the most weakening influence.

The numerical results of the parametric study are presented in terms of ultimate strength against the b/ℓ parameter for the three values of b/t studied (40, 60 and 100). The form of the curves obtained prompted the author to attempt to present the results for design purposes using a format based on an analogy with column strength curves.

The conclusions regarding the interaction between the shear lag and buckling effects are compared with Maquoi and Massonnet's[22] proposal for design rules. They were also tested on stiffened flange cases where only overall buckling interacted with shear lag effects.

5.2   CRITERIA USED TO SELECT DIMENSIONS AND MATERIAL PROPERTIES
          FOR NUMERICAL EXAMPLES

To maintain some relation between all the cases studied and to reduce the number of intervening parameters the same moment of inertia and ratios of cross-sectional area of each flange and the combined area

of the webs $(A_{cf}/A_w$ and $A_{tf}/A_w)$were assumed, unless otherwise specified.
As found by Moffatt and Dowling[13], these ratios are relatively minor
parameters influencing the elastic shear lag effects on the flanges at
the point-loaded cross sections. They were assumed to be equal to
unity in this study for all three cross-sections (Fig. 1.4).

To enable the same moment of inertia to be assumed throughout,
the cross-sectional dimensions of the webs were kept constant with the
following values (Fig. 1.3):

$$d = 900 \text{ mm} \quad ; \quad t_w = 18 \text{ mm} \qquad\qquad 5.1$$

Thus, the cross-sectional areas are

$$A_{cf} = A_{tf} = A_w = 32400 \text{ mm}^2 \qquad\qquad 5.2$$

In the case of stiffened flanges this only approximately maintains the
cross-sectional moment of inertia.

To fix the value of the flange cross-sectional area establishes
a relation between the width and thickness of an unstiffened flange,
that is, A_{cf} = bt. These dimensions are then automatically determined
once a value for the slenderness parameter b/t is assumed. Consequently,
for each value of b/ℓ required, the length ℓ has to be calculated from
the value of the width b.

The buckling mode of stiffened flanges associated with an
inwards deflection of the flange (positive bending of the stiffeners)
is governed by two main geometric parameters: the slenderness of the
plate panels b'/t, and the column slenderness ℓ/r of the stiffener and
associated plate width taken as the full panel width b' (Fig. 5.1).
The local buckling of the stiffener outstand is dependent on the depth-
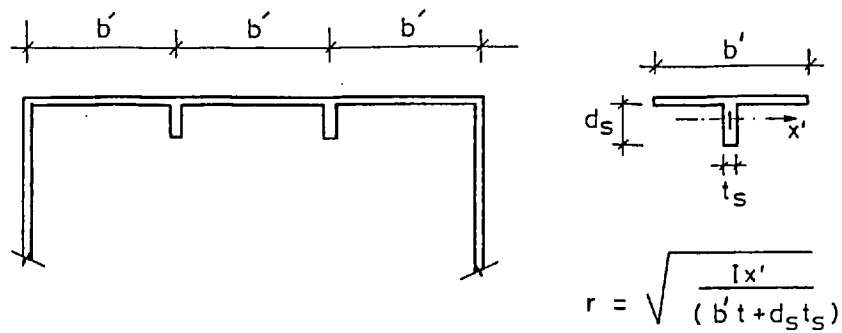thickness ratio d_s/t_s.

Fig. 5.1   Stiffener and associated plate width

Given α, b'/t and the number of plate panels or stiffeners, it is possible to calculate from expressions (1.7) and (1.8) the panel dimensions b' and t, the total width b and the cross-sectional area of each stiffener.   As before ℓ has to be determined from the value of b for each value of b/ℓ.

The actual dimensions of the stiffener cross section are then calculated by either fixing a value for ℓ/r or for d_s/t_s.   In the examples presented in this thesis ℓ/r was generally selected as the given parameter and d_s and t_s adjusted accordingly.   This led in some cases to unrealistic values for d_s/t_s but, as the present analytical model is not suitable for studying the modes of failure associated with stiffener torsional buckling, this was considered to be acceptable. All the box girder plate components were assumed to be made of a very ductile mild steel with the same Poisson's ratio and Young's modulus:

$$\nu = 0.3 \quad ; \quad E = 205\,800 \ N/mm^2 \qquad\qquad 5.3$$

In stiffened flanges, unless specified otherwise, the same material was assumed for the plate and the stiffeners thus making the equivalent stiffening factor α' (defined in (1.9)) equal to α.   The same uniaxial

yield stress was used in most of the examples corresponding to a steel characterised by

$$\sigma_o = 235 \text{ N/mm}^2 \quad \text{or} \quad \sqrt{\sigma_o/E} = 0.0338 \qquad 5.4$$

To meet the assumption that the webs remain elastic a very high value (ten times the above value) was assigned to the yield stress.

5.3   EFFECTS AND CHOICE OF INITIAL GEOMETRIC IMPERFECTIONS

The influence of varying the amplitude of the geometric imperfection on the buckling mode of failure was studied at first.   The results showed that, as in isolated plates in compression, larger initial deflections produce, in general, lower and less pronounced peaks in the stress-strain curves.   This is illustrated in Fig. 5.2 where the behaviour of a $b/\ell = 1$ slender flange is represented for different amplitudes of a double half-sine wave imperfection.

The associated problem of determining the initial shape that produces the biggest weakening effect was more difficult to study mainly due to the lack of information on elastic buckling mode shapes for the shear lag type of loading.

In the present problem, the net compression force peaks at the point load position.   For unstiffened plates initial distortions which included a downward bow in this zone proved to be more weakening than initial shapes of the same form as the preferred buckling modes under uniform compression.   For example, for $b/\ell = 0.5$ an imperfection with two longitudinal waves with the shape of the critical mode in axial compression, and thus antisymmetric in relation to the mid-span section, produced a collapse load eight per cent higher than a symmetric imperfection with three half waves.   This is shown on Fig. 5.3.
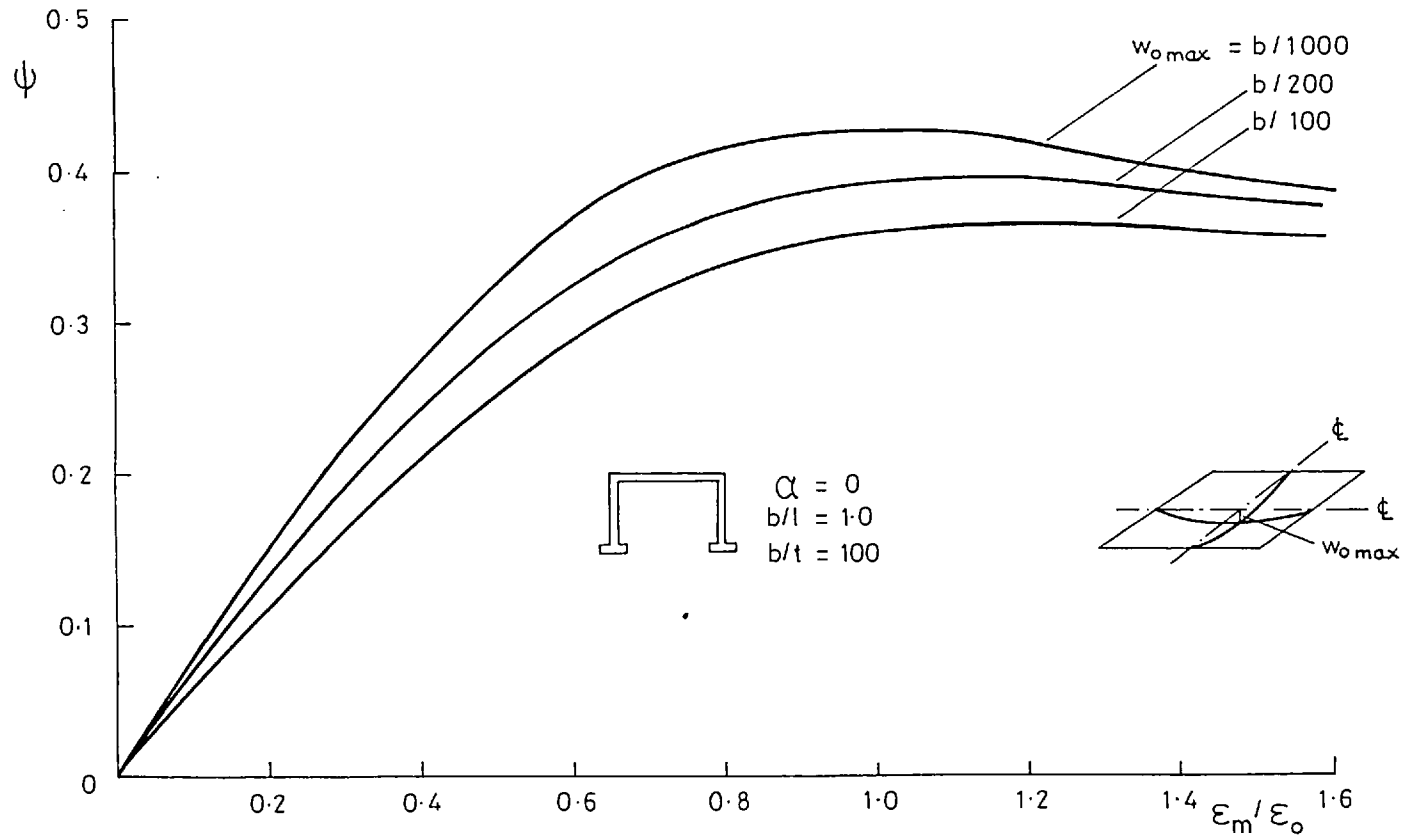
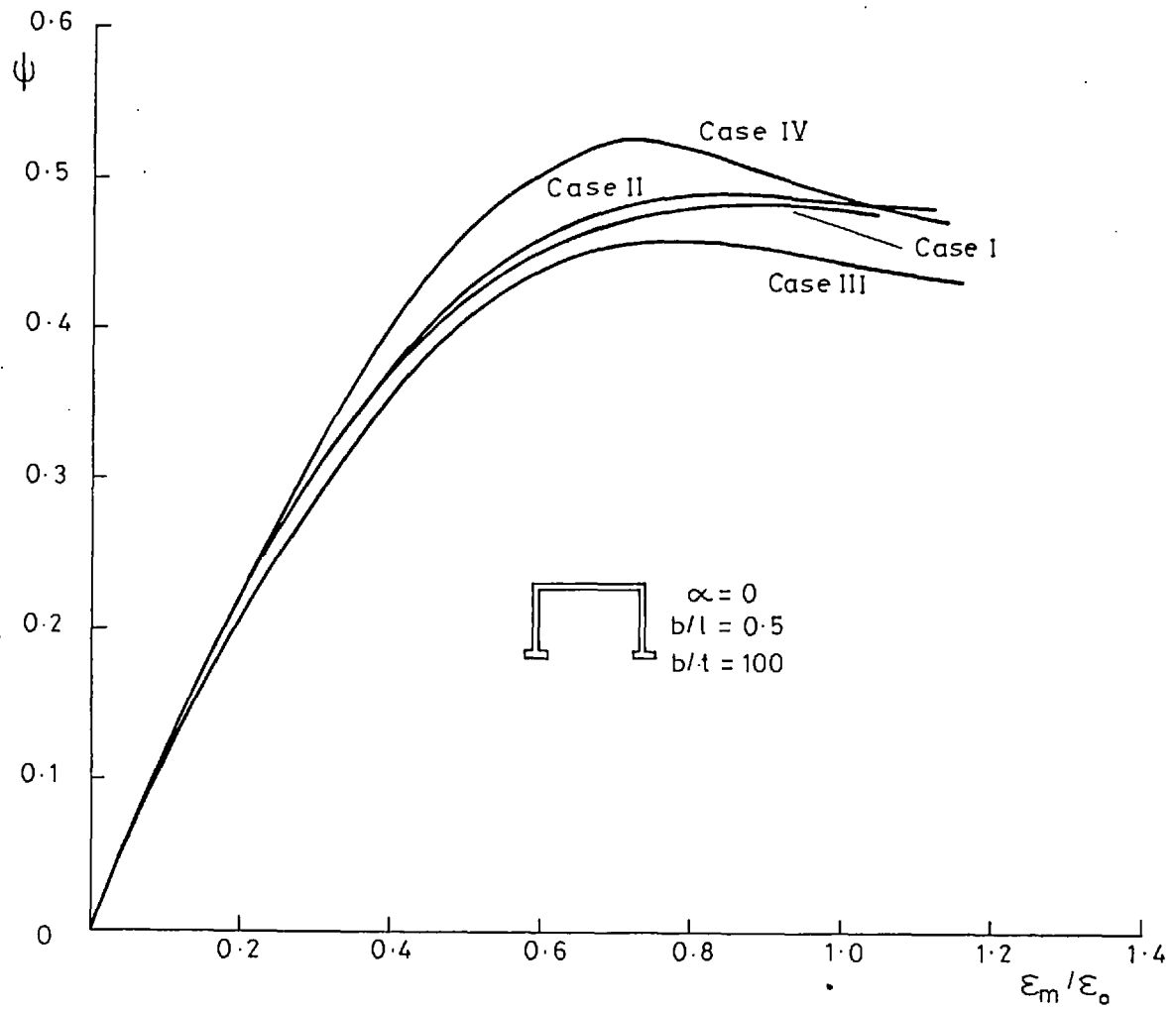Fig 5·2 Effect of varying the amplitude of the initial imperfections

Fig. 5.3   Effects of different shape of initial imperfections in the
behaviour of a b/ℓ = 0.5 flange (elastic webs)

The same transverse half-sine wave shape was used with various shapes in the longitudinal direction. These were obtained for cases with symmetry about mid-span by combining, in different proportions, one and three half-sine waves. In the antisymmetric case two half-sine waves were used. The longitudinal profiles of these shapes are shown in Fig. 5.4. The maximum amplitude of the downward bow (w_{omax}) was the same in all cases and equal to b/200.
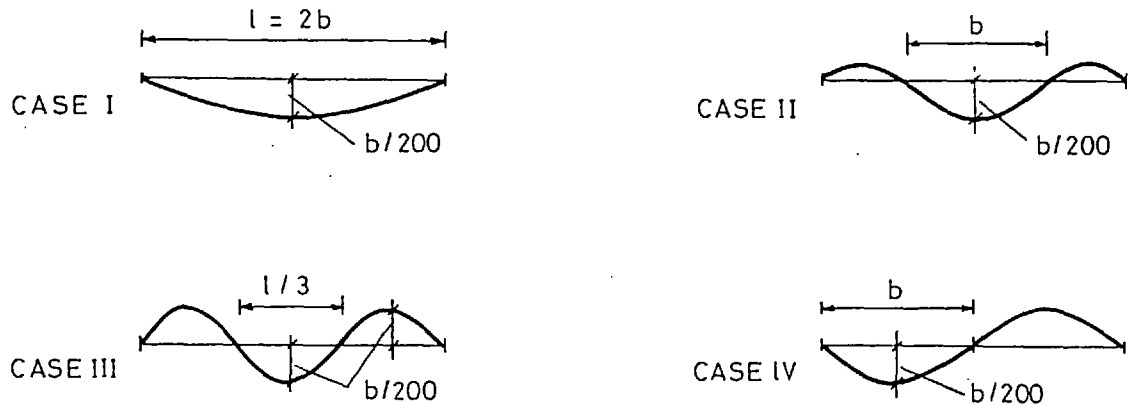

Fig. 5.4   Longitudinal profiles of initial imperfections assumed for a b/ℓ = 0.5 flange

The development of the longitudinal profile of the central line with loading is shown in Fig. 5.5 for all the cases. The deflections shown are measured from a cylindrical surface generated by the deflected line of the web-flange connection. These profiles illustrate how buckling in different modes is influenced by the shape of the initial imperfection.

By comparing the profiles of Case I and Case IV, for example, it is possible to understand why the ultimate compressive force at mid-span is higher in the latter. In this case, a nodal line, corresponding in the profiles to the point of contraflecture, acts like a transverse stiffener to the most compressed central zone, thus reinforcing it against buckling.
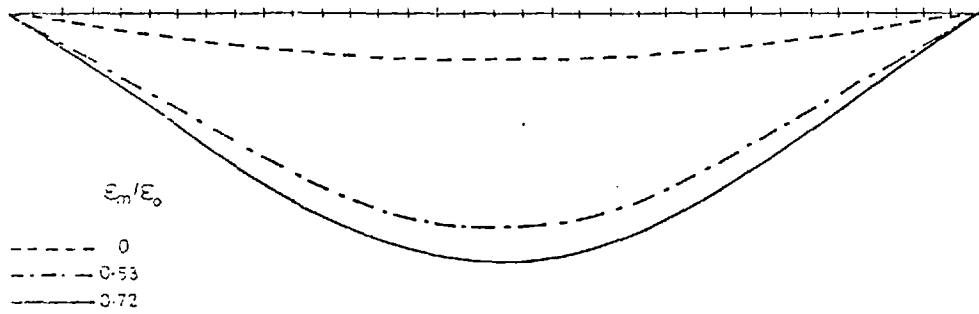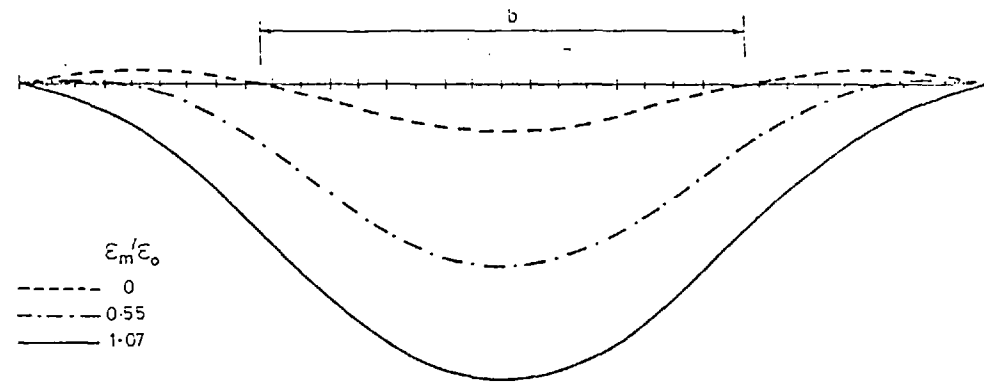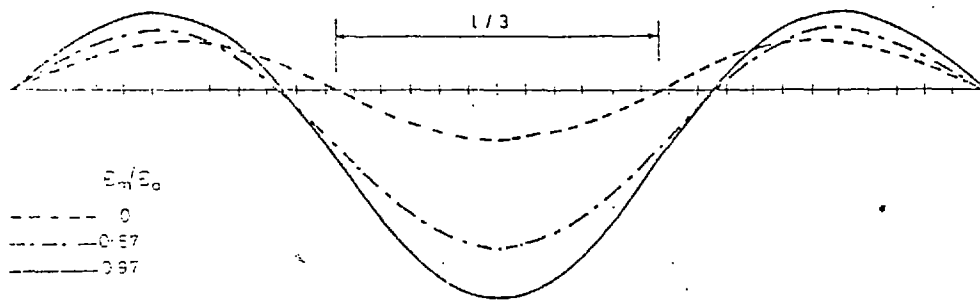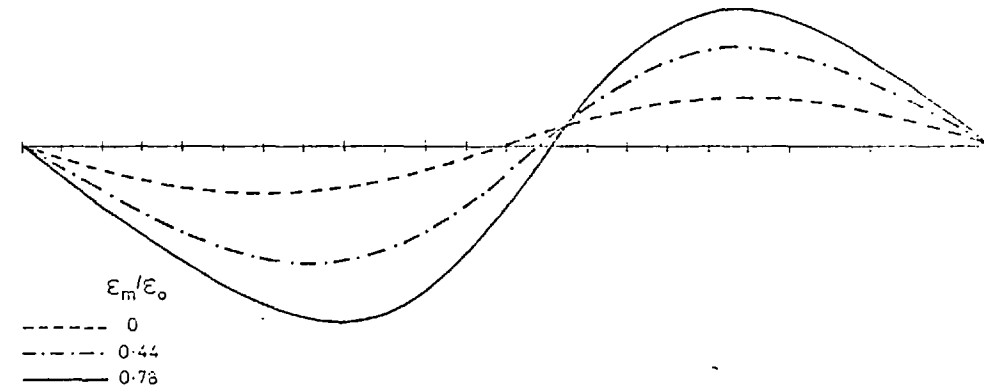
Note: Deflections due to web bending were deducted

Fig 5·5 Development of deflections with loading for different shapes of initial imperfections.
Longitudinal profiles of central line (b/l = 0·5 ; b/t = 100)

For Case II, the plate buckles from an initial three wave shape into a one wave form. In this case there is some delay in the development of large deflections which explains, perhaps, the attainment of a higher peak load than in Case I. Case III proves to be the 'weakest'.

These observations seem to suggest that for this type of loading an imperfection whose shape weakens the central most stressed zone, by having a downward bow at the centre while leaving the flange ends sufficiently flat, would have the most weakening effects. Such a shape would provide 'strong' load paths from the ends of the web-flange connections, which remain elastic, to the central zone.

When these suggestions were published recently[71], Wang drew the author's attention to an earlier paper[72] in which he had studied numerically (using the finite differences technique) the elastic buckling of flat plates under compressive forces uniformly distributed across the width but varying axially as shown in Fig. 5.6.
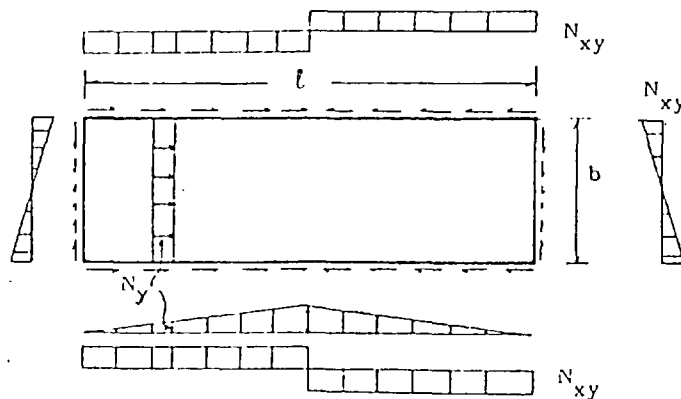
Fig. 5.6   Stress distributions in flange assumed in reference (72)

The assumed stress distributions were selected to represent the situation of a flange of a box girder under point load at mid-span neglecting shear lag effects.   Little information is given in reference (72) about the buckling mode shapes obtained but they are said to present a pronounced wave at the centre with relatively 'flat' zones near the ends (see example in Fig. 5.7).   This provides some corroboration
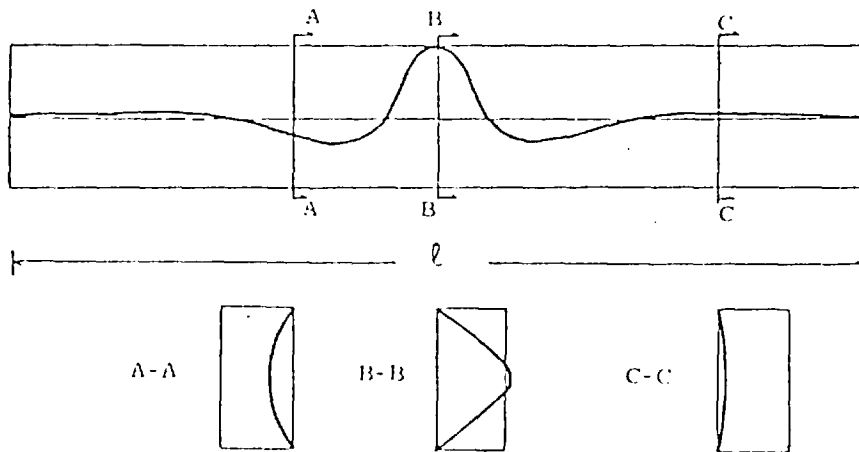
Fig. 5.7   Example of buckling mode shape obtained for a b/ℓ = 1/6 flange loaded as in Fig. 5.6 (longitudinal profile along central line*)

of the suggestions about the most weakening imperfection made above. This problem however deserves more attention than was given in the present, limited, investigation.

Eventually, a shape with three equal half-waves (Case III) was adopted in the parametric study for the initial imperfections of flanges with b/ℓ ⩽ 0.5.   For aspect ratios between 0.5 and 1.0 either the shape of Case I or Case II was used, depending on which produced the lowest

* from reference (72)

value of ψ_{max}. For consistency, the maximum amplitude of the central

bow was kept constant with a value given by b/200. This decision is

linked to recent recommendations on tolerances in plated structures[73].

This choice corresponds to assuming that the ratio w_{omax}/t is

proportional to the plate slenderness b/t, or to the non-dimensional

slenderness* β (as the same material properties were assumed for all

the plates). For correlating the results in a study of the influence

of material properties, the proportionality between w_{omax}/t and β

proved to be a convenient way of describing the effects of initial dis-

tortions.

For all the stiffened flanges used in the parametric study the

overall shape of the initial distortion consisted of one half-sine wave

in both directions. The maximum amplitude of this 'dishing' was also

taken as b/200. That is, no transverse modulation of this overall

sinusoidal distortion, corresponding to plate panel deflection between

stiffeners, was assumed.

Such imperfections are perhaps too severe, compared to normal

tolerances, since they correspond, when three equal plate panels are assumed,

to a stiffener longitudinal deflection which varies between ℓ/230 for

b/ℓ = 1 to ℓ/690 for b/ℓ = 1/3. However, as these flanges were only

considered in a very restricted investigation the assumptions are again

considered to be acceptable.

5.4   INFLUENCE OF MATERIAL PROPERTIES

The upper bound to the capacity of an unstiffened flange when

it is governed by the shear strength of the longitudinal edges is given

* defined in expression (5.5)

by expression (4.10). This expression is independent of the plate

slenderness and material properties. On the other hand, the inelastic

buckling of isolated unstiffened plates is governed by the non-dimensional

plate slenderness β, when account of material properties is taken in

the comparison of different cases. This parameter is defined as

$$\beta = (b/t)\sqrt{\sigma_o/E} \qquad\qquad 5.5$$

This suggests that by keeping β constant it may be possible to obtain

the same values of ψ_{max} in flanges with the same aspect ratio b/ℓ but

with different values of b/t. This would eliminate the need for con-

sidering the influence of different materials and thus allow the para-

metric study to be conducted on the bases of the b/ℓ and b/t parameters

only, and allow the same yield stresses to be used throughout. This

possibility was investigated and proved to be acceptable by comparing

the behaviour of flanges with $b/t = 60$ as considered in the parametric

study (i.e. with $\sqrt{\sigma_o/E} = 0.0338$), with flanges with $b/t = 100$ and a

yield stress reduced in order to produce the same value of β, i.e.

$\beta = 2.028$.

As described before, the nondimensional amplitude of the initial

distortions (w_{omax}/t) was assumed for the parametric study to be pro-

portional to the slenderness b/t or to β. Based on this criterion

the ratio w_{omax}/t was maintained equal to the one used in the $b/t = 60$

case i.e., $w_{omax}/t = 0.3$.

The results of this study are shown in Fig. 5.8 for two values

of the b/ℓ ratio (1 and 1/3). In both cases the agreement between the

behaviour of the two flanges with different materials is very good.

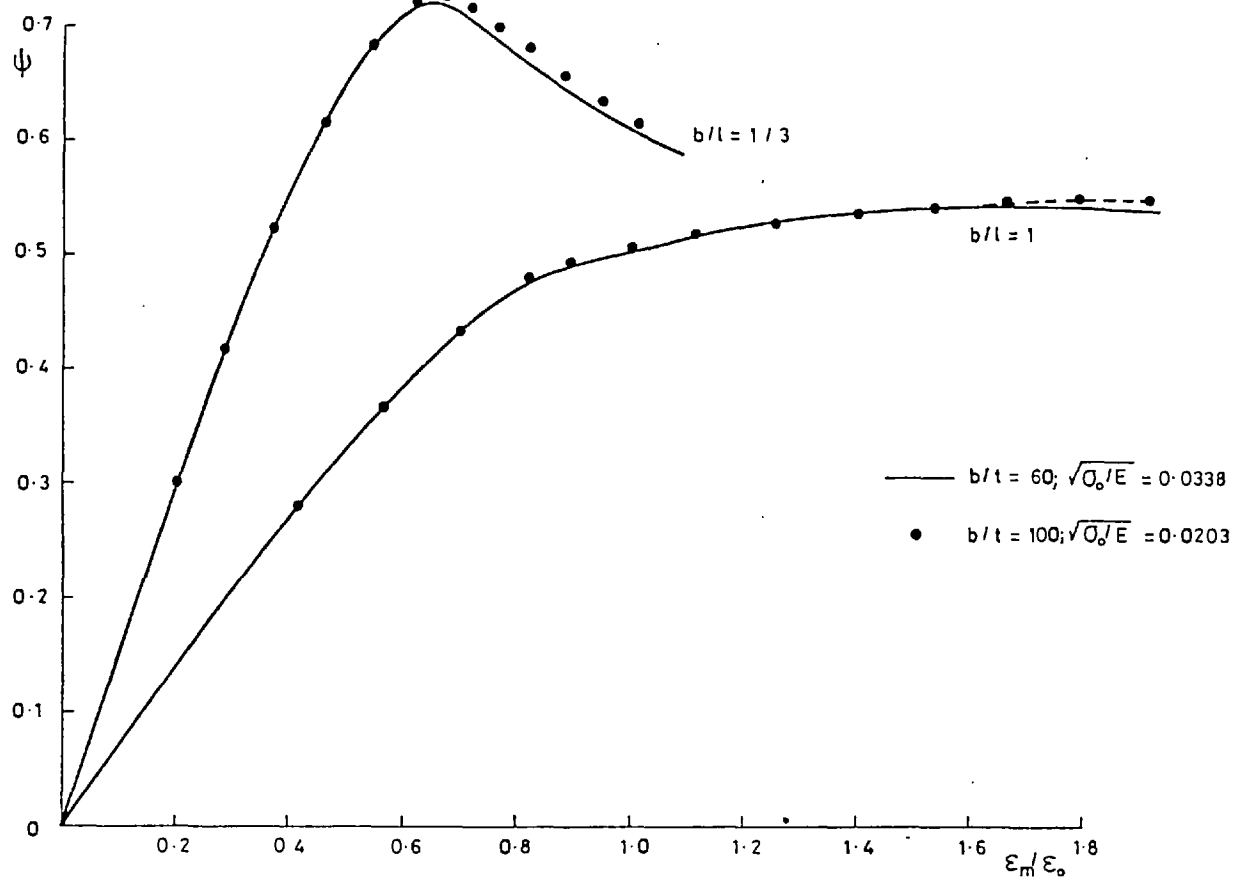This suggests that the shear lag effects are at least relatively inde-

Fig 5·8   Study of material properties. Comparison between flanges
          with different dimensions but same non-dimensional slenderness ($\beta = 2·028$)

pendent of material properties. These only need to be considered on the failure component associated with inelastic buckling. These results also suggest that, in the presence of shear lag, the buckling mode component in the flange collapse can be treated in the same way as the inelastic buckling of isolated plates in compression i.e. its influence for different grades of material can be related to the factor β.

As suggested in section 4.2 it is probable that the residual stresses also have their main effects associated only to this buckling mode of failure. These effects could then be incorporated in the study by simply allowing for an appropriate reduction in the upper bound corresponding to inelastic buckling calculated from studies of isolated plates.

5.5   SUMMARY OF PARAMETRIC STUDY RESULTS

5.5.1   Unstiffened Flanges

The results of varying the main parameters are summarised in Fig. 5.9 where the maximum values of ψ are plotted against b/ℓ for the three values of slenderness ratio. Some more results are needed to clarify the shape of the curves obtained for each slenderness for small values of b/ℓ.

The plotted points suggest that these curves would have initial values of ψ_{max} close to buckling effective width ratios such as those proposed by Winter[74] for plates in axial uniform compression*. For larger values of b/ℓ these curves seem to merge into the upper bound line given by expression (4.10). In between these two zones the inter-action of the two modes of failure referred to before is clear.
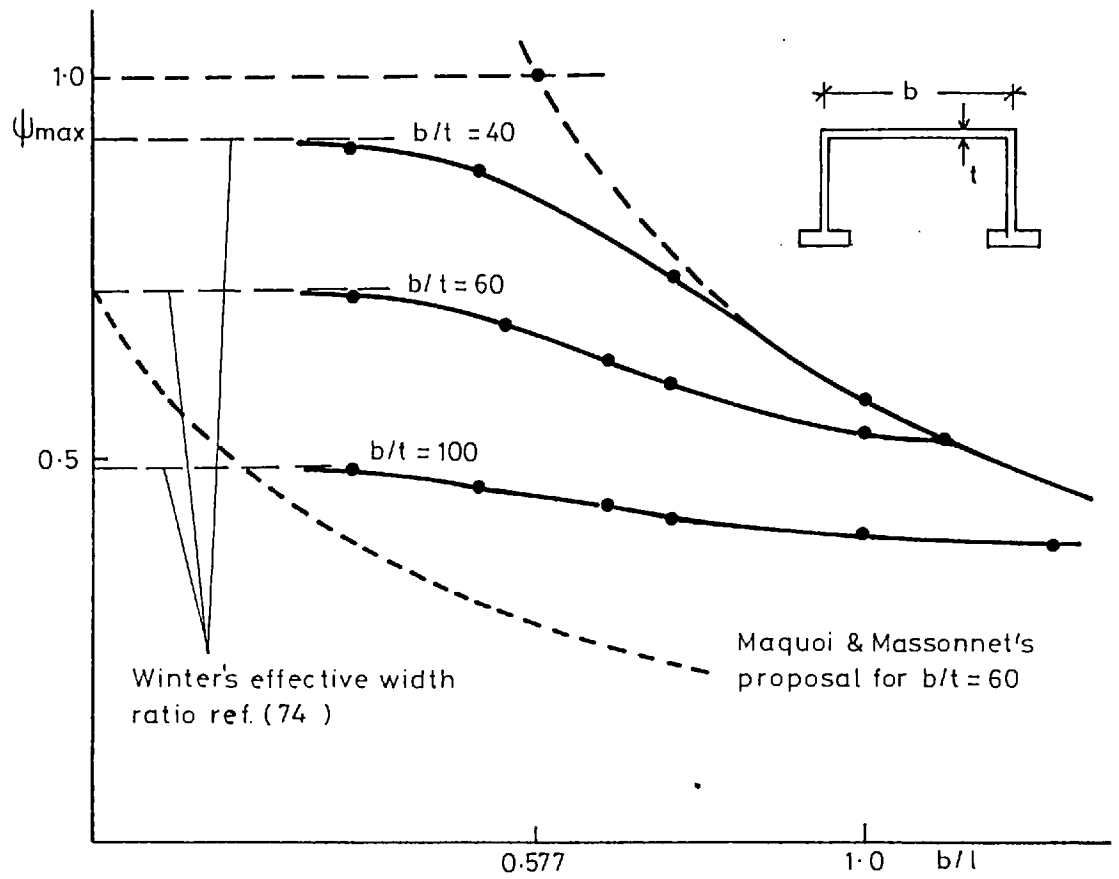
* given by $\psi_b = 1.9/\beta - 0.9/\beta^2$.

Fig 5·9   Parametric study results

Unstiffened compression flanges ($\sqrt{\sigma_o/E}$ =0·0338)

The existence of an initial plateau, though not well defined, indicates that for smaller values of b/ℓ full redistribution can be assumed and that the flange strength is governed by inelastic buckling considerations. The size of this plateau seems relatively smaller for more slender plates, indicating that interaction with the shear lag mode of failure starts 'earlier' for these flanges.

The convergence of results to the upper bound line and the merging of the curves also needs clarifying since it is associated with the difficult modelling of plastic flow around the longitudinal edges under high shear straining. In this zone, however, the predominance of the mode of failure associated with the shear strength of the edges shows the flange capacity given by the maximum shear flow these edges can transmit.

Although the detection of the two modes of failure was possible since the early stages of this research project[75] the identification of the associated upper bounds was fundamental to an understanding and proper interpretation of the results.

The shapes of the curves are dependent on the initial distortions assumed in the study but the effects of the imperfections should be comparable for all the various slendernesses and some correlation between the three curves must exist.

The similarity of the curves of Fig. 5.9 with column strengh-slenderness curves suggests a way of presenting results i.e. by use of Perry-Robertson type curves. This was attempted employing the following quantities:

$$b/\ell^* \;=\; (b/\ell)/(1/\sqrt{3}\ \psi_b) \qquad\qquad 5.6$$

and $\quad\psi^* \;=\; \psi_{max}/\psi_b \qquad\qquad\qquad\qquad 5.7$
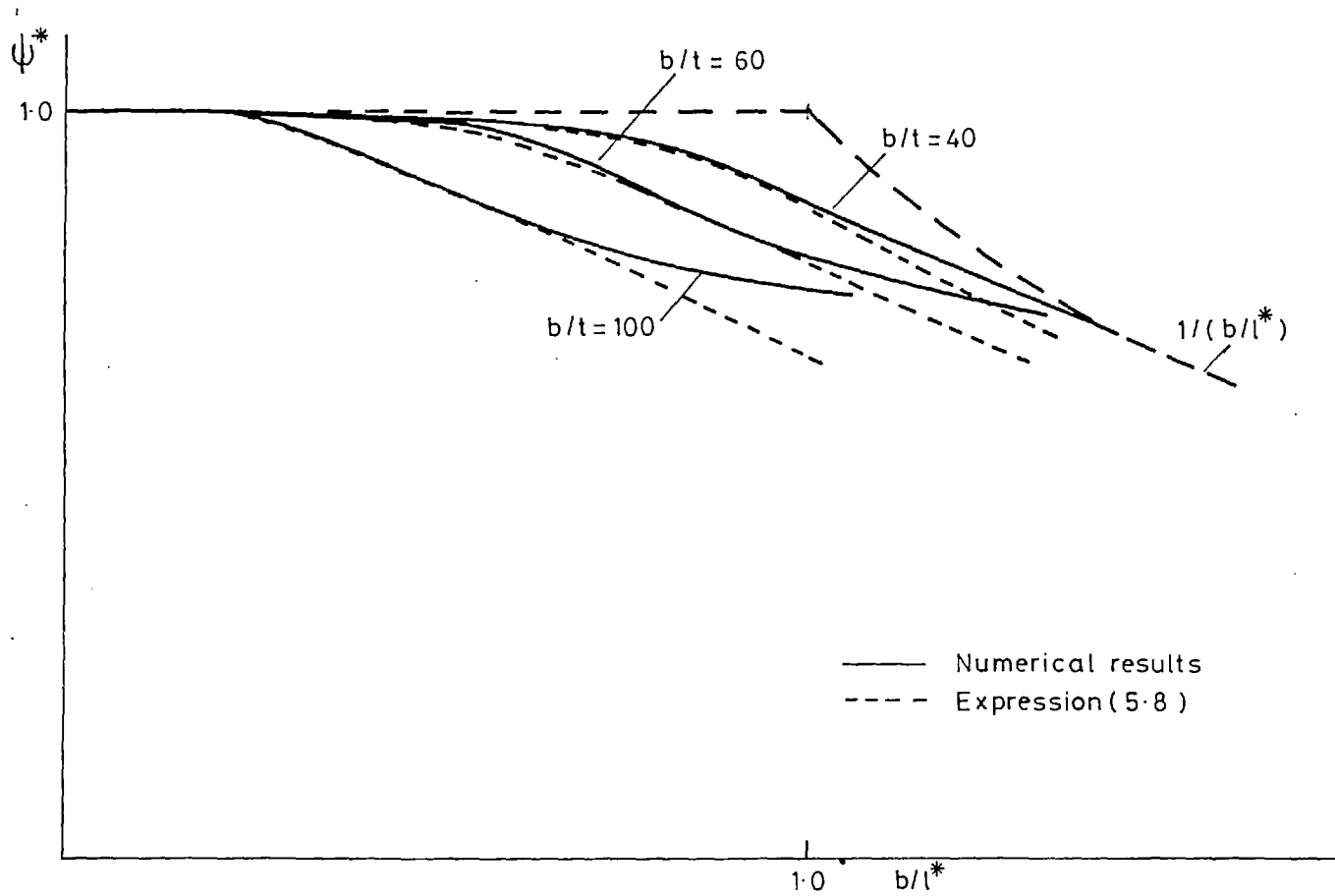
Fig. 5.10   Unstiffened flanges.   Curve fitting to numerical results

where ψ_b is the value of the inelastic buckling effective width ratio i.e. the value of ψ_{max} corresponding to the apparent plateau for each b/t.

If the results are presented in this new system of coordinates the curves are of the form indicated in Fig. 5.10. Although more results are needed to define these curves accurately an attempt was made to formulate an empirical expression to fit them. This expression is

$$\left(\frac{1}{b/\ell^*} - \psi^*\right)(1-\psi^*) = \eta\left(\frac{\psi^*}{b/\ell^*}\right) \qquad 5.8$$

where

$$\eta = \delta(b/\ell^* - b/\ell_0^*) \text{ for } b/\ell^* \geqslant b/\ell_0^*$$

or

$$= 0 \qquad \text{for } b/\ell^* < b/\ell_0^* \qquad 5.9$$

with δ a parameter to be adjusted for the various slendernesses and b/ℓ_0^* representing the size of a possible initial plateau. A curve fitting exercise produced the parameters,

$$b/\ell_0^* = 0.45 - 2.5 \times 10^{-3} \, b/t$$

and

$$\delta = 2 \times 10^{-5} \, (b/t)^2 \qquad 5.10$$

The corresponding curves are also presented in Fig. 5.10. They show that this approach can represent well the results of the parametric study for small values of b/ℓ^* (the more significant ones). Although all relevant parameters were considered in expressions (5.8-5.10) these are rather complicated. It would probably be sufficient for design purposes to take advantage of the reduced system of coordinates and propose a lower bound curve. This could be used to estimate the amount of redistribution that can be assumed in a flange given the inelastic buckling load and the aspect ratio.

5.5.2 Comparison with Maquoi and Massonnet's Proposal

The Maquoi and Massonnet's[22] proposal to derive collapse effective width ratios by multiplying shear lag and inelastic buckling effective width ratios produces over conservative results. This is shown in Fig. 5.9 where such values* for plates with $b/t = 60$ have been compared with the present results, and may be seen to bear little resemblance. Their proposal seems therefore to be unacceptable.

5.5.3 Stiffened Flanges

The conclusions from the study of unstiffened flanges, regarding the explanation of the interaction of modes of failure in terms of corresponding upper bounds to flange capacity, were also tested for simple stiffened flanges†.

For slenderness $b'/t = 40$ panel buckling was not expected to be predominant and an illustration of the influence of the upper bound (4.10) when $\alpha = 0.25$ is presented in Fig. 5.11 for two different stiffener rigidities, i.e. $\ell/r = 40$ and 80. The influence of the stiffeners and the corresponding increase of the shear lag effect can be seen in the convergence of results to the theoretical upper limit as predicted when deriving expression (4.10). The different values of the eventual plateaux can be explained by the influence of ℓ/r on the overall buckling strength. These values can be compared in the same figure with the inelastic buckling effective width ratio of a $b/\ell = 1$ and $\ell/r = 40$ plate in axial compression obtained from Fig. 4.10. The pattern of interaction

---

* *obtained by multiplying elastic shear lag effective width ratios, given for example in reference (14), by the inelastic buckling effective width ratio, i.e. the value of ψ_{max} corresponding to the plateau (ψ_b).*

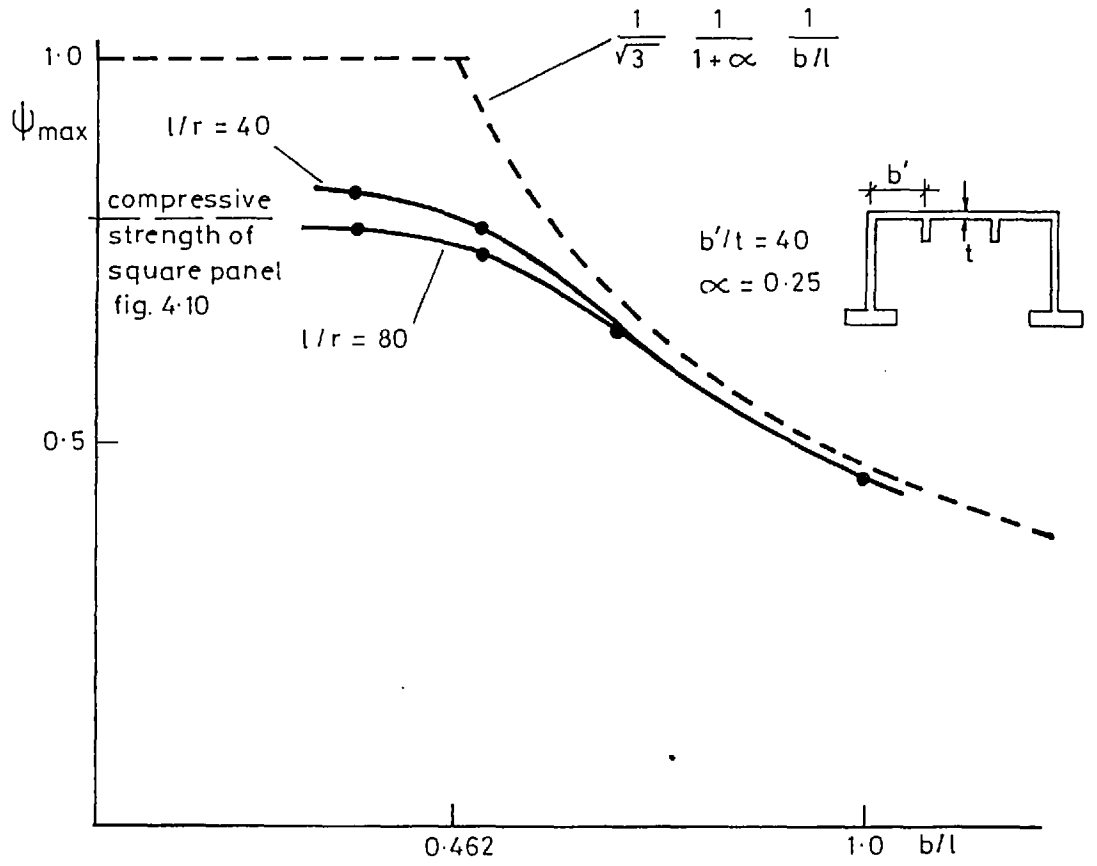† *with only three plate panels.*

Fig 5·11 Interaction between shear lag and
overall buckling in stiffened flanges

between the overall buckling mode and the failure by exhausting the edges shear capacity is thus similar to the one found for unstiffened flanges. However, the b/ℓ zone where interaction between these modes takes place seems more reduced than in the cases of unstiffened plates.
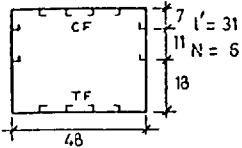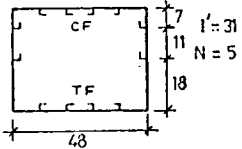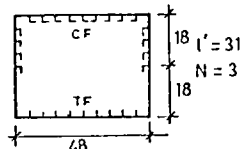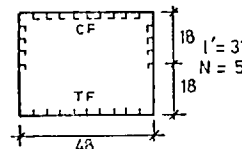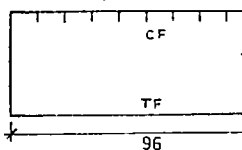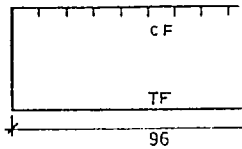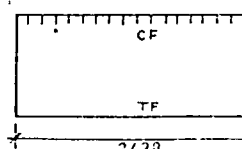
CHAPTER   6

REAPPRAISAL OF SOME TEST RESULTS ON LARGE SCALE MODEL BOX GIRDERS

6.1   GENERAL DESCRIPTION OF TESTING PROCEDURES

The major part of the programme of tests on large scale steel box girders conducted at Imperial College between 1971 and 1976 was initiated by the Merrison Committee of Inquiry. As described briefly in Chapter 1, three box girder models (Models 1, 3 and 9) were designed to investigate the effects of shear lag and tested as simply supported beams under mid-span point loading. To study the influence of shear and shear lag their behaviour was compared with that of other models (Models 2, 4 and 10) with the same cross-sectional dimensions but loaded with a two-point loading system to generate a pure bending moment condition over their length. The flanges of the first models could then be compared with similar flange plates in approximately uniform axial loading for quantitative assessment of shear lag effects. The overall and cross-sectional dimensions of these models are summarised in Table 6.1 where the material properties are also given.

In the point loaded Model 9, the ratio b/ℓ was increased to exaggerate the shear lag effects. The flange collapsed deflecting downwards (plate panels in compression), while in the failure of the companion Model 10 (loaded in pure bending) the flange buckled by compression of the stiffeners outstand, deflecting upwards. It was thus difficult to compare, as intended, the behaviour of the two flanges. Another model (Model 12) was later designed to induce, under point loading condition, the same mode of failure as in Model 10 although the local slenderness

Table 6.1 Principal dimensions of models and properties of materials

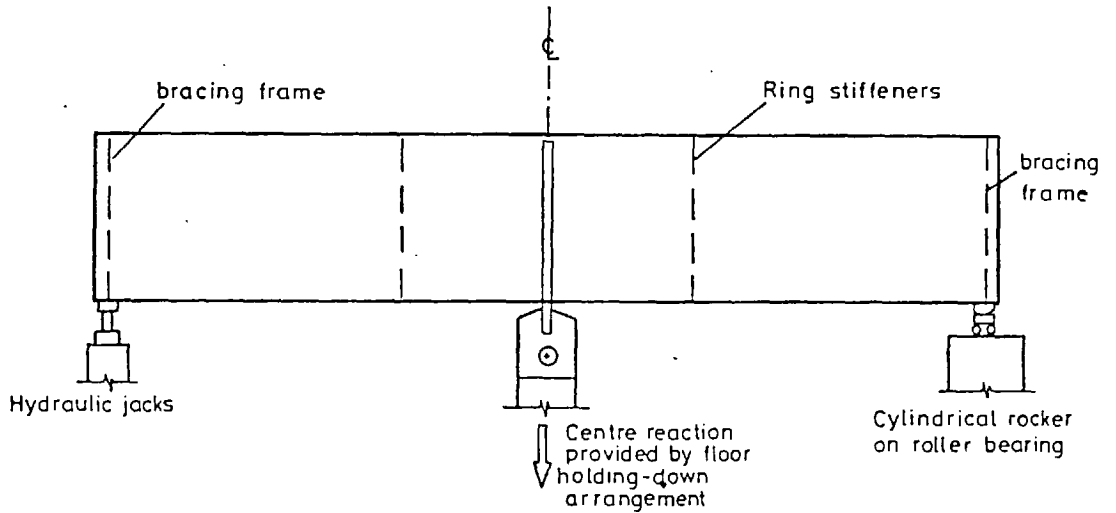| Model No.	Cross section of model dimensions, in	Component	Nominal size, in	t*, in	σ_o tonf/sq.in	E tonf/sq.in
1	$l'=31$ $N=6$ 18 48 (CF, TF)	CF	3/16	0.195	16.0	13000
		TF	3/16	0.195	16.0	13000
		W	1/8	0.133	17.7	13900
		LS	2 × 5/8 × 3/16 L	–	21.3	13000
		TS	3 × 2 × 1/4 L	–	20.3	12600
		D	1/4	–	16.5	12900
2	$l'=31$ $N=5$ 18 48 (CF, TF)	CF	3/16	0.192	19.3	13500
		TF	3/16	0.192	19.3	13500
		W	1/8	0.133	13.7	14000
		LS	2 × 5/8 × 3/16 L	–	17.9	12400
		TS	3 × 2 × 1/4 L	–	20.1	12700
3	$l'=31$ $N=3$ 18 48 (CF, TF)	CF	3/16	0.198	14.3	13400
		TF	3/16	0.195	14.0	13500
		W	3/16	0.196	18.2	13900
		LS(CF)LS(W)	2 × 5/8 × 3/16 L	–	18.6	12900
		LS(TF)	2 × 1/4 Flat	–	19.7	12900
		TS	4 × 2½ × 1/4 L	–	19.7	13400
4	$l'=31$ $N=5$ 18 48 (CF, TF)	CF	3/16	0.198	14.3	13400
		TF	3/16	0.195	14.0	13500
		W	3/16	0.196	18.2	13900
		LS(CF)LS(W)	2 × 5/8 × 3/16 L	–	18.6	12900
		LS(TF)LS(W)	2 × 1/4 Plate	–	19.7	13400
		TS	4 × 2½ × 1/4 L	–	19.7	13000
		D	1/4	0.258	19.4	13500
9	$l'=62$ $N=3$ 36 96 (CF, TF)	CF	3/16	0.192	21.6	13300
		TF	1/4	0.268	20.4	13900
		W	1/2	0.500	18.0	13500
		LS	$2\frac{3}{4}$ × 5/16 Flat	0.312	18.5	13300
		TS	5 × 3 × 3/8 L	·	18.7	13200
10	$l'=62$ $N=3$ 36 96 (CF, TF)	CF	3/16	0.194	21.7	13400
		TF	1/4	0.242	22.0	13700
		W	1/2	0.500	18.0	13500
		LS	$2\frac{3}{4}$ × 5/16 Flat	0.312	18.5	13300
		TS	5 × 3 × 3/8 L	–	18.7	13200

Model No.	Cross section of model dimensions, in	Component	Nominal size, mm	t*, mm	σ_o N/mm²	N/mm²
12	$l'=1575$ $N=3$ 915 2438 (CF, TF)	CF	5	4.90	396.3	202500
		LS	80 × 3.5	80.64×3.38	238.9	202050
		TF	6	6.15	339.8	211590
		W	12.5	12.01	328.8	201570

TF Tension flange   CF Compression flange   LS(CF) Longitudinal stiffener on compression flange
W   Web   LS Longitudinal stiffener LS(TF) Longitudinal stiffener on tension flange
D   Diaphragm   TS Transverse stiffener   LS(W)   Longitudinal stiffener on web
                          l' Length of bays
                          N   Number of bays along span of model
                          t* Measured thickness

Cylindrical bearing pads

Ring stiffeners   Diaphragm   Longitudinal stiffeners

36"

100 ton hydraulic jacks to each web   These longitudinal stiffeners were omitted on Model 1   Cylindrical rocker on roller bearing under each web

(a)   POINT LOAD RIG, MODELS 1 & 3

bracing frame   Ring stiffeners

bracing frame

Hydraulic jacks

Centre reaction provided by floor holding-down arrangement

(b)   POINT LOAD RIG, MODELS 9 & 12

Loading arm   Model   Loading arm

Jacks   Jacks

$30 \times 12 \times \frac{5}{8}$" plates (with pin-joints at each end) linking loading arm to reaction beam on laboratory floor

7'-9"

(c)   PURE MOMENT RIG, MODEL 10
(MODELS 2 & 4 SIMILAR)

Fig 6·1 Test rigs for models

Fig 6·2   Model 9: Cross-section and Details of Loading Lugs
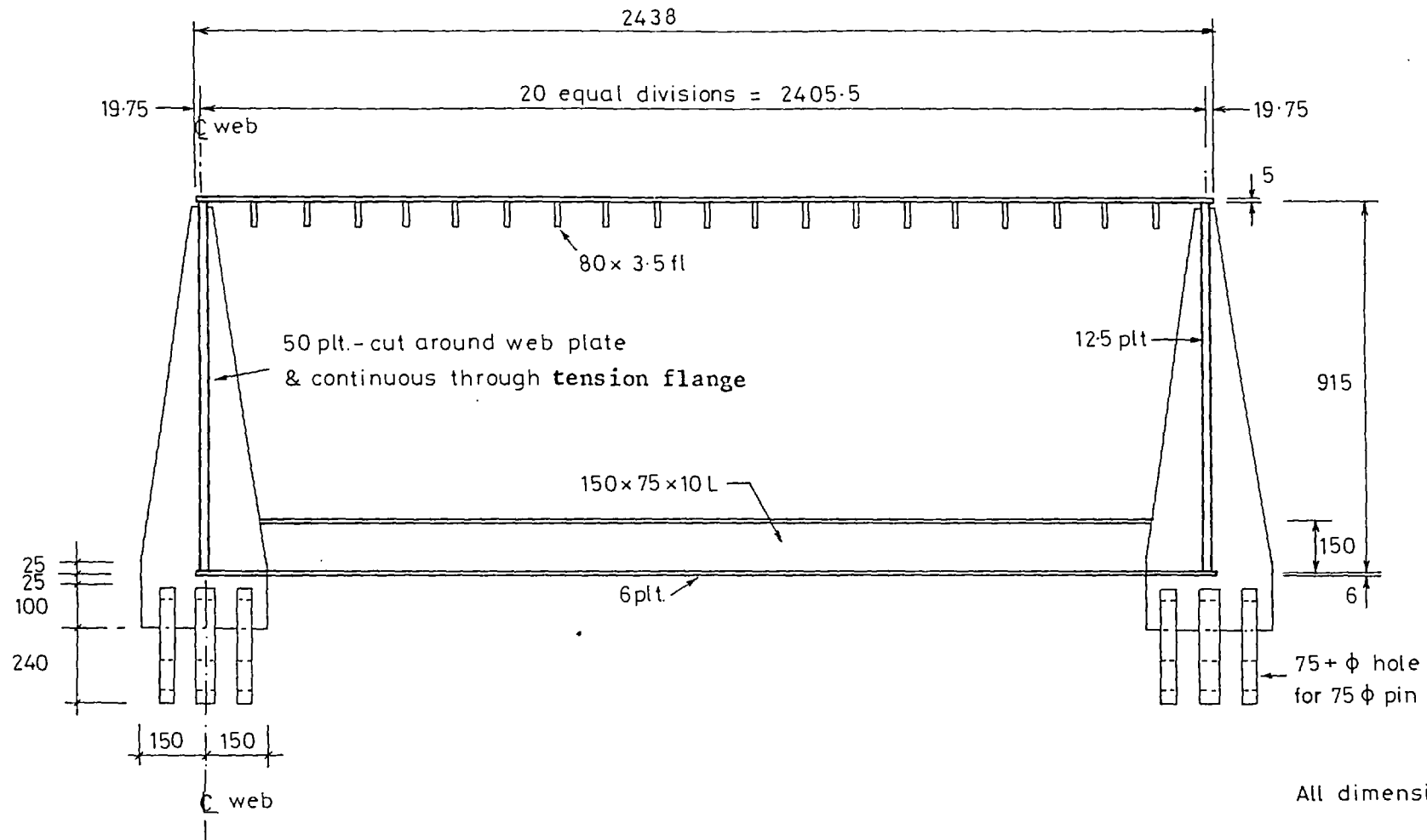
Fig 6·3 Model 12: Cross-section and Details of Loading Lugs

2438

20 equal divisions = 2405·5

19·75

₵ web

19·75

5

80 × 3·5 fl

50 plt.- cut around web plate
& continuous through **tension flange**

12·5 plt

915

150 × 75 × 10 L

6 plt.

150

6

25
25
100

240

75 + φ hole
for 75 φ pin

150   150

₵ web

All dimensions in mm

was greatly increased. A b/ℓ ratio similar to that of Model 9 was chosen. This model was designed using metric plate thicknesses for which reason its dimensions, also in Table 6.1, are given in millimetres. The author played an active part in the testing and analysis of results of Model 12.
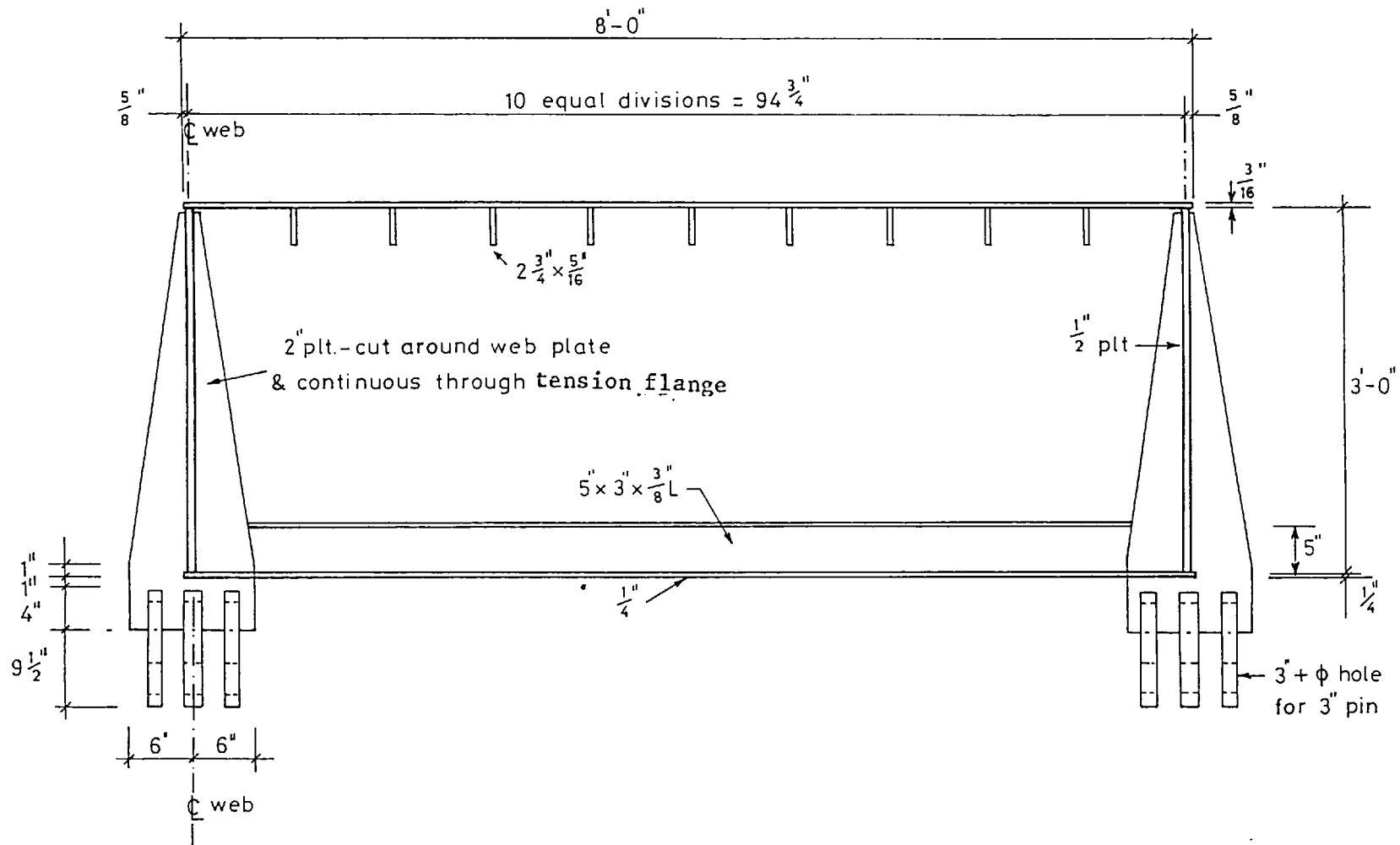
The loading systems used in the tests are represented in Fig. 6.1. In Models 1 and 3 a central load bearing diaphragm was used producing the high stress concentrations at the web-flange connection referred to in section 2.5.4. This was avoided in Models 9 and 12 by using tapered loading stiffeners to apply the point loads to the webs (Figs. 6.2 and 6.3). This explains the differences between the two point loading rigs represented in Fig. 6.1.

6.2   BASIS FOR REAPPRAISAL OF EXPERIMENTAL DATA

An interpretation of the experimental results from this series of tests based on the theoretical predictions of flange behaviour, obtained as a conclusion of the present study, is undertaken in this chapter. Only the aspects of the models' behaviour that were considered relevant for this reappraisal of test evidence are mentioned. Attention will be focussed on Models 9 and 12 where, because of the geometries, shear lag effects are more pronounced. More details of construction and testing can be found in references (29-32,76).

It was reported by Moolani[32] that by comparing the ultimate moments of the models in each pair (1 and 2, 3 and 4, 9 and 10) there was no evidence of significant weakening in flange strength caused by shear lag. It was also found that the experimental results agreed satisfactorily with theoretical predictions of flange capacity in

uniform compression, obtained using an inelastic beam-column theory developed for the analysis of box girder flanges[32]. The conclusion was that full redistribution had taken place in all the three models tested under point load.

Web failure was not a premature limitation to the mobilisation of the full capacity of the flanges. Even in Model 1, where preliminary tests indicated the need to strengthen the web against buckling, after this was done, the collapse occurred as a combination of compression flange and web failure near mid-span. Some interaction may have reduced the individual ultimate capacities of these components but the web alone did not govern the mode of collapse. In Model 9, yielding of the webs near the mid-span region occurred before ultimate load was reached. On the basis of the numerical research on the application of the upper bounds to the flange capacity (section 4.2) this again should not have limited the possibility of achieving the full flange capacity.

To comment on the behaviour of the models in the context of these upper bounds, the values of the α, α' and b/ℓ parameters were calculated as were the slenderness of the plate panels and the stiffener parametres ℓ/r and d_s/t_s (see Table 6.2).

It was shown in Chapter 5 that by representing the upper bounds to the flange capacity in the ψ and b/ℓ coordinate system (corresponding to the edge shear strength and the strength in axial compression), it is possible to assess, in certain conditions, if redistribution can be achieved. This is done by locating the flange (by its value of b/ℓ) in the region limited by the upper bounds. If the value of b/ℓ is much smaller than the one corresponding to the intersection of the two upper bounds (defined in expression (5.6) as $b/\ell*$) full redistribution

Table 6.2

Model No.	α	α'	b/ℓ	b'/t	ℓ/r	d_s/t_s	ψ_{max}	b/ℓ^*
1	0.197	0.262	0.256	48.8	53.9	–	0.654	0.700
3	0.437	0.405	0.256	24.	44.7	–	–	–
9	0.424	0.363	0.509	49.3	75.4	8.8	0.663	0.639
12	0.440	0.265	0.509	24.5	66.0	23.8	–	–

may be possible.   If b/ℓ is greater than b/ℓ* then the edge shear

strength governs the flange capacity.   For values of b/ℓ near b/ℓ*

the possibility of interaction between the two modes may reduce the

flange capacity corresponding to either of the two upper bounds.   To

estimate this reduction the representation of the upper bounds in the

system of reduced coordinates used in Fig. 5.10 may be useful.

The reliability of this approach depends on the confidence that

can be placed on the derivation of the upper bounds and on the possibility

of assuming an appropriate transition curve to assess interaction.

For Models 1 and 9 the compressive strength of the stiffened

panels was calculated analytically by Moolani[32] and the corresponding

values of ψ_{max} are given in Table   6.2 .   Assuming for all

cases that the upper bounds corresponding to the edge shear capacity

can be calculated neglecting the effects of buckling of the edge panels,

expression (4.9) can be used to obtain for these two cases the b/ℓ*

values (Table 6.2).

It would have been interesting to use the present numerical solu-

tion to calculate the compressive strength of the flange of Model 9 for

comparison (those of models 1 and 3 do not have flat type stiffeners),

and that of Model 12.   However, the number of stiffeners in the flanges

is greater than the maximum of six that can be treated in the program

to date.

6.3   INTERPRETATION OF TEST RESULTS

6.3.1   Models 1 and 3

In the case of Model 1 the aspect ratio b/ℓ is sufficiently

smaller (0.256, see Table 6.2) than the b/ℓ* value (0.700) to be possible

to predict that the shear lag effects should not have noticeably reduced the flange capacity. This difference is enough to accommodate any reduction in the upper bound corresponding to the edge shear failure due to buckling. The fact that a diaphragm existed at mid-span which could prevent the development of overall large deflections, thus reducing even more the risk of any possible interaction of this mode of failure with the inelastic buckling mode, makes such a prediction more reliable.

Given the characteristics of Model 3, the compressive strength of its flange should be higher than that of Model 1. On the other hand the equivalent stiffening factor was substantially higher (0.405). Both these factors reduce the $b/\ell*$ value. However, even for ψ_{max} = 1.0 the $b/\ell*$ correspondent to α' = 0.405 is 0.411 which is still 1.6 times the value of b/ℓ. As the possibility of edge panel buckling was reduced in this case (due to the use of stocky plate panels), it should make it possible to predict, perhaps with even more confidence, that the full flange strength was mobilised at collapse. These simple criteria are thus sufficient to explain the experimental results which showed that full redistribution was achieved.

6.3.2 Model 9

To apply the same method to Model 9, the value of b/ℓ = 0.509 should now be compared with $b/\ell*$ = 0.639 (Table 6.2). Although b/ℓ is still smaller than $b/\ell*$, the difference between the two is smaller than in the previous cases, indicating that interaction of the two modes of failure was more likely to have reduced the flange ultimate capacity in this box. However, this does not seem to have been the case judging from the conclusions of the experiments[32].
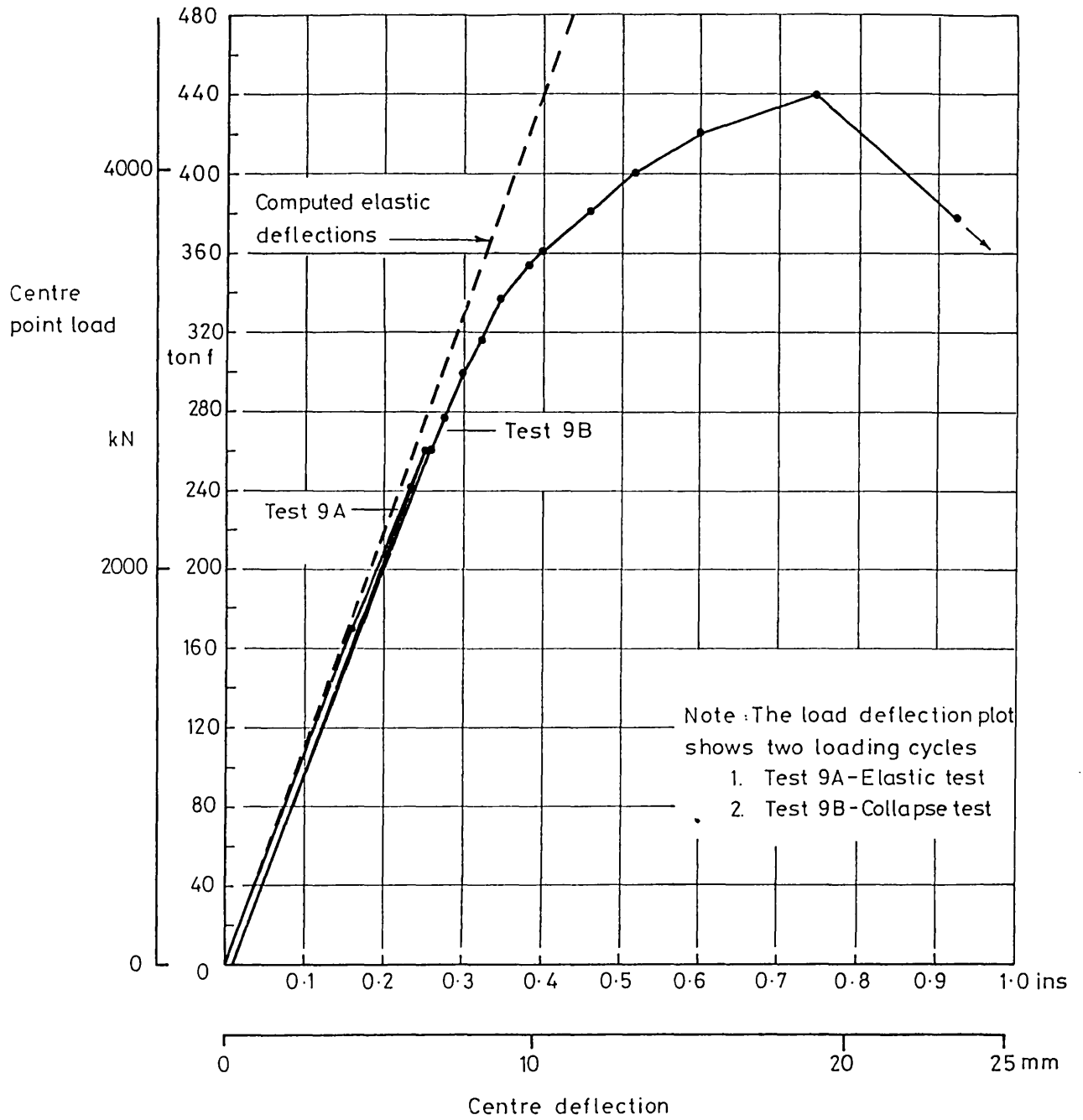
Fig 6·4
Model 9: Load-deflection curves

Some characteristics of the behaviour of this model may be useful to the understanding of these conclusions. The initial imperfect shape of the compression flange included an upwards bow of the central bay. Although the column slenderness of the stiffeners and associated plate was high (75.4) they had a stocky cross section. Up to near collapse the central stiffeners were observed to deflect upwards without buckling.

This could explain why the effects of overall large deflections may also have been avoided during redistribution and interaction between the modes of failure again reduced. This effect was demonstrated in the study of the influence of the shape of imperfections in the collapse of a $b/\ell = 0.5$ flange (section 5.3). There, an imperfection producing a stiffening effect at mid-span (case IV, Fig. 5.4) could reduce the mode interaction and increase the flange capacity.

It should also be emphasised that in stiffened flanges the interaction between these modes seems to be less pronounced than that found for unstiffened flanges. This is a conclusion that can be inferred from the results of Fig. 5.11.

Another aspect of the behaviour of this model deserves comment. This refers to the pattern of development of panel buckles noticed before collapse. After a preliminary test (Test 9A, Fig. 6.4) collapse was reached at a centre point load of 440 tonf (Test 9B, Fig. 6.4), with all the stiffeners in the central bay deflecting inwards. Extensive yielding across the flange in the mid-span region was observed.

The mechanism of stress redistribution was initiated by the formation of buckles at the edge panels at mid-span. This could be expected from the value of panel slenderness of nearly 50. The for-
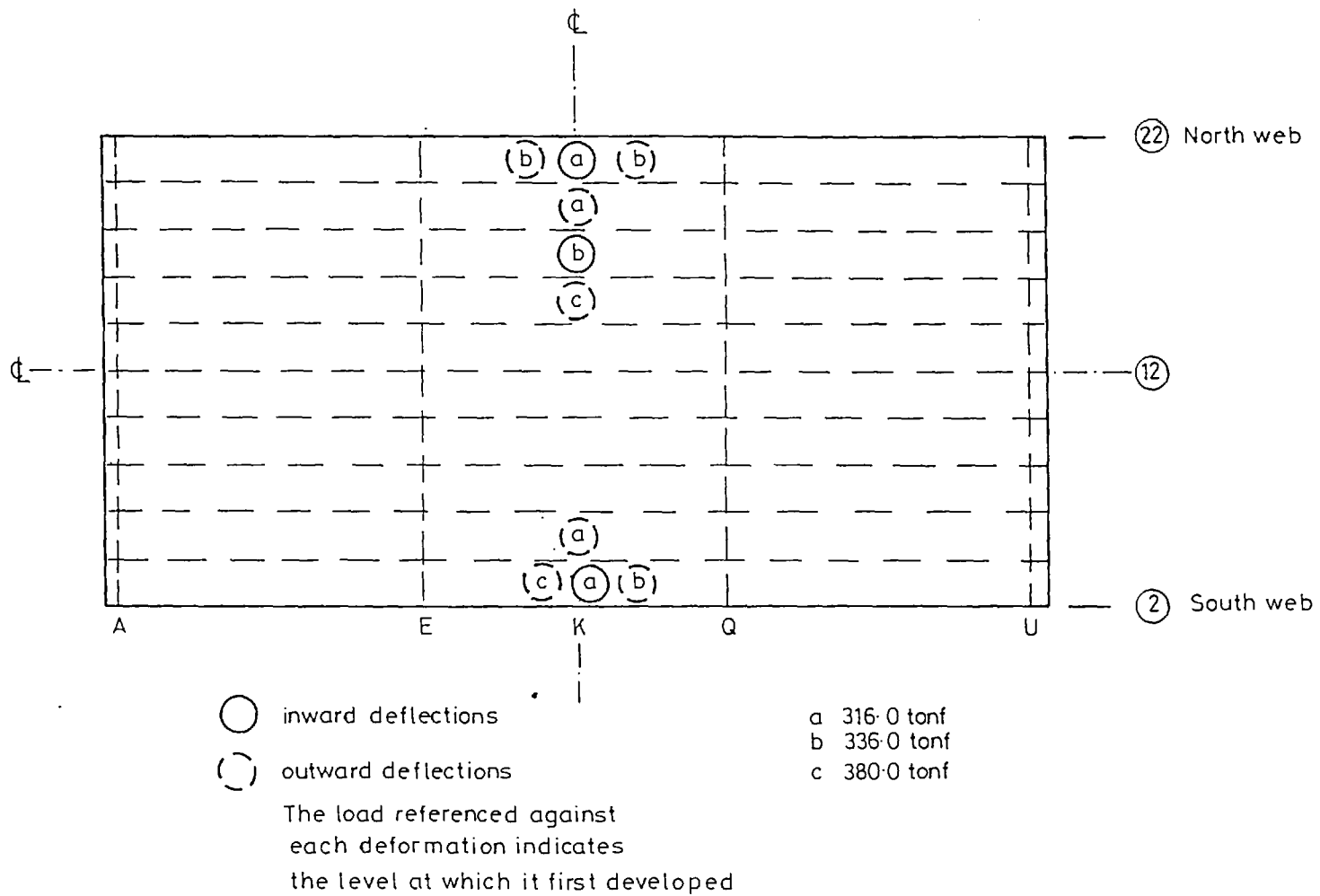
Fig 6·5   Model 9
Test 9B · Development of compression flange plate panel buckles

mation of these buckles progressed across the flange towards the centre and along the edges (Fig. 6.5). This phenomenon can be explained by the close proximity of the two upper bound values for the flange capacity mentioned above. A similar propagation of buckles was obtained numerically in the example of Fig. 4.13c, where they form earlier in the edge panels and increase in depth before those in the central panel develop.

The significance of the post-ultimate strength behaviour of the edge plate panels in the context of redistribution was identified in reference (28). This was based on the observations made in relation to Model 9 that after buckling of the edge panels they had to continue to sustain considerable straining without substantial unloading, while the capacity of the central ones was being mobilised. The relevance of these conditions to full redistribution is clear and was discussed in section 4.4.2 in relation to the example of Fig. 4.13c. The process of redistribution is also governed by the total shear flow which the edge panels can transmit and in a sufficiently long beam a fall-off in the carrying capacity of the edge panels at mid-span does not stop the process of mobilisation of the central zone.

It was already stated that the characteristics of Model 9 indicate that this shear flow did not limit the full flange capacity to be reached. This is confirmed by the fact that extensive parts of the longitudinal edges remained elastic up to collapse. On the other hand, even if due to the relatively high panel slenderness

the shear strength of the edge panels was reduced by buckling action and the corresponding upper bound lowered, this strength should still be sufficient to mobilise the central part of the flange. This is due to the fact that interaction with overall buckling was avoided.

The full yielding of the unstiffened tension flange over the mid-span cross section noticed[32] at the maximum sustained load is also predictable in terms of the upper bounds to the capacity of the flange (Chapter 4).

The aspect ratio b/ℓ of the flange (0.509 - Table 6.2) is just smaller than the critical value of 0.577 (expression 4.10) beyond which the edge shear strength would also limit the reaching of maximum yield tension force. Although the maximum strength of the compression flange was much smaller than the full plastic capacity of the tension flange, the ultimate bending moment of resistance at mid-span is not reached until both strengths are exhausted. This corresponds to the mechanism of redistribution of longitudinal stresses within the cross section at collapse discussed in section 4.1. It occurs because the shear strength of the webs is not a limiting factor. These continued to carry more shear beyond the load which produced a fully yielded mid-span cross section as has been proved numerically to be possible.

6.3.3   Model 12

The general characteristics of this model are given in Tables 6.1 and 6.2. It was designed to study shear lag effects in a flange collapsing by failure of the stiffeners in compression. This model had approximately the same aspect ratio b/ℓ and the same geometric stiffening factor α as Model 9. However, as the stiffener material
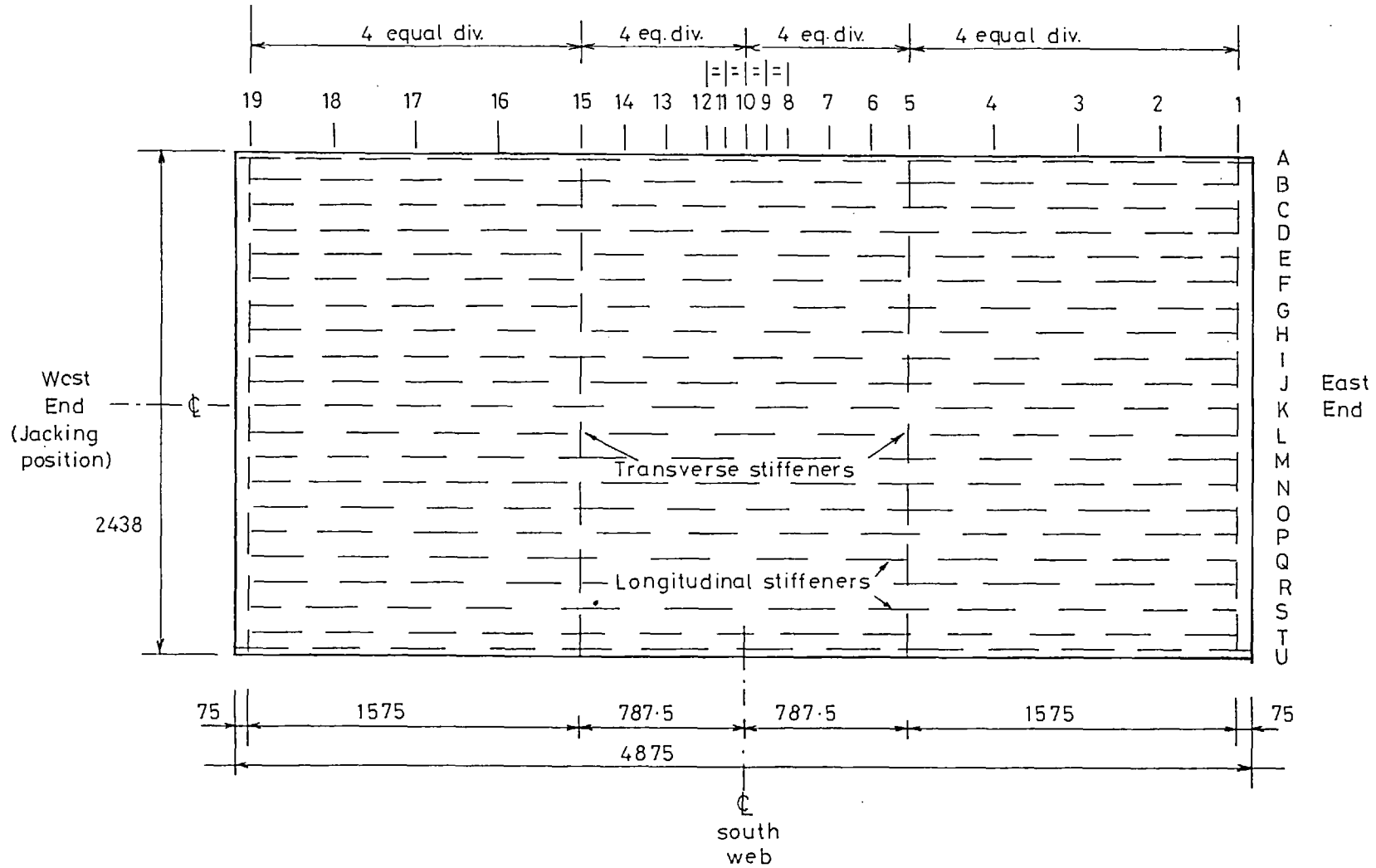
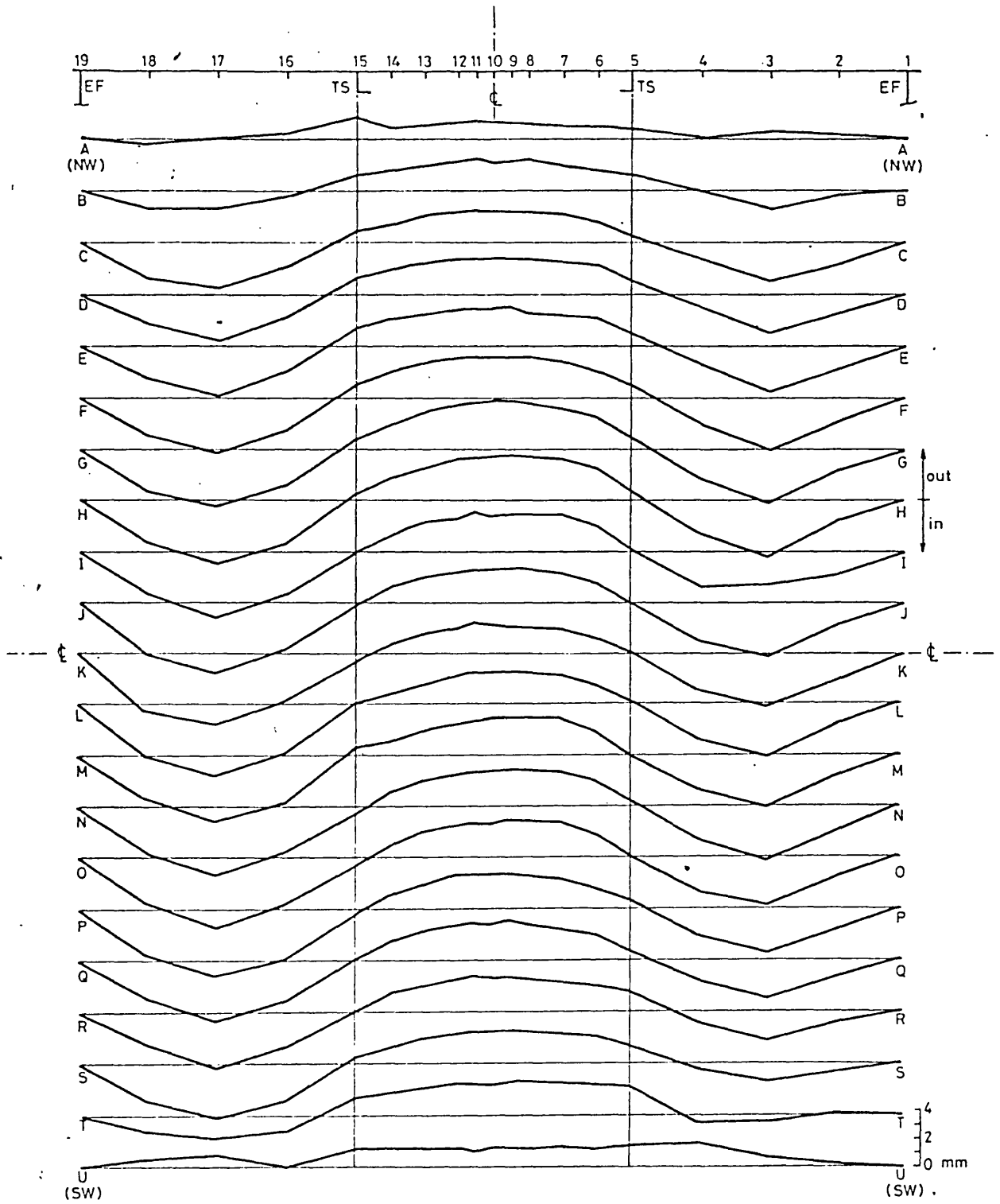Fig 6·6 Model 12: Compression flange showing reference grid

Fig 6·7 Model 12 Compression flange initial deformations:
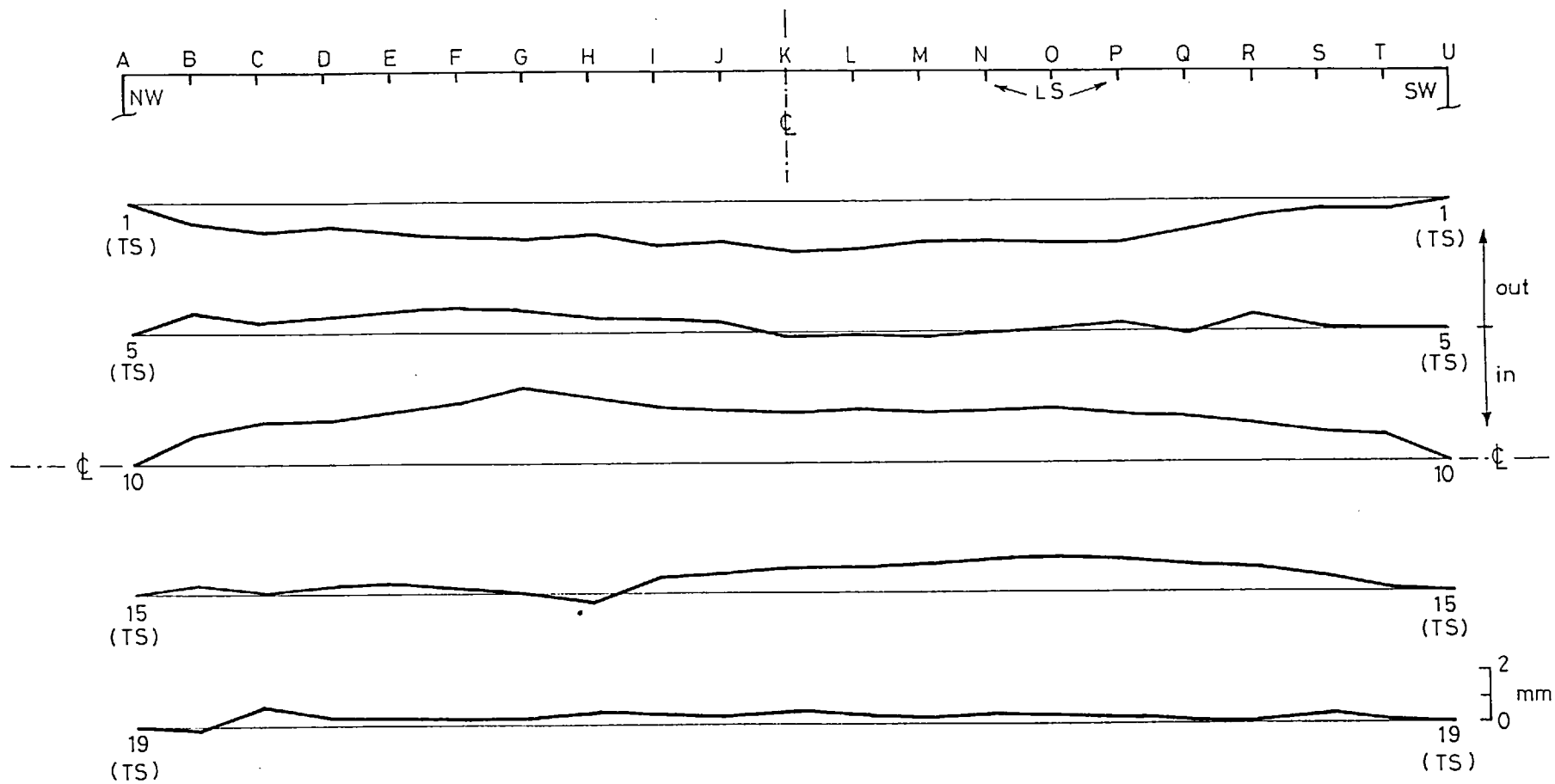Profiles along webs and longitudinal stiffeners

Fig 6·8 Model 12

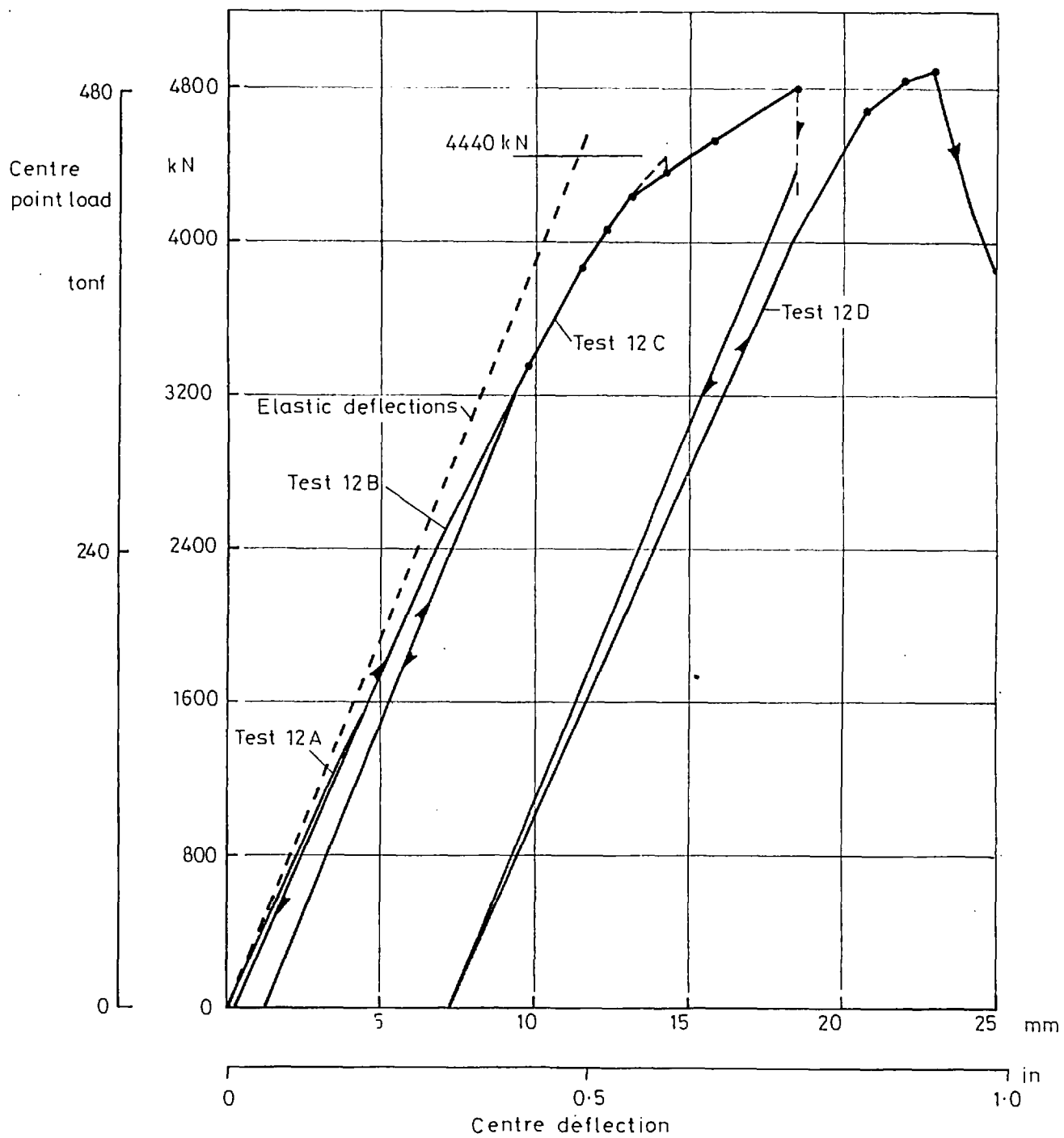Compression flange initial deformations: Transverse profiles

Fig 6·9

Model 12: Load-deflection curves

had a lower yield stress   the equivalent stiffening factor α' was smaller than the Model 9 value.   On the other hand providing the mode of failure was similar to that of Model 9 the flange strength should have been greater, and these two factors combined produce approximately the same value for b/ℓ^*.   Had Model 12 failed by plate compression the reduction of ultimate flange capacity by shear lag effects would thus be even smaller than that found in Model 9.   To induce the required mode of failure a greater number of stiffeners with more slender cross sections was used and the slenderness of the plate panels was thus lowered (Fig. 6.3 and Table 6.2).   This reduced the risk of any premature panel buckling.

At the same time the compression flange was fabricated with a distorted shape containing an upwards bow in the central bay and a downwards deflection in the end bays.   These imperfections were measured accurately with the help of a theodolite and are presented in Figs. 6.7 and 6.8 referring to the grid indicated in Fig. 6.6.

After some preliminary tests to chart the elastic response (Tests 12A and B) the model was loaded to collapse (Test 12C).   The general behaviour is summarised in the load-deflection curves of Fig. 6.9.   Details of testing are to be published in a special report[76] and are omitted in this discussion.

At a central point load of about 4440 kN, the stiffeners F, G and H situated to one side of the box at about the quarter width failed by sudden tripping near the mid-span cross section.   This is signalled in the load-deflection curve by a drop in the carrying capacity of the model and the situation obtained at that stage is shown in photographs (Fig. 6.10).   A view of the flange underside taken at that load level
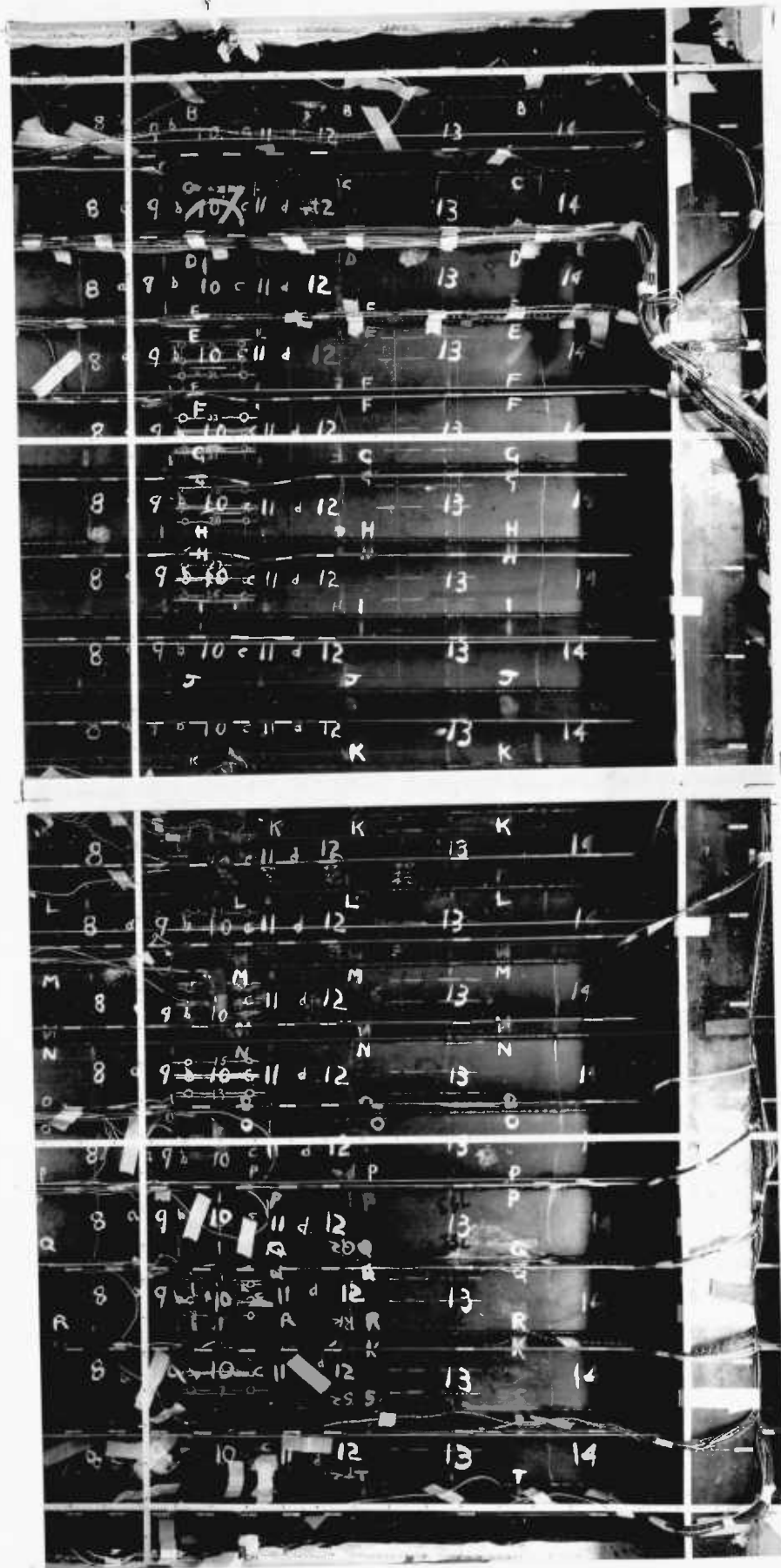
Fig. 6.10   Model 12 - view of underside of central bay showing failure
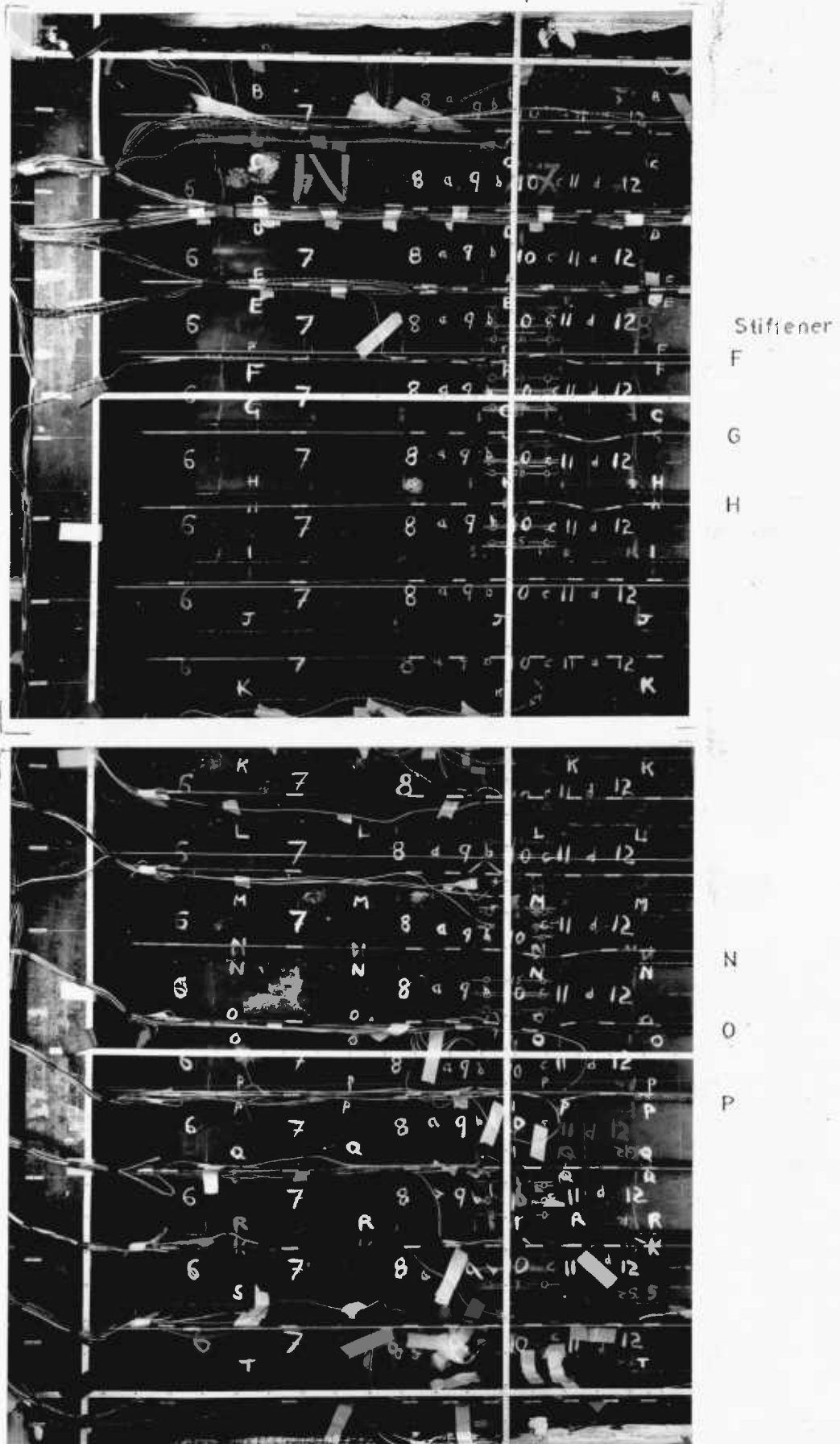of stiffeners F, G and H (Test 12C - at 4440 kN point load)

Fig. 6.11   Model 12 – view of underside of central bay showing failure
of stiffeners F, G, H, N, O and P (Test 12C – at 4540 kN
point load)

from points close to the west end side transverse stiffener is shown. The local buckles of those stiffeners can be identified by the displaced position of the targets that were fixed to the tips of the outstands. After equilibrium was reestablished the loading was increased again and a similar failure of stiffeners N, O and P located at the other quarter width soon followed (at about 4540 kN). This is shown in photographs (Fig. 6.11) taken from points closer to the east side transverse stiffener which can be seen in the photographs.

After more loading was applied local buckles were noticed on stiffeners B and T (adjacent to the webs) at the ends of the central bay near the connections to the transverse stiffeners. This was followed by similar failures of stiffeners C, D, Q and S. The load at which this occurred was not accurately recorded but photographs taken at 4640 kN already show this failure on stiffeners B and T. By now stiffeners E and I on one side of the longitudinal central line and M on the other had also failed by tripping near mid-span. Soon afterwards, at approximately 4800 kN, the bracing frame at the end where the jacking was applied failed and the testing was stopped. At that stage the pattern of buckles on the stiffener outstands had not altered and stiffeners J, K and L appeared to remain straight and R showed a pronounced overall lateral deflection. After unloading permanent deformations were visible in all the stiffeners that had buckled at mid-span and in the stiffeners adjacent to the webs (B and T).

The final collapse was achieved in a later loading test (Test 12D) after appropriate reinforcement was provided to the end bracing frames. The ultimate load was accompanied by an overall buckling of the central bay deflecting upwards[76].

The somewhat unexpected first failure of the quarter-width stiffeners in Test 12C is a very interesting feature of the behaviour of this model. In Model 10, which was loaded to produce uniform compression in the flange, the general buckling mode was of a similar nature i.e. compression of the stiffener outstands (with the central bay panel deflecting upwards). However, the stiffeners failed almost all at the same time with a smooth lateral deflection at mid-span. It appears therefore, that the difference in behaviour is associated with the interaction of shear lag effects with this buckling failure mode.

By examining the growth of deflections in the compression flange during Test 12C, using the longitudinal and transverse profiles in Fig. 6.12 and 6.13, it is possible to see that the stiffeners near the webs followed the overall deflection of the girder. However, at some stage the stiffeners which failed first (F, G and H) started deflecting upwards. This upwards movement increased with loading and was quite pronounced at the load that caused their failure. The transverse profiles of Fig. 6.13 show that stiffeners N, O and P followed closely the web deflections until the others failed and suddenly deflected upwards in the same manner. The profiles also show that simultaneously the stiffeners adjacent to the webs had increased downwards deflections. During Test 12C the central stiffeners maintained a deflected shape that followed the overall bending of the webs.

The variations of longitudinal strains on the plate over the stiffener lines and at the tip of the stiffener outstands at mid-span are shown in Fig. 6.14. These indicate an initial bending of all the stiffeners following the overall deflection and a reversal of this bending pattern in the stiffeners that failed by tripping at mid-span.
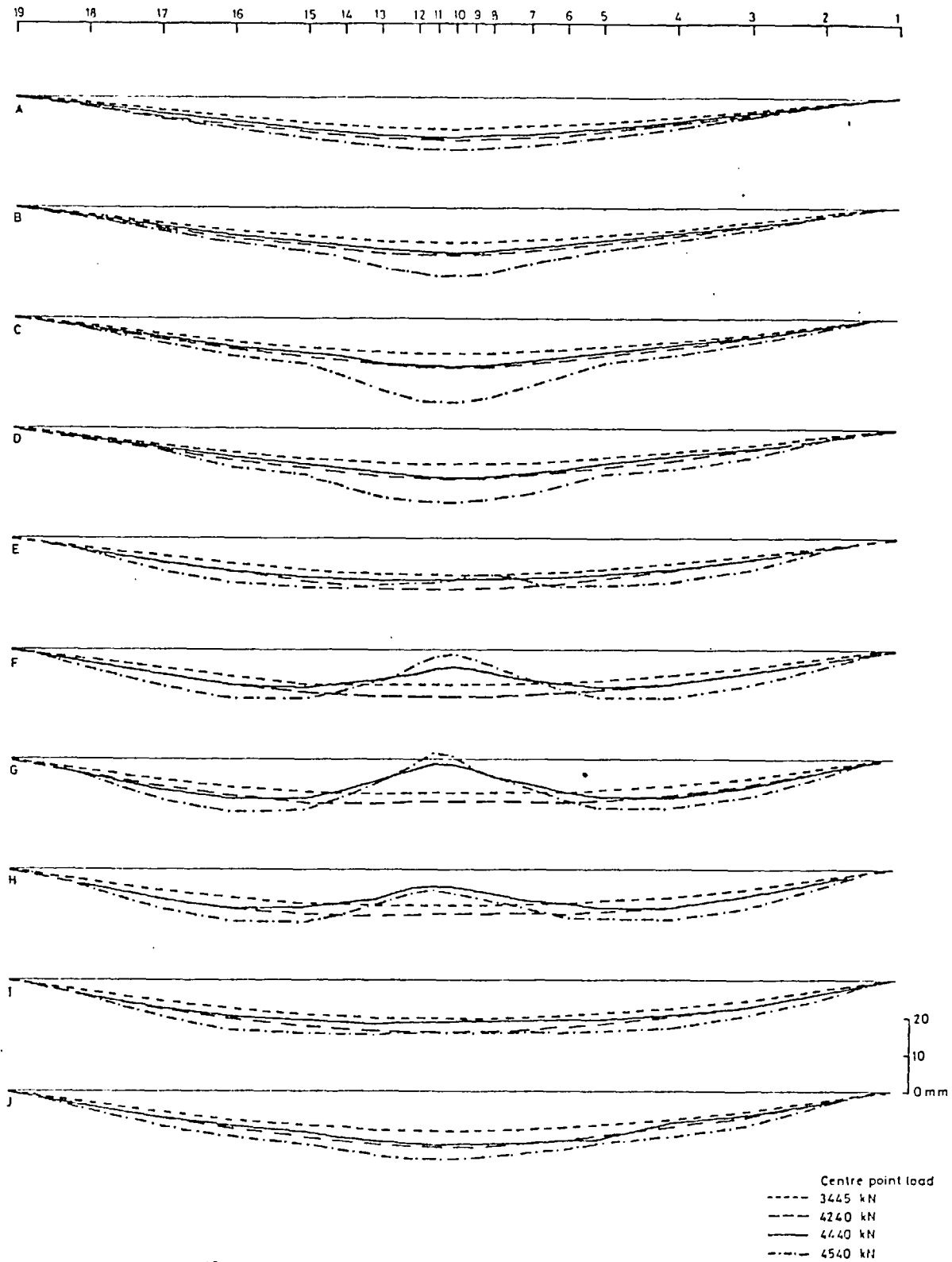
Fig 6·12   a. Test 12C Compression flange deflections   under load
Profiles along webs and longitudinal stiffeners
(initial and previous residual deflections
are not included)
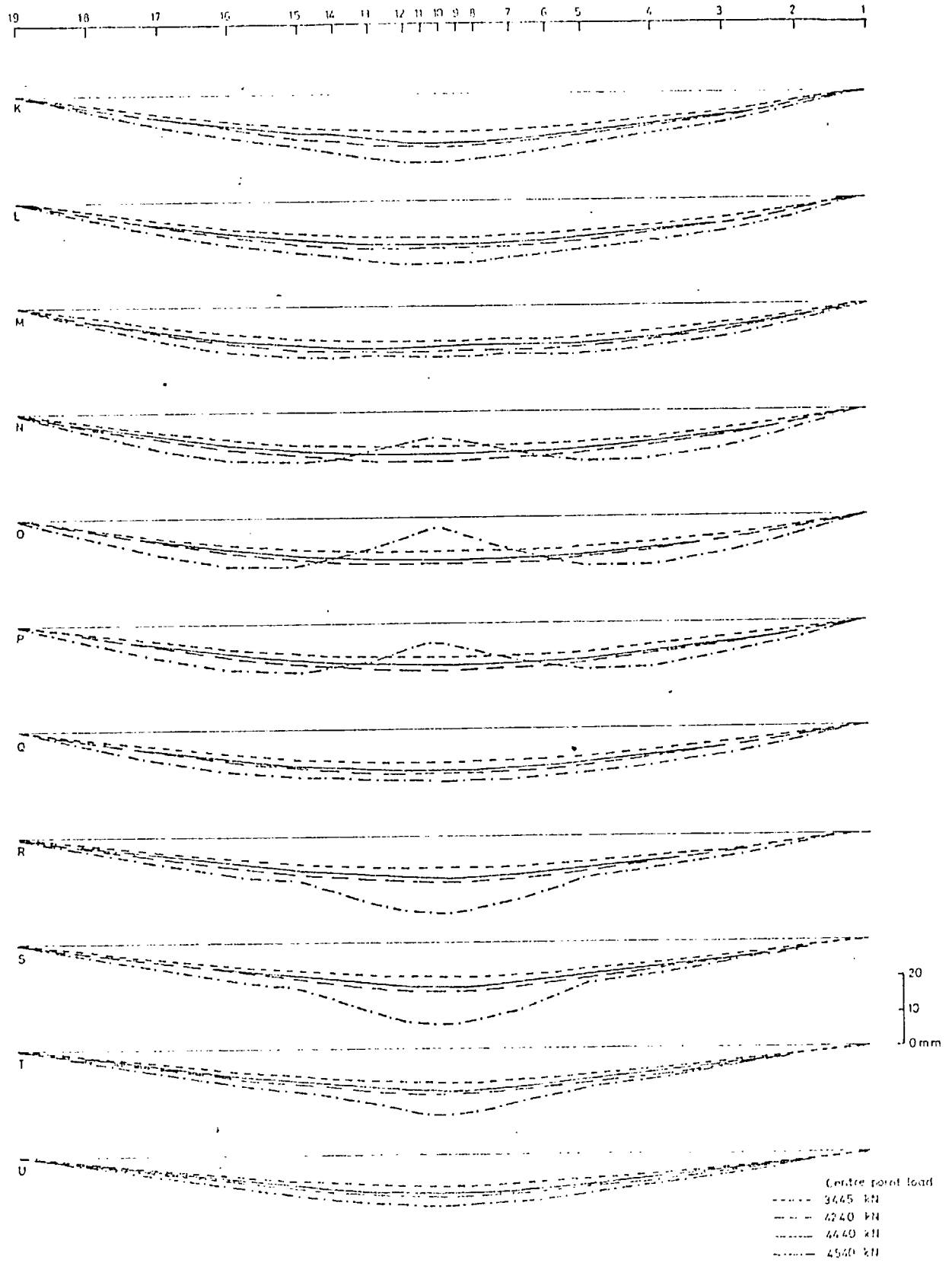
Fig 6.12 b — continuation
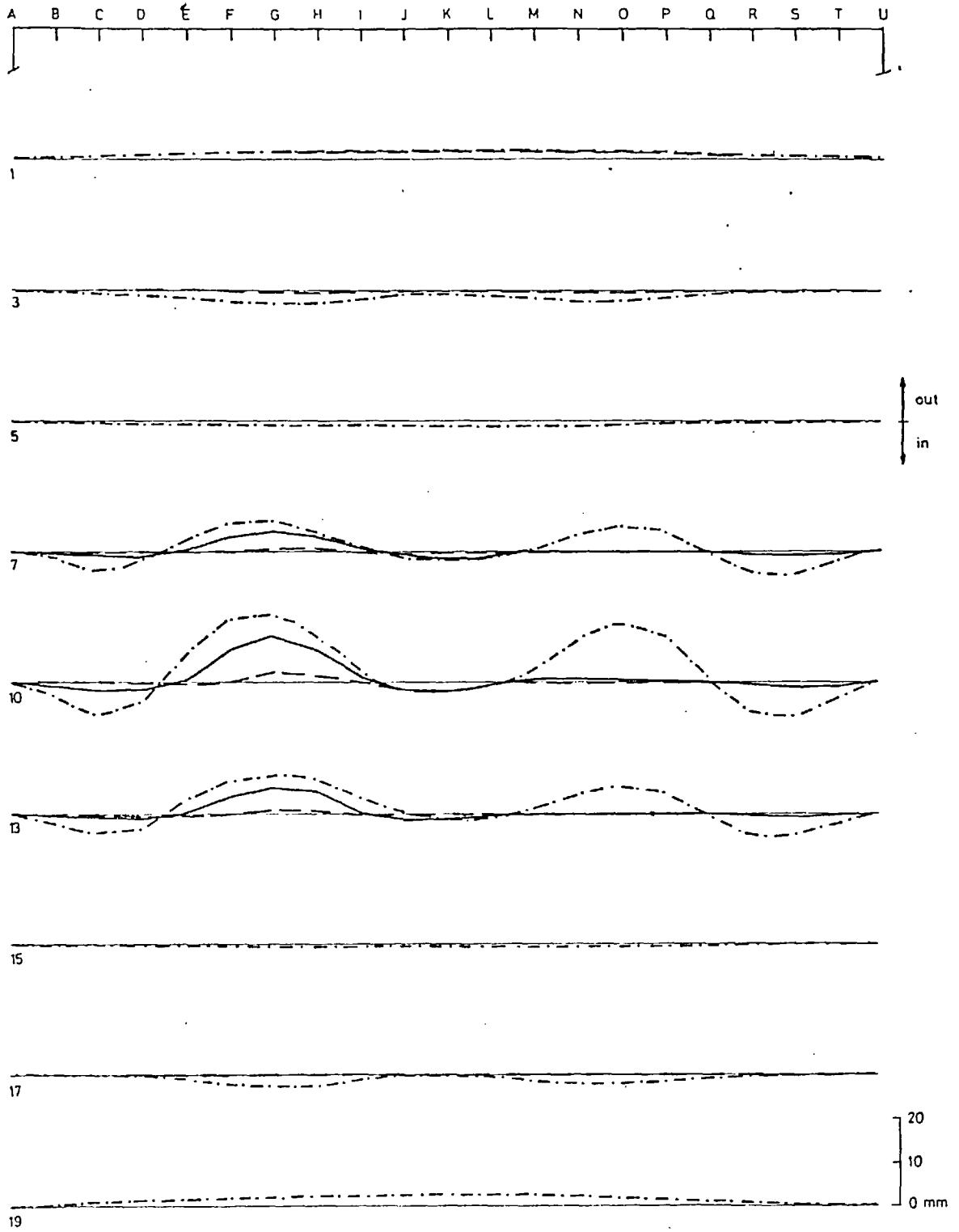
Fig 6·13

Test 12 C Deflections under load, transverse profiles
(initial and previous residual deflections
are not included)

Centre point load

— — — 4240 kN
————— 4440 kN
—·—·— 4540 kN
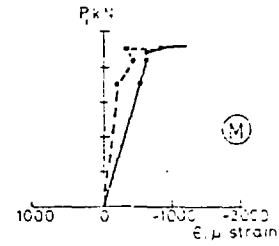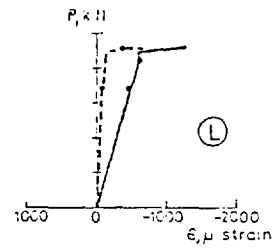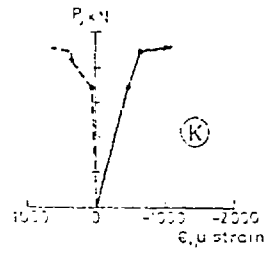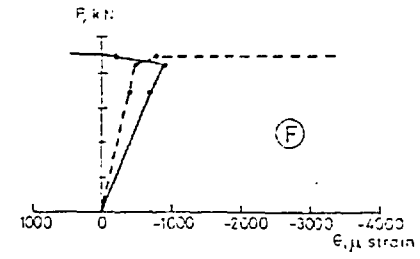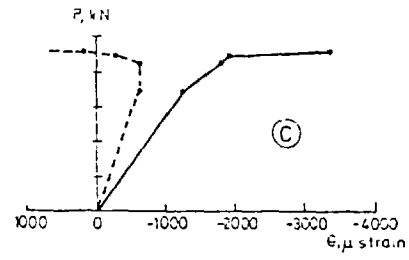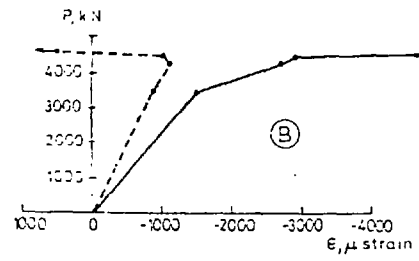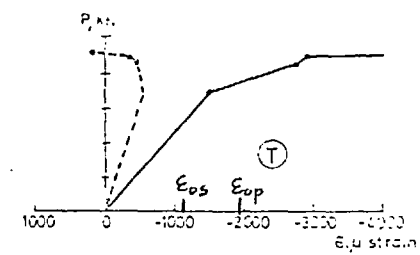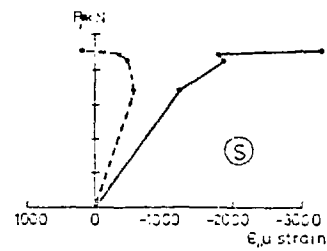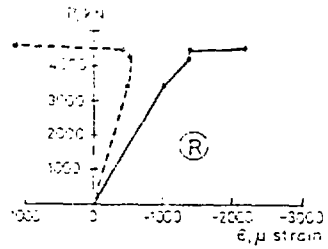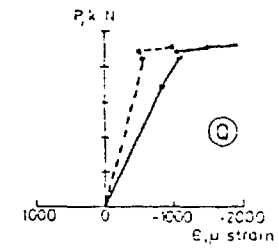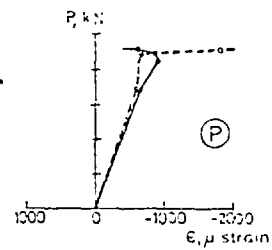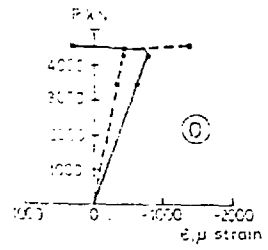
Fig 6·14 Test 12C : Strain in longitudinal stiffeners
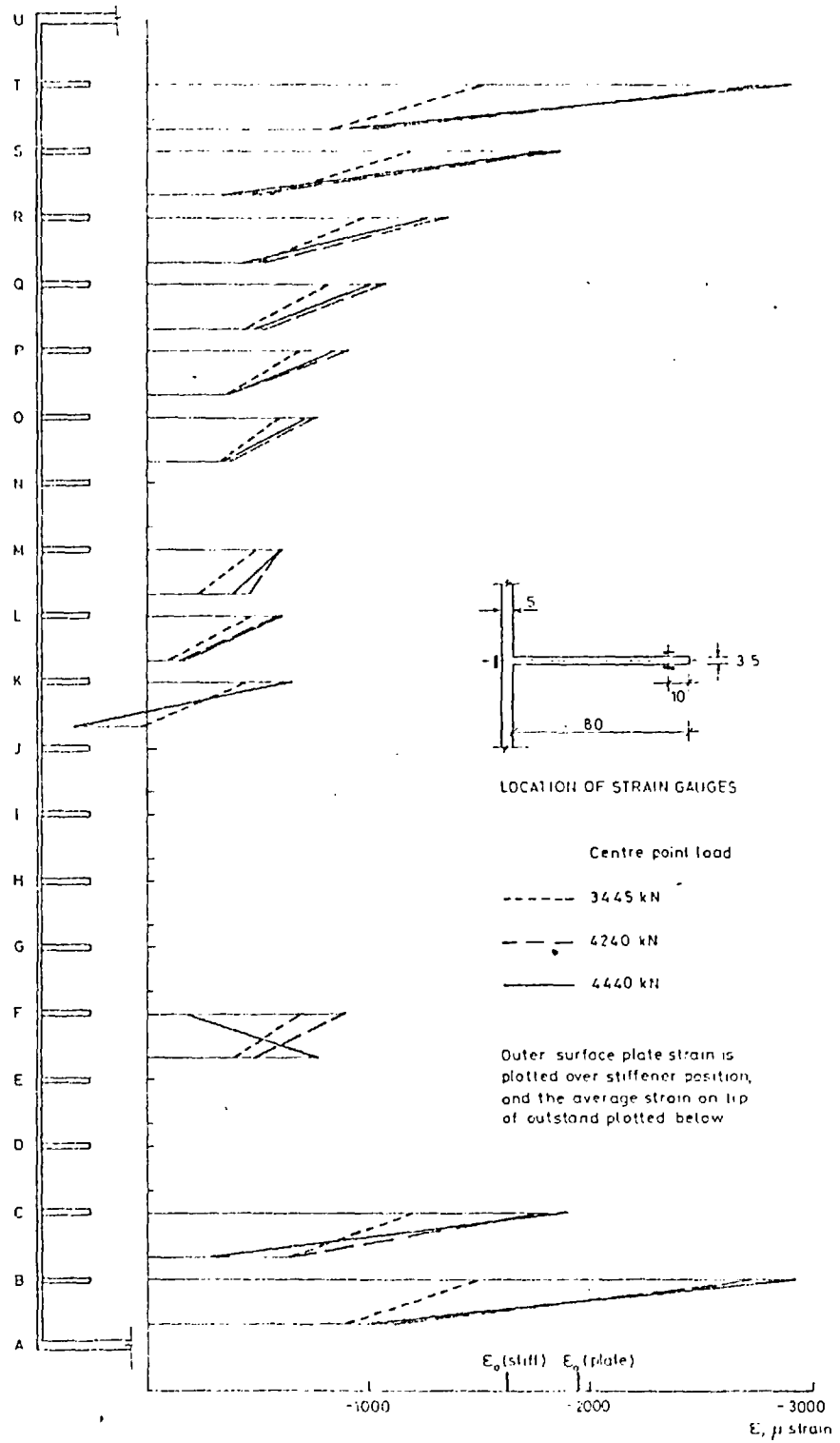
Fig 6.15 Test 12C – Longitudinal strain in stiffeners at mid-span
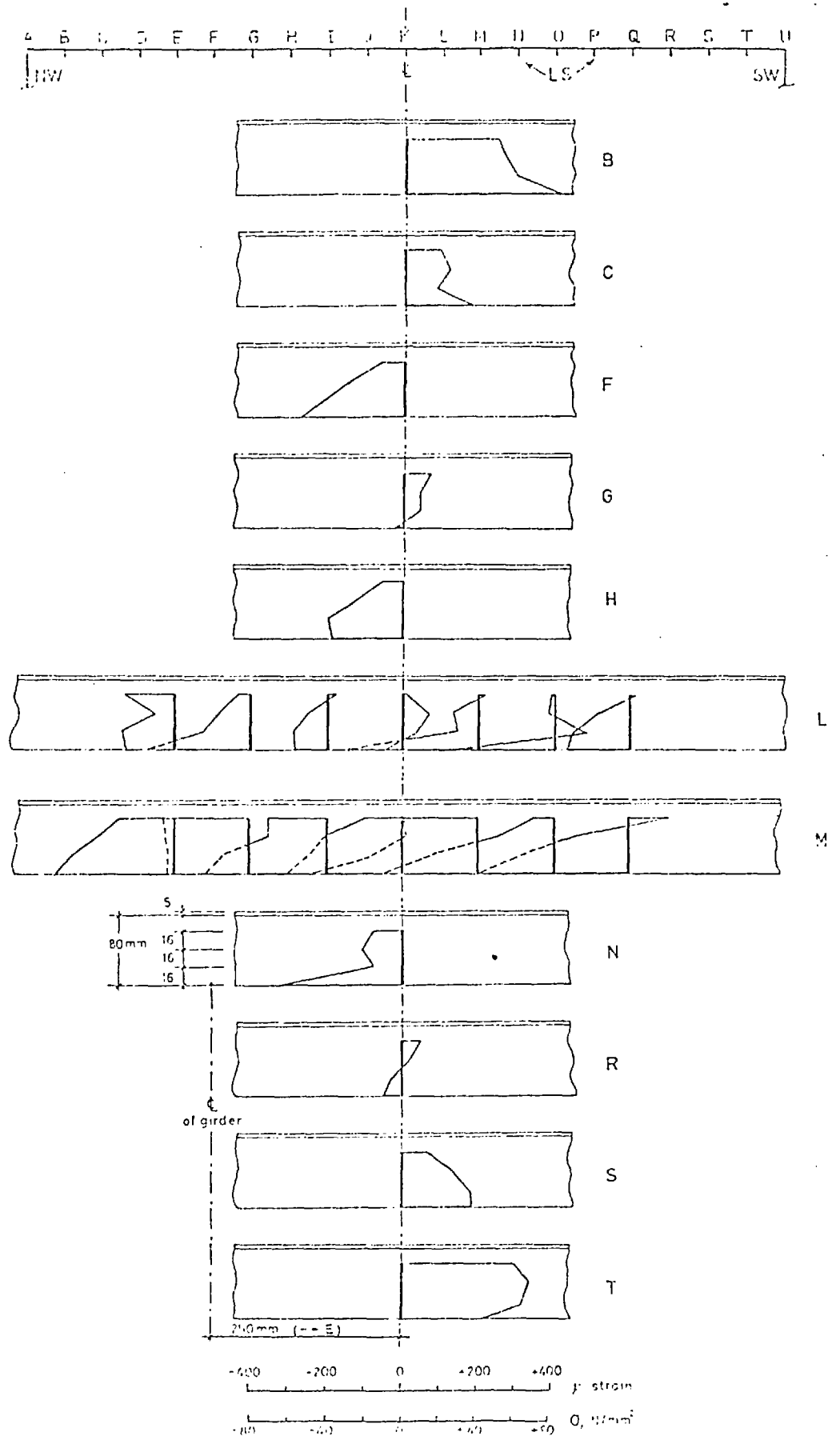
Fig. 6.16 Residual welding strains in longitudinal stiffeners
Stiffeners B,C,S,T after fabrication, remainder after
erection for testing

The average compression straining across the width follows a shear lag type of distribution.

From this evidence alone a first interpretation of the failure mode can be proposed. The distribution of average straining across the width due to overall bending peaks near the webs and has a minimum value at the centre due to shear lag. On this strain distribution are super-imposed bending strains varying over the depth of the stiffeners caused by the webs deflecting downwards. The stiffeners tend to develop ten-sile strains at their tips. These deflections are reduced towards the centre and would therefore produce an anticlastic distortion of the central bay panel i.e. a type of"bending lag"occurs. If due to the shape of initial imperfections a tendency to deflect upwards is intro-duced, the resulting distribution of bending strains in the stiffener outstands could produce tensile straining near the webs and compressive strains at the centre. These strains superimposed on the average shear lag type of strain distribution can produce maximum compression in the tips of stiffeners away from the webs or the centre line. This could also explain why, in a shear lag type of environment, the stiffeners near the webs develop bending moments at the connection to the transverse stiffeners producing high compressive strains on the tip of the outstands which fail, like those of Model 12, at their ends. These moments correspond to the restraint imposed by the transverse stiffeners and adjacent longitudinally stiffened bays to the rotation of the ends necessary to follow the downwards pulling action of the webs.

The transverse profile of the initial deflections at mid-span shows a small peak nearly over the F, G and H stiffeners(Fig.6.8). However, at first examination this does not indicate why only these stiffeners

reversed the initial trend to deflect downwards and why they subsequently

buckled upwards following the sign of their initial bow.   It might

also be of interest to record that at the quarter width stiffeners

compressive residual stresses were measured after erection (Fig. 6.16)

and these may have contributed to the earlier failure of these stiffeners.

However, these stresses also occur in the central stiffeners and

thus could not have been responsible for the reversal of

deflections.

The reversing of deflections and change of sign in the corres-

ponding strains is perhaps more clear in the representation of the varia-

tion of strains over the depth of the stiffeners used in Fig. 6.15.

The superposition of the two systems of strains mentioned above is evi-

dent.   Up to a point load of 4240 kN the overall deflection is reflected

by the regular pattern of bending strains.   The anticlastic curvature

of the panel is indicated by the decrease of the bending component

(bending downwards) from the webs towards the centre.

An attempt to interpret numerically the behaviour of this flange

was made using the program developed for the present research.   As the

program can only consider to date up to seven plate panels, the dimensions

of the numerical model (Fig. 6.17) were adjusted to maintain within this

constraint the principal characteristics of Model 12. That is, the same

values for the governing parameters α, α', b/ℓ, b'/t and ℓ/r (see Table

6.2) were used.   The material properties of the various components

were retained and the real thicknesses of the flanges and web plates

were also used.   Consequently, the width of the flange of the numerical

model corresponds to seven panels of the real flange, and the total

length and cross-sectional dimensions of the stiffeners (d_s and t_s) were

calculated to obtain the same values for α, b/ℓ and ℓ/r. The value of d_s/t_s cannot be simultaneously controlled and therefore a smaller value was used in the numerical model than that employed in Model 12. However, as stiffener local buckling cannot be treated in the present numerical solution this should not affect the exercise. As the deflections of the webs were found to have an important influence on the flange behaviour, the depth of the webs was reduced to produce comparable overall bending rigidities between theoretical and experimental model (i.e. to obtain approximately the same value for the ratio I/ℓ^2, where I is the cross-sectional moment of inertia).
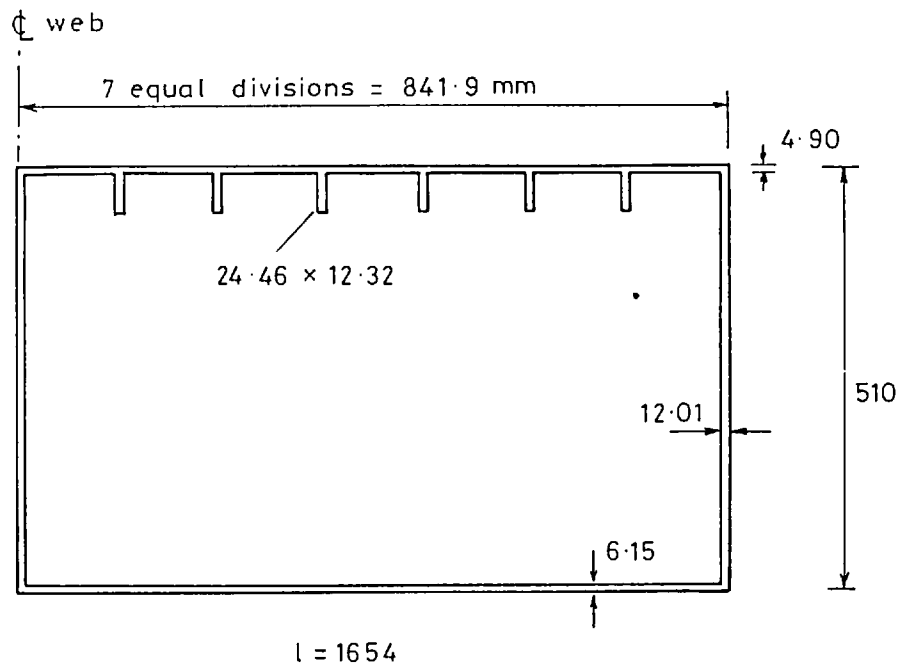
Fig. 6.17 Dimensions for numerical simulation of Model 12

To simulate the effects of the transverse stiffeners the shape of the initial deflections was assumed to have three equal half sine waves in the longitudinal direction.

The program was used to study the effects of initial imperfections with different profiles on the flange behaviour. The results obtained by varying the maximum amplitude of these profiles showed that if its value was taken to be proportional to the initial distortions measured in Model 12, the overall deflection of the girder was sufficient to reverse the initial deflection over the central 'bay' after a small level of loading. This was mainly due to the transverse bending rigidity of the modelled flange being relatively higher (only seven plate panels) than that of the real structure. This reversal was noted in Model 9 which also had small upwards initial distortions over the central bay but failed by a downwards deflection of this panel. By exaggerating the amplitude of the upwards distortions it was possible, however, to make the numerical model deflect in this direction. This is shown in Fig. 6.18a where a transverse profile with a half sine-wave shape was used. In this case, the flange maintained an almost horizontal transverse profile at the third-length cross sections, thus indicating that the effects of the transverse stiffeners had been satisfactorily modelled. In the same figure the strains in the stiffeners are plotted against the flange capacity measured by the inelastic effective width ratio ψ. As expected from the shape of the deflections, the average strain follows a shear lag distribution and the bending components (measured by the difference in the strains near the plate and at the tip of the outstands) increase from the web towards the centre. The deflection of the web reduces the bending strains in the adjacent stiffener. This pattern of strains in the stiffeners is relatively easy to produce to

show the interaction between shear lag effects and buckling by compression of these stiffener outstands (panel deflecting upwards).

The results of superimposing on the one half-sine wave shape of the transverse profile different proportions of a five half-sine wave profile are presented in Figs. 6.18b and 6.18c. This component enhanced the downwards deflections in the stiffeners adjacent to the webs and at the same time activated the upwards movement of the second stiffeners (at quarter-width). In both cases the influence of the imposed web deflection was to eventually reverse the upwards movement induced by the shape of the initial distortion in the central zone. This is partially due to the approximation used to model the transverse stiffeners but is also due to the high transverse bending rigidity as mentioned above.

When this occurs the results can no longer be used because at the third-length sections downwards deflections also take place thus 'removing' the simulated 'transverse stiffeners'. However, this is only initiated at load levels beyond $\psi = 0.35$ and before that level the strain variations may still be useful to explain the behaviour of Model 12. It was not possible in any of the cases investigated to produce a significant downwards initial bending movement following the deflection of the webs as was noticed in Model 12. However, in both the cases of Figs. 6.18b and 6.18c it was possible to model the downwards deflection of the stiffener adjacent to the web(which increases without affecting the upwards movement of the second stiffener) and to produce in the central stiffeners a reversal of the deflection earlier than in the quarter-width stiffener(this is more clearly shown in Fig. 3.18c). The average strain in the stiffener adjacent to the web is reduced in these
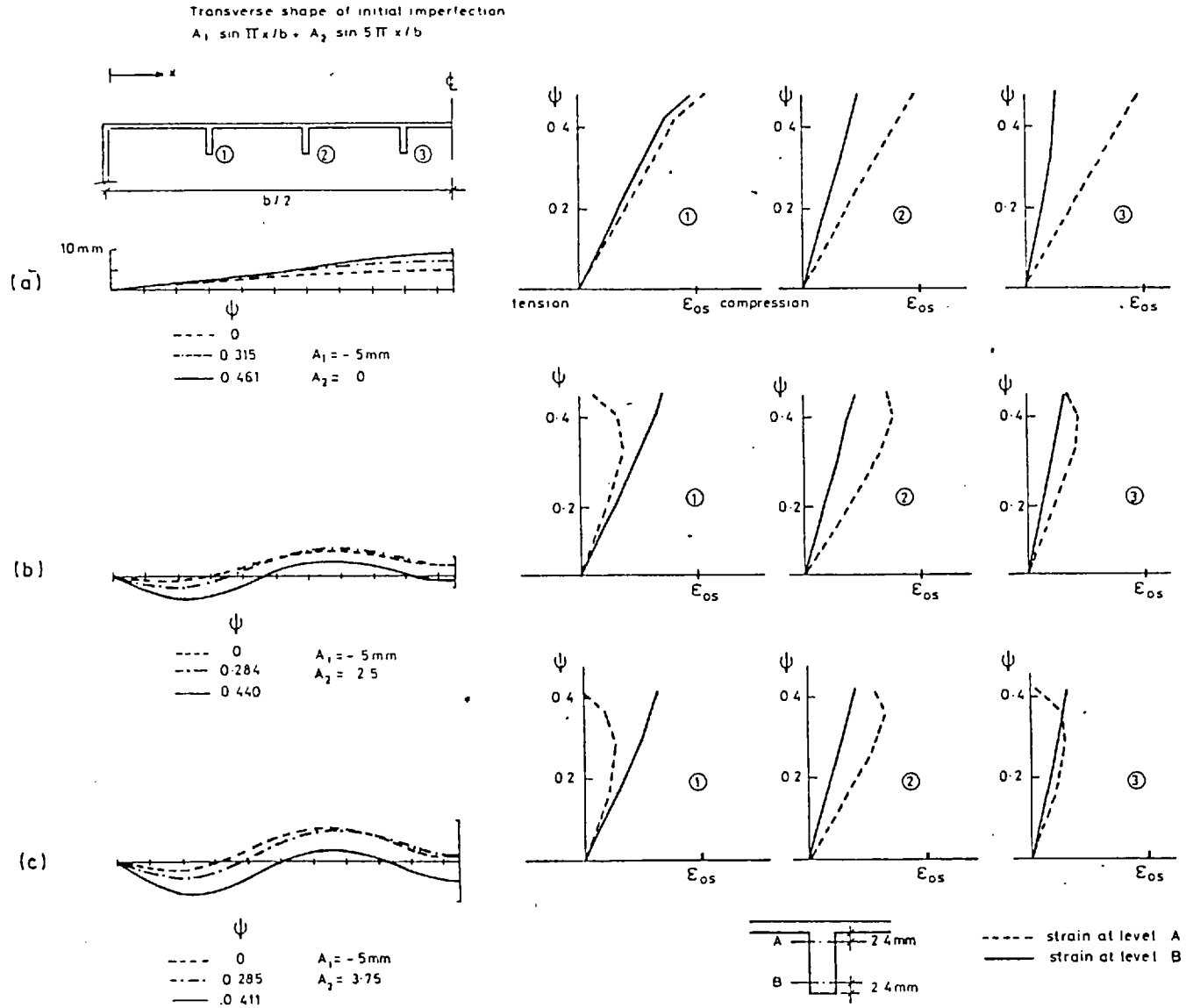
Fig 6·18 Numerical simulation of Model 12. Deflections and strains in stiffeners at mid-span for different initial imperfections

cases from what it should be if caused only by shear lag, because of a tension component developing due to large deflections.

With the exception of the central stiffeners the pattern of strains obtained in these approximate numerical experiments provides additional evidence to reinforce the explanation for the behaviour of Model 12 which was proposed earlier. Thus the fact that the stiffeners at the quarter-width were the first to reverse the trend to follow the downwards web deflections can be understood. It is related to the fact that at the quarter-widths the shear lag average compression was sufficient to counteract the downwards pull produced by the webs, whereas in the centre, although the web effects were smaller, the level of compression was not capable of activating the tendency introduced by the initial imperfections.

In unstiffened flanges it was also found that an upwards initial distortion over the centre could be reversed by the girder overall deflections. This also depended on the amplitude of the distortions and on the ratio of plate transverse rigidity to main girder rigidity. However, from the numerical observations made in relation to Model 12, it is possible to conclude that in stiffened flanges the interaction of shear lag with buckling by compression of the stiffener outstands is highly dependent on those factors and on the shape of the initial distortions. In the case of a stiffened flange of course, the transverse rigidity is greatly enhanced by the presence of any transverse stiffeners. An important characteristic of this interaction is that failure can be initiated at a point of the most heavily stressed flange cross section other than one adjacent to the web or at the centre of the panel.

CHAPTER   7

CONCLUSIONS AND FUTURE WORK

7.1   CONCLUSIONS

(1)   The analytical model and its solution developed for the research work reported in this thesis has proved to be suitable for the study of the combined effects of shear lag and material and geometric nonlinearities in the behaviour of wide flanges such as those used in box girders. The simplified formulation of the discrete stiffener-plate interaction was sufficient to investigate the differences associated with orthotropy of form in the context of shear lag/buckling interaction. In this respect the aims of the project have been accomplished.

(2)   Two distinct collapse modes have been identified for unstiffened compression flanges of simply supported box beams with point loading at mid-span.   For long narrow flanges the full compressive strength of the flange may be reached at the centre; but for short wide flanges the flange strength may be governed by the shear capacity of the web-flange junction.   Over a range of medium flange aspect ratios interaction of the two collapse modes must be considered.

(3)   Simple upper bound expressions have been presented which reflect the limitations placed on flange strength by web and flange in-plane shear capacity.

(4)   A study of the influence of material properties on unstiffened flanges has shown that the mode of failure associated with the shear capacity of the web-flange connection is independent of such properties. This mode of failure is governed by the aspect ratio b/ℓ.   The study

showed that the influence of these properties on the collapse mode associated with inelastic buckling in compression can be incorporated in the non-dimensional slenderness parameter β as used for isolated plates. The interaction of the two modes of failure can be studied for unstiffened flanges on the basis of these two parametres.

(5)   Curves have been presented for a range of initially distorted unstiffened flange plates of varying slendernesses which can be used to establish effective widths needed in design calculations of the ultimate limit state of such beams. These effective widths account both for the effects of shear lag and inelastic buckling.

(6)   Although the research was not concerned with serviceability limits, these curves, if used together with results for elastic shear lag effective width ratios, can serve to estimate the degrees of yielding associated with the attainment of maximum capacity. It should then be possible to establish what degree of redistribution can be adopted, based on an acceptable level of permanent set.

(7)   One possible way of presenting design curves for flange ultimate capacity using a Perry type expression and taking advantage of the upper bound expressions has been outlined, although it should be possible to establish a simpler design approach.

(8)   The simple expedient of using an effective width ratio based on the product of shear lag and buckling effective width ratios has been shown to be unduly conservative.

(9)   Results have also been presented for the case of a stiffened flange with varying stiffener slendernesses in which overall buckling of the stiffened flange may also be a limiting collapse mode. The way in which shear lag influences collapse has been demonstrated.

(10)   It has been shown that a condition for full redistribution in stiffened flanges is associated with the inelastic buckling capacity of the edge panels to transmit shear.   This condition must be considered in conjunction with the need[28] for the stiffener/plate combination near the edges to sustain without significant unloading (see section 1.1) a high level of compression straining.

(11)   For cases where buckling of the edge panels does not reduce their shear strength a method for predicting the possibility of full redistribution has been proposed.   This followed the observation of the characteristics of the interaction between the overall buckling mode of failure and the shear failure of the flange edge.   It consists of examining the position of the flange (as represented by its b/ℓ ratio) in maximum capacity/aspect ratio space in relation to the upper bounds corresponding to these two modes of failure.

(12)   The method summarised in (11) has been used to reappraise the results of box girder tests carried out previously at Imperial College.

(13)   The techniques developed have also been used to interpret the results of a large scale model, reported here for the first time, which was tested by the author and his colleagues.

(14)   The work within this thesis has been used to check and modify the proposed rules for inelastic shear lag effects in the draft Steel Bridge Code, BS5400, Part 3.

(15)   Another longer term experimental programme (see Appendix II) has been designed by the author to provide further checks on the findings of this thesis.   All the equipment and test specimens are ready for testing at

the time of submission of this thesis.   The provision of this information should enable other interested research workers to devise complementary tests.

7.2   FUTURE WORK

(1)   The limitations of the analytical model used in the present research have been outlined in detail in the description of the various aspects of its formulation.   These refer in particular to neglecting large deflection effects in the behaviour of the webs which were assumed to be disconnected from the flange regarding compatibility of rotations and in-plane transverse restraints.   These effects need to be considered in the investigation of web-flange buckling interaction to study stress redistribution between web and flanges in shear lag situations.   It was suggested that these effects may be included in the study of the flange ultimate capacity by an appropriate reduction of the upper bounds corresponding to the shear strength of the web-flange connections.   This requires confirmation.

(2)   The stiffener formulation is not yet capable of considering stiffener tripping and modes of failure where this occurs were not studied.   The method of dealing with rotational boundary conditions at the ends of a stiffened plate in compression, which were found to be very important, needs to be improved for comparison with different testing procedures.   Some numerical aspects related to the consideration of the discrete effects of stiffeners also need improvement since at present only a limited number of stiffeners can be assumed and these are insufficent to model real flanges.   The possibility of considering the effects of transverse stiffeners must also be included in the numerical modelling of the box girder flanges.

(3)   The elastic-plastic effects of the torsional rigidity and lateral bending of stiffeners and of the rotational and in-plane restraints from the web need to be considered in the study of the capacity of edge panels to transmit shear.   This will enable the limitation imposed on stiffened flange capacity by the edge shear mechanism of failure to be quantified.   The consideration of those boundary restraints in the edge panels will facilitate the study of the influence on the process of stress redistribution, of the reduction in the carrying capacity of the more strained edge plate panels and stiffeners when they prematurely buckle in a shear lag environment.   This limitation to the possibility of full redistribution was not investigated in this research.   For these studies the rig that has been designed and constructed for testing flange plates with accurately simulated boundary conditions will be of great use.

(4)   The problem of residual stresses was not covered in the present work and needs to be investigated.   A suggestion was made regarding the inclusion of their effects on the mode of failure associated with in-elastic buckling in compression, but this is a speculative suggestion that requires to be properly substantiated.

(5)   Although conclusions regarding the influence of initial distortions and the general characteristics of the most weakening initial shape were derived, this problem requires a more systematic investigation to enable a more clear understanding of the problem of preferred buckling mode shapes in a shear lag environment.

(6)   More research is needed to extend the conclusions regarding stress redistribution obtained for simply supported beams to continuous girders. The organisation of this research could follow, as a guide line, the steps

taken by Moffatt and Dowling[13] in the treatment of elastic shear lag effects in these structures. An obvious first step towards that extension must be the study of flange failure in non-symmetric point loading cases.

REFERENCES

1. Schade,H.A. The effective breadth of stiffened plating under bending loads. Transactions of the Society of Naval Architects and Marine Engineers, Vol 59, 1951.

2. von Kármán, T. Die mittragende Breite. August-Föppl-Festschrift, Springer-Verlag, Berlin, 1924.

3. Chwalla, E. Die Formeln zur Berechnung der "voll mittragenden Breite" dünner Gurt-und Rippenplatten. Der Stahlbau, 1936.

4. Metzner, W. Die mittragende Breite. Luftfahrtforschung, 1929.

5. Dischinger, F. Die mitwirkende Breite des Plattenbalkens, Taschenbuch für Bauingenieure I. Springer-Verlag, Berlin, 1955.

6. Kuhn, P., and Chiarito, P.T. Shear lag in beams. Methods of analysis and experimental analysis. Report No 739, National Advisory Committee for Aeronautics, 1941.

7. Williams, D. Theory of Aircraft Structures. Edward Arnold Ltd, London, 1960.

8. Yuille, I.M. Shear lag in stiffened plating. Transactions of the Society of Naval Architects and Marine Engineers, Vol 61, 1953.

9. Winter, G. Stress distribution in and equivalent width of flanges of wide, thin-wall steel beams. National Advisory Committee for Aeronautics, Technical Note 784, 1940.

10. Kondo, K., Komatsu, S., and Nakai, H. Theoretical and experimental researches on the effective width of girder bridge with steel deck plate. Transactions of the Japan Society of Civil Engineers, Vol 86, October 1962.

11. Abdel-Sayed, G. Effective width of steel deck-plate in bridges. Journal of the Structural Division, Proceedings of the American Society of Civil Engineers, Vol 95, July 1969.

12. Malcolm, D.J., and Redwood, R.G. Shear lag in stiffened box girders. Journal of the Structural Division, Proceedings of the American Society of Civil Engineers, Vol 96, July 1970.

13. Moffatt, K.R., and Dowling, P.J. Steel box girders, Parametric study on the shear lag phenomenon in steel box girder bridges. CESLIC Report BG17. Engineering Structures Laboratories, Imperial College of Science and Technology, London, 1972.

14. Moffatt, K.R. and Dowling, P.J. Shear lag in steel box girder bridges. The Structural Engineer, Vol 53, October 1975.

15. Inquiry into the basis of design and method of erection of steel box girder bridges: Interim design and workmanship rules, Parts I to IV. Her Majesty's Stationery Office, London, 1973.

16. British Standard Specification BS5400. Steel, concrete and composite bridges, Part 3 (to be published): Code of practice for design of steel bridges. British Standards Institution, London.

17. British Standard Specification BS5400. Steel, concrete and composite bridges. Part 5: Code of practice for design of composite bridges. British Standards Institution, London, 1979.

18. Lamas, A.R.G. Combined effect of shear lag and buckling on flange efficiency. Final Report, ECCS 2nd International Colloquium on Stability of Steel Structures, Liège, April 1977.

19. Inquiry into the basis of design and method of erection of steel box girder bridges: Interim Report. Her Majesty's Stationery Office, London, 1971.

20. Horne, M.R. Structural action in steel box girders, CIRIA Guide 3, Construction Industry Research and Information Association, London, April 1977.

21. Bogunovic, V. Uber die Stabilität der Rippenkonstruction. Der Stahlbau, Vol 24, 1955.

22. Maquoi, R., and Massonnet, C. Interaction between shear lag and post-buckling behaviour in box girders. Steel Plated Structures, P.J. Dowling et al. eds., Crosby Lockwood Staples, London, 1977.

23. Maquoi, R. and Massonnet, C. Théorie non-linéaire de la résistance post critique des grandes poutres en caisson raidies. IABSE Publications, Vol 31-II, 1971.

24. Massonnet, C., and Maquoi, R. Recent progress in the field of structural stability of steel structures. IABSE Publications, Survey S-5/78, 1978.

25. Faulkner, D. A review of effective plating for use in the analysis of stiffened plating in bending and compression. Journal of Ship Research, Vol 19, No 1, March 1975.

26. Albrecht, G. Beitrag zur mittragenden Breite von Plattenbalken im elasto-plastischen Bereich. Ruhr-Universität Bochum, Technical Report No 76-7, July 1976.

27. Roik, K. Effective breadth and shear lag in plate girder bridges with elastic and elasto-plastic material behaviour. Steel Plated Structures, P.J. Dowling et al. eds., Crosby Lockwood Staples, London, 1977.

28. Dowling, P.J., Moolani, F.M., and Frieze, P.A. The effect of shear lag on the ultimate strength of box girders. Steel Plated Structures, P.J. Dowling et al. eds., Crosby Lockwood Staples, London, 1977.

29. Dowling, P.J. Experimental investigations on boxes. Proceedings of Informal Meeting on Steel Box Girder Bridges, Institution of Civil Engineers, London, 1973.

30. Guile, P.J.D., Moolani, F.M. and Dowling, P.J. Steel box girders, Models 9 and 10, Progress Report 1: Construction, instrumentation and residual strain measurements, CESLIC Report BG33. Engineering Structures Laboratories, Imperial College of Science and Technology, London, 1975.

31. Moolani, F.M., and Dowling, P.J. Steel box girders, Models 9 and 10, Progress Report 2: Tests to study the effects of shear lag on the collapse of steel box girders, CESLIC Report BG34. Engineering Structures Laboratories, Imperial College of Science and Technology, London, 1975.

32. Moolani, F.M. Ultimate load behaviour of steel box girder stiffened compression flanges. PhD Thesis, University of London, 1976.

33. Carlsen, C.A., Søreide, T.H. and Nordsve, N.T. Ultimate load analysis of the compression flange of a box girder. Preliminary Report, ECCS 2nd International Colloquium on Stability of Steel Structures, Liège, April 1977.

34. Crisfield, M.A. Shear lag and the ultimate load capacity of box-girder bridges. Final Report, ECCS 2nd International Colloquium on Stability of Steel Structures, Liège, April 1977.

35. Harding, J.E, Hobbs, R.E. and Neal, B.G. The elasto-plastic analysis of imperfect square plates under in-plane loading. Proceedings of the Institution of Civil Engineers, Part 2, Vol. 63, March 1977.

36. Frieze, P.A., Hobbs, R.E. and Dowling, P.J. Application of dynamic relaxation to the large deflection elasto-plastic analysis of plates. Computers and Structures, Vol 8, No 2, April 1978.

37. Marguerre, K. Zur Theorie der gekrümmten Platte grosser Formänderung. Proceedings of the 5th International Congress on Applied Mechanics, Cambridge, 1938.

38. Basu, A.K., Djahani, P. and Dowling, P.J. Elastic post-buckling behaviour of discretely stiffened plates. Preliminary Report, ECCS 2nd International Colloquium on Stability of Steel Structures, Liège, April 1977.

39. Marcal, P.V. and Pilgrim, W.R. A stiffness method for elastic-plastic shells of revolution. Journal of Strain Analysis, Vol 1, No 4, 1966.

40. Crisfield, M.A. Large-deflection elasto-plastic buckling analysis of plates using finite elements, TRRL Report LR593. Transport and Road Research Laboratory, Crowthorne, Berkshire, 1973.

41. Crisfield, M.A. Some approximations in the non-linear analysis of rectangular plates using finite elements, TRRL Report SR51 UC. Transport and Road Research Laboratory, Crowthorne, Berkshire, 1974.

42. Frieze, P.A. Ultimate load behaviour of steel box girders and their components. PhD Thesis, University of London, 1975.

43. Crisfield, M.A. On an approximate yield criterion for thin steel shells, TRRL Report 658. Transport and Road Research Laboratory, Crowthorne, Berkshire, 1974.

44. Djahani, P. Large deflection analysis of discretely stiffened plates. PhD Thesis, University of London, 1977.

45. Tvergaard, V. and Needleman, A. Mode interaction in an eccentrically stiffened elastic-plastic panel under compression. DCAMM Report No 69. The Technical University of Denmark, Lyngby, 1974.

46. Ilyushin, A.A.   Plasticité. Editions Eyrolles, Paris, 1965.

47. Robinson, M.   A comparison of yield surfaces for thin shells. International Journal of Mechanical Sciences, Vol 13, No 4, 1971.

48. Burgoyne, C.J.   Discussion (to be published) on paper by P.A. Frieze, Elasto-plastic buckling on short thin-walled beams and columns. Proceedings of the Institution of Civil Engineers, Part 2, Vol 65, December 1978.

49. Ivanov, G.V.   Approximating the final relationship between the forces and moments of shells under the Mises plasticity condition (in Russian). Inzhenernyi Zhurnal Mekhanika Tverdogo Tela, Vol 2, No 6, 1967.

50. Haydl, H.M. and Sherbourne, A.N.   Limit loads of circular plates under combined loading. Journal of Applied Mechanics, September 1973.

51. Olszak, W. and Sawczuk, A.   Inelastic behaviour in shells. P. Noordhoff Ltd, Groningen, 1967.

52. Drucker, D.C.   Plasticity. Proceddings of 1st Symposium on Naval Structural Mechanics, Goodier and Hoff eds., Pergamon Press, Oxford, 1959.

53. Save, M.   On yield conditions in generalised stresses. Quarterly of Applied Mathematics, Vol 19, No 3, 1961.

54. Onat, E.T.   Plastic shells. Proceedings, Symposium of IASS, Warsaw, 1963. Olszak and Sawczuk eds., North-Holland Pub. Co, Amsterdam, 1964.

55. Horne, M.R., Montague, P. and Narayanan, R.   Influence on strength of compression panels of stiffener section, spacing and welded connection. Proceedings of the Institution of Civil Engineers, Part 2, Vol 63, March 1977.

56. Weller, T. and Singer, J.   Experimental studies on the buckling under axial compression of integrally stringer-stiffened circular cylindrical shells.   Journal of Applied Mechanics, Vol 44, December 1977.

57. Koiter, W.T.   On the diffusion of load from a stiffener into a sheet. Quarterly Journal of Mechanics and Applied Mathematics, Vol 8, 1955.

58. Caldwell, J.B.   Diffusion of load from a boom into a rectangular sheet. Quarterly Journal of Mechanics and Applied Mathematics, Vol 11, 1958.

59. Frieze, P.A. and Dowling, P.J.   Interactive buckling analysis of box sections using dynamic relaxation.   Computers and Structures, Vol 9, No 5, 1978.

60. Wittrick, W.H.   Stress singularities at diaphragm-web-flange junctions in box girders.   Proceedings of the Institution of Civil Engineers, Vol 59, Part 2, March 1975.

61. Williams, M.L.   Stress singularities resulting from various boundary conditions in angular corners of plates in extension.   Journal of Applied Mechanics, Vol 19, December 1952.

62. Day, A.S.   An introduction to dynamic relaxation. The Engineer, Vol 219, January 1965.

63. Wood, W.L.   Comparison of dynamic relaxation with three other iterative methods. The Engineer, Vol 221, November 1967.

64. Rushton, K.R.   Dynamic relaxation solution for the large deflection of plates with specified boundary stresses. Journal of Strain Analysis, Vol 4, No 2, 1969.

65. Cassell, A.C.   Shells of revolution under arbitrary loading and the use of fictitious densities in dynamic relaxation. Proceedings of the Institution of Civil Engineers, Vol 45, January 1970.

66. Cassell, A.C. and Hobbs, R.E.   Dynamic relaxation. Proceedings, Symposium of IUTAM, Liège, Publication of the University of Liège, 1971.

67. Chaplin, T.K.   Discussion on paper by R.S. Alwar and N. Ramachandra Rao, Large elastic deformations of clamped skewed plates by dynamic relaxation. Computers and Structures, Vol 8, 1978.

68. Zienkiewicz, O.C.   The finite element method in engineering science. McGraw-Hill, London, 1971.

69. Lowe, P.A.   Prediction of loading causing inserviceability of reinforced concrete and composite highway bridges. PhD Thesis, University of London, 1969.

70. Webb, S.E.   The behaviour of stiffened plating under combined in-plane and lateral loading. PhD Thesis, University of London (to be published).

71. Lamas, A.R.G. and Dowling, P.J. Effect of shear lag on the inelastic buckling behaviour of thin-walled structures. Proceedings of the International Conference on Thin-Walled Structures, University of Strathclyde, Glasgow, April 1979.

72. Wang, S.T. and Tien, Y.L. Buckling of plates and beam sections under stress gradient. Research and Developments in cold-formed steel design and construction, W.W. Yu and J.H. Senne eds., Department of Civil Engineering, University of Missouri-Rolla, 1975.

73. Dowling, P.J., Frieze, P.A. and Harding, J.E. Imperfection sensitivity of steel plates under complex edge loading. Preliminary Report, ECCS 2nd International Conference on Stability of Steel Structures, Liège, April, 1977.

74. Winter, G. Strength of thin steel compression flanges. Preliminary Publications, IABSE 4th Congress, Cambridge and London, 1952.

75. Dowling, P.J. and Lamas, A.R.G. Interaction between shear lag and buckling in plates at collapse. Proceedings of Annual Technical Meeting of the Structural Stability Research Council, Boston, 1978.

76. Frieze, P.A., Lamas, A.R.G. and Dowling, P.J. Steel box girders, Model 12, Test to study the effect of shear lag on the collapse of a box girder flange with stiffeners of slender cross section, CESLIC Report BG 48. Engineering Structures Laboratories, Imperial College of Science and Technology, London (to be published).

NOTATION

Latin and Greek Symbols

A_{cf}, A_{tf}	total cross-sectional area of compression flange including stiffeners and of tension flange, respectively
A_w	cross-sectional area of the two box webs
A_p	cross-sectional area of plate component of a stiffened flange
A_s	total cross-sectional area of flange stiffeners
b	width of flange measured between webs
b'	width of plate panels measured between stiffeners
b_e	elastic effective width of flange
d	depth of web
d_s	depth of a stiffener
E	Young's modulus
F_y, F_z	plate-stiffener interaction line forces
f	yield function in stress resultant space $(f(N_i), N_i = 1, \ldots, 6)$
ℓ	length of simply supported box girder or isolated plate
M_{ult}	ultimate bending moment of a box girder cross section
$N_x, N_y, N_{xy}, M_x, M_y, M_{xy}$	in-plane and flexural components of vector of generalised total stress resultants $(\underset{\sim}{N})$
N_i	ith component of vector of generalised total stress resultants
N_s, M_s	resultant of axial stresses at a stiffener cross section and moment of these stresses in relation to an axis parallel to x direction and centred at plate mid-plane level
Q_t, Q_m, Q_{tm}	non-dimensional quadratic forms of stress resultants used in the definition of the yield function (expressions 2.19)

Q_x, Q_y	transverse shear forces
r	radius of gyration of stiffener cross section and associated plate of width b' (Fig. 5.1)
T_f	total flow of shear stresses over half length of a web-flange connection
t	thickness of flange plate
t_w	thickness of web plate
t_s	thickness of a stiffener
u, v, w	displacement components in x,y and z directions, of a point in the plate mid-plane initially at a position defined by x,y and $z = w_o(x,y)$
x, y, z	coordinate directions
V_x	Kirchoff transverse shear forces at plate edge parallel to y-direction
w_o	function of x and y defining plate initially imperfect shape
w_{omax}	maximum amplitude of initial shape $w_o(x,y)$
$\Delta x, \Delta y$	finite differences mesh spacing in x and y directions
α	geometric stiffening factor $(\alpha \doteq A_s/A_p)$
α'	equivalent stiffening factor $(\alpha' = \alpha\sigma_{os}/\sigma_{op})$
β	non-dimensional plate slenderness $(\beta = (b/t)\sqrt{\sigma_o/E})$
γ	flow parameter or plastic strain multiplier
$\varepsilon_x, \varepsilon_y, \varepsilon_{xy},$ $\chi_x, \chi_y, \chi_{xy}$	in-plane and curvature components of vector of generalised strains
ε_o	yield strain $(\varepsilon_o = \sigma_o/E)$
λ, μ	parameters used in definition of Ilyushin's yield criterion (expressions 2.17 and 2.20)
ν	Poisson's ratio
σ_{av}	average of longitudinal stresses over flange cross section (expression 1.4)

$\sigma_{max}, \sigma_{min}$ maximum and minimum values of longitudinal stresses over flange cross section

σ_o uniaxial yield stress

σ_{ocf} equivalent yield stress of compression flange (expression 1.5)

σ_{otf} yield stress of tension flange plate

σ_{op} "   "   " stiffened flange plate

σ_{os} "   "   " stiffeners

σ_{ow} "   "   " web plates

ψ inelastic effective width ratio of flange cross section (expression 1.3)

ψ_b inelastic buckling effective width ratio

ψ_{max} maximum value of ψ measuring flange ultimate capacity

ψ^* ψ_{max}/ψ_b (expression 5.7)

Subscripts

cf   compression flange

tf   tension flange

w   web

s   stiffener

p   quantity related to flange plate or a value calculated in a previous load increment

x,y   in-plane directions

xy   shear and twist directions

z   quantity measured at distance z from plate mid-plane

Superscripts

i,j   position in finite differences mesh arrangement in x and y direction

e   elastic

p   plastic

Matrices and Vectors

$\underset{\sim}{C}$ matrix of elastic-plastic plate tangential rigidities

$\underset{\sim}{C}^e$ matrix of elastic plate rigidities

$\underset{\sim}{f}$,   column vector of partial derivatives of yield function
in relation to total generalised stress resultants

$\underset{\sim}{N}, \underset{\sim}{\Delta N}$ column vectors of total and incremental generalised
stress resultants

$\underset{\sim}{\varepsilon}, \underset{\sim}{\Delta\varepsilon}$ column vectors of total and incremental generalised
strain resultants

Abbreviations

FD   finite differences

DR   dynamic relaxation

Symbols not mentioned within this list are defined in the text.

APPENDIX   I

NUMERICAL TREATMENT OF EQUILIBRIUM

ALONG SPECIAL NODAL LINES

I.1   LONGITUDINAL EQUILIBRIUM ALONG WEB-FLANGE CONNECTIONS

The 'finite element' approach to this problem was described

in Section 3.2.2.   A typical distribution of stresses with a longitu-

dinal component acting on the sides of the element of Fig. 3.6 is

shown in Fig. I.1 where the element is represented unfolded in a plan

view.   This refers to the connection of the web to the compression

flange but the treatment of the connection to the tension flange is

identical.   For convenience the web-flange line is designated by the

ith nodal line and the other longitudinal nodal lines are referred to

accordingly.

The average of the shear stresses acting on each longitudinal

side is assumed to be approximated by the mid-side value.   On the left

hand side this is given by the first internal web shear node value

$N_{xyw}^{i-1,j}$.   At the right hand side the mid-side value can be calculated

by a second order polynomial interpolation over the first three shear

nodes on the jth line of the compression flange ($N_{xy}^{i,j}$, $N_{xy}^{i+1,j}$ and $N_{xy}^{i+2,j}$).

This is a consequence of using an element extending equally in the

transverse direction over the web and the flange.   This was chosen for

convenience of damping, in the DR process, the   corresponding equation

of motion as a web equation without having to resort to a more compli-

cated assessment of the damping factors and fictitious densities.   It

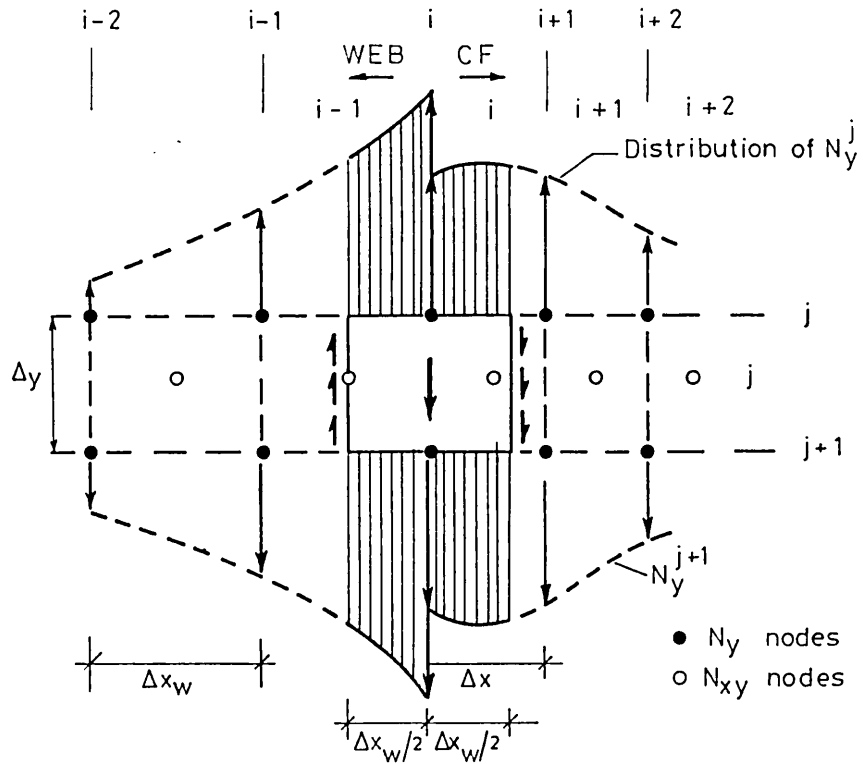requires mesh spacings in the x-direction such that

Fig. I.1   Stress components acting in the longitudinal direction on element of web-flange connection
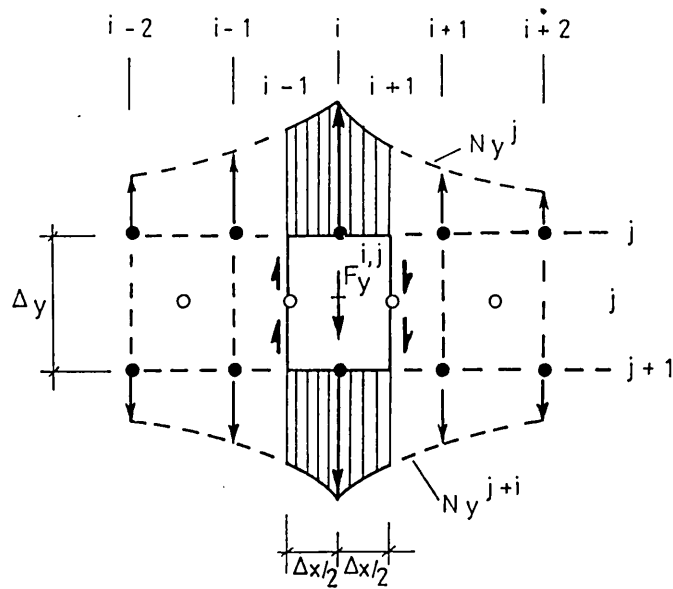

Fig. II.2 Stress components and stiffener force acting in the longitudinal direction on element of   plate over stiffener line

$$\Delta x_w > \Delta x_{cf} \qquad \text{and} \qquad \Delta x_w > \Delta x_{tf} \qquad\qquad \text{I.1}$$

To apply equation 3.2 to express the equilibrium of the element in the y-direction the longitudinal stresses acting on the transverse sides have to be integrated. For this purpose, the variation of N_y over these sides can also be described on each plate by polynomial approximations using the first three N_y nodes on the left and right of the common edge.

After expanding equation 3.2 and dividing by $\Delta x_w \Delta y$, the longitudinal equilibrium of the 'finite element' can be expressed by:

$$\frac{1}{24\Delta y}\left(a_1(N_y^{i,j+1} - N_y^{i,j}) + a_2(N_y^{i+1,j+1} - N_y^{i+1,j}) - a_3(N_y^{i+2,j+1} - N_y^{i+2,j})\right)$$

$$+ \frac{1}{24\Delta y}\left(8(N_{yw}^{i,j+1} - N_{yw}^{i,j}) + 5(N_{yw}^{i-1,j+1} - N_{yw}^{i-1,j}) - (N_{yw}^{i-2,j+1} - N_{yw}^{i-2,j})\right)$$

$$+ \frac{1}{\Delta x}\left(a_4 N_{xy}^{i,j} + a_5 N_{xy}^{i+1,j} + a_6 N_{xy}^{i+2,j} - N_{xyw}^{i-1,j}\right) = 0 \qquad\qquad \text{I.2}$$

where
$$a_1 = \frac{1}{2}a_7{}^2 - \frac{9}{2}a_7 + 12 \qquad\qquad a_4 = \frac{1}{8}a_8{}^2 - \frac{3}{4}a_8 + 1$$

$$a_2 = -a_7{}^2 + 6a_7 \qquad\qquad a_5 = -\frac{1}{4}a_8^2 + a_8$$

$$a_3 = -\frac{1}{2}a_7{}^2 + \frac{3}{2}a_7 \qquad\qquad a_6 = \frac{1}{8}a_8{}^2 - \frac{1}{4}a_8$$

$$a_7 = \Delta x_w/\Delta x \qquad\qquad a_8 = \Delta x_w/\Delta x - 1$$

I.2 LONGITUDINAL EQUILIBRIUM ALONG STIFFENER LINES

The 'finite element' used for this case is represented in Fig. 3.8. As for the equilibrium at the web-flange connection the relevant stresses acting on the element are represented in Fig. I.2. The element is centred at a v node over the stiffener line.

The average of the shear stresses on each longitudinal side
is assumed to be given by values at the shear nodes   situated over
the sides.   The same applies to the longitudinal line force F_y repre-
senting the action of the stiffener on the element whose value calcu-
lated at the v node is designated by $F_y^{i,j}$.
The same approach used to integrate the longitudinal stresses in I.1
over each half of the transverse sides is used in this case with the
advantage that now all the sides coincide with nodal lines.

Expanding again equation 3.2 and dividing by $\Delta x \Delta y$ the equilibrium
equation to use for the calculation of v displacements over the stiffener
lines follows:

$$\frac{1}{24\Delta y}\left(16(N_y^{i,j+1}-N_y^{i,j}) + 5(N_y^{i+1,j+1}-N_y^{i+1,j}) + 5(N_y^{i-1,j+1}-N_y^{i-1,j})\right.$$

$$- (N_y^{i+2,j+1}-N_y^{i+2,j}) - (N_y^{i-2,j+1}-N_y^{i-2,j}))$$

$$+ \frac{1}{\Delta x}(N_{xy}^{i,j} - N_{xy}^{i-1,j} + F_y^{i,j}) = 0 \qquad\qquad \text{I.3}$$

I.3   TRANSVERSE EQUILIBRIUM OVER THE POINT LOADING CROSS SECTION

The 'finite elements' used in this case are centred at the
$u^{i,j}$ nodes located over this section.   This approach for expressing
equilibrium by taking into account cuspings of in-plane stresses due to
the point loading effects, was restricted to cases where longitudinal
symmetry about this section was assumed.   The elements thus lie half
within the quarter of the box being analysed and the other half is
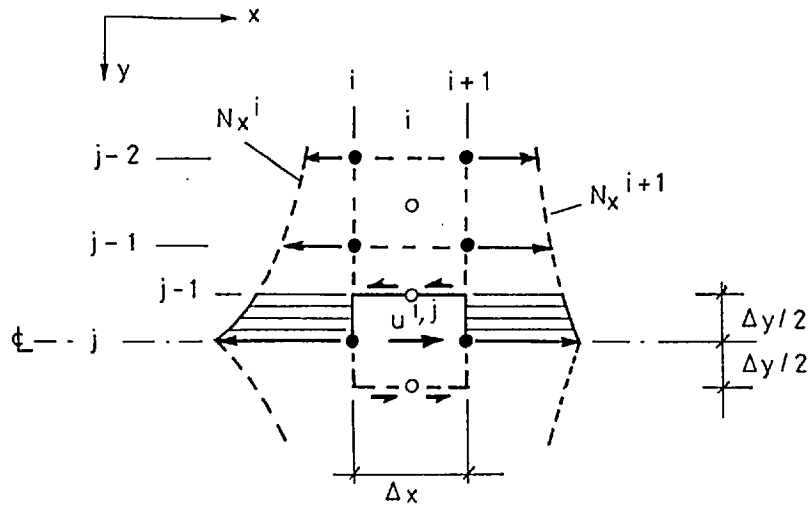'fictitious'.

Fig. I.3   Stresses acting in the transverse direction on finite element
of plate over mid-span cross section

The stresses now contributing to the equilibrium in the x-direc-
tion are the N_x stresses over the longitudinal sides which are symmetric
in relation to the mid-span central line, and the shear stresses at the
transverse sides which have an antisymmetric distribution.   The effects
of the shear stresses cancel and the integration of the N_x stresses using
the same technique as described in I.1 and I.2 is much simplified.   It
only involves values at the mid-span cross section and the values over the
two previous j lines. The equilibrium equation to be used for the $u^{i,j}$
nodes is, therefore, as follows:

$$\frac{1}{12\Delta x} \left(8(N_x^{i+1,j} + N_x^{i,j}) + 5(N_x^{i+1,j-1} - N_x^{i,j-1}) - (N_x^{i+1,j-2} - N_x^{i,j-2})\right) = 0$$

I.4

APPENDIX   II

FLANGE TESTING RIG

II.1   GENERAL

An experimental programme of tests has been proposed to vali-
date the theoretical appraisal discussed in this thesis.   The author
has been responsible for the design of a rig that will be used in the
near future.for tests on isolated flange plates.

The main features of this rig were outlined in the Introduction
and this Appendix serves to discuss the same in more detail.

II.2   CONCEPTION OF RIG

It is proposed to use the rig for the testing of small scale
mild steel flange plates of 2 and 4 mm thickness.   Point loading will
be applied to simulate the most severe shear lag effects developed in
box girders.

This loading arrangement could best be achieved by applying
the load to the webs of a modelled box girder of open cross section.
To avoid yielding and buckling the webs are to be made of stocky sec-
tions of very high strength steel.

The need to separate the flanges from rotational and in-plane
restraints from the webs followed as a consequence of utilising stocky
webs.   This had the additional advantage of corresponding to the boun-
dary conditions assumed in the analytical model and of ensuring that the
webs could be re-used whilst the flange plates were replaceable.

The web-flange connection should accordingly impose compati-
bility of longitudinal displacements while allowing the flange edge to

be free to rotate and pull-in. This required a discrete type of web-flange connection as opposed to a continuous one.

II.3   FLANGE PLATE AND LOADING WEB ASSEMBLY

The loading of the flange plate edge is achieved through a series of pins (Fig. II.1). These are regularly spaced on each face of the plate.
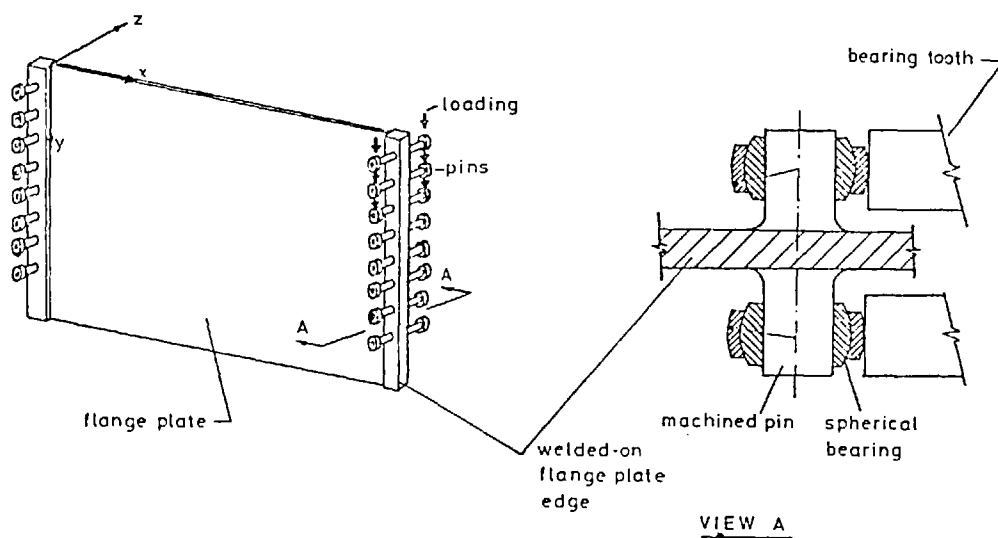
Fig II· 1   Discrete application of edge loading

Spherical bearings are located on the pins and these are caused to engage on teeth machined in the upper beam of the loading web (Fig. II.2 and detail Fig. II.3). When the web deflects under load these are compressed longitudinally towards the mid-span cross section. The bearings are positioned symmetrically in relation to the plate mid-plane and the applied loads should have a resultant at that level. To

upper beam of
loading web assembly

teeth

holes for plate
holding fingers

supporting stiffener

adjustable
wedges

1·375 ⌀

lugs for holding fingers

web plate of
loading web assembly

lower beam of
loading web assembly

loading stiffener

12·050

18·270

26·045

11·400

WEB ELEVATION (inside view)

Note : dimensions in inches
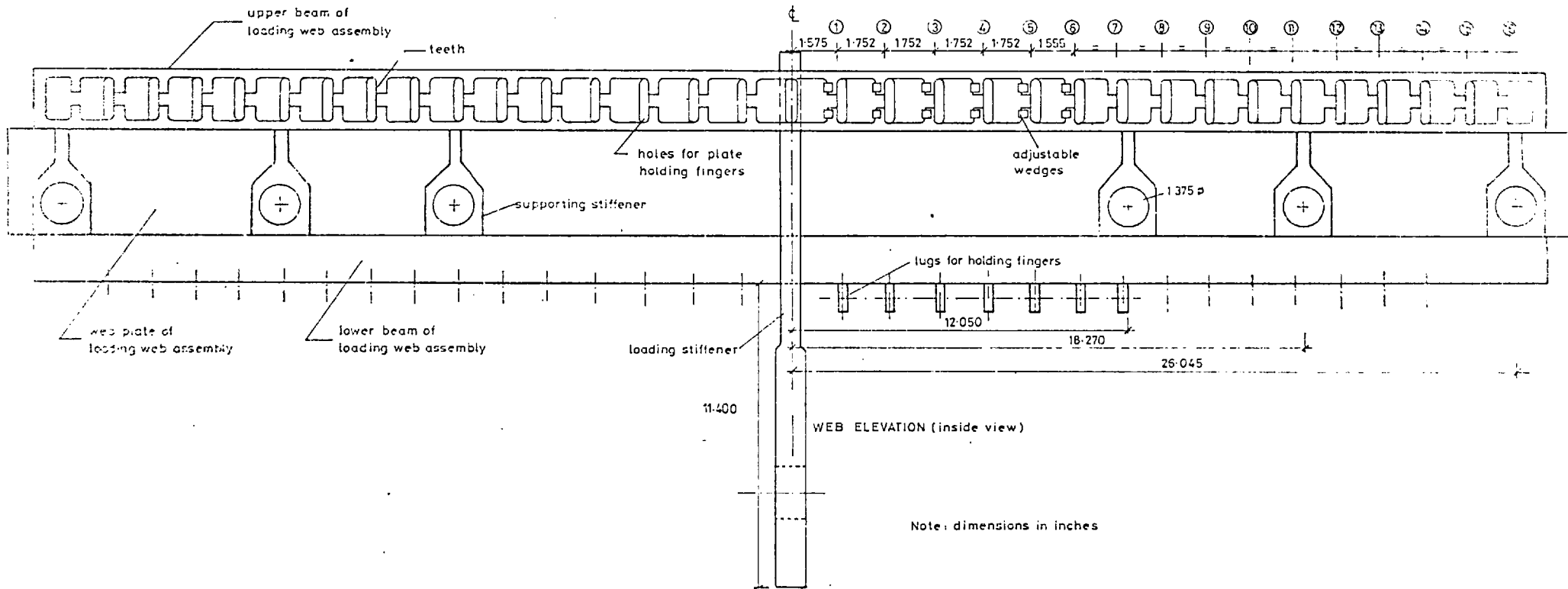
FigII·2   Detail of elevation of loading web assembly

Holes in upper beam of loading web to locate fingers for vertical support of flange plate edge (see fig II 6)

pin ⑤   ►C   pin ⑥

1 686

524   433

σ ·4998 ·5002 σ ·3748 ·3752

·581

·4375 ·4355

·3125 ·3105

144

·207

·4815

·638   ·520

6mm = ·236"

4mm

·700

spherical bearing
machined pin
wedge
bearing tooth
reduced section of welded-on flange plate edge
upper beam of loading web

►C

VIEW A

·395   ·685

machined pin

FLANGE PLATE

VIEW A

welded-on flange plate edge

slots for location of rollers of holding arm fingers

Section C-C

note : All dimensions in mm

Fig II·3   Details of upper beam of loading webs at teeth ⑤ and ⑥

217

Section AA

① ② ③ ④ ⑤ ⑥ ⑦
A ►
A ►

Section AA

ǁ pins ⑥ ·375" dia

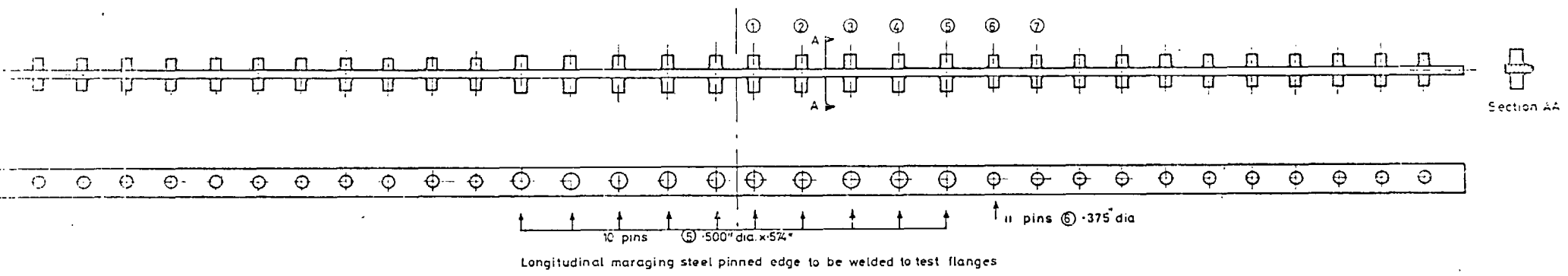10 pins   ⑤ ·500" dia. x 5¼"

Longitudinal maraging steel pinned edge to be welded to test flanges

Fig II·4   Detail of loading pins and
flange edge

·930

·748

spherical bearing for pins 1-5

spherical bearing for other pins

·900

Travel

1·600

1·270

·3125

·524

·433

adjustable wedge

·059

9°

locking nut

·335

·375

web tooth

teeth 1-5

·355

·685

1·690

note : all dimensions in inches
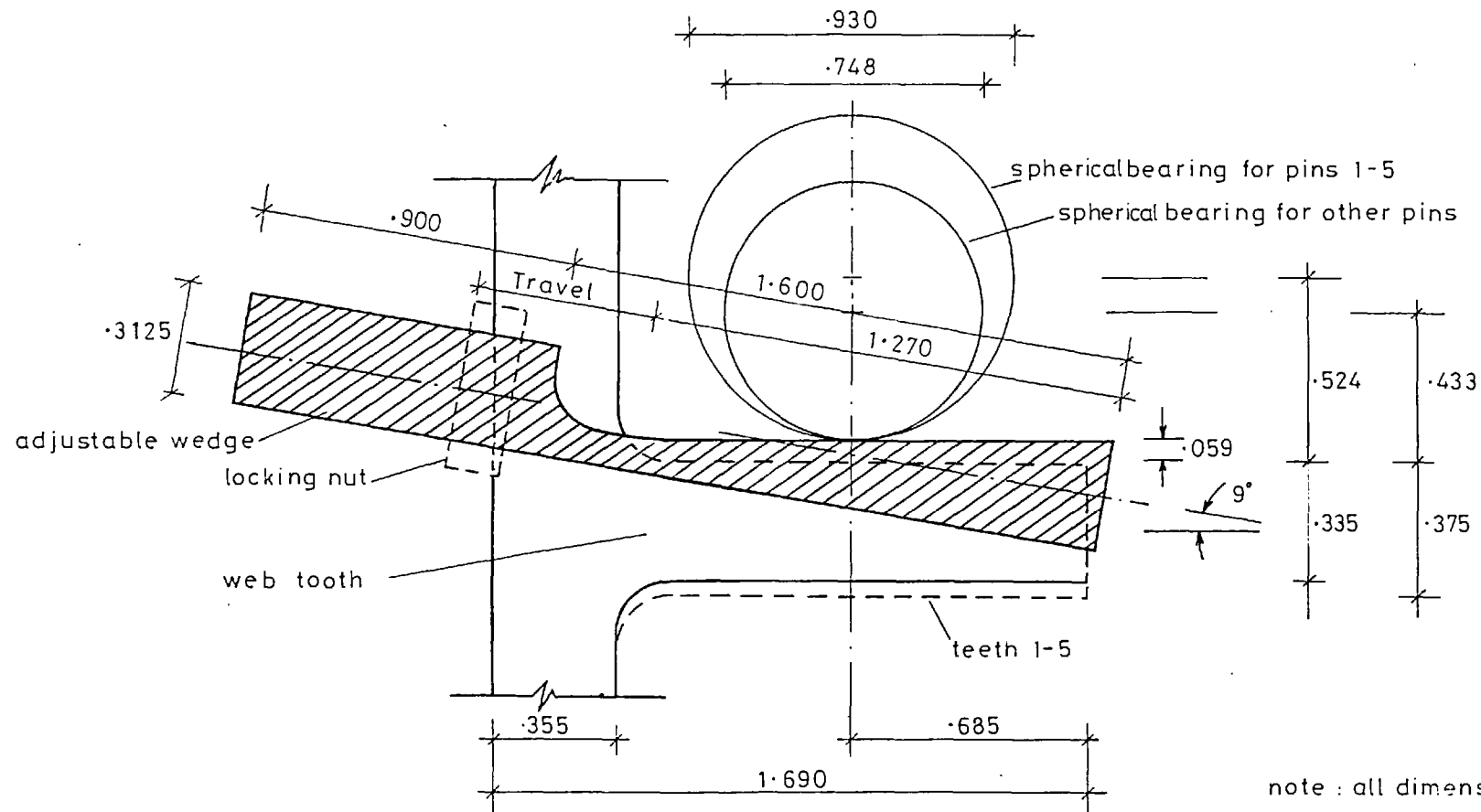
Fig II·5 Detail of wedge.—Plan view

eccentric pin for vertical adjustment of lower finger

fixed upper finger

adjustable lower finger

upper beam of web assembly

web of web assembly

lower beam of web assembly

pivot of holding arms

SECTION AA

fixed upper finger

3mm ∅ roller

10mm

flange plate

4mm

adjustable lower finger
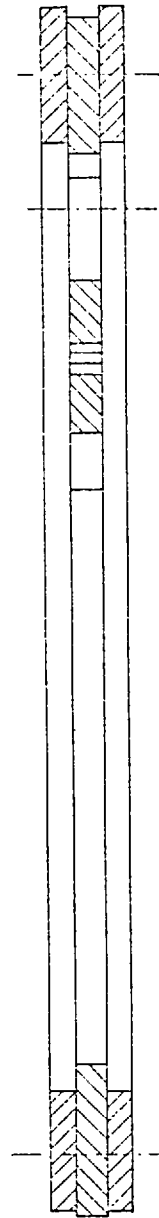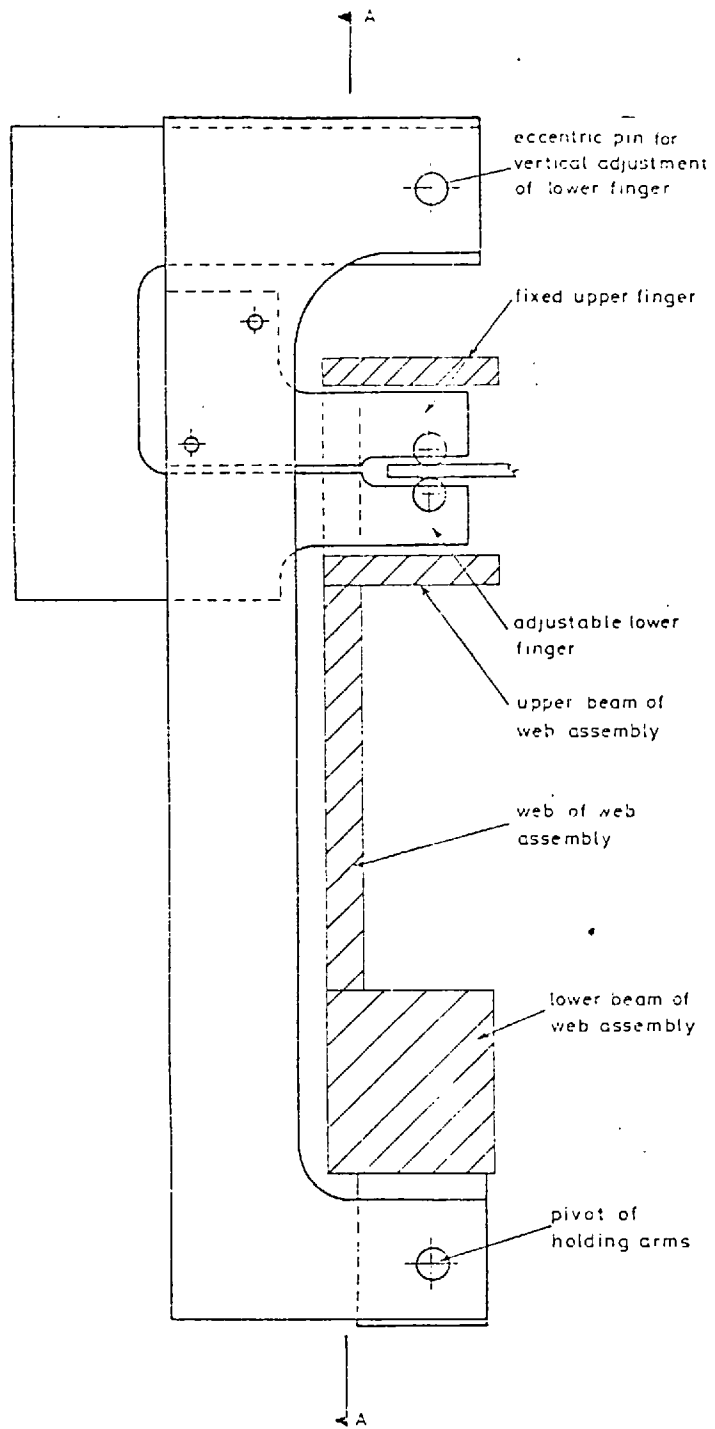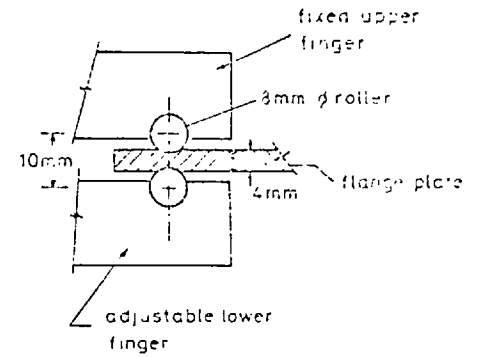
DETAIL OF FINGER

Fig II 6.
Details of holding arm

avoid stress concentrations and localised yielding at the connection of the pins to the plate the pins and the flange edge were machined from the same length of maraging steel*. The resulting strips (represented in Fig. II.4) are to be welded to the edges of the mild steel flange specimens. It will thus be possible to stress relieve the plate after welding and subsequently treat the whole at the aging temperature of the maraging steel to harden the edges which can be re-used.

This loading arrangement depends on specially designed and fabricated doubly spherical bearings. A pilot study was made to ensure that the bearings would behave satisfactorily under the unusual type of point contact load. The double spherical surface (a sphere inside a sphere) is necessary to mechanically allow simultaneous rotation of the pinned edge (around a longitudinal line at plate mid-plane level) with in-plane transverse movement.

Due to the maraging steel welded flange edge strip it is expected that there will be some restraint to complete freedom to pull-in. These effects may be significant after the onset of plasticity at the edge of the plate but will have to be calibrated and allowed for. To ensure initial contact of the bearings with the teeth of the upper beam of the web assembly, wedged packing pieces are inserted in broached square grooves between the bearings and the teeth. These wedges are adjustable and can be locked when in position. They were made of hardened silver steel (Fig. II.5). For the broaching of the inclined grooves a special jig had to be designed.

The web flange mechanical connection does not provide vertical support to the edges of the plate. Longitudinally, this is supplied by 'holding arms' (Fig. II.6) located between the pins. These arms are

* the same material used for the webs and described later.

hinged at the bottom of the web assembly to allow free to pull-in
movement of the plate edge.   Two 'fingers' connected to these arms pass
through holes in the wall of the upper beam of the web assembly to hold
the plate edge between cylindrical rollers.   These rollers are located
in cylindrical slots machined on both faces of the flange plate edges
(see detail Fig. II.6).   The top finger is fixed to the arm and the
lower one pivots independently.   The rotation of the arm allows free to
pull-in transverse displacement of the plate edge whilst the independent
rotation of the lower finger accommodates edge rotations.   The pivot
around which this lower finger can rotate (Fig. II.6) is eccentrically
machined to allow initial vertical adjustment during assemblage.   When
the roller is in contact with the plate the pivot position is locked.
The drilling of holes in the arm pieces for the hinged connections and
for the rollers was accurately controlled using a drilling jig.

At the ends of the model the flange plates will be connected by
welding to mild steel flexible diaphragms bolted to stiffeners on the
web.   This will provide vertical support and approximate the theoretical
boundary conditions assumed at the supports in the analytical model.
That is, tangential restraint, free rotation and free to pull-in dis-
placement conditions.

II.4   MATERIALS AND FABRICATION OF LOADING WEB ASSEMBLIES

From numerical evidence it was found that the webs should be
able to impose on the edges at the centre of the flange plates longi-
tudinal strains 4-5 times the yield strain of mild steel.   In the
search for a suitable material for the webs, machineability and control
of distortions after heat treatment had to be considered.   Maraging
steel meets all these requirements having a Young's modulus conveniently

lower than mild steel. In the anealed state (soft state) it can be machined and requires low temperatures (480°C) in the hardening (aging) process. Though not presenting any yield stress plateau it is sufficiently extensible before rupture to avoid danger of brittle failure. Maraging steel of G110 type was chosen in a compromise between strength and economy. Its main mechanical characteristics are:

Young's modulus	=	186	kN/mm^2
2% proof stress	=	1.770	"
Tensile strength	=	1.850	"
Poisson's ratio	=	0.3	

The web assembly shown in Fig. II.2 was fabricated by welding to a thick plate two blocks of approximately square cross section. These sections were welded together at the Welding Institute using an argon-arc process. To avoid post-welding distortions a rigid frame for clamping was built to hold the pieces in position. Very little distortion was found after welding apart from a small lateral bowing, almost longitudinally symmetric, in both webs. All the subsequent machining was conducted with the webs laying flat clamped to this frame, with the frame in turn fixed to the machine bed. The lateral bowing of the webs being longitudinally symmetric can be corrected by the diaphragm bracing plates which will be used to keep the webs in position in the testing rig. These plates are to be bolted to stiffeners welded to the webs at the support locations. The top blocks on the webs were accurately machined to house the teeth that transmit the shear lag type of loading to the plate edge bearings. The bottom blocks act as tension flanges to lower, as much as possible, the location of the neutral axis of the assemblage. The length of the webs, and consequently the maximum length of the plates
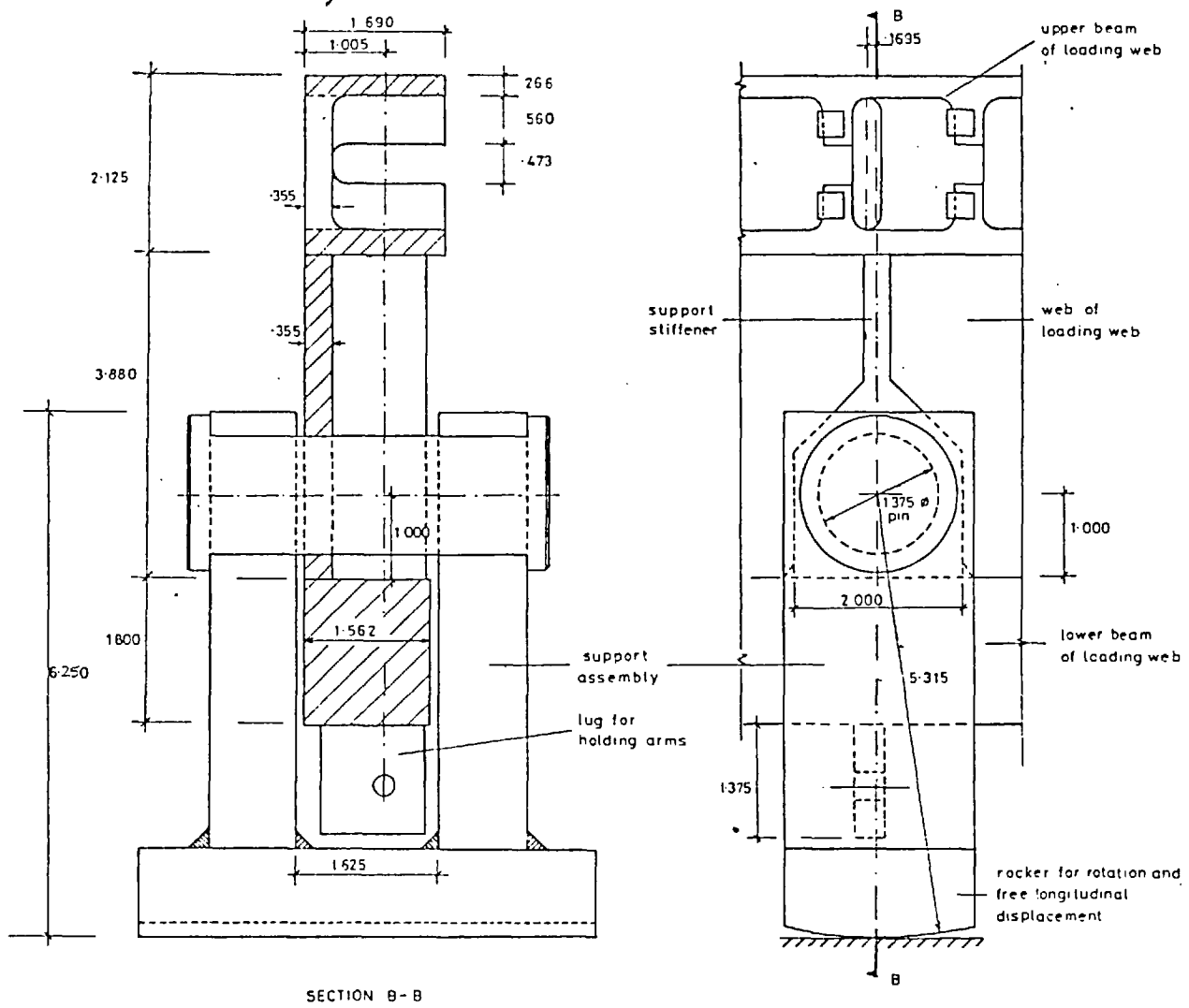
SECTION B-B

Fig II·7 Detail of supports and web cross-sectional dimensions (inches)

to be tested, was chosen so that they could be machined in the longer machine bed available in the Departmental Workshop. The cross-sectional dimensions resulted from a compromise to obtain a flexural modulus such that in the shorter spans the high strains required at the level of the testing plates could be generated with safe point loads.

II.5   LOADING ARRANGEMENTS

Point loads are to be applied through strong loading stiffeners at the mid-span of the loading web assemblies. These stiffeners were cut around the pieces of the web assembly to give them continuity and welded to the whole (see Fig. II.2).

The webs can be supported at three different symmetric positions for testing plates of different lengths. The supports are also made of maraging steel. They support the webs through pins with axes located for stability at approximately the level of the web neutral axis. These were designed with rockers to allow rotation and free longitudinal displacement (Fig. II.7).

The loading system (Fig. II.8) is self-equilibrated. Hydraulic jacks with a capacity of 800 kN/web will be used. These jacks will be located between the bottom flange of reaction beams, which support the webs, and 'saddle' rings (Fig. II.9) which are pinned to the web loading stiffeners.

The loading arrangement of the saddle rings is shown in Fig. II.10. The saddles are constrained to move vertically by adjustable bearings fixed to the webs of the supporting beams. They are also connected to each other transversely for additional stability. The reaction beams are braced by transverse supporting girders which provide at the same time
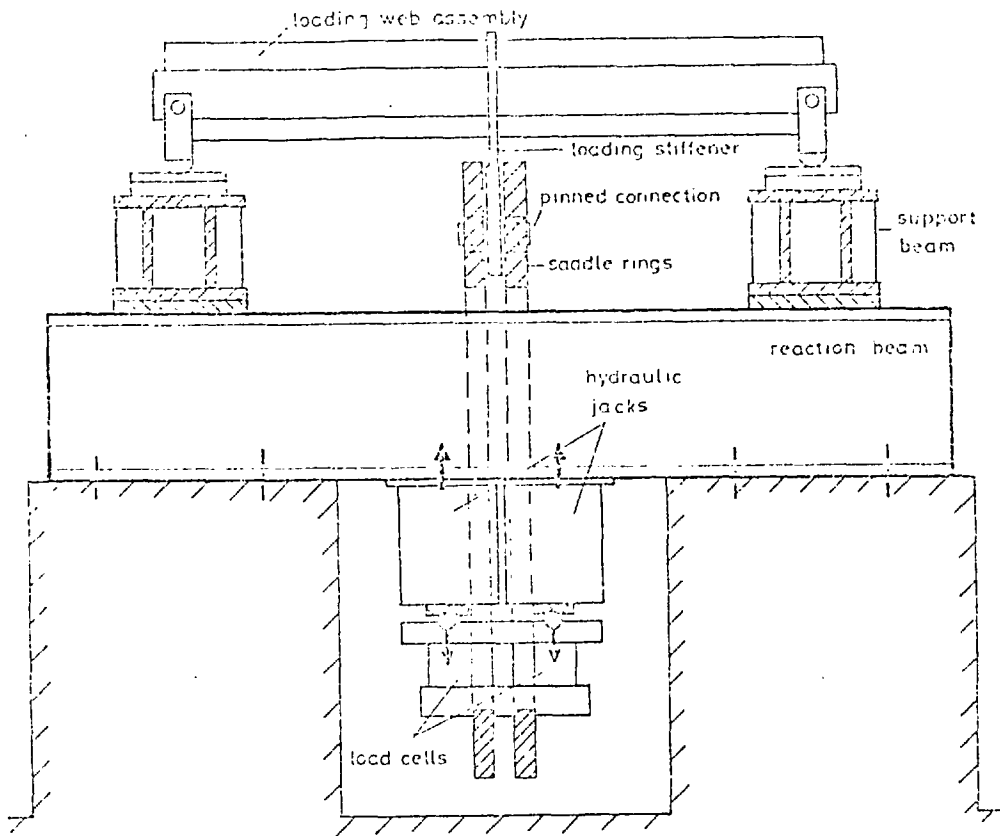
Fig II·8 Sketch of loading system

the packing height necessary to accommodate the depth of the loading saddle rings.

The distance between the reaction beams' can be varied according to the width of the plates to be tested. The webs are simultaneously moved by using bracing diaphragm plates of different lengths.

Details of the fabrication and the safety frame to avoid longitudinal differential movement of the webs are omitted in this brief description and this frame is not represented in the figures.
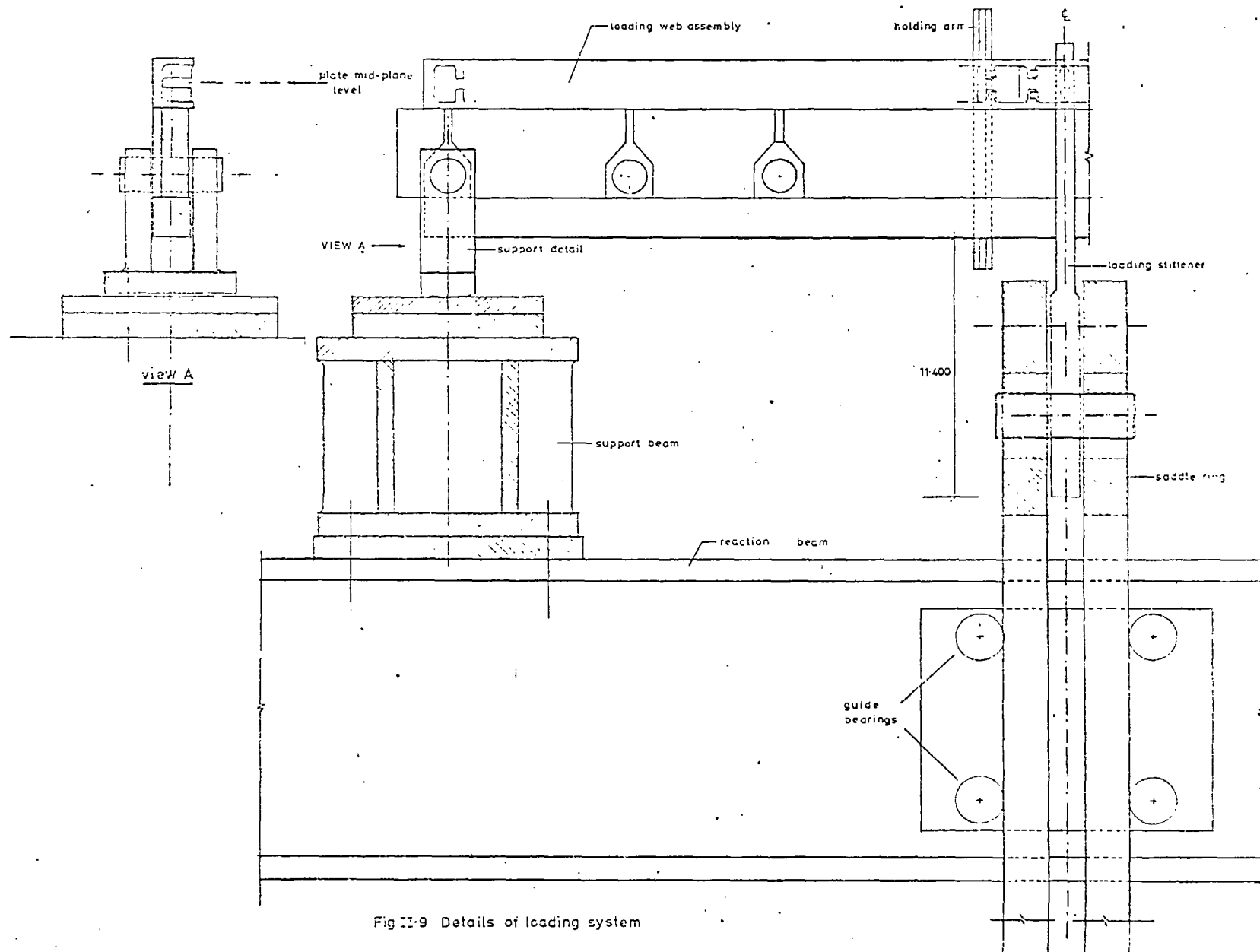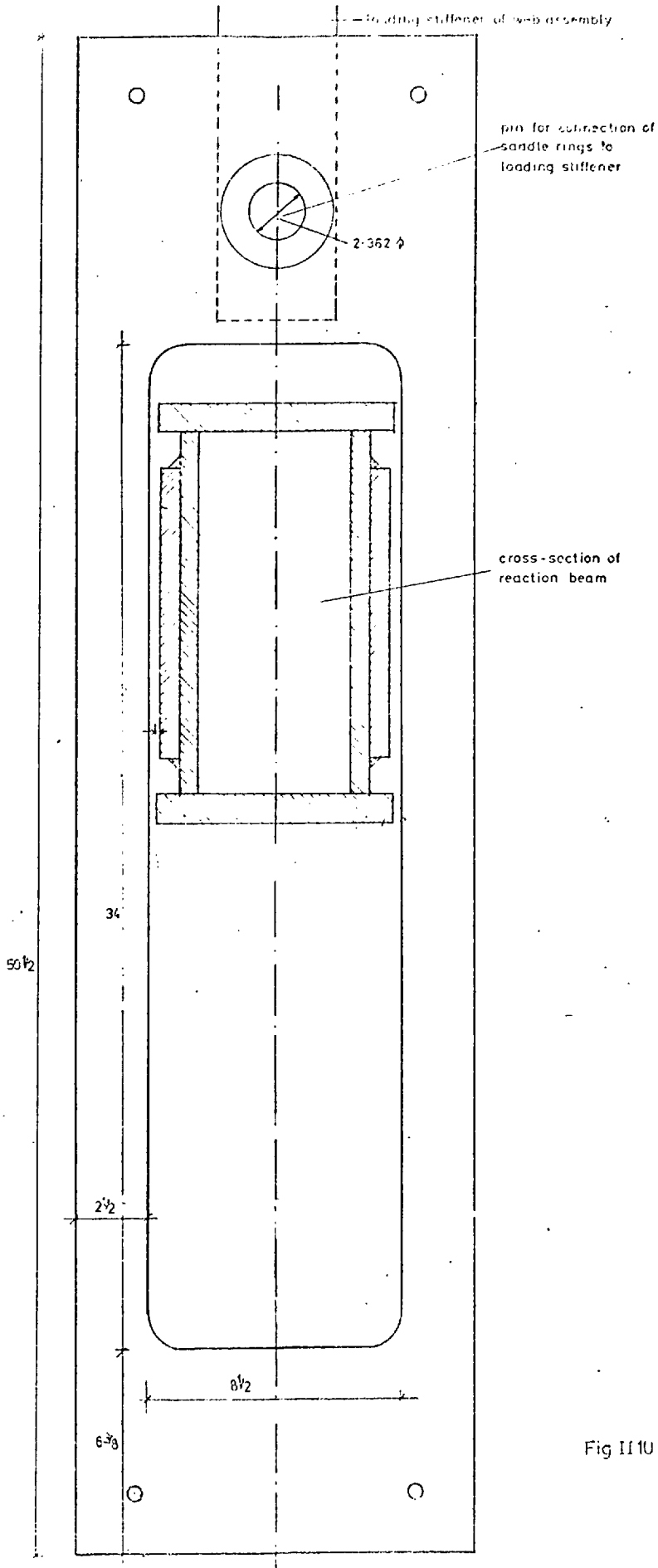
Fig II·9 Details of loading system

Labels in figure:
- loading web assembly
- holding arm
- plate mid-plane level
- VIEW A
- support detail
- loading stiffener
- view A
- support beam
- 11·400
- saddle ring
- reaction beam
- guide bearings

loading stiffener of web assembly

pin for connection of
saddle rings to
loading stiffener

2·362 φ

cross-section of
reaction beam

50½

34

2½

8½

6⅞

Fig II1U Details of saddle rings